



UNIVERSITÀ  
DEGLI STUDI  
DI PADOVA

Università degli Studi di Padova

Dipartimento di Scienze Biomediche

CORSO DI DOTTORATO DI RICERCA IN SCIENZE BIOMEDICHE  
31° CICLO

# Regulation of the Mitochondrial Permeability Transition Pore by Arginine Residue(s) and their Role in the Dimerization of F-ATP Synthase

**Coordinator:** Prof. Paolo Bernardi

**Supervisor:** Prof. Paolo Bernardi

**Ph.D. student:** Lishu Guo



*There is more to us than we know. If we can be made to see it, perhaps for the rest of our lives we will be unwilling to settle for less.*

—Kurt Hahn - 1886-1974, Educator

**父母之爱子，则为之计深远。**

*If parents do love their children, then they have to consider for them in the long run.*

— **感恩父母。** *Thanks to my parents.*



# TABLE OF CONTENTS

Summary.....	5
Sommario.....	7
Abbreviations .....	9
Table of Figures .....	13
Table of Tables .....	14
<b>1 INTRODUCTION .....</b>	<b>15</b>
<b>1.1 Mitochondria.....</b>	<b>16</b>
1.1.1 Mitochondrial architecture .....	16
1.1.2 Mitochondrial bioenergetics.....	19
1.1.3 Mitochondrial signaling.....	23
1.1.4 Mitochondrial channels.....	26
<b>1.2 The permeability transition pore (PTP).....</b>	<b>30</b>
1.2.1 Regulation of PTP .....	30
1.2.2 Cyclophilin D and regulation of the PTP in different species.....	33
1.2.3 The role of PTP in pathophysiology .....	34
1.2.4 Molecular structure. Early hypotheses .....	35
<b>1.3 The mitochondrial ATP synthase .....</b>	<b>38</b>
1.3.1 Structure and function of F-ATP synthase .....	38
1.3.2 Assembly of F-ATP synthase .....	43
1.3.3 Dimerization of F-ATP synthase and subunits e and g .....	45
1.3.3.1 Dimerization of F-ATP synthase.....	45
1.3.3.2 The subunits e and g in yeast.....	47
1.3.4 F-ATP synthase and the PTP.....	48
1.3.5 PTP modulation by arginine residues.....	51
1.3.5.1 The modification of arginine residues.....	51
1.3.5.2 Effects of arginine modification by glyoxals on PTP.....	52
<b>1.4 Objectives and key results.....</b>	<b>54</b>

<b>2</b>	<b>MATERIALS and METHODS .....</b>	<b>55</b>
2.1	Reagents and cells .....	56
2.2	Yeast mutant generation.....	56
2.3	Yeast mitochondria isolation.....	58
2.4	Mouse liver mitochondria isolation.....	59
2.5	Cell permeabilization .....	59
2.6	Chemical modification with glyoxals .....	59
2.7	Isolation of mitochondria from cells .....	60
2.8	Mitochondrial Ca <sup>2+</sup> retention capacity.....	60
2.9	Mitochondrial swelling assay .....	60
2.10	ATP hydrolysis assay .....	60
2.11	Oxygen consumption rate assay .....	61
2.12	Yeast cell lysis .....	61
2.13	Cross-linking experiments .....	61
2.14	Western blotting.....	61
2.15	Blue native gel electrophoresis.....	62
2.16	Silver staining .....	62
2.17	Electrophysiology .....	63
2.18	Serial-dilution spotting assay.....	63
2.19	Fluorescence dye rhod-2 loading.....	64
2.20	BAPTA-AM mitochondria loading.....	64
<b>3</b>	<b>RESULTS and DISCUSSION .....</b>	<b>65</b>
3.1	OH-PGO is able to generate channel activity comparable to MMC in purified F-ATP synthase .....	66
3.2	Matrix Ca <sup>2+</sup> is an essential permissive factor for opening of the PTP	67
3.3	Species-specificity of the PTP regulation by arginine residue(s) .....	71
3.3.1	The species-specific effects of PGO on the PTP .....	71
3.3.2	The role of subunit g in conferring this species-specificity .....	73
3.4	Arginine 107 of yeast subunit g mediates the sensitivity of PTP to PGO .....	74

3.5	Arginine 8 of yeast subunit e is required for dimerization of F-ATP synthase .....	77
3.5.1	Substitution of Arg 8 in subunit e affects dimerization of the F-ATP synthase complex .....	77
3.5.2	Ablation or loss of subunit g affects accommodation of subunit e in the F-ATP synthase dimers .....	78
3.5.3	Glu 83 of subunit g interacts with Arg 8 of subunit e .....	79
3.5.4	Expression level of subunits e and g in the mutants .....	81
3.5.5	Substitutions of Arg 8 of subunit e affect the channel features .....	82
4	ACKNOWLEDGMENT .....	84
5	APPENDIX .....	85
5.1	Publication 1 .....	85
5.2	Publication 2 .....	85
6	REFERENCES .....	109





# Summary

The mitochondrial permeability transition (PT) is a  $\text{Ca}^{2+}$ -dependent permeability increase of the inner membrane, mediated by the permeability transition pore (PTP). The mammalian PTP displays a range of conductance states, which can be as high as 1.2 nS corresponding to a pore with a diameter of about 2 nm. Depending on open time and channel size, the PTP can participate in  $\text{Ca}^{2+}$  homeostasis or cell death. Regulation of the PTP is complex; opening is favored by cyclophilin D (CyPD), Pi, and oxidative stress while it is inhibited by matrix  $\text{H}^+$ ,  $\text{Mg}^{2+}$ , adenine nucleotides and cyclosporin A (CsA). In the 1990s, through the use of modifiers of SH groups and of relatively specific histidine and arginine reagents, a few discrete regulatory sites of the PTP have been defined. Recent evidence suggests that PTP forms from F-ATP synthase. Consistent with this, PTP blockade by matrix  $\text{H}^+$  is mediated by the unique conserved histidine residue of oligomycin sensitivity conferral protein (OSCP).

The first part of my work was focused on the identification of the arginine residue(s) conferring PTP regulation by glyoxals within the general hypothesis that the PTP originates from F-ATP synthase. Eriksson and co-workers discovered the PTP-modulatory effects of arginine-selective reagents, and focused on the structure-function relationship of arginine-glyoxal adducts in the regulation of PTP opening and closure in rat liver mitochondria. Phenylglyoxal (PGO) is the most extensively used arginine-specific reagent. I have observed for the first time that PGO affects the PT in a species-specific manner (inhibition in mouse and yeast, induction in human and *Drosophila* mitochondria), indicating that the ability to modulate the PTP by PGO has been conserved but differs across species. Following the assumptions (i) that the observed differences depend on specific features of the PTP rather than on the existence of species-specific reactive sites, and (ii) that these sites are located on the F-ATP synthase, I have been able to show that the effect of PGO on the PT is specifically mediated by Arg 107 of subunit g, the only arginine residue of this subunit that has been conserved across species. Yeast mitochondria lacking subunit g or bearing a subunit g R107A mutation were totally resistant to PT inhibition by PGO. Taking advantage of the species-specific differences but conserved reactivity with PGO, I have observed that substitution of yeast subunit g with its human counterpart confers the “human” phenotype to yeast, suggesting that the species-specific effect of PGO is more likely to depend on structural differences between the yeast and human F-ATP synthase than on the R107-PGO adduct as such. This finding is a step forward in the molecular understanding of PTP regulation, and further supports the hypothesis that the PTP forms from F-ATP synthase.

The second part of my work was dedicated to reinvestigate the role of  $\text{Ca}^{2+}$  as a permissive factor for PTP opening. The most recent hypothesis about the mechanism of PTP formation is that interaction of  $\text{Ca}^{2+}$  with the metal binding site of  $\beta$  subunit (which usually contributes to coordinate

the binding of Mg-ATP) causes a conformational change that is propagated to the inner membrane through the lateral stalk, which eventually leads to PTP formation. If  $\text{Ca}^{2+}$  must bind to the catalytic site of F-ATP synthase for the PT to occur, then  $\text{Ca}^{2+}$  should be a key permissive factor for PTP opening, while other inducers should affect either the accessibility of the metal binding site or the transmission of the  $\text{Ca}^{2+}$ -dependent conformational change to the inner membrane. Yet a PT occurred in the absence of added  $\text{Ca}^{2+}$  with several inducers including *p*-hydroxyphenylgloxal (OH-PGO), one of the arginine reagents that favor PTP opening in rat liver mitochondria; and phenylarsine oxide (PhAsO), a dithiol cross-linker that is a potent PTP inducer. I have observed that pore opening can occur in presence of EGTA after the treatment of mitochondria with OH-PGO and PhAsO, but also that the inducing effect is prevented by depletion of matrix  $\text{Ca}^{2+}$  with the ionophore A23187 or by chelation of matrix  $\text{Ca}^{2+}$  with BAPTA. These observations indicate that in the absence of matrix  $\text{Ca}^{2+}$  PTP cannot be activated by OH-PGO and PhAsO.

Another part of my work was to test whether charged amino acids of yeast subunits e and g are involved in their interaction, thus playing a role in the dimerization of F-ATP synthase. I have identified Arg 8 of subunit e as a critical residue in mediating e-g interactions, most likely through an electrostatic bond with Glu 83 of subunit g. We have also observed that dimers purified after blue-native electrophoresis from mutants of Arg 8 show decreased PTP channel conductance and activity, indicating that this residue might directly participate in generating the full conductance channel.

# Sommario

La transizione di permeabilità mitocondriale (PT) è un aumento  $\text{Ca}^{2+}$ -dipendente della permeabilità della membrana interna, mediato dal poro di transizione della permeabilità (PTP). Il PTP di mammifero mostra una certa gamma di stati di conduttanza, che possono arrivare fino a 1.2 nS corrispondenti ad un canale con un diametro di circa 2 nm. A seconda della durata delle aperture e della dimensione del canale, il PTP può partecipare all'omeostasi del  $\text{Ca}^{2+}$  o alla morte cellulare. La regolazione del PTP è complessa; l'apertura è favorita dalla ciclofilina D (CyPD), Pi e dallo stress ossidativo mentre è inibita dal pH acido di matrice, dal  $\text{Mg}^{2+}$ , dai nucleotidi adeninici e dalla ciclosporina A (CsA). Negli anni '90, attraverso l'uso di modificatori di gruppi SH e di reagenti relativamente specifici di istidina e arginina, sono stati definiti alcuni siti regolatori del PTP. Prove recenti suggeriscono che PTP si forma dalla F-ATP sintasi. Coerentemente con questo, l'inibizione del PTP dagli  $\text{H}^+$  di matrice è mediata dalla protonazione di un'istidina conservata presente nella subunità OSCP dell'enzima.

La prima parte del mio lavoro è stata dedicata all'identificazione dei residui di arginina che conferiscono la sensibilità del PTP ai gliosali, assumendo che il PTP si formi dalla F-ATP sintasi. Eriksson e collaboratori hanno investigato la modulazione del PTP da parte di agenti selettivi per le arginine, focalizzandosi sullo studio degli effetti degli addotti arginina-gliosale in mitocondri isolati dal fegato di ratto. Il fenilgliosale (PGO) è il reagente specifico per le arginine più comunemente usato. Ho osservato per la prima volta che il PGO influenza il PTP in modo specie-specifico (causando inibizione in topo e nel lievito, mentre induzione in drosofila e nell'uomo), indicando che, nonostante la sua capacità modulatoria sia diversa tra i vari organismi, la sua reattività è invece conservata. Assumendo (i) che le differenze osservate dipendono da caratteristiche specifiche del PTP piuttosto che dall'esistenza di siti reattivi specie-specifici e (ii) che questi siti si trovano sulla F-ATP sintasi, ho potuto dimostrare che l'effetto del PGO è mediato in modo specifico dalla Arg 107 della subunità g della F-ATP sintasi, peraltro conservata tra le specie. I mitocondri di lievito privi di subunità g o esprimenti una subunità g con la mutazione R107A sono totalmente resistenti all'inibizione del PT da PGO. Inoltre, la sostituzione della subunità g del lievito con la sua controparte umana conferisce un fenotipo "umano" al PTP di lievito relativamente all'effetto del PGO, confermando che la Arg 107 è il giusto target e che le differenze specie-specifiche della modulazione da PGO sono probabilmente attribuibili a diversità strutturali dell'enzima. Questa scoperta è un passo avanti nella comprensione molecolare della regolazione PTP, e supporta ulteriormente l'ipotesi che il PTP si generi dalla F-ATP sintasi.

La seconda parte del mio lavoro è stata dedicata a reinvestigare il ruolo del  $\text{Ca}^{2+}$  come fattore permissivo per l'apertura del PTP. L'ipotesi più recente sul meccanismo di formazione del PTP è che il legame del  $\text{Ca}^{2+}$  al sito di legame del metallo della subunità  $\beta$  (che contribuisce a coordinare il

legame di Mg-ATP) causa un cambiamento conformazionale che viene propagato alle subunità inserite nella membrana interna attraverso il gambo laterale, portando all'apertura del PTP. Assumendo che il  $\text{Ca}^{2+}$  giochi questo ruolo, tutti gli altri induttori dovrebbero influenzare l'accessibilità del sito di legame del metallo o la trasmissione del cambiamento conformazionale alla membrana interna. Eppure la PT si verifica ugualmente in assenza di  $\text{Ca}^{2+}$  aggiunto utilizzando diversi induttori compreso il *p*-idrossifenilgliossale (OH-PGO), uno dei reagenti di arginina che favorisce l'apertura del PTP nei mitocondri del fegato di ratto; e la fenilarsina ossido (PhAsO), un reagente dei ditioli e potente induttore del PTP. Tuttavia, nei miei studi ho osservato che l'apertura del PTP può sì verificarsi in presenza di EGTA dopo il trattamento dei mitocondri con OH-PGO e PhAsO, ma l'effetto di induzione termina con l'esaurimento del  $\text{Ca}^{2+}$  di matrice causato dallo ionoforo A23187 o con la chelazione del catione con BAPTA. Queste osservazioni indicano che in assenza del  $\text{Ca}^{2+}$  di matrice il PTP non può essere attivato da altri modulatori, confermando il ruolo permissivo e strettamente necessario del catione.

Un'altra parte del mio lavoro è stata testare se amminoacidi carichi delle subunità di lievito e e g sono coinvolti nella loro reciproca interazione, svolgendo quindi un ruolo chiave nella dimerizzazione della F-ATP sintasi. Grazie ad una mutagenesi sito specifica, ho identificato la Arg 8 della subunità e come residuo critico per tale interazione, agendo molto probabilmente attraverso legami elettrostatici con la Glu 83 della subunità g. Abbiamo anche osservato che i dimeri purificati da BN gels da mutanti privi dell'Arg 8 mostrano una diminuzione della conduttanza e dell'attività di canale del PTP, indicando che questo residuo potrebbe partecipare direttamente alla generazione di un canale correttamente assemblato.

## Abbreviations

ADP	Adenosine diphosphate
AGEs	Advanced glycation end-products
AKT	Protein kinase B
AMPK	AMP-activated protein kinase
ANT	Adenine nucleotide translocase
ATP	Adenosine triphosphate
ATR	Atractyloside
BAD	2,3-Butanedione
BAPTA-AM	1,2-bis(2-aminophenoxy)ethane-N,N,N',N'-tetraacetic acid tetrakis(acetoxymethyl ester)
BCL-2 antagonist/killer	Bak
BCL-2-associated X protein	Bax
B cell lymphoma 2	Bcl-2
BKA	Bongkreikic acid
BSA	Bovine serum albumin
Bz	Benzodiazepine
CI	Complex I of the respiratory chain
CII	Complex II of the respiratory chain
CIII	Complex III of the respiratory chain
CIV	Complex IV of the respiratory chain
CaMKII	Ca <sup>2+</sup> -calmodulin-dependent protein kinase II
CAT	Carboxyatractyloside
CoA	Coenzyme A
CoQ	Coenzyme Q
cpYFP	Circularly permuted yellow fluorescent protein
CRC	Ca <sup>2+</sup> retention capacity
CsA	Cyclosporin A
Cu(OP) <sub>2</sub>	Copper- <i>o</i> -phenanthroline
Cyt <i>c</i>	Cytochrome <i>c</i>
CypD	Cyclophilin D
[Ca <sup>2+</sup> ] <sub>m</sub>	Free matrix Ca <sup>2+</sup>
DAPIT	Diabetes-associated protein in insulin-sensitive tissues
DMEM	Dulbecco's modified Eagle's medium
DTT	Dithiothreitol

Drp1	Dynamamin-related protein
EGTA	Ethylene glycol-bis( $\beta$ -aminoethyl ether)-N,N,N',N'-tetraacetic acid
EMRE	Essential MCU regulator
ER	Endoplasmic reticulum
ERK	Extracellular signal regulated kinase
ETC	Electron transport chain
FADH <sub>2</sub>	A reduced form of flavin adenine dinucleotide
FBS	Fetal bovine serum
FCCP	Carbonyl cyanide <i>p</i> -trifluoromethoxyphenylhydrazone
FMN	Flavin mononucleotide
F <sub>6</sub>	Coupling factor 6
GO	Glyoxal
GOs	Glyoxals
GSH	Glutathione
GTP	Guanine triphosphate
HIF-1	Hypoxia-inducible factor 1
IMM	Inner mitochondrial membrane
IMS	Intermembrane space
INAC	the inner membrane assembly complex
IP <sub>3</sub> R	Inositol trisphosphate receptor
KO	Knock out
Letm1	Leucine-zipper-EF-hand-containing transmembrane protein 1
LPLs	Lysophospholipids
MAMs	Mitochondrial-associated membranes
MAPK	Mitogen-activated protein kinase
MCU	Mitochondrial Ca <sup>2+</sup> uniporter
Mfn1/2	Mitofusins
MGO	Methylglyoxal
MICU1	Mitochondrial calcium uptake 1
MLM	Mouse liver mitochondria
MMC	Mitochondrial megachannel
MPC	Mitochondrial pyruvate carrier
mTOR	Mammalian target of rapamycin
MW	Molecular weight
NAD <sup>+</sup>	Oxidized nicotinamide adenine dinucleotide

NADH	Nicotinamide adenine dinucleotide
NCLX	Na <sup>+</sup> -Ca <sup>2+</sup> exchanger
NDI	NADH dehydrogenase
NEM	N-Ethylmaleimide
OH-PGO	<i>p</i> -hydroxyphenylglyoxal
OMM	Outer mitochondrial membrane
OPA1	Optic atrophy-1
OSCP	Oligomycin sensitivity conferral protein
OXPHOS	Oxidative phosphorylation
PAGE	Polyacrylamide gel electrophoresis
PBS	Phosphate buffered saline
PCR	Polymerase chain reaction
PGO	Phenylglyoxal
PhAsO	Phenylarsine oxide
Pi	Inorganic phosphate
PiC	Phosphate carrier
PI3K	Phosphoinositide 3-kinase
PLA2	Phospholipase A <sub>2</sub>
pmf	Proton motive force
PPIase	Peptidyl-prolyl <i>cis-trans</i> isomerase
PT	Permeability transition
PTMs	Post-translational modifications
PTP	Permeability transition pore
RET	Reversed electron transfer
Rh123	Rhodamine 123
Rhod-2 AM	
1-[2-Amino-5-(3-dimethylamino-6-dimethylammonio-9-xanthenyl)phenoxy]-2-(2-amino-5-methylphenoxy)ethane-N,N,N',N'-tetraacetic acid, 1-[2-amino-5-(3-dimethylamino-6-dimethylammonio-9-xanthenyl)phenoxy]-2-(2-amino-5-methylphenoxy)ethane-N,N,N',N'-tetraacetic acid, tetraacetoxymethyl ester	
RLM	Rat liver mitochondria
ROS	Reactive oxygen species
RR	Ruthenium red
RyR	Ryanodine receptor
SDH	Succinate dehydrogenase

SDS	Sodium dodecyl sulphate
SIRT3	Sirtuin-3
SQR	Succinate-ubiquinone oxidoreductase
SR	Sarcoplasmic reticulum
TCA	Tricarboxylic acid
TMD	Transmembrane domain
TOM	Translocase of the outer mitochondrial membrane
tPTP	Transient PTP opening
TSPO	Translocator protein
Ub <sub>0</sub>	Ubiquinone 0
UbQ	Ubiquinone
UCP	Uncoupling protein
VDAC	Voltage-dependent anion channels
WT	Wild-type
YM	Yeast mitochondria
$\Delta\psi_m$	Mitochondrial transmembrane potential
6.8PL	6.8 kDa proteolipid



## Table of Figures

Fig. 1.1 The origin of eukaryotes: the endosymbiosis of mitochondria ancestors by proto eukaryotes. .....	16
Fig. 1.2. The structure of the mitochondrion .....	19
Fig. 1.3. The mammalian OXPHOS system and the TCA cycle .....	23
Fig. 1.4. Mitochondrial-dependent signaling pathways.....	25
Fig. 1.5. Mitochondrial channels and transporters.....	29
Fig. 1.6. Regulators of the mitochondrial permeability transition pore .....	32
Fig. 1.7. Putative components of the PTP.....	37
Fig. 1.8. Timeline for the characterization of the molecular structure of F-ATP synthase .....	43
Fig. 1.9. Assembly pathways of human and yeast F-ATP synthase .....	45
Fig. 1.10. F-ATP synthase organization and molecular structure of the yeast Fo dimeric domain...47	
Fig. 1.11. Proposed model for PTP opening.....	50
Fig. 1.12. Structure of PGO- and OH-PGO-arginine adducts .....	52
Fig. 1.13. Effect of phenylglyoxal derivatives on the PTP depending on the net negative charge or hydrogen bonds.....	53
Fig. 3.1. OH-PGO is able to trigger PTP opening in planar lipid bilayer in the presence of Ca <sup>2+</sup> ....	67
Fig. 3.2.1. Differential permeability induced by PhAsO and OH-PGO in absence and presence of EGTA.....	68
Fig. 3.2.2. Effect of A23187 and BAPTA-AM on intramitochondrial Ca <sup>2+</sup> level monitored by Rhod- 2 fluorescence .....	69
Fig. 3.2.3. Depletion of matrix Ca <sup>2+</sup> by A23187 inhibits the PTP induction by PhAsO and OH-PGO .....	69
Fig. 3.2.4. Mitochondrial BAPTA loading inhibits the PTP induction by different concentrations of PhAsO and OH-PGO .....	70
Fig. 3.3.1. The effects of PGO on the PTP have been conserved but differ between species .....	72
Fig. 3.3.2. Expression of human subunit g in yeast prevents the inhibitory effect of PGO.....	74
Fig. 3.4. R107 of yeast F-ATP synthase subunit g mediates the effects of PGO on the CRC .....	76
Fig. 3.5.1. Single amino acid substitutions of Arg 8 of yeast subunit e affect F-ATP synthase dimerization .....	78
Fig. 3.5.2. Ablation or loss of subunit g affects accommodation of subunit e in F-ATP synthase dimers.....	79
Fig. 3.5.3. Sequence and structure of yeast subunit e and g. ....	80
Fig. 3.5.4. Glu 83 of subunit g interacts with Arg 8 of subunit e favoring F-ATP synthase dimerization .....	81

Fig. 3.5.5. Expression level of subunits e and g in the mutants.....	82
Fig. 3.5.6. Substitutions of Arg 8 of subunit e affects channel features .....	83

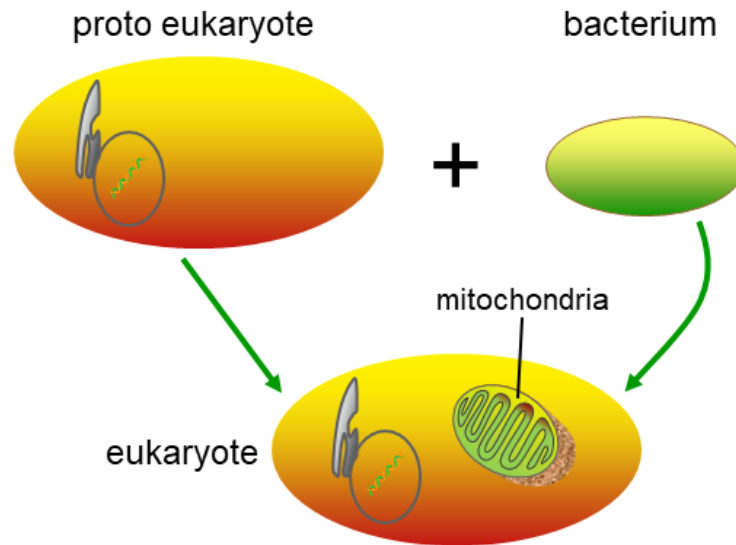
## Table of Tables

Table 1. Summary of the PTP properties of <i>S. cerevisiae</i> , <i>D. melanogaster</i> and mammals .....	34
Table 2. Subunit compositions of mammalian and yeast mitochondrial ATP synthase.....	42
Table 3. Number and position of arginine residues conserved between F-ATP synthase of <i>S. cerevisiae</i> , <i>H. sapiens</i> and <i>M. musculus</i> .....	73

# 1 INTRODUCTION

## 1.1 Mitochondria

The endosymbiotic theory, a well-established evolutionary theory, explains how the host cell and ingested bacteria became dependent on one another for survival, and suggests that mitochondria are derived from bacteria by a symbiosis process (1–3). Endosymbiosis occurs through engulfing and retention of unicellular organisms (1–3), as shown in Fig. 1.1.



**Fig. 1.1 The origin of eukaryotes: the endosymbiosis of mitochondria ancestors by proto eukaryotes.**

The transition from an endosymbiotic bacterium to a mitochondrion as an organelle required many evolutionary changes, including the development of a protein-import system and of membrane-embedded transporters for ions and metabolites; the integration of metabolism and of the replication cycle between host and symbiont, and a dramatic reduction of genome size that matched the transfer of genetic information to the nucleus (4,5). Mitochondria retained their own DNA and translation/transcription materials, most of which are related to the expression of genes encoding proteins involved in cellular respiration (6,7).

### 1.1.1 Mitochondrial architecture

Although mitochondria have been recognized as early as the 1850s, they were clearly defined when microscopes and tissue-staining techniques were developed by the end of the 1800s. Around 1890, Richard Altmann recognized ubiquitous filamentous structures within nearly all cells and called them “bioblasts”. Altmann proposed that these granule-like structures were elementary living unites responsible for vital metabolic processes. The term “mitochondrion” was introduced eight years later by Carl Benda, from the Greek words “mitos” (thread) and “chondros” (granule) (8).

In 1952 the first high-resolution electron micrographs of mitochondria were published and became the “official portrait” of mitochondria (9). Mitochondria are small rod-shaped or spherical organelles located in the cytoplasm with a diameter ranging from 0.5 to 1.0  $\mu\text{m}$ , which are found in nearly all eukaryotes including animals, fungi and plants. Each mitochondrion is bound by two membranes, the outer and inner membrane made up of phospholipids and proteins, which separate two aqueous compartments, the intermembrane space (IMS) and the matrix (Fig. 1.2).

The outer membrane is smooth and is closely related to endoplasmic reticulum (ER), which contributes the transport of protein and phospholipids from ER to mitochondria (10). The outer membrane is freely permeable to molecules up to 5 kDa. The permeability of outer membrane is conferred by a large number of special proteins known as the porins. The mitochondrial porins are also termed the voltage-dependent anion channels (VDAC), and function as gatekeepers for the entry and exit of mitochondrial metabolites, allowing the passage of nutrient molecules, energy-related molecules like adenine nucleotides, and ions from the cytoplasm without leakage of IMS proteins like cytochrome *c* (cyt *c*) (11–13). More than 1,000 different proteins are imported from the cytosol into mitochondria mostly through the translocase of the outer mitochondrial membrane (TOM) system. The preproteins are recognized and translocated through a channel formed by Tom40 within outer membrane and transferred to the presequence translocase (Tim23 complex) within the IMM (14). The translocation contact sites formed by the TOM and Tim23 translocases are so narrow that folded proteins cannot pass through, so that preproteins have to be translocated in an unfolded conformation (13–15).

The IMS protein cyt *c*, primarily recognized as an electron carrier in the electron transport chain (ETC), is also required to promote caspase 9 activation following the permeabilization of the outer mitochondrial membrane (OMM) (16). The integrity of OMM is also highly controlled by pro- and anti-apoptotic members of the B cell lymphoma 2 (Bcl-2) protein family, such as Bcl-2-associated X protein (Bax), Bcl-2 antagonist or killer (Bak) and Bcl-2 itself. As a consequence of OMM permeabilization, the release of IMS proteins including cyt *c* leads to decreased respiration and initiates extrinsic and intrinsic caspase-dependent apoptotic pathways, which may eventually cause apoptotic cell death (17–19).

The inner mitochondrial membrane (IMM) remains in quite close contact with the OMM, albeit only at a few sites. IMM has a similar lipid composition to the bacterial membrane, which can be explained by the endosymbiont hypothesis (1–3) (Fig. 1.1). In contrast to OMM, which has a 50:50 protein-to-lipid ratio, IMM has a ratio of 80:20 and contains all the enzymes necessary for oxidation of reduced cofactors generated by the Krebs cycle and by fatty acid oxidation. IMM is almost impermeable to ions and substrates while it is very permeable to oxygen,  $\text{CO}_2$  and  $\text{H}_2\text{O}$ . The IMM is highly wrinkled and folded, and is organized into layers called cristae, which are highly enriched

in F-ATP synthase dimeric units organized into long rows that contribute to create the typical membrane curvature. The cristae allow a greater surface area for processes that occur across the IMM including electron transport, F-ATP synthesis, protein import and transport of ions and metabolites (20).

The mitochondrial matrix is the space delimited by the IMM. The matrix contains mitochondrial DNA (mtDNA), ribosomes, dissolved oxygen, water, carbon dioxide and enzymes responsible for energy conservation, such as the citric acid cycle reactions and oxidative phosphorylation (OXPHOS). Because of the IMM cristae, the matrix components can easily and promptly diffuse to inner membrane complexes and transport proteins (13,20).

Mitochondrial dynamics were first observed with light microscopy about 100 years ago (22). Mitochondria are highly dynamic structures moving along cytoskeletal tracks, continuously undergoing fission and fusion events that control mitochondrial morphology (22). Many human diseases have been discovered to be caused by mutations in fission and fusion proteins, thus mitochondrial fission and fusion are considered cornerstones for cell survival (22–24). Mammalian mitochondria are endowed with a set of proteins to regulate their dynamics, Dynamin-related protein 1 (Drp1) for fission, mitofusins (Mfn1/2) and optic atrophy-1 (OPA1) for fusion (22,25). Mitochondrial dynamics and mitophagy (the process of removal of defective mitochondria) are recognized as two critical processes underlying mitochondrial homeostasis (23,24). Frequent fusion and fission events enable the redistribution of mitochondrial components and accelerate efficient clearance of damaged mitochondrial components by the autophagic machinery. The integrated interplay between fusion, fission, and autophagy contributes to maintenance of mitochondrial quality and function (23,24).

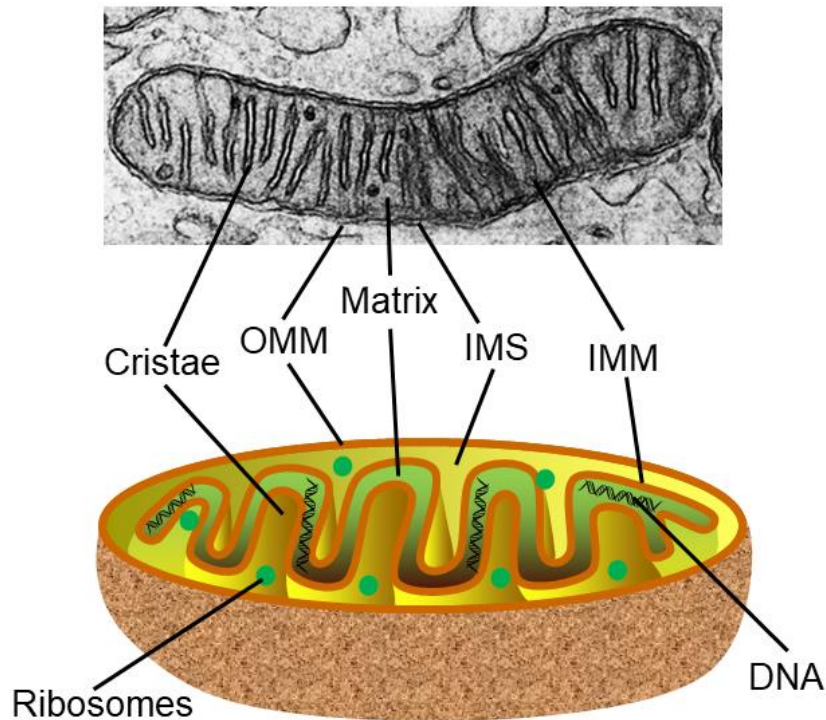


**Fig. 1.2. The structure of the mitochondrion.** OMM: outer mitochondrial membrane, IMS: intermembrane space, IMM: inner mitochondrial membrane.

### 1.1.2 Mitochondrial bioenergetics

All living matter requires energy transformations to drive energetically dynamical life processes. Energy can be stored in the chemical bonds of molecules in the cell, and breakdown of chemical bonds leads to release of energy. The energy stored in the chemical bonds is called chemical energy, and adenosine triphosphate (ATP), referred to as “cellular energy currency”, is an immediate source of chemical energy. There are three major processes for generation of ATP: (i) Glycolysis, i.e. catabolism of glucose with production of two pyruvic acid molecules and two ATP molecules per molecule of glucose. In eukaryotic organisms, glycolysis takes place in the cytosol; (ii) The citric acid cycle, also known as the tricarboxylic acid cycle (TCA) or Krebs cycle, a series of chemical reactions to generate energy through the oxidation of acetate derived from carbohydrates, fats, and proteins into  $\text{CO}_2$ . TCA cycle is a closed loop: the last step regenerates the compound used in the first step. Like the conversion of pyruvate to acetyl coenzyme A (acetyl CoA), TCA cycle takes place in the mitochondrial matrix. The two-carbon acetyl groups from acetyl-CoA combines with the four-carbon oxaloacetate to form the six-carbon molecule citrate. The citrate loses 1 molecule  $\text{H}_2\text{O}$  resulting its isomer-isocitrate, which is oxidized to a five-carbon molecule,  $\alpha$ -ketoglutarate, together with the release of 1 molecule of  $\text{CO}_2$  and release of two electrons ( $e^-$ ) that reduce  $\text{NAD}^+$  to NADH. Oxidation of  $\alpha$ -ketoglutarate generates succinyl-CoA with the release of 1 molecule of  $\text{CO}_2$ . The “high energy” succinyl-CoA is converted to succinate through the substitution of CoA with a

high energy bond-phosphate group. At the same time, one equivalent of guanine triphosphate (GTP) or ATP (depending on the cell type) is formed through substrate-level phosphorylation. During the conversion of succinate into fumarate, flavin adenine dinucleotide (FAD) is reduced to FADH<sub>2</sub>. H<sub>2</sub>O is added to fumarate resulting the formation of malate. Oxidation of malate regenerates oxaloacetate accompanied with reduction of NAD<sup>+</sup> to NADH (26); (iii) OXPHOS occurs within mitochondrial cristae, to generate 32 to 34 ATP molecules from the complete oxidation of 1 glucose, which is about 16 times of ATP production from glycolysis. OXPHOS is a critical activity that serves as the major source of energy in cells. The chemiosmotic hypothesis was first proposed by Peter D. Mitchell in 1961, who suggested that ATP is generated by using the electrochemical H<sup>+</sup> gradient across biological membranes (27). Now overwhelming evidence support his proposal that chemiosmotic coupling is a general mechanism of ATP generation. During OXPHOS, e<sup>-</sup> derived from NADH and FADH<sub>2</sub> are transferred to O<sub>2</sub>, accompanied by H<sup>+</sup> pumping by respiratory Complexes I, III and IV with generation of a H<sup>+</sup> electrochemical gradient, which is then used to drive the synthesis of ATP from ADP and Pi by the F-ATP synthase or Complex V (28) (Fig. 1.3). The electron transport chain (ETC), also known as the respiratory chain, is composed by a series of multisubunit protein complexes embedded in the IMM.

**Complex I (CI)**, NADH-ubiquinone oxidoreductase, is the first and largest enzyme of the respiratory complexes and is L shaped. NADH brings free energy to ETC by binding to CI and is converted to NAD<sup>+</sup> to generate e<sup>-</sup> that are then passed down the hydrophilic arm of CI via a series of iron-sulphur (Fe-S) clusters to the redox carrier coenzyme Q (CoQ). CI is deemed to be the pacemaker of the mitochondrial respiration (26,29). CI is a major site of reactive oxygen species (ROS) generation and a significant contributor to cellular oxidative stress in many degenerative diseases. CI consists of 45 subunits and has a molecular mass of 980 kDa. Both mitochondrial and bacterial enzymes contain similar redox components, flavin mononucleotide (FMN) and 8-9 Fe-S clusters. The site of NADH oxidation by the tightly bound FMN is located towards the extremity of the hydrophilic domain, implying that ROS is produced at the flavin site of CI. The hydrophobic arm of CI is embedded in the membrane and the hydrophilic peripheral arm protrudes into the mitochondrial matrix or the bacterial cytoplasm. Contrary to earlier expectations that CI lacks redox groups in the hydrophobic domain, recent studies of CI from *Thermus thermophilus* and *Escherichia coli* have suggested that conformational changes induced by the electron transfer in the hydrophilic domain must in some way be transmitted to the hydrophobic domain leading to proton pumping (28,29). The simpler prokaryotic enzyme generally consists of 14 conserved “core” subunits (seven hydrophilic and seven hydrophobic) with a total mass of about 550 kDa. In a bacterial convention, the 14 core subunits are named NuoA-NuoM, or Nqo1-Nqo14 (in an alternative bacterial nomenclature) (30,31). CI and NADH dehydrogenase (NDI) have been



independently lost in multiple yeast lineages, for example, *P. tannophilus* and *O. polymorpha* have lost NDI yet maintain CI (32). Yet not all yeast lineages possess a proton-translocating CI, for example, the two most widely studied yeast strains *S. cerevisiae* and *S. pombe* have lost CI. These two strains are Crabtree-positive yeasts, where the OXPHOS system is suppressed by high fermentation, and they use fermentation even in the presence of oxygen (33). Some scientists suggested that the loss of CI was associated with aerobic fermentation and proposed that to synthesize a single polypeptide of NDI for an organism was more advantageous than to synthesize a large CI, which contributed to rapid cell proliferation. On the other hand, repression of the ETC in fermentative yeast would lead to the loss of CI (32). Studies of a mitochondrial CI from the yeast *Yarrowia lipolytica* demonstrated that the general structural features are quite similar to the bacterial complex, while in addition to the 14 core subunits common to the bacterial complex, CI contains no less than 31 or 32 supernumerary subunits with a total mass of 950 kDa. The hydrophobic domain subunits (ND1, -2, -3, -4, -4L, -5 and -6) are encoded by mtDNA, and the hydrophilic domain, 7 of 8 Fe-S clusters provide the electron wire. The  $e^-$  are passed down the hydrophilic arm via Fe-S clusters to the lipid soluble redox carrier CoQ, also known as ubiquinone (UbQ), then are transferred directly to complex III (34).

**Complex II (CII)**, succinate dehydrogenase (SDH) or succinate-ubiquinone oxidoreductase (SQR), receives  $e^-$  from succinate as part of the TCA cycle. CII, the only membrane-bound member of the TCA cycle, usually consists of four nuclear encoded subunits: SDHA (70 kDa), SDHB (30 kDa), SDHC (15 kDa) and SDHD (13 kDa), termed Sdh1-4 in yeast and SdhA-SdhD in bacteria. A FAD prosthetic group of SDHA subunit participates in the TCA cycle and converts succinate into fumarate. In this process, CII accepts the  $e^-$  from FADH<sub>2</sub> and transfers them to SDHB subunit, which has three Fe-S clusters arranged to force the movement of  $e^-$  to SDHC and SDHD subunits to the heme and UbQ prosthetic groups. Heme stabilizes the  $e^-$  adjacent to UbQ and UbQ is reduced to UbQH<sub>2</sub>. UbQH<sub>2</sub> then transfers  $e^-$  to CIII, where it is re-oxidized, returning to CII (35). In contrast to other complexes, CII does not pump protons across the membrane.

**Complex III (CIII)**, also termed the cyt *bc*1 complex, catalyzes the transfer of  $e^-$  from UQH<sub>2</sub> to cyt *c*, and the associated proton translocation. CIII apparently always exists as a homodimer with a mass of about 460 kDa, and the monomer consists of 10-11 subunits with H shape (36). CIII functions through a Q-cycle mechanism. Q<sub>p</sub> (near P-phase (cytoplasm)) and Q<sub>n</sub> (near N-phase (matrix)) are the two binding sites for UQH<sub>2</sub>. A molecule of UQH<sub>2</sub> binds to the Q<sub>p</sub> site which is close to the Rieske protein. The first  $e^-$  from UbQH<sub>2</sub> is transferred to the 2Fe-2S center then passed down the chain to cyt *c*<sub>1</sub>, and the second  $e^-$  is transferred to cyt *b*<sub>L</sub>. Q<sub>n</sub> is the second UbQ processing site where UbQ is reduced to UbQH<sub>2</sub>. Because this reaction requires two  $e^-$ , the Q<sub>p</sub> site has to turn over twice, oxidizing two UbQH<sub>2</sub>, releasing 4H<sup>+</sup> and delivering two  $e^-$ . The overall reaction

catalyzed by CIII involves the net oxidation of one UQH<sub>2</sub> and the reduction of two cyt *c*<sub>1</sub>, the release of 4H<sup>+</sup> at P-phase and the uptake of 2H<sup>+</sup> from N-phase (37).

Cellular aging increases the production of ROS, a major contributing factor in many aging-related diseases. CI and CIII have been recognized as two main sites for the generation of superoxide and ROS. When the FMN site of CI is reduced because of the high matrix NADH/NAD<sup>+</sup> ratio, or when there is no ATP production but high proton motive force (pmf or  $\Delta p$ ) and a reduced CoQ pool, e<sup>-</sup> won't flow forward along the ETC and instead flow back to CI (38,39), a process known as reverse electron transfer (RET), which can be abolished by the inhibitor rotenone (38,39) and be induced by accumulation of succinate (40). CIII transfers e<sup>-</sup> from the CoQ pool to cyt *c*. The structural integrity of CIII is important for maximal rate of catalysis and minimal rate of e<sup>-</sup> leakage toward O<sub>2</sub> (41). With the supply of reduced CoQ (CoQH<sub>2</sub>) and inhibition of the Q<sub>i</sub> site by antimycin, CIII can be induced to produce large amounts of superoxide at the Q<sub>o</sub> site. However, under physiological conditions superoxide production by uninhibited CIII is negligible compared with that by CI during RET (38,41).

**Complex IV (CIV)**, also termed cytochrome oxidase, is a member of the heme–copper oxidase family. CIV transfer e<sup>-</sup> from cyt *c* to O<sub>2</sub> through its metal centers: the copper A (Cu<sub>A</sub>) center, heme *a* and Cu<sub>B</sub>. Cyt *c* accepts an e<sup>-</sup> from cyt *c*<sub>1</sub> and donates it to Cu<sub>A</sub> center, which is the initial e<sup>-</sup> acceptor of CIV. Heme *a* is close to the Cu<sub>A</sub> center and accepts e<sup>-</sup> from Cu<sub>A</sub>. The second heme, heme *a*<sub>3</sub>, is within 5Å of Heme *a* and it is the site where O<sub>2</sub> binds before it is reduced to H<sub>2</sub>O, and it is also the site of binding of several inhibitors including cyanide, azide, nitric oxide, and carbon monoxide. A third copper atom, known as Cu<sub>B</sub>, is adjacent to heme *a*<sub>3</sub>. Most investigators favour a mechanism in which the route of proton pumping passes close to the heme *a*<sub>3</sub>/Cu<sub>B</sub>, where O<sub>2</sub> is reduced (42,43).

Electron transport through CI, CIII, and CIV is coupled to the transport of protons out from the mitochondrial matrix, which generates electrochemical H<sup>+</sup> gradient across the IMM. The complex V (CV), also termed F-ATP synthase, then uses the energy stored in this gradient to make ATP (44). The structure and function of F-ATP synthase will be described in Part 1.3.1.

It has been widely accepted that CI, CIII and CIV can form supercomplexes, which were defined as “respirasome” in 2008 (45). Most CII, CIV and a relevant fraction of CIII stand alone, and the majority of CI is stabilized by the CIII dimer, with or without CIV (46,47). The respirasome functions to minimize the generation of ROS during e<sup>-</sup> transport through the ETC (46). The biogenesis and assembly of respirasome are highly relevant to mitochondrial proper function, and are related to many pathologies, such as neuromuscular disorders, heart failure, aging etc. Nonetheless, the accurate assembly process of respirasome is still behind the curtain (47).



the caspase cascade and leads to cell death (16). In both prokaryotes and eukaryotes, protein lysine acetylation by TCA cycle metabolite acetyl-coA is present to control diverse cellular functions. ROS emerged as intrinsic mitochondrial signaling molecules to communicate their fitness with the rest of the cell under physiological and pathological conditions. Mitochondrial release of ROS can activate expression of hypoxia-responsive genes responsible for metabolic adaptation to low O<sub>2</sub>. Hypoxic conditions can stimulate mitochondria to release ROS, resulting in the stabilization of hypoxia inducible factors (HIFs) (48,49). The HIFs are essential for many physiological progresses. Hypoxia-inducible factor 1 (HIF-1) is a heterodimer consisting of a HIF-1 $\beta$  subunit and a HIF-1 $\alpha$  subunit. HIF-1 is an oxygen-sensitive transcriptional activator and activates the transcription of many genes involved in angiogenesis, glucose metabolism, cell proliferation and metastasis. As an oxygen sensor, HIF-1 coordinates cellular transcriptional response to hypoxia to maintain cellular homeostasis under low O<sub>2</sub> stress (50,51).

Emerging evidence suggests that PI3K/Akt/mTOR signaling contributes to HIF-1 $\alpha$ -regulated cellular glucose metabolism. Activated mTOR induces the translation of HIF-1 $\alpha$  resulting in aerobic glycolysis. The activation of Akt–mTOR–HIF-1 $\alpha$  pathway by hypoxia causes increase of aerobic glycolysis, which contributes multidrug resistance of various human cancers (52,53). The NAD-dependent deacetylases, sirtuins, have been recognized to be crucial for the management of stress response of cells (54). Sirtuin-3, SIRT3, can reversibly bind to CI, and regulate its acetylation and activity of ETC. SIRT3 has also been demonstrated to play an important role in maintenance of basal ATP levels and hence, overall energy homeostasis (55). SIRT3 has been shown to promote autophagy by activation of the LKB1-AMPK-mTOR signaling pathway (56). The SIRT3/AMPK/HIF-1 $\alpha$  pathway could be a potential therapeutic target in a variety of human diseases. MAPK signaling pathway is another pivotal and intensively studied signaling pathway in hypoxic conditions, which positively regulates the expression and activity of HIF-1 $\alpha$  (57). Interestingly, ROS, a messenger of several signaling pathways, can induce MAPK phosphorylation and activate MAPK signaling pathways that modulate Complex I activity (58) (Fig. 1.4b).

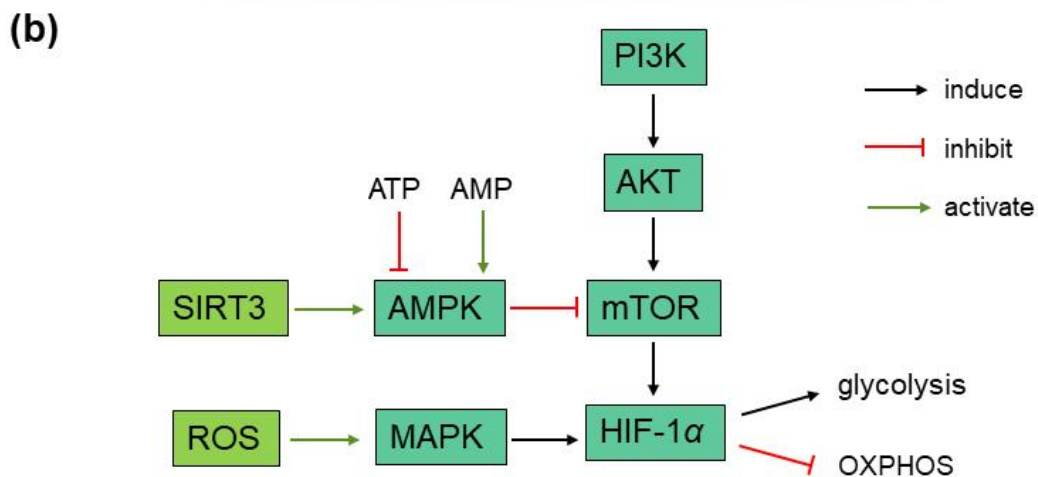
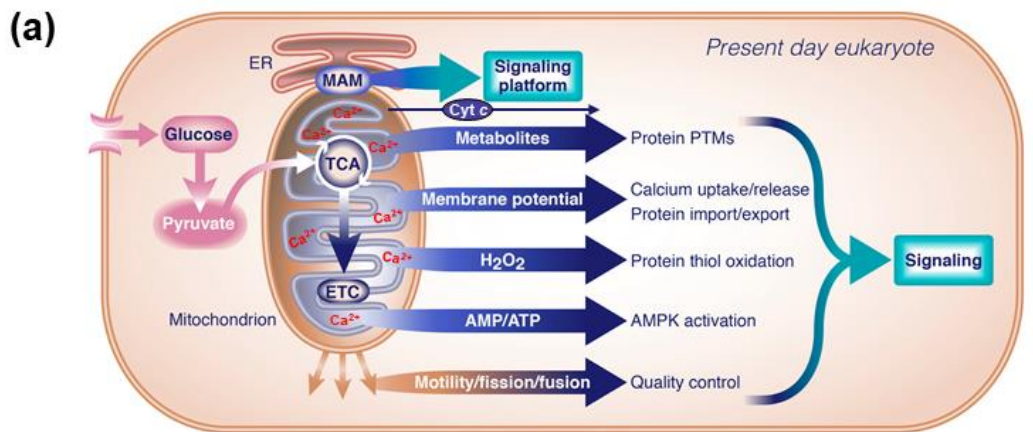


**Fig. 1.4. Mitochondrial-dependent signaling pathways.** (a) Mitochondria have multiple mechanisms to communicate with the rest of a cell. Among all, the release of *cyt c*, metabolites and ROS, activation of AMPK, changes of membrane potential and  $\text{Ca}^{2+}$  homeostasis, as well as the mitochondrial dynamics. Modified from Fig. 1 of Ref. (48). (b) A simplified scheme of major signaling pathways controlling mitochondrial biogenesis and function. ER: endoplasmic reticulum; MAMs: mitochondrial-associated membranes; PTMs: post-translational modifications; AMPK: AMP-activated protein kinase; PI3K: phosphoinositide 3-kinase; AKT: protein kinase B; mTOR: mammalian target of rapamycin; MAPK: mitogen-activated protein kinase.

Millions of years of endosymbiosis between mitochondria and the host cells has resulted not only in the cooperation in energy conservation but also in the collaborative approach to  $\text{Ca}^{2+}$  signaling. Mitochondria-cytosolic communication finely tunes energy supply to energy demand. ATP hydrolysis in the cytosol provides ADP to mitochondria to stimulate OXPHOS by mitochondrial respiration.  $\text{Ca}^{2+}$  signals primarily orchestrate the “stimulus-response-metabolism coupling” of ATP synthesis between the cytosol and matrix (59). Mitochondria serve as a target of  $\text{Ca}^{2+}$  signaling, which can regulate mitochondrial oxidative metabolism and is involved in OXPHOS disorders (60–62).  $\text{Ca}^{2+}$  signals govern most processes that require increased energy supply, such as secretion, motility, contraction, electrical excitability, so cellular  $\text{Ca}^{2+}$  homeostasis is fundamental for cell metabolism, proliferation, and apoptosis (26,62,63). The cross-talk between mitochondria and ER plays an important role in the maintenance of  $\text{Ca}^{2+}$  homeostasis. Synchronous activation of inositol trisphosphate receptor ( $\text{IP}_3\text{R}$ ) or Ryanodine receptor ( $\text{RyR}$ ) results in a localized  $\text{Ca}^{2+}$  concentration

( $[Ca^{2+}]$ ) increase at the ER/sarcoplasmic reticulum (SR)-mitochondrial junction, respectively, which sequentially evokes the activation of mitochondrial  $Ca^{2+}$  uptake sites (62,64,65). MAMs provide microdomains for ER-mitochondria  $Ca^{2+}$  transfer. MAMs, hotspots of  $Ca^{2+}$  signaling, are increasingly appreciated as vital players in many cellular processes, such as mitochondrial bioenergetic, cell fate decision, autophagy, mitophagy, mitochondrial dynamics, cancer, immunity and aging (66,67).

Mitochondria take up  $Ca^{2+}$  across the IMM through a  $Ca^{2+}$ -selective channel known as the mitochondrial  $Ca^{2+}$  uniporter (MCU), which equilibrates  $Ca^{2+}$  with its electrochemical gradient (68,69). In energized mitochondria this favors  $Ca^{2+}$  accumulation, which is driven by the inside-negative transmembrane potential ( $\Delta\psi_m$ ) (70). The extrusion of  $Ca^{2+}$  is probably coupled to the entry of  $H^+$  via the putative  $H^+/Ca^{2+}$  exchanger in liver mitochondria, or indirectly in heart or brain mitochondria where  $Ca^{2+}$  efflux occurs through a combination of an electrogenic  $3Na^+-Ca^{2+}$  exchanger and  $H^+/Na^+$  exchanger (71–73). The general consensus is that free matrix  $Ca^{2+}$  ( $[Ca^{2+}]_m$ ) is in the range of 0.5-2  $\mu M$ , and that matrix  $Ca^{2+}$ -Pi complexes can rapidly dissociate to maintain  $[Ca^{2+}]_m$  at a constant value (74). When the level of  $[Ca^{2+}]_m$  reaches a threshold value, which is usually assumed to be higher than the physiological concentration, the mitochondrial permeability transition can occur (see Part 1.2).

#### 1.1.4 Mitochondrial channels

A large variety of mitochondrial carriers, exchangers and channels are required for the transport of proteins, ions, and metabolites to establish communication between mitochondria and other cellular compartments and maintain mitochondrial function and biogenesis. Opening of mitochondrial ion channels would cause collapse of membrane potential, mitochondrial uncoupling, mitochondrial dysfunction and cell apoptosis. Many studies have revealed the existence of many regulated mitochondrial channels and are unraveling their regulation and function (Fig. 5).

VDAC, also termed porin, was the first channel discovered in mitochondria, followed by extensive studies over the past 30 years (75). VDAC is a 30 kDa pore-forming protein located in the OMM of all eukaryotic mitochondria. Two isoforms are known in yeast (yVDAC1 and yVDAC2) and three (VDAC1, VDAC2, and VDAC3) in mammals (76). VDAC is the most abundant ion channel of OMM, a  $\beta$ -barrel channel allowing passage of hydrophilic molecules up to 5 kDa. Diffusion of hydrophilic ions and metabolites via VDAC follows their concentration gradient across the OMM (77). VDAC also mediates  $Ca^{2+}$  diffusion regulated by its  $Ca^{2+}$ -binding site(s), and also functions in the  $Ca^{2+}$  cross-talk between ER and mitochondria, hence it plays a fundamental role in regulation of mitochondrial  $Ca^{2+}$  homeostasis. VDAC interacts with many partner proteins such as the TOM, Bcl-

2 family and hexokinase (HK), which links VDAC to other cellular functions like protein import, apoptosis, metabolite regulation and tumorigenesis. Tom40, the main component of TOM complex, is a conserved protein import channel. Tom40 forms a 19-stranded  $\beta$ -barrel with an N-terminal  $\alpha$ -helix linked to VDAC. VDAC1, the most expressed VDAC isoform, has been identified to be a multifunctional protein and play a crucial role in cellular metabolism and mitochondrial function. VDAC1 regulates Bcl-2 family members, and its interaction with Bax yields a complex with much higher conductance than VDAC1 alone, which can be prevented by Bcl-xL. VDAC1 is assembled into monomers, dimers and oligomers, and its oligomeric state can be affected by the interaction with Bcl-2 and Bcl-xL. VDAC1 oligomeric state regulates VDAC1 function, including stabilization of the protein, serving as a platform for the oligomerization of other proteins such as HK and creatine kinase (CK), and mediating the release of cyt *c* (77–81). HK lies at the apex of the glycolytic pathway and has been found to be over-expressed in the tumor cell. HK protects against mitochondria-mediated apoptosis via interaction with VDAC1, and VDAC1-bound HK is over-expressed in cancer cells. Translocator protein (TSPO), also known as the peripheral benzodiazepine receptor, is a highly hydrophobic 18 kDa protein mainly found in the OMM. TSPO is a multi-functional protein involved in regulation of cholesterol transport, heme synthesis, apoptosis, tumorigenesis and cell proliferation (82,83). The regulation of mitophagy by TSPO is dependent on VDAC, to which TSPO binds to, reducing mitochondrial coupling and enhancing ROS overproduction that leads to cell apoptosis (77–81).

The IMM is much less permeable than the OMM and is only freely permeable to the very simplest molecules like H<sub>2</sub>O, CO<sub>2</sub> and O<sub>2</sub>. Sophisticated antiport systems and ion channels embedded in the IMM allow specific molecules to cross this barrier, as shown in Fig. 1.5.

MCU, a Ca<sup>2+</sup>-selective ion channel, drives Ca<sup>2+</sup> into mitochondrial matrix down its electrochemical gradient (68,69). The coiled-coil domain-containing protein 109A (Ccdc109a) has been proposed to be responsible for channel formation and required for channel activity. MCU-dependent Ca<sup>2+</sup> uptake has been demonstrated to be modulated by several regulators. Mitochondrial Ca<sup>2+</sup> uniporter regulator 1 (MCUR1), also known as CCDC90a, acts as a positive modulator while no evidence shows it has a direct effect on the activity of MCU. Mitochondrial calcium uptake 1 (MICU1), a 54 kDa membrane protein previously known as CBARA1 and EFHA3, possesses two Ca<sup>2+</sup> binding EF-hand motifs and acts as a positive regulator of MCU (84). Later, MICU1 has been found to be a gatekeeper for MCU-dependent Ca<sup>2+</sup> accumulation, thus, it is predicted to be a negative regulator essential to avoid matrix Ca<sup>2+</sup> overload (85). MICU1 is unlikely to contribute to MCU channel formation because it possesses only one very short transmembrane domain (TMD). Essential MCU regulator (EMRE), a 10 kDa protein located in the IMM, contains a single predicted TMD (86). EMRE is essential for the interaction between MCU and MICU1/MICU2 and required for the Ca<sup>2+</sup>-

dependent uptake by MCU (87).  $\text{Ca}^{2+}$ -calmodulin-dependent protein kinase II (CaMKII) resides in the mitochondrial matrix. CaMKII is a positive regulator of MCU through its interaction with MCU and promoting  $\text{Ca}^{2+}$  entry into matrix (88). CaMKII has been found to become highly activated in some pathophysiological conditions, for example, ischemia-reperfusion (89). Mitochondrial  $\text{Ca}^{2+}$  uniporter b (MCUb), previously named Ccdc109b, is a 33 kDa protein with two TMDs. MCVb is an MCU paralogue that shares 50% similarity with MCU. The overexpression of MCVb reduces mitochondrial  $\text{Ca}^{2+}$  uptake, suggesting that MCVb inhibits MCU activity (90). The  $\text{Ca}^{2+}$  transport activity of MCU can be inhibited by 0.2  $\mu\text{M}$  ruthenium red (RR) (91) or even lower concentrations of ruthenium 360 (92). The downregulation of MCU impairs  $\text{Ca}^{2+}$  uptake thus increase the resistance to cell apoptosis, suggesting that MCU may be involved in tumorigenesis (81,93–95).

As to  $\text{Ca}^{2+}$  efflux from matrix,  $\text{Na}^+$ - $\text{Ca}^{2+}$  exchanger (NCLX) is a mitochondrial  $\text{Na}^+$ -dependent  $\text{Ca}^{2+}$  efflux pathway (71). PTP may participate in  $\text{Ca}^{2+}$  homeostasis as a  $\text{Ca}^{2+}$  release channel, also allowing equilibration of other various ions and solutes (96), which will be described in Part 1.2.

The uncoupling protein (UCP) family is a  $\text{H}^+$  channel or transporter located in the IMM. Uncoupling protein 1 (UCP1), also known as thermogenin, mediates “proton leak” allowing fast oxidation of substrates without ATP production, energy being dissipated as heat (97). UCP2 (98) has revealed structural similarity to the adenine nucleotide translocase (ANT). High expression of UCP2 can decrease ROS production, suggesting that UCP2 acts as a sensor of oxidative stress. UCP4 and UCP5 are less homologous and principally expressed in the central nervous system (99,100).

The following mitochondrial  $\text{K}^+$ -selective channels have been described in the IMM: ATP-dependent  $\text{K}^+$  (mito $\text{K}_{\text{ATP}}$ ) channels, big-conductance  $\text{Ca}^{2+}$ -activated  $\text{K}^+$  (mito $\text{BK}_{\text{Ca}}$ ) channel, intermediate-conductance  $\text{Ca}^{2+}$ -activated  $\text{K}^+$  (IKCa) channel, small-conductance  $\text{Ca}^{2+}$ -activated  $\text{K}^+$  (SKCa) channel, voltage-gated Kv1.3  $\text{K}^+$  channel, TASK-3 two-pore  $\text{K}^+$  channel (mitoTASK-3) and pH-sensitive  $\text{K}^+$  channel. The mitochondrial  $\text{K}^+$  channels have been implicated in various pathophysiological processes involved cell death by modulating  $\Delta\psi_{\text{m}}$ ,  $\text{Ca}^{2+}$  signaling, matrix volume and generation of ROS (81).

Mitochondrial carriers are proteins that transport essential molecules, such as metabolites, adenine nucleotides and phosphate, across the mitochondrial inner membrane. The human genome encodes 48 mitochondrial carriers with likely 39 different functions (101). These carriers transport substrates and products that are necessary for the OXPHOS reaction. The ANT and the phosphate carrier (PiC) are essential for OXPHOS, and will be described in Part 1.2.4. Glycolysis takes place in the cytosol and its final product, pyruvate, is transported into the mitochondrion for the conversion into acetyl-CoA by a reaction requiring high levels of CoA (101). The mitochondrial pyruvate carrier (MPC) transfers pyruvate from cytosol to the mitochondrial matrix (102). The *MPC1* and *MPC2* genes



encode two subunits of the MPC, MPC1 and MPC2, respectively, which are both required for the assembly and activity of the MPC complex (103,104). MPC function appears to be abnormal in some forms of cancer (105). I refer the reader to recent reviews (106,107) for other mitochondrial carriers which are not discussed here.

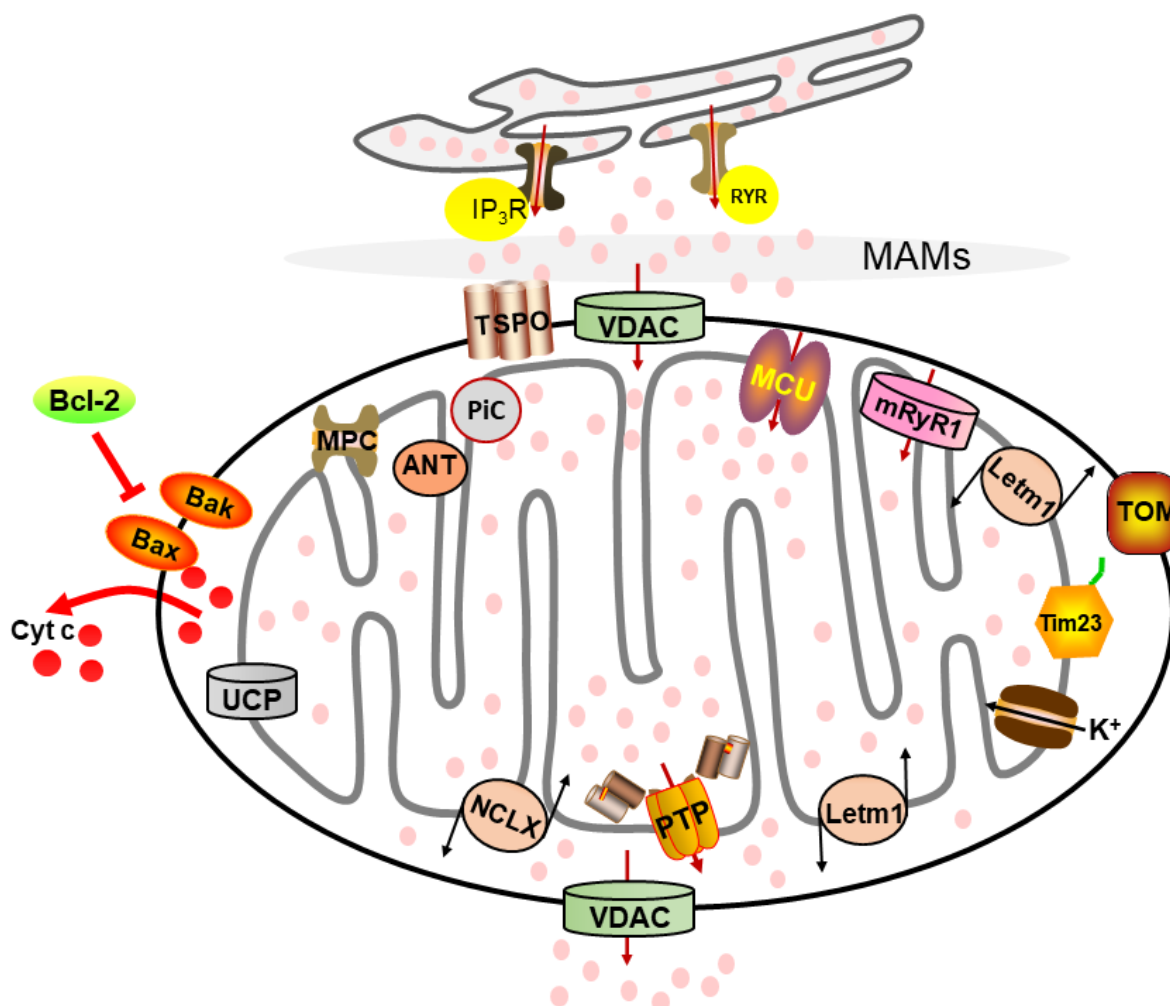


**Fig. 1.5. Mitochondrial channels and transporters.**  $\text{Ca}^{2+}$  release from ER mainly occurs through  $\text{IP}_3\text{R}$  and  $\text{RyR}$ .  $\text{VDAC}$  provides a pathway for metabolite transport and  $\text{Ca}^{2+}$  diffusion across the OMM.  $\text{TSPO}$  is mainly found in OMM and acts as a cholesterol transporter.  $\text{TOM}$  complex located in the OMM allows import of proteins into the IMS.  $\text{MCU}$  located in the IMM transports  $\text{Ca}^{2+}$  into the matrix. The  $\text{PTP}$  and  $\text{NCLX}$  located in IMM contribute to  $\text{Ca}^{2+}$  efflux. Proteins could be recognized and translocated by  $\text{TIM/TOM}$  complex. Different potassium-selective channels are present in the IMM and are classified by their physiological modulators. The  $\text{UCP}$  mediates proton leak across the IMM.  $\text{ANT}$  is located in the IMM is responsible for the import ADP into the matrix and the export of synthesized ATP.  $\text{PiC}$  is the primary transporter of  $\text{Pi}$  into matrix across the IMM. ER: endoplasmic reticulum;  $\text{IP}_3\text{R}$ : inositol 1,4,5-trisphosphate receptor;  $\text{RyR}$ : ryanodine receptor; MAMs: mitochondrial associated membranes; OMM: outer mitochondrial membrane;  $\text{VDAC}$ : voltage-dependent anion channel;  $\text{TSPO}$ : translocator protein;  $\text{TOM}$ : translocase of the outer membrane; IMS: intermembrane space;  $\text{Bax}$ : bcl-2-associated X protein;  $\text{Bak}$ : bcl-2 homologous antagonist killer; IMM: inner mitochondrial membrane;  $\text{MCU}$ : mitochondrial  $\text{Ca}^{2+}$  uniporter;  $\text{mRyR1}$ : mitochondrial  $\text{RyR}$  type 1;  $\text{Letm1}$ : Leucine zipper-EF-hand containing transmembrane protein 1;  $\text{PTP}$ : mitochondrial permeability transition pore;  $\text{NCLX}$ :  $\text{Na}^+/\text{Ca}^{2+}$  exchanger;  $\text{Tim23}$ : translocase of the inner mitochondrial membrane 23;  $\text{UCP}$ : uncoupling protein;  $\text{ANT}$ : adenine nucleotide translocator;  $\text{PiC}$ : phosphate carrier.

## 1.2 The permeability transition pore (PTP)

The mitochondrial permeability transition (PT) is an abrupt increase of IMM permeability to solutes with molecular mass up to 1.5 kDa mediated by the mitochondrial permeability transition pore (PTP) (108). The term “permeability transition” was coined by Haworth and Hunter, who established most characteristics of the PTP (109–114). The PT has been previously considered as a form of “Ca<sup>2+</sup> induced unspecific membrane damage” because the PTP is nonselective or quite poorly selective. The discovery that mammalian PT can be inhibited by cyclosporin A (CsA) (115–118), a paramount finding, led to the hypothesis that the PTP is a regulated channel. This hypothesis, in fact, had already been put forward by Haworth and Hunter who identified many of the inducers and inhibitors of the PT (109–114).

About 30 years ago, the introduction of patch-clamp technique allows to detect the individual channel activity of very small cells. In 1987, it was found that the OMM possesses a voltage-dependent ion channel, which is different from VDAC (119). In 1989, a channel with a high-conductance of ~1.3 ns, the so-called “mitochondrial megachannel” (MMC) was identified (120,121). Solute exclusion studies demonstrated that the maximum molecular weight (MW) admitted into the mitochondrial matrix is 1.5 kDa and the estimated pore diameter is 2-3 nm (81,122). The MMC activity can be inhibited by CsA and possesses all the key regulatory features of the PTP (123,124).

### 1.2.1 Regulation of PTP

The PT is defined as an unselective permeabilization of the IMM due to the opening of PTP. The PT is activated by Ca<sup>2+</sup>, and may serve as a Ca<sup>2+</sup> release channel involved in cellular Ca<sup>2+</sup> homeostasis (125). Mitochondrial matrix Ca<sup>2+</sup> is essential for the PT to occur (126), but the amount of Ca<sup>2+</sup> required to activate PTP opening varies depending on the species, organ of origin of the mitochondria, and on the presence of one of a variety of “inducers”, compounds that cannot open the pore but favor the Ca<sup>2+</sup>-dependent opening (122). The PTP has two binding sites for divalent cations, a matrix site that promotes pore opening when occupied by Ca<sup>2+</sup> while all other tested cations (such as Sr<sup>2+</sup>, Mn<sup>2+</sup>, Ba<sup>2+</sup>) have an inhibitory effect, and an external site whose occupancy results in PTP inhibition even when occupied by Ca<sup>2+</sup> (127). Ca<sup>2+</sup>-induced PT is fully reversible by Ca<sup>2+</sup> chelation with EGTA (128–131). In saline media mitochondrial resealing is followed by repolarization, shrinkage and recovery of the initial volume provided that cyt *c* (which is released in the swelling process) is added back, indicating that no permanent damage to the IMM occurs as a consequence of the PT (131).

The PTP is a voltage-dependent channel, with high  $\Delta\psi_m$  favoring the closed conformation and depolarization leading to the open conformation (132). Hunter and Haworth have shown that

energization is not required for PT occurrence and may offer a protective mechanism against  $\text{Ca}^{2+}$ -induced transition. Addition of either carbonyl cyanide *p*-trifluoromethoxyphenylhydrazone (FCCP) or oligomycin plus antimycin induces a rapid PT to occur (112). Regulation of the PTP by  $\Delta\psi_m$  implies the existence of a voltage sensor, a device that can sense the change of  $\Delta\psi_m$  and transduce the information to the PTP, decoding it into a modulation of the open probability. Arginine residues frequently play a role in voltage sensing by ion channels. The voltage-activated ion channels such as  $\text{K}^+$ ,  $\text{Na}^+$  and  $\text{Ca}^{2+}$  channels possess modular voltage-sensing domains, a notable example being the highly charged S1-S4 domains that contain many critical arginine residues (133–135). Arginine residues play an important role in modulation of PTP opening as well, and this will be described in detail in Part 1.3.5.

The PT is inhibited by acidic matrix pH through protonation of histidyl residues, which can be prevented by carbethoxylation with diethyl pyrocarbonate (DPC) (136). Nicolli et al. found that the addition of DPC prior to mitochondrial depolarization can allow PTP opening by FCCP, which would otherwise be inhibited by matrix acidification (136). It is worth noting that the PT can also be influenced by pH indirectly through compounds whose accumulation in the matrix depends on its pH. For example, acidic pH facilitates  $\text{Pi}$  uptake, and the inhibitory effects of pH on the PTP may be masked by an increased rate of  $\text{Pi}$  uptake (137).

PTP-dependent  $\text{Ca}^{2+}$  efflux is increased by the oxidation of SH groups and is prevented by their reaction with N-Ethylmaleimide (NEM) (138,139). The depletion of glutathione (GSH), an important cellular antioxidant, prevents  $\text{H}_2\text{O}_2$ -induced mitochondrial  $\text{Ca}^{2+}$  release mediated by the PTP (140). PTP opening is also favored by oxidation of GSH, suggesting that the transition is influenced by the redox state of the GSH pool (141). The PT can also be modulated by oxidation of pyridine nucleotides through the so-called “P-site”, which was proposed to be in redox equilibrium with  $\text{NADH}/\text{NAD}^+$  and  $\text{NADPH}/\text{NADP}^+$ . Indeed, oxidation of mitochondrial pyridine nucleotides can sensitize PTP opening to  $\text{Ca}^{2+}$  under conditions where the GSH pool is maintained in the fully reduced state, suggesting that the PTP is mediated by oxidation at two separate sites: “S-site” and “P-site” (141). The oxidation of pyridine nucleotides and of SH groups are tightly linked, and oxidation of critical SH groups forming disulfide (S-S) bonds is the end result, which could directly induce an open conformation of the PTP. Oxidative stress may have additional effects, e.g., collapse of mitochondrial membrane potential through lipid peroxidation and induction of  $\text{H}^+$  and ion leaks (122). It is worth noting that the formation of S-S bonds is influenced by matrix pH, and that a lowering of matrix pH favors their formation due to a lowering of their  $\text{pK}_a$  values, which makes them more prone to interact with neighboring residues and to oxidation (142). NADH acts synergistically with ADP to inhibit the PT (77). ADP, ATP,  $\text{Mg}^{2+}$  alone or in combination show protective effect of  $\text{Ca}^{2+}$ -induced PT.

Fatty acids and lysophospholipids (LPLs) favor PTP opening, which may be a result of mitochondrial depolarization (143,144). Early hypotheses regarding the  $\text{Ca}^{2+}$ -induced PT suggested that its occurrence can be induced by perturbation of the phospholipid bilayer caused by  $\text{Ca}^{2+}$ -dependent phospholipase  $\text{A}_2$  (PLA $_2$ ), with accumulation of free fatty acids and LPLs (143,144). However, the discovery that the inhibitory effect of CsA on the PT is independent of the inhibition of PLA $_2$ , suggested that a proteinaceous pore is likely responsible for the PT occurrence (115–118). However, it should be noted that the inhibitory effect of CsA on the PT can be transient, while a combination with inhibition of PLA $_2$  leads to a long-lasting inhibition on the PT (145). It is worth mentioning that exogenous fatty acids cause mitochondrial swelling and uncoupling, which can be prevented by bovine serum albumin (BSA) via its ability to bind fatty acids (146). In summary, PTP open-closed transitions are highly regulated by multiple effectors at discrete sites, which are summarized Fig. 1.6. PTP modulation by CyPD will be covered in a specific paragraph.

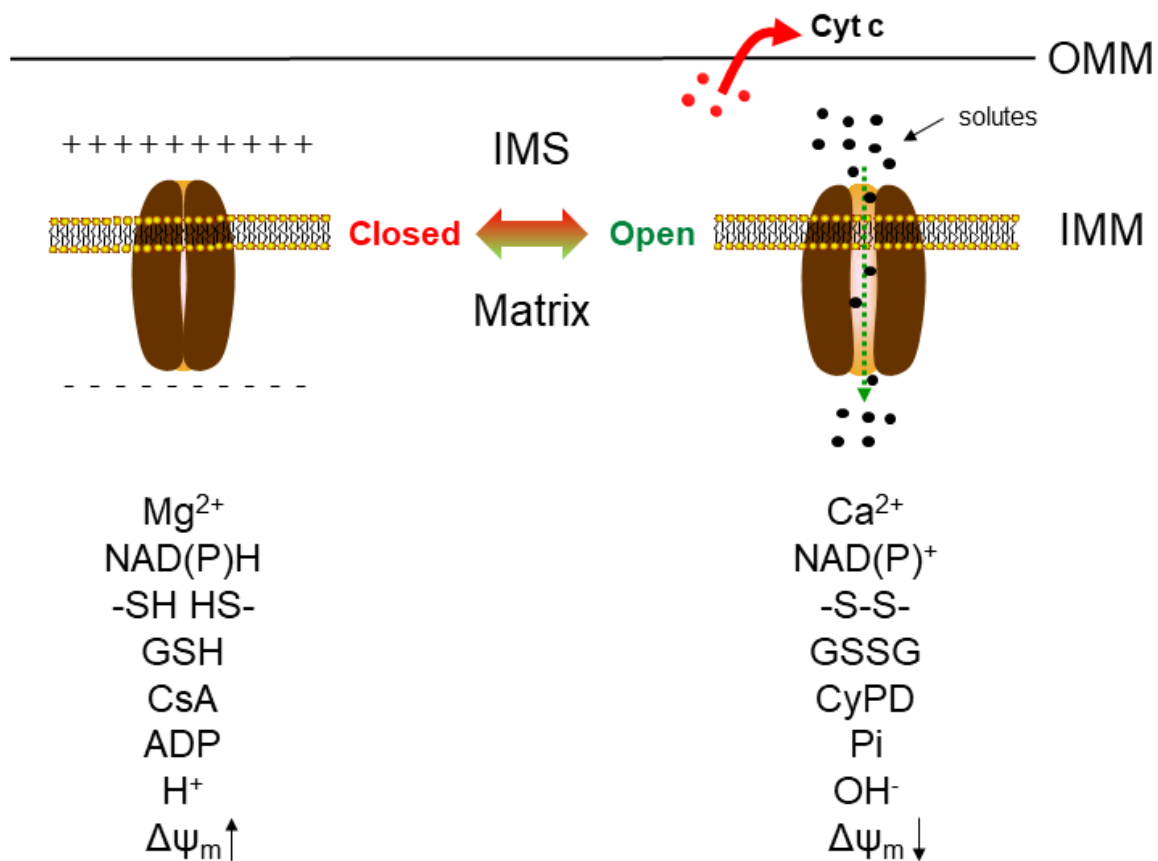


**Fig. 1.6. Regulators of the mitochondrial permeability transition pore.** *Left*, factors that prevent the occurrence of PT. *Right*, factors that favor the occurrence of PT. PTP opening can cause mitochondrial swelling, rupture of the outer membrane, release of pro-apoptotic proteins like cytochrome *c* leading to cell death. OMM: outer mitochondrial membrane; IMS: intermembrane space; IMM: inner mitochondrial membrane; Cyt *c*: cytochrome *c*; NADH: nicotinamide adenine dinucleotide; NAD $^{+}$ : oxidized nicotinamide adenine dinucleotide; -SH: thiol group; -S-S-: disulfide bond; GSH: glutathione; GSSG: glutathione disulfide; CsA: cyclosporin A; CyPD: cyclophilin D; ADP: adenosine diphosphate; Pi: phosphate;  $\text{H}^{+}$ : acidic pH;  $\text{OH}^{-}$ : alkaline pH;  $\Delta\psi_m$ : mitochondrial transmembrane potential.

## 1.2.2 Cyclophilin D and regulation of the PTP in different species

Cyclophilins (CyPs) are a family of ubiquitous proteins endowed with PPIase activity that has been highly conserved in evolution (147). CyPD, the unique mammalian mitochondrial matrix cyclophilin, is the mitochondrial receptor for CsA (148). Binding of CyPD to PTP sensitizes the pore to  $\text{Ca}^{2+}$ , while its detachment following binding to CsA suppresses pore opening (148–150). The genetic ablation of CyPD encoded by *Ppif* gene in mice demonstrated that CyPD acts as an activator of the pore but it is not a structural component. CyPD ablation desensitizes PTP opening to  $\text{Ca}^{2+}$  but PTP opening can still be triggered by higher  $\text{Ca}^{2+}$  loads (151–154).

Yeast mitochondria possess a matrix CyP (CPR3) that catalyzes CsA-sensitive protein folding (155,156). yPTP is insensitive to CsA (157) and CPR3 deletion does not desensitize the yPTP to  $\text{Ca}^{2+}$ , suggesting that CPR3 does not bind to the pore or that its binding does not affect the pore (158). As mentioned above, a recent publication disputes this conclusion because in agar-embedded yeast mitochondria and cells, yPTP appears to be modulated by CPR3 and sensitive to CsA (159). Thus, while differences may certainly exist, some of these may depend on specific experimental conditions.

The presence of Pi is necessary for mitochondria to take up substantial amounts of  $\text{Ca}^{2+}$ , because the transport of Pi prevents the buildup of a relevant  $\text{H}^+$  chemical gradient, thus allowing regeneration of the membrane potential, and of a  $\text{Ca}^{2+}$  concentration gradient, which would prevent further  $\text{Ca}^{2+}$  uptake (160). This makes it difficult to understand the inducing effects of Pi, because by forming  $\text{Ca}^{2+}$ -Pi complexes (which decrease matrix free  $\text{Ca}^{2+}$ ) in principle should decrease rather than increase the probability of pore opening (161). Pi appears to act as an inducer of the mammalian PTP because it favors the interaction of CyPD with the pore, possibly at the oligomycin sensitivity conferral protein (OSCP) of F-ATP synthase (162,163). Indeed, Pi desensitizes the mammalian PTP to  $\text{Ca}^{2+}$  in mitochondria devoid of CyPD or treated with CsA, suggesting that Pi as such would indeed act as a desensitizer by decreasing matrix free  $\text{Ca}^{2+}$  (164). Interestingly, Pi desensitizes the PTP to  $\text{Ca}^{2+}$  in yeast (157,158) and in *Drosophila melanogaster* mitochondria (which lack mitochondrial cyclophilin) (165) and where the PTP is insensitive to CsA. Table 1 summarizes the properties of PTP in *S. cerevisiae*, *D. melanogaster* and mammals.

Species	Conductance (pS)	Matrix Ca <sup>2+</sup>	Matrix Mg <sup>2+</sup> /ADP	Pi	CsA	Matrix CyP
<i>S. cerevisiae</i>	300	activates	inhibits	inhibits	no effect	yes
<i>D. melanogaster</i>	53	activates	inhibits	inhibits	no effect	no
mammals	500	activates	inhibits	activates	inhibits	yes

**Table 1. Summary of the PTP properties of *S. cerevisiae*, *D. melanogaster* and mammals.**

### 1.2.3 The role of PTP in pathophysiology

Mitochondria play a critical role in regulation of cellular Ca<sup>2+</sup> homeostasis (125,126). The transient or flickering opening of PTP may provide a pathway for fast Ca<sup>2+</sup> release from mitochondria preventing matrix Ca<sup>2+</sup> overload, thus participating in physiological Ca<sup>2+</sup> homeostasis (96,125,126,166). Long-lasting openings of the PTP, which cause mitochondrial swelling, are followed by OMM rupture with release of cyt *c* from the IMS, an event that in mammalian cells can trigger apoptosis (125,126). Whether the pore plays a similar role in yeast is still a matter of debate. Yeast does not possess a mitochondrial Ca<sup>2+</sup> uniporter to mediate rapid Ca<sup>2+</sup> uptake, nor it forms the apoptosome complex required for the activation of effector caspases. Yet yeast mitochondria can undergo membrane permeabilization in response to Ca<sup>2+</sup>, leading to the release of cyt *c* which certainly causes decreased respiration and ATP production. These events, together with the activation of the yeast metacaspase Ycalp, are proximal events in yeast programmed cell death (167). Thus, as for mammals, PTP opening might represent an important cell death pathway also for yeast. An interesting set of observation concerns *D. melanogaster*, which does possess a RR-sensitive MCU and can release Ca<sup>2+</sup> following a train of Ca<sup>2+</sup> pulses, which is reminiscent of the consequences of PTP opening (165). At variance from mammals, however, during Ca<sup>2+</sup> release *Drosophila* mitochondria do not undergo swelling and cyt *c* release. Consistent with its proposed role in PTP formation, the *Drosophila* channel formed by F-ATP synthase display a current of a mere 53 pS (168). These data suggested that due to its small size the PTP of *Drosophila* may participate in Ca<sup>2+</sup> homeostasis but not in cell death, consistent with the fact that *Drosophila* apoptosis only involves cytoplasmic factors (161).

Transient PTP opening (tPTP) leads to mitochondrial uncoupling and triggers a burst of superoxide anion. The ROS generated at ETC which is promoted by tPTP may be followed by a process of ROS-induced ROS release (170). “Superoxide flashes”, an event that individual mitochondria can undergo with spontaneous burst of superoxide generation, have been observed in mitochondria

expressing a circularly permuted yellow fluorescent protein (cpYFP) (171). Flashes can be triggered by tPTP and be terminated by matrix acidification (172) and are regulated by CyPD (173). Whether the flashes are partially or totally caused by the alkalization of the mitochondrial matrix is under debate (171,174,175). The cpYFP was shown to be highly responsive to pH but not to superoxide, which led some Authors to question the existence of “superoxide flashes” (174,175). It should be mentioned that superoxide elevation results in the loss of NAD(P)H/GSH that may, in turn, promote the generation of superoxide and/or enhance the half-life of superoxide, followed by the pH change and collapse of  $\Delta\psi_m$ . Superoxide flashes contribute to increased oxidative stress, suggesting that they may serve as a quantitative biomarker for oxidative stress-related diseases (171). Increased cellular oxidative stress coincides with elevation of matrix  $Ca^{2+}$  and sensitization of PTP opening, and may be followed by release of cyt *c* from IMS and activation of the intrinsic pathway to apoptosis. That oxidative stress regulates PTP opening and cell death has been suggested to be conserved across species (125,167).

Mitochondrial PT has been recognized to play an important role in diseases, and the encouraging finding that CsA inhibits PTP opening led to an effort to target the PTP for therapeutic intervention. Ablation of CyPD or treatment with CsA each confers remarkable protection against ischemia-reperfusion injury of the heart (176) and brain (154), implicating PTP as a target for cardioprotection and neurodegenerative disorder treatment. Collagen VI diseases appear to be the best documented muscular dystrophy involving CyPD. The cyclophilin inhibitor alisporivir is a derivative of CsA that does not inhibit calcineurin. Alisporivir can restore respiratory function and improve muscle ultrastructure in a zebrafish model of Duchenne muscular dystrophy (177). In some cancer cell lines, extracellular signal regulated kinase (ERK) is active and desensitizes PTP through its inhibition of GSK3. The inhibition of PTP can be abolished by activation of GSK3-dependent phosphorylation of CyPD via inhibition of ERK. The enhancement of PTP opening leads to cancer cell apoptosis (125). The regulators of PTP could be therefore be of help in the treatment of various diseases.

#### **1.2.4 Molecular structure. Early hypotheses**

Over the last few decades, a series of biochemical studies lead to the hypothesis that the PTP is a multiprotein complex likely spanning the inner and outer mitochondrial membranes, composed by ANT, CyPD, VDAC, TSPO, PiC and Bcl-2 family, as shown in Fig. 1.7.

The adenine nucleotide translocase (ANT) is a 32 kDa protein located in the IMM (178). ANT acts as a transporter responsible for exchange of cytosolic ADP into matrix and mitochondrial ATP across IMM. Carboxyatractyloside (CAT) and bongkreikic acid (BKA) are the two classical inhibitors of ANT. One molecule of CAT or BKA reacts with ANT resulting a complex with a MW

of 60 kDa, suggesting that ANT protein exists as a dimer (179,180). The idea that ANT is a pore-forming component of the PTP originates from the findings that  $\text{Ca}^{2+}$ -induced PT is activated and inhibited by the ANT inhibitors atractyloside (ATR) and BKA, respectively (181). Further investigations showed that CAT stimulates PTP opening through promotion of its 'c' conformation and BKA inhibits the channel activity through stabilization its 'm' conformation (114,179). ANT reconstituted alone or in combination with CyPD and VDAC into proteoliposomes displays channel activities which resemble the properties of PTP (182–184). CyPD can bind to ANT and VDAC, which led to the hypothesis that the inhibitory effect of CsA on the PT is caused by its binding to CyPD, which thus prevents the interaction between CyPD and ANT (118,182,185). The Bax/Bcl-2 family, apoptosis-regulatory proteins, can interact with ANT as well (181,185). However, mitochondria from mouse liver with the genetic inactivation of ANT1 and ANT2 isoforms (*Ant1* and *Ant2* genes) can still undergo PT although more  $\text{Ca}^{2+}$  is required, suggesting that ANT is a non-essential component of PTP although it contributes to its regulation (186).

VDAC is the putative component of PTP in OMM, consistent with the observation that purified VDAC displays similar electrophysiological properties to those of PTP and functions as a nonselective pore to ions (187). This hypothesis was supported by studies in which extracts of VDAC, ANT and CyPD reconstituted into proteoliposomes displayed CsA-sensitive permeabilization to solutes (182). However, the involvement of VDAC in the PTP formation was similarly ruled out based on genetic inactivation studies. Mitochondria from *Vdac1*-null mice can still exhibit  $\text{Ca}^{2+}$ - and oxidative stress- induced PT indistinguishable from WT, and VDAC are dispensable for Bcl-2 family member-driven cell death (188,189). Also the yeast PTP channel is still present in strains devoid of both of VDAC and ANT, and yPTP is unaffected by several inducers of the mammalian PTP like carboxyatractylate (inhibitor of the ANT), ligands of TSPO, and prooxidants (190,191).

The IMM PiC is the primary transporter for Pi. In energized mitochondria Pi is accumulated through the PiC, which therefore plays an essential role in mitochondrial OXPHOS (192). Pi is known to favor PTP opening (116,129,193), which would be consistent with the finding that PiC overexpression promotes cell apoptosis. PiC was further proposed to be a component of the PTP because its interaction with CyPD facilitates the PT to occur (194). However, the subsequent observations that PiC knockdown inhibits neither the mitochondrial  $\text{Ca}^{2+}$  accumulation nor the  $\text{Ca}^{2+}$ -induced PT, suggested that PiC is not a critical component of PTP (195,196). Nevertheless, deletion of the gene encoding PiC protein in heart blunts the  $\text{Ca}^{2+}$ -stimulated PT and leads to a greater  $\text{Ca}^{2+}$  retention capacity (CRC). This desensitization of PTP opening attenuates cardiac ischemic-reperfusion injury (197). These observations suggest that PiC is not directly involved in PTP formation but rather than it can affect the pore indirectly by modifying matrix Pi levels and pH.



Patch clamp experiments in liposomes containing yeast PiC did detect a conductance of 25 pS, which is way too small for a direct correlation with PTP/MMC (81).

TSPO has been suggested to interact with VDAC and ANT (198) and to play a role in regulation of PTP opening (199,200). However, mitochondria from mice in which TSPO is conditionally eliminated display indistinguishable PTP properties from the WT control, suggesting that this protein is not involved in PTP formation (201).

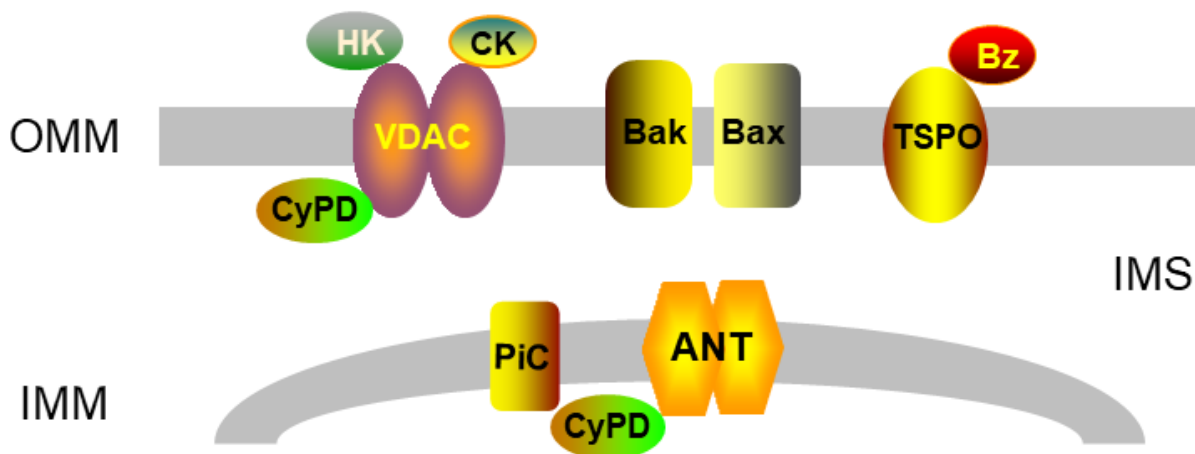


**Fig. 1.7. Putative components of the PTP.** The original paradigm of the PTP includes VDAC, ANT and CyPD as main components. Genetic studies revealed that VDAC, ANT and PiC are dispensable for PTP formation but are rather involved in its regulation. CyPD acts as a regulator through its binding to PTP in the mitochondrial matrix. TSPO plays a regulatory role as well. OMM: outer mitochondrial membrane; IMM: inner mitochondrial membrane; IMS: intermembrane space; VDAC: voltage-dependent anion channel; HK: hexokinase; CK: creatine kinase; CyPD: cyclophilin D; ANT: adenine nucleotide translocase; Bax: bcl-2-associated X protein; Bak: bcl-2 homologous antagonist killer; PiC: phosphate carrier; TSPO: translocator protein; Bz: benzodiazepine.

Bax and Bak, the pro-apoptotic Bcl-2 family members, oligomerize to permeabilize the OMM, leading to the release of cyt *c* (202). In addition to their role in cell apoptosis, they have been implicated in the formation and regulation of the PTP through their ability to increase the permeability of OMM allowing PTP opening-induced mitochondrial swelling and organelle rupture (203). Bax/Bak-null mitochondria are resistant to PTP opening and reconstitution of Bax/Bak-deficient cells or mitochondria with WT Bax or an oligomerization-impaired Bax restores both PTP opening and the permeability of OMM, which can be prevented by CsA or Ca<sup>2+</sup> chelation (203–205). Collectively, genetic studies provide no evidence for Bax/Bak in the direct regulation or formation of the PTP, while Bax and Bak may be important for PTP to progress to organelle rupture at the OMM when the PTP is activated by Ca<sup>2+</sup> or oxidative stress.

CI has been suggested to be part of the PTP, or to play a role in regulating the pore by Fontaine et al. in 1998 (206). PTP opening is facilitated by e<sup>-</sup> flow through CI (but not through CII, CIII or CIV) and can be inhibited by ubiquinone 0 (Ub<sub>0</sub>) (206,207) and by rotenone (208). Rotenone displays

stronger inhibitory effect on PTP opening in mitochondria from tissues that express lower levels of CyPD, while inhibition is negligible in organs and cells with high expression levels of CyPD. These findings suggested that inhibition of CI by rotenone modulates the PTP through a site masked by CyPD (209). Oxidation of succinate can strongly support mitochondrial ROS generation due to RET at CI. The modulatory effect of PTP by CI could be due, in part at least, to its contribution to oxidative stress by producing ROS (210).

It should be mentioned that He and Lemasters have proposed a different model for the PTP, which could account for some intriguing aspects of pore modulation. The model posits that the PTP can originate from membrane proteins that underwent misfolding after oxidative (or other forms of) stress (211), and is similar to the idea that the PT is due to general oxidative damage to membrane proteins rather than a consequence of the opening of a channel (212). Formation of conductive pathways through the misfolded protein clusters would normally be prevented by proteins with chaperone activity (like CyPD). According to this hypothesis opening of “unregulated” pores would occur when the number of protein clusters exceeds chaperones, and this feature would explain occurrence of pores that are not sensitive to CsA (211). The model has the merit to account for the existence of CsA-insensitive pores and for the lack of selectivity, but it is hard to reconcile with the fine regulation of channel activity by  $\text{Ca}^{2+}$ ,  $\text{Mg}^{2+}$ , adenine nucleotides as well as for channel block by mildly acidic pH (125).

## 1.3 The mitochondrial ATP synthase

The mitochondrial ATP synthase, also termed  $\text{F}_1\text{F}_0$ -ATP synthase (F-type ATPase, F-ATP synthase) or complex V, is responsible for the synthesis of ATP driven by the electrochemical  $\text{H}^+$  gradient across the IMM, as originally proposed by Peter Mitchell in 1961 in the chemiosmotic hypothesis, which is a landmark in the field of bioenergetics (213).

### 1.3.1 Structure and function of F-ATP synthase

The mitochondrial ATP synthase is a rotary motor coupled to the “proton motive force” existing across the IMM (pmf or  $\Delta p$ ), whose molecular architecture is well conserved from bacteria and chloroplasts to mammals (213). The ATP synthase is a multisubunit complex with a MW of about 600 kDa, composed by a soluble  $\text{F}_1$  sector that functions as the catalytic core and a membrane-embedded  $\text{F}_0$  sector linked to the  $\text{F}_1$  sector by central and peripheral stalks (125,213).

The  $\text{F}_1$  sector consists of the five subunits denoted  $\alpha$ ,  $\beta$ ,  $\gamma$ ,  $\delta$  and  $\epsilon$  with a 3:3:1:1:1 stoichiometry (214). The atomic structure of  $\text{F}_1$ -ATPase was determined by X-ray crystallography in 1994. Subunits  $\alpha$  and  $\beta$  are organized into an  $\alpha_3\beta_3$  hexamer, and subunit  $\gamma$  is located inside the  $\alpha_3\beta_3$

complex (215). The structure of the rotary central stalk consisting of subunits  $\gamma$ ,  $\delta$  and  $\epsilon$  was revealed in 2000. Subunit  $\gamma$  interacts with subunits  $\delta$  and  $\epsilon$  at the foot of the central stalk contacting the c-ring, which are all key element in coupling pmf to the the  $\alpha_3\beta_3$  complex (216). Definition of the structure of the membrane-embedded domain had more technical difficulties than the soluble domain. In 1999, the crystal structure of c<sub>10</sub>-ring from *Saccharomyces cerevisiae* together with the F<sub>1</sub> domain was obtained. The molecular architecture reveals that the c oligomer is tightly attached to subunits  $\gamma$  and  $\delta$ , and acts as part of the rotary motor. The c<sub>10</sub>-ring faces a single subunit a through which the H<sup>+</sup> flow, thus generating rotation of the enzyme at a rate of about 150 revolutions per second. Each full rotation produces 3 molecules of ATP. The number of c subunits dictates the number of H<sup>+</sup> required to make one molecule of ATP, which corresponds to a 120° rotation of subunit  $\gamma$  (217,218). The size of the c-ring differs between species. A c<sub>10</sub>-c<sub>15</sub> ring has been determined in fungi, eubacteria, and plant chloroplasts. Mammalian F-ATP synthase possesses a c<sub>8</sub>-ring, implying that the bioenergetic cost to make each ATP molecule is 2.7 H<sup>+</sup> (218). A conserved arginine in subunit a at a position equivalent to 159 in mammals (the presequence amino acids are included) plays an essential role in the H<sup>+</sup> translocation-coupled c-ring rotation at the F<sub>O</sub>-a/c-ring interface by preventing a futile H<sup>+</sup> shortcut (219). In *S. cerevisiae*, glutamate 59 in each c subunit interacts with the conserved arginine in subunit a (arginine 186 in *S. cerevisiae* including the ten presequence amino acids) coordinating its protonation. This conserved arginine acts like a pendulum: when deprotonated, glutamate 59 is paired with arginine 186, but it is re-protonated when the arginine switches to the either side followed by return to subunit a/c-ring interface and release of H<sup>+</sup>, which is coupled to the rotation of c-ring (220).

The F<sub>1</sub> sector is also linked to the F<sub>O</sub> domain through the peripheral stalk that acts as a stator. The stator of the mammalian enzyme is a subcomplex composed by single copies of subunits b, d, coupling factor 6 (F<sub>6</sub>) and OSCP (221). The subunit composition of the peripheral stalk in bacteria and chloroplasts substantially differs from those in eukaryote and the peripheral stalk is composed by subunit  $\delta$ , which is homologous with OSCP, and either two identical copies of subunit b in bacteria or single copies of subunit b and b' in chloroplasts. In bovine mitochondria, N-terminus of OSCP binds to the uppermost region of the stator *via* the N-termini of the three subunits  $\alpha$ , while the C-terminus of OSCP interacts with the C-terminus of subunit b. The  $\alpha$ -helix of subunit b, stiffened by subunits F<sub>6</sub> and d, protrudes to the IMM. Each of the six additional proteins in mammalian F<sub>O</sub> domain (subunits A6L (ATP8), diabetes-associated protein in insulin-sensitive tissues (DAPIT), 6.8 kDa proteolipid (6.8PL), e, g, f) possesses a single predicted transmembrane  $\alpha$ -helix (221,222). A low-resolution structure of bovine F-ATP synthase by cryo-electron microscopy (EM) suggests that c<sub>8</sub>-ring contacts subunit a in a small region, and the TMD of subunit b does not interact with c<sub>8</sub>-ring while subunits e and g extend from the distal of subunit a to c<sub>8</sub>-ring

(223). ATP8 and ATP6 are mitochondrial DNA (mtDNA) encoding mammalian A6L and subunit a, respectively. Cross-linking detection reveals that C-terminus of ATP8, as a part of the stator, interacts with the peripheral stalk in the matrix. It is predicted that the N-termini of other additional subunits are in the same side likely in the matrix (224). The molecular structure of F<sub>1</sub> domain, the peripheral stalk and c<sub>8</sub>-ring have been determined in bovine mitochondrial enzyme, but that of the residual F<sub>0</sub> domain remains to be established. It is assumed that the structure of F<sub>0</sub> region of the mammalian enzyme is similar to yeast species.

The yeast mitochondrial ATP synthase consists of 13 different subunits ( $\alpha$ ,  $\beta$ ,  $\gamma$ ,  $\delta$ ,  $\epsilon$ , a, c, OSCP, b, d, f, h and 8) necessary for the assembly and catalysis of the complex, which is between the number of *E. coli* enzyme (8 subunits) and bovine enzyme (16 subunits). The additional 5 subunits that are not essential for the activity of yeast enzyme, so called supernumerary subunits, are subunits e, g, i/j, k, l. But yeast subunit i encoded by ATP18 is involved in the activity of F-ATP synthase and its ablation results in a decline of OXPHOS (225). It has been recently proposed that yeast subunit j and mammalian 6.8PL, as well as yeast subunit k and mammalian DAPIT are functional orthologs (226).

In yeast, differently from mammals, subunits a, c and 8 are encoded by mtDNA ATP6, ATP9 and ATP8, respectively (225,227,228). These non-essential components (subunits e, g, k, i), and subunits a, h, b have been suggested to mediate the dimerization of the enzyme, which will be described in Part 1.3.3. The subunit compositions of mammalian and yeast mitochondrial ATP synthase are as shown in Table 2.

Structure of a complete F-ATP synthase dimer from yeast *Yarrowia lipolytica* reveals that the horizontal helices of subunit a surround c-ring. Subunit e and g do not directly contact two monomers to form dimers but they induce an IMM curvature of  $\sim 100^\circ$  resulting in mitochondrial cristae. The C-terminus of subunit i/j, which has been previously mistaken for subunit f, contains conserved charged residues that are directly involved in the dimer formation (229,230). Recently, Rubinstein group has determined the complete atomic structure of dimeric F<sub>0</sub> domain from *S. cerevisiae* by cryo-EM (230). The transmembrane  $\alpha$ -helix of subunit b contacts with subunits e and g. The N-terminus of subunit f binds to the foot of the peripheral stalk. The N-terminal  $\alpha$ -helix of subunit 8 embedded in the IMM interacts with subunit a. The TMD of subunits b together with subunits 8 and f contributes to the base of the lateral stalk, and subunit d acts as a clamp. Thus subunits 8 and f are categorized as the compositions of the lateral stalk. Two strands of subunit a from each monomer form a dimer interface. The subunit i/j and subunit a directly contact between two monomers and forms dimers. The N-terminal  $\alpha$ -helix of subunit e begins within the IMM and extends into the IMS interacting with subunit k. Subunit g contains two N-terminal  $\alpha$ -helices, one of

which interacts with subunit e and is exposed to the matrix (230). Fig. 1.8 reports the history of the F-ATP synthase structures.

High-resolution crystallographic studies have identified 4 inhibitory sites that inhibit bovine mitochondrial ATP synthase: the aurovertin B-binding site, the efrapeptin-binding site, the catalytic site and the site to which the inhibitor protein IF<sub>1</sub> binds (231). IF<sub>1</sub> is a natural regulatory mitochondria protein encoded by ATP5IF1 gene, which displays inhibitory effect on F-ATP synthase. IF<sub>1</sub> does not disturb the coupling activity and ATP synthesis of the enzyme, but it prevents ATP hydrolysis (232,233). At a pH below 6.7, IF<sub>1</sub> is dimeric and binds to F<sub>1</sub> catalytic core with a stoichiometry of 1:1 thus prevents the enzyme from hydrolyzing ATP. At pH 8.0, the dimeric IF<sub>1</sub> associated with each other and form tetramer, and that the oligomeric states mask its inhibitory region leads to its inactivity (233–235). In chloroplasts and bacteria, there are no homologues of IF<sub>1</sub> in the mitochondria, and they develop another mechanism to inhibit the activity of F-ATP synthase (233,235). IF<sub>1</sub> lacks the C-terminal dimerization region in yeast, and it lacks most of the dimerization region in bovine. The structure of the monomeric IF<sub>1</sub> reveals that it binds to a  $\alpha_{DP}$ - $\beta_{DP}$  catalytic interface and contacts subunit  $\gamma$  (216,236,237). The bound IF<sub>1</sub> will be released when the pmf is present and the direction of rotor reverses, followed by the recovery of ATP synthesis, which indicates that IF<sub>1</sub> plays a role in preventing futile ATP hydrolysis (213). A well conserved regulatory mechanism of the enzyme ATPase activity is “ADP inhibition”. In de-energized mitochondria, F-ATP synthase is inactivated when MgADP is bound to the catalytic core, while ADP will be released after the mitochondria are energized followed by increased enzyme activity. In bacteria and chloroplasts subunit  $\epsilon$  is involved in the modulation of this process: the conformational change of subunit  $\epsilon$  from the contracted to the extended inhibits and prevents futile ATP hydrolysis, which is proposed to be determined by the direction of subunit  $\gamma$  rotation (238). Knock out (KO) of subunit  $\epsilon$  in mammals leads to a decreased activity and content of the enzyme, paralleled by a decreased content of subunits  $\alpha$ ,  $\beta$ , a and d but accumulation of subunit c. The absence of subunit  $\epsilon$  results in an oligomycin-insensitive enzyme. These findings suggest that subunit  $\epsilon$  is essential for F<sub>1</sub> stability and proton coupling. An understanding of these regulators of the enzyme may provide therapeutic rational for F-ATP synthase linked pathophysiological disorder (239).

<b>Mammal (subunit/gene)</b>	<b>Yeast (subunit/gene)</b>	<b>Genome</b>	<b>Importance</b>
<i><b>α / Atp5a1</b></i>	<i><b>α / ATP1</b></i>	Nuclear	Essential
<i><b>β / Atp5b</b></i>	<i><b>β / ATP2</b></i>	Nuclear	Essential
<i><b>γ / Atp5c1</b></i>	<i><b>γ / ATP3</b></i>	Nuclear	Essential
<i><b>δ / Atp5d</b></i>	<i><b>δ / ATP16</b></i>	Nuclear	Essential
<i><b>ε / Atp5e</b></i>	<i><b>ε / ATP15</b></i>	Nuclear	Important
<i><b>a / Mtatp6</b></i>	<i><b>a / ATP6</b></i>	Mt.	Essential
<i><b>C1 / Atp5g1</b></i>	<i><b>c / ATP9</b></i>	Nuclear (mammal); Mt. (yeast)	Essential
<i><b>C2 / Atp5g2</b></i>			
<i><b>C3 / Atp5g3</b></i>			
<i><b>OSCP / Atp5o</b></i>	<i><b>OSCP / ATP5</b></i>	Nuclear	Essential
<i><b>b / Atp5f1</b></i>	<i><b>b / ATP4</b></i>	Nuclear	Essential
<i><b>d / Atp5h</b></i>	<i><b>d / ATP7</b></i>	Nuclear	Essential
<i><b>F<sub>6</sub> / Atp5j</b></i>	<i><b>h / ATP14</b></i>	Nuclear	Essential
<i><b>e / Atp5i</b></i>	<i><b>e / TIM11</b></i>	Nuclear	Dispensable
<i><b>f / Atp5j2</b></i>	<i><b>f / ATP17</b></i>	Nuclear	Essential
<i><b>g / Atp5l</b></i>	<i><b>g / ATP20</b></i>	Nuclear	Dispensable
<i><b>A6L / Mtatp8</b></i>	<i><b>8 / ATP8</b></i>	Mt.	Essential
<i><b>IF<sub>1</sub> / Atp5if1</b></i>	<i><b>IF<sub>1</sub> / Inh1p</b></i>	Nuclear	Dispensable
<i><b>DAPIT / Usmg5</b></i>		Nuclear	Important
<i><b>6.8PL / Mp68</b></i>		Nuclear	Important
	<i><b>j (i) / ATP18</b></i>	Nuclear	Essential
	<i><b>k / ATP19</b></i>	Nuclear	Dispensable
	<i><b>l</b></i>	Nuclear	Unkown

**Table 2. Subunit compositions of mammalian and yeast mitochondrial ATP synthase.** Italics words indicate the corresponding encoding genes. “Genome” indicates gene localization (into nuclear or mitochondrial DNA). “Importance” indicates whether the corresponding protein is essential or dispensable for the activity of F-ATP synthase.

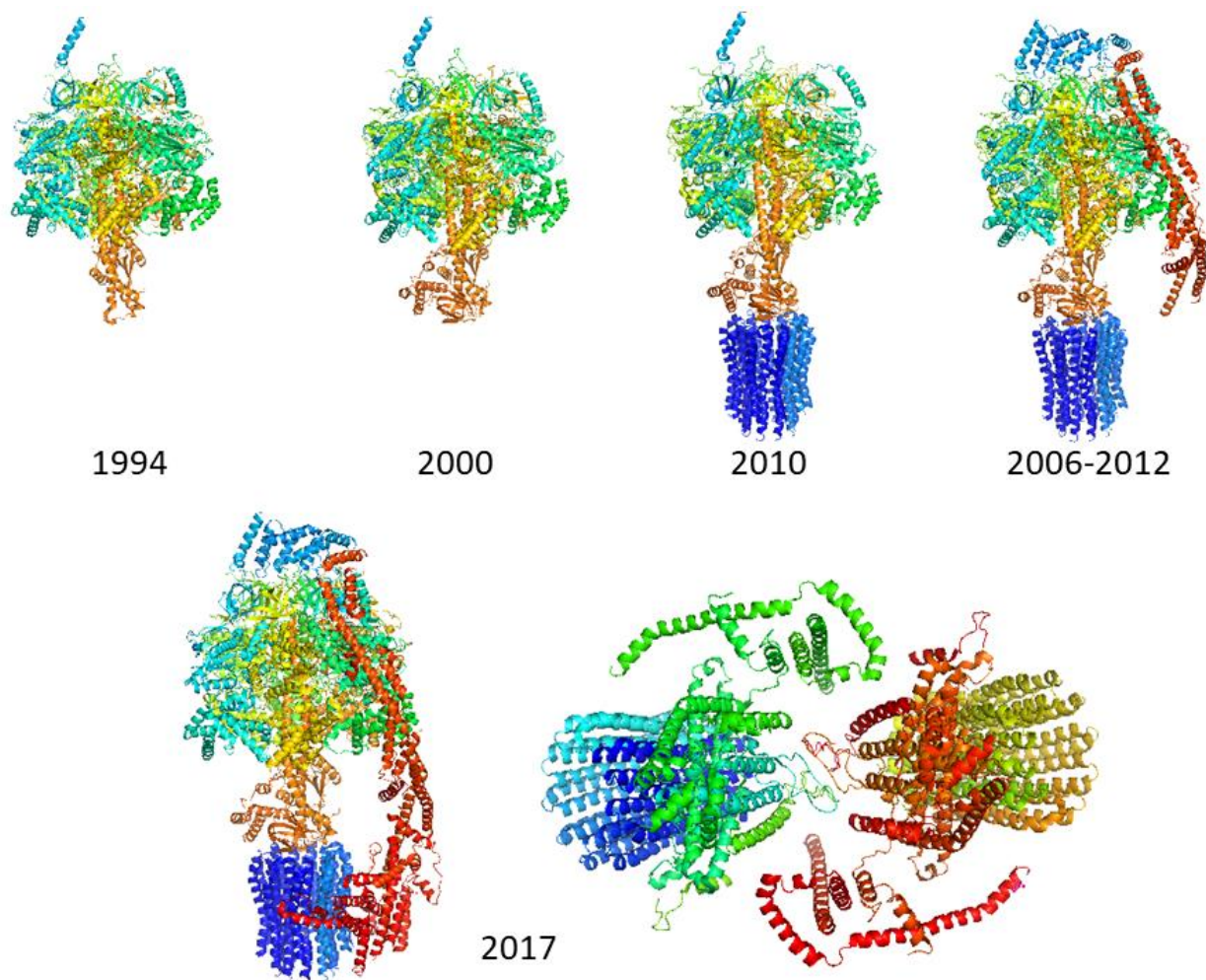


**Fig. 1.8. Timeline for the characterization of the molecular structure of F-ATP synthase.** In 1994, the first crystal structure of  $\alpha_3\beta_3$  complex and incomplete subunit  $\gamma$  was determined by X-ray crystallography in bovine heart mitochondria (215). In 2000, the structure of F<sub>1</sub> sector was completed in bovine F-ATP synthase (217,240) and the structure of subunits  $\delta$  and  $\epsilon$  and their interaction with missing part of subunit  $\gamma$  were added. In 2006, the stator, also called peripheral stalk, was revealed in bovine mitochondria (221,222). In 2010, the structure of the F<sub>1</sub>-c8-ring complex was determined in bovine F-ATP synthase by cryo-EM (218). In 2012, the structure of membrane extrinsic part of the stator and its association with F<sub>1</sub> sector were determined (223). By then, the structure of the membrane extrinsic section of the bovine enzyme was complete by cryo-EM. In 2017, the atomic structure of dimeric F<sub>O</sub> domain of yeast enzyme from *S. cerevisiae* strain was determined by cryo-EM (230). All the structure shown were modified from 3D structure (PDB: 6B2Z).

### 1.3.2 Assembly of F-ATP synthase

Human mitochondrial ATP synthase is a complex composed by 29 proteins (226). The assembly of the enzyme is a complex process, which has been recently identified by CRISPR-Cas9 based disruption of individual genes in human cell lines (226,241,242). As already mentioned, ATP6 and ATP8 are mitochondrially-encoded, and the other subunits are nuclear-encoded and imported into the matrix. The membrane extrinsic part likely forms independently of membrane-embedded domain. The assembly of F<sub>1</sub>-c<sub>8</sub> subcomplex is a key intermediate, which first binds to the lateral stalk associated with the membrane subunits e, g and f, another separate assembly intermediate

(226,241–243). Subsequently, ATP6 and ATP8 are integrated into this intermediate and stabilized by 6.8PL (226,241,242). Indeed, in human  $\rho^0$  cells lacking mitochondrial genes ATP6 and ATP8, F<sub>1</sub>-c<sub>8</sub> subcomplex is stably expressed, and an almost full assembly of F-ATP synthase is identified, suggesting that the insertion of subunits a and A6L is the last step to complete the enzyme assembly (244). Tmem70 is a membrane protein that mediates the enzyme assembly. The absence of Tmem70 results in the accumulation of F<sub>1</sub> sector without any F<sub>O</sub> subunits associated, indicating that Tmem70 factor promotes the interaction of F<sub>1</sub> and c-ring. The binding with Tmem70 stabilizes the F<sub>1</sub> catalytic core favoring formation of a F<sub>1</sub>-c<sub>8</sub> subcomplex (245). DAPIT is the most peripheral subunit, and is easily be removed from the enzyme under mild detergent treatment. DAPIT, a homologue of yeast subunit k, seems to play a role in the oligomerization of the enzyme and in mitochondrial cristae formation (226).

The assembly pathway of yeast F-ATP synthase has been extensively studied and appears to be a similar process as in human mitochondria, but some mechanisms differ. Yeast subunit a is synthesized as a precursor protein and initially interacts with the chaperone ATP10 followed by the binding with the peptidase ATP23 (246). The inner membrane assembly complex (INAC) has been found to be required for the maturation of subunit a by ATP23, and is also essential for liaising the subunit a with c-oligomer (247). Yeast subunit a and ATP8, together with ATP23, ATP10 and INAC, first bind to the lateral stalk or the F<sub>1</sub>-lateral stalk complex, and then associate with c<sub>10</sub>-ring (248). In F<sub>1</sub> sector, binding of subunits  $\alpha$  and  $\beta$  to ATP11 and ATP12 prevents their aggregation that otherwise blocks the enzyme formation (249). The association of  $\alpha_3\beta_3$  complex with the central stalk results in the release of ATP11 and ATP12 (250). The membrane-embedded supernumerary subunits i/j, k, e, f, g are incorporated into the enzyme at the last to promote the dimerization (251) (Fig. 1.9).



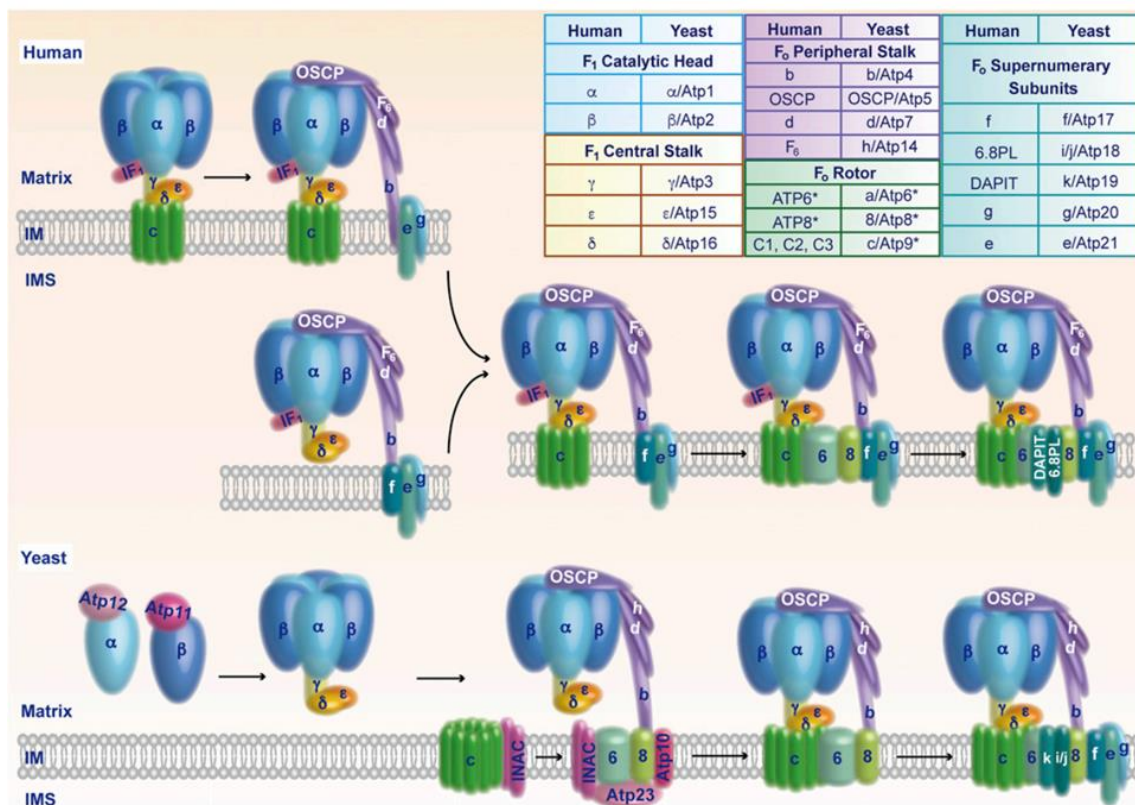


**Fig. 1.9. Assembly pathways of human and yeast F-ATP synthase.** *Upper*, assembly of human F-ATP synthase. *Lower*, assembly of yeast F-ATP synthase. *Inset*, subunit compositions of human and yeast F-ATP synthase. \*, proteins encoded by mtDNA. Figure is from Ref. (251).

### 1.3.3 Dimerization of F-ATP synthase and subunits e and g

#### 1.3.3.1 Dimerization of F-ATP synthase

Cryoelectron tomograms of the IMM have consistently revealed that F-ATP synthase is arranged in V-shaped dimers, which form long rows of oligomers located along the highly curved cristae edges, an organization which is highly conserved across species except in prokaryotes and chloroplasts (252). Dimers interact within the IMM through the F<sub>o</sub> subunits with the peripheral stalks turned away from each other, as shown in Fig. 1.10. Pioneering studies in yeast have unquestionably linked the dimeric state of the enzyme to the proper cristae formation (220–229). Dimer ribbons of the enzyme thus contribute to mitochondrial performance (229–232). Yet it has been demonstrated that the F<sub>o</sub> region of monomers is sufficient to induce curvature of the lipid bilayer (223,266). A quantitative molecular-simulation analysis suggested that this membrane deformation, which is an unusual membrane topology, drives self-association of the dimers into dimer rows to minimize the overall elastic strain of the membrane. The process would be due not due to direct protein-protein interactions or a specific lipid composition of the membrane (252).

Numerous biochemical and genetic studies have established that in yeast subunits a, b, h, and i/j, as well as the dimer-specific subunits e, g and k are involved in dimerization of the enzyme (267). In particular, subunits e and g have been extensively studied. These subunits are called dimer-specific subunits, as well as supernumerary subunits. Indeed, they are exclusively associated to F-ATP synthase dimers and their ablation leads to disappearance of the dimers and formation of a onion-like ultrastructure of mitochondria (221,229–232). They are not essential for cellular growth on non-fermentable medium (262,263) and in the null mutant lacking subunit e or g, the oligomycin sensitivity and enzymatic activity of F-ATP synthase are unaltered (262). A peculiar behavior of yeast is that the absence of subunit e leads to disappearance of both subunit g and k, while normal expression of subunit e can be observed in the mutants lacking subunit g or k (262). Subunit k appears to be not essential for the dimeric state of yeast enzyme (262), but it likely contribute to stabilize the dimeric F-ATP synthase (268).

The most recent high resolution atomic structure of the yeast dimer (230) reveals that (i) in each monomer subunits e, g and N-terminal of subunit b, with the further support from subunit k, enforce the membrane curvature; (ii) subunits i/j and two strands of subunit a from each monomer form the dimer interface, which is stabilized by the interaction of subunits e and g. Consistently with this structure, previous studies established that (iii) subunit b of one monomer can spontaneously form a homodimer with subunit b of another monomer by formation of a disulfide bridge at a position located in the intermembrane space (257); (iv) the yeast strain lacking the first transmembrane helix of subunit b loses both the dimers and the IMM curvature, while the mutant maintains functional F-ATP synthase (255,265); (v) the absence of the first TMD of subunit b causes strongly decreased expression of subunit g (255); (vi) homodimerization of subunit i turned out to be independent of subunits e and g (253). These observations contribute to explain why a small fraction of dimers is detectable in the null mutants lacking subunit e or g (269). Because the N-terminus of subunit b has been identified next to subunit g also by cross-linking analysis (256), it is proposed that subunit b accommodates the interaction with subunit g, which interacts with subunit e to favor the dimerization of the enzyme (255,256). Part of my studies have been dedicated to define the charged amino acids involved in the physical association of the dimer-specific subunits e and g that stabilize the yeast enzyme dimers.

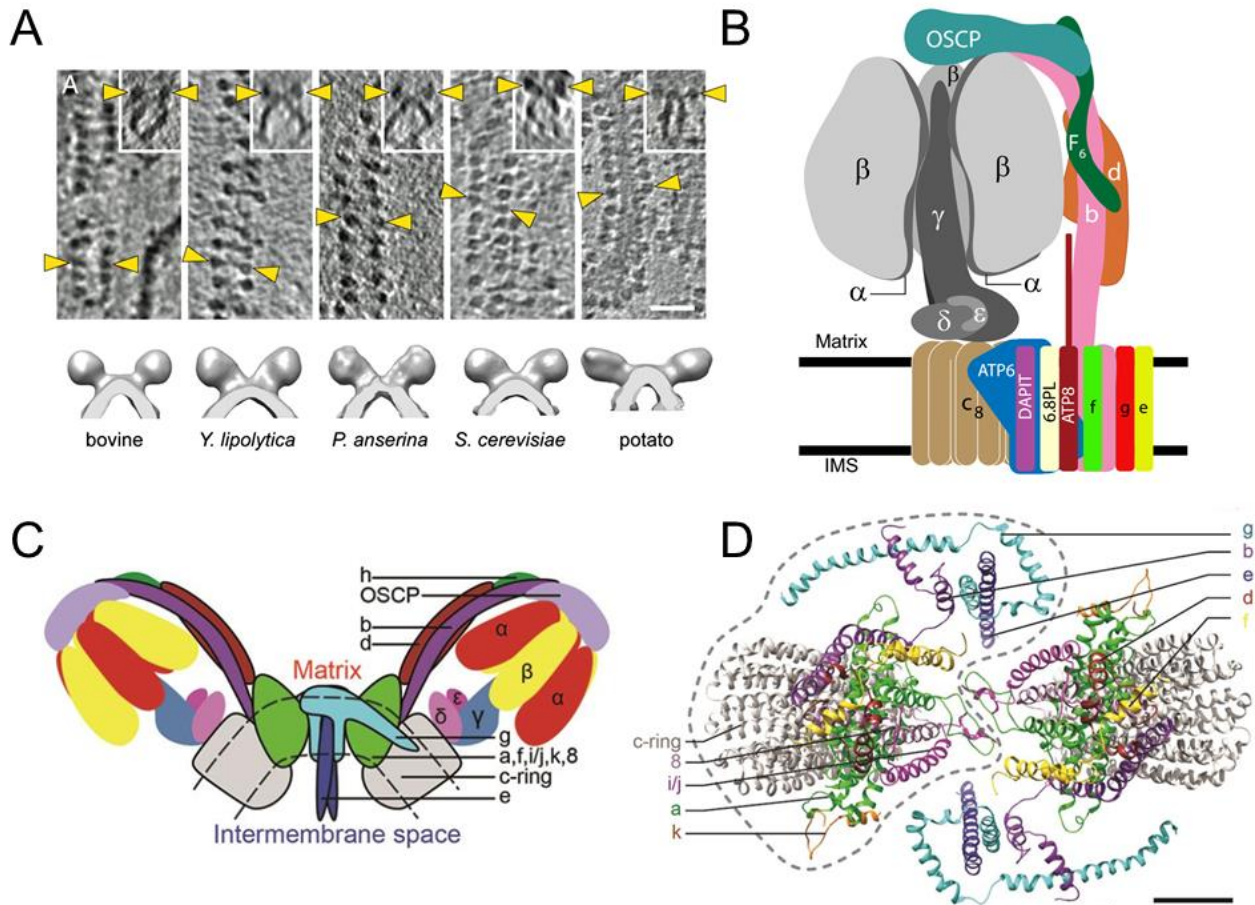


**Fig. 1.10. F-ATP synthase organization and molecular structure of the yeast  $F_o$  dimeric domain.** A, Rows of F-ATP synthase dimers in the mitochondrial membrane from five different species. Figure is from Ref (270). B, organization of subunits in the monomeric mammalian F-ATP synthase. Figure is from Ref (226). C, cartoon of dimeric yeast F-ATP synthase. D, top view of dimeric  $F_o$  domain of yeast enzyme showing localization and structure of indicated subunits. Panels C and D are from Ref. (230).

### 1.3.3.2 The subunits e and g in yeast

Both e- and g-subunits have a unique TMD inserted with the same orientation in the IMM and a soluble domain localized on opposite sides of the membrane, with the C-terminal of subunit e exposed to the IMS. Both harbour an endogenous cysteine (eC28 and gC75, this latter conserved in the bovine enzyme) and possess a conserved coiled-coil motif located in their TMD. Alteration in this GxxxG motif of subunit e (by insertion of an alanine and by replacement of glycine with leucine) leads to the loss of subunit g and the loss of dimeric/oligomeric forms of the enzyme (259). Indeed, subunit g is quite unstable, i.e. its expression is influenced also by alterations of subunit b (255), suggesting that it plays an important role at the interfaces between monomers allowing dimerization/oligomerization of the yeast enzyme (259). Conversely, cross-linking of Cys 28 of subunit e with  $Cu^{2+}$ , which results in formation of subunit e homodimers, increases the stability of F-ATP synthase oligomeric forms in digitonin extracts, demonstrating the involvement of the dimerization motif of subunit e in the formation of F-ATP synthase oligomeric structures (258).

Consistently, cross-linking by  $\text{Cu}^{2+}$  followed by gel electrophoresis analysis of mitochondria from the subunit g C75S/L109C mutant reveals that homodimers of subunit e or subunit g are only present in the F-ATP synthase oligomers (258,260), confirming that e/e and g/g interactions participate in the putative oligomerization interface.

The interaction between subunits e and g seems to play an important role in the dimerization of the enzyme, although the involvement of their respective GxxxG motifs has been questioned. Actually, Gly105 of subunit g GxxxG motif is the last residue of the TMD while subunit e GxxxG motif is located in the middle of the TMD (259,260). Moreover, the stability of subunit g is unaffected by mutation of the Gly 105 or by introduction of a cysteine at position 110 or 112 (261). These data suggest that an intact subunit g GxxxG motif may not be the sole basis for either the interaction between subunit e and g, or for the homodimerization of subunit g (261).

Charged amino acids are often partners for protein-protein interactions, which are required to stabilize the assembly of complex and protein-protein oligomerization including heterodimerization (271–274). We hypothesized that the charged amino acids in subunits e and g could be involved in the physical interaction between each other.

### 1.3.4 F-ATP synthase and the PTP

The most recent hypothesis about the nature of the PTP is that it originates from the conformational change induced by  $\text{Ca}^{2+}$ -binding to the catalytic core of F-ATP synthase (126,163,275,276).

OSCP subunit, located at the “crown” of the peripheral stalk of the enzyme, was identified as binding site for CyPD (162,163). These findings led to the subsequent demonstration that gel-excised dimers of F-ATP synthase from bovine heart mitochondria reconstituted into lipid bilayers display channel activity that coincides with that expected of the PTP/MMC, while channel activity could not be observed with monomers (163). It was also shown that selective inhibitors of the PTP do not compromise the catalytic activity of the enzyme and *vice versa*, that inhibitors of catalysis do not affect the PTP (125). From the ensemble of these observations it was suggested that the PTP may form at the interface between two monomers, while it appears unlikely that this can occur at regions involved in the catalytic activity of the enzyme (163), i.e. the c-ring, as will be discussed later. This proposal has been supported by studies in *S. cerevisiae* (158) and *D. melanogaster* (168); by the finding that ablation of yeast subunit e and g, which are essential for dimerization of yeast enzyme, desensitizes the PTP to  $\text{Ca}^{2+}$  (158); and by recent mutagenesis studies (275,277). Table 1 summarizes the features of the PTP from different species.

Although the molecular nature of the PTP has been a long-standing mystery, a few discrete regulatory sites of PTP have been defined in the 1990s (128,273) through the use of modifiers of sulfhydryl (279) and of relatively specific histidine (136) and arginine reagents (280–284). If these

residues are located on the F-ATP synthase, it should now be possible to identify them by genetic manipulation. Subunit  $\beta$  contains two binding sites for divalent metals ( $\text{Me}^{2+}$ ). These sites usually are occupied by  $\text{Mg}^{2+}$ , which can be replaced by  $\text{Ca}^{2+}$  when the matrix  $\text{Ca}^{2+}$  rises (278). In contrast to  $\text{Mg}^{2+}$ -ATP hydrolysis,  $\text{Ca}^{2+}$ -ATP hydrolysis could not drive proton pumping, implicating an uncoupling mechanism that could be consistent with PTP opening (285). Thr163 of subunit  $\beta$  was identified to mediate  $\text{Me}^{2+}$ -dependent activity of F-ATP synthase in human HeLa cells. The T163S mutation inhibited  $\text{Ca}^{2+}$ -ATP hydrolysis and favored  $\text{Mg}^{2+}$ -ATP hydrolysis, as was previously shown for the T159S mutation (the position equivalent to mammalian T163) in *Rhodospirillum rubrum* (286,287). This point mutation desensitized the PTP to  $\text{Ca}^{2+}$  and protected from PTP-dependent cell death (275). Based on molecular dynamics simulations, it was proposed that a spatial rearrangement can be induced by the larger van der Waals radius of  $\text{Ca}^{2+}$  binding, resulting in increased overall  $\text{F}_1$  rigidity.  $\text{Ca}^{2+}$  binding-induced conformational changes might be transmitted through the peripheral stalk via OSCP to the inner membrane where the PTP eventually forms (126,275).

Mitochondrial matrix acidic pH prevents PTP opening through reversible histidine protonation, and addition of DPC (which reacts with histidine residues) allowed pore opening at acidic pH (136). A unique histidine that is highly conserved in OSCP subunit has been identified to regulate the PTP by matrix  $\text{H}^+$ . H112Q or H112Y mutations indeed abolished the sensitivity of PTP to matrix acidification in human HEK293 cells without affecting catalytic activity of the enzyme (277).

Taken, together, these findings are solid evidence that that PTP forms from F-ATP synthase. Fig. 1.11 reports a model depicting this hypothesis.

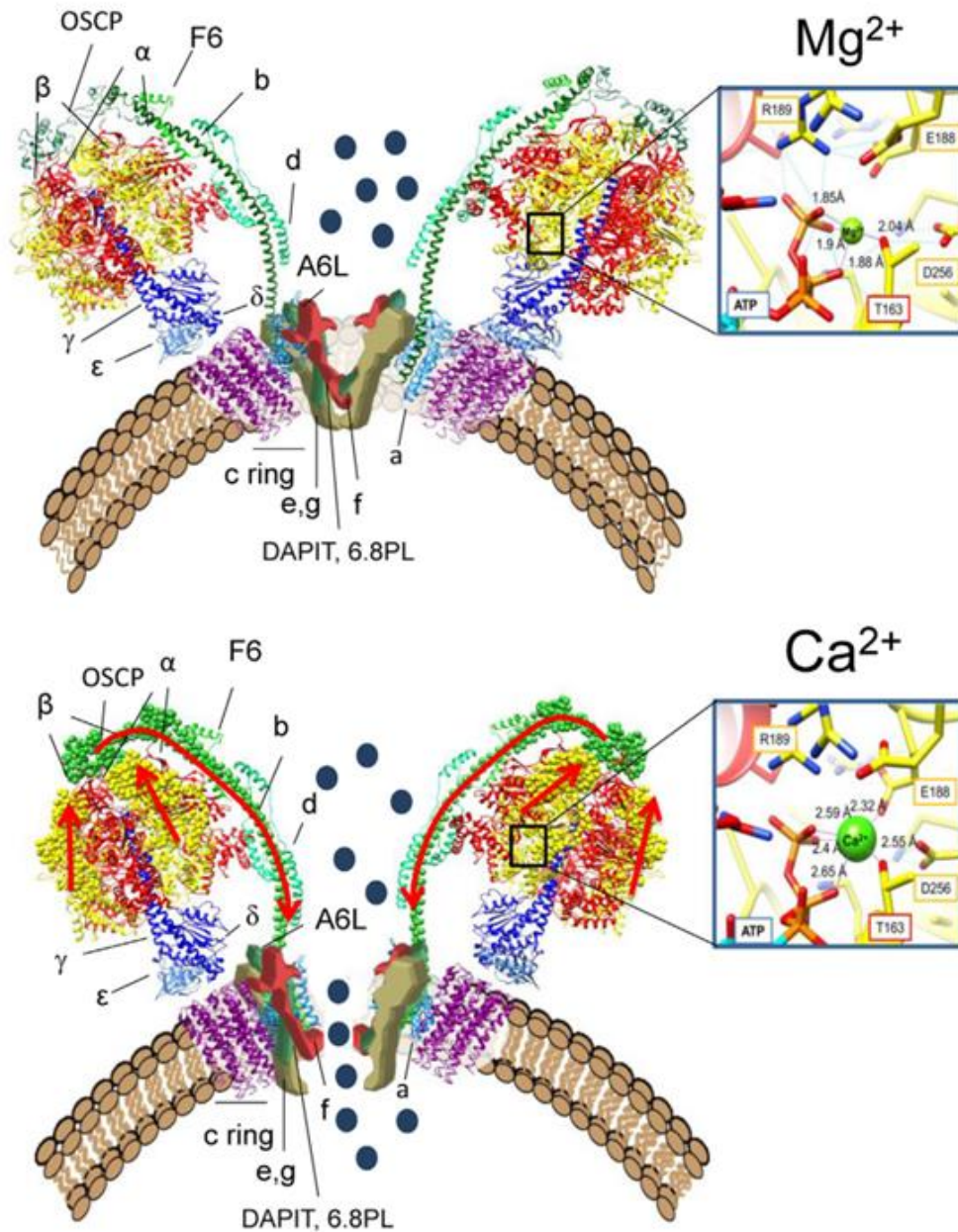


**Fig. 1.11. Proposed model for PTP opening.** F-ATP synthase dimers with  $Mg^{2+}$  (upper) or  $Ca^{2+}$  (lower) bound to the catalytic sites (insets). Subunits  $\alpha$  in red; subunit  $\beta$  in yellow; the lateral stalk (subunits OSCP, b, d, F6) is in green; subunits  $\gamma$ ,  $\delta$ ,  $\epsilon$  are in blue; c-ring is in magenta and subunit a is in light blue. Subunits A6L, f, e and g are also indicated. Lower, the structural region proposed to participate in the conformational change occurring upon  $Ca^{2+}$  binding is highlighted by sphere representation and the overall transmission along the lateral stalk is indicated by red arrows. Dark blue dots represent ion and solutes.

Evidence that F-ATP synthase may form the PTP came also from independent studies from other laboratories. Bonora et al. used siRNA methods to downregulate and forced plasmid expression to transiently overexpress subunit c, and observed consistent changes of PTP opening that matched increased resistance to cell death after knockdown (288). Alavian et al. showed that patch-clamping of liposomes reconstituted with the c subunit revealed high-conductance channel activity induced by  $Ca^{2+}$ . Furthermore, deletion of c subunit prevented the occurrence of PT and attenuated ROS-

induced cell death (289). However, an atomistic simulation study suggested that the properties of the c-ring are incompatible with the features of the PPT/MMC. Indeed, the lipid-filled c-ring is not permeable to ions, H<sub>2</sub>O and osmolytes (290).

The hypothesis that PTP forms from F-ATP synthase has been questioned by two studies based on disruption of the F-ATP synthase subunit c (241) and of subunits b and OSCP (242). In both cases (i) assembly of the enzyme was severely affected resulting in a “vestigial” complex where neither dimers nor normally-sized monomers were apparently assembled; and (ii) respiratory activity was dramatically decreased (241,242). In the case of deletion of the peripheral stalk subunits the decreased respiratory activity was due to lack of assembly of complex I, severe decrease of complex III and moderate decrease of complex IV expression (242). The authors report that in permeabilized cells Ca<sup>2+</sup> is taken up normally irrespective of the deletions, that onset of the PTP (as measured by Ca<sup>2+</sup> release after accumulation of a train of Ca<sup>2+</sup> pulses) still occurs and is sensitive to treatment with CsA, which desensitized the PTP to the same extent in the wild type and in the null cells (241,242). As noted by Bernardi and Lippe, however, swelling in KCl media was substantially decreased in the mutants of the peripheral stalk, suggesting that the pore size had become much smaller (276). An additional problem is that in mitochondria the maximal rate of Ca<sup>2+</sup> uptake is limited by the rate of H<sup>+</sup> pumping by the respiratory chain (291), and it is not clear why the rate of Ca<sup>2+</sup> uptake was instead reportedly unaffected in the KO cells, which had a negligible respiratory activity.

## **1.3.5 PTP modulation by arginine residues**

### **1.3.5.1 The modification of arginine residues**

Phenylglyoxal (PGO) is the most extensively used arginine reagent and it is probably the most selective (292). The approach for modification of arginine residues in proteins by PGO was developed by Takahashi in 1968 (293). PGO reacts with arginine within proteins with a 2:1 stoichiometry (293) (Fig. 1.12A). Under mild conditions, PGO reacts more rapidly and more selectively than glyoxal (GO) or methylglyoxal (MGO) (293,294). A similar reaction takes place with *p*-hydroxyphenylglyoxal (OH-PGO) (Fig. 1.12B).

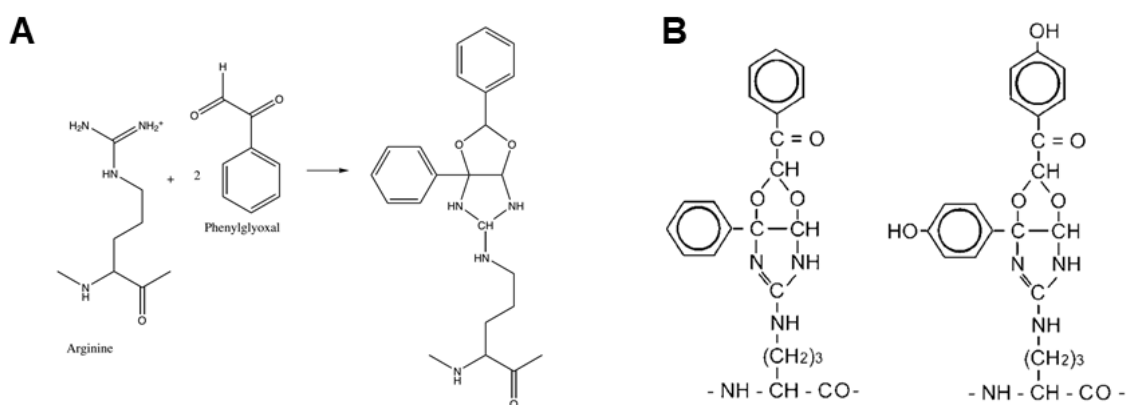


**Fig. 1.12. Structure of PGO- and OH-PGO-arginine adducts.** A, reaction of PGO with arginine in proteins with a stoichiometry of 2:1. The diagram is from Ref. (292) and identified by Takahashi in 1968(293). B, structure of the arginine adducts of PGO (left) and OH-PGO (right). The molecular mass of OH-PGO adduct is 32 Da higher than that of PGO adduct, which corresponds to the two hydroxy groups. The structure is from Ref. (282).

Arginine residues are quite frequent in protein active or binding sites, and are the hotspots for modifications by MGO (295–297). MGO, an  $\alpha$ -dicarbonyl byproduct of glycolysis, is the major precursor in the formation of advanced glycation end-products (AGEs) that contributes to the pathophysiology associated with aging and the long-term complications of diabetes (298–303). Protein glycation is also detectable in yeast (304,305).

### 1.3.5.2 Effects of arginine modification by glyoxals on PTP

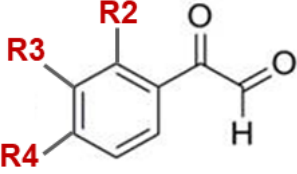
Eriksson and co-workers have observed that modification with arginine-specific reagents modulates the PTP of rat liver mitochondria (RLM) with inhibitory or inducing effects that depend on the net charge and hydrogen-bonding capacity of the adduct(s) (280–284). The regulation of PTP by arginine modification was first addressed in 1997 by Eriksson et al., with the discovery that treatment of RLM with PGO or with 2,3 butanedione (another widely used arginine reagents) inhibits the PTP triggered by uncoupler after matrix  $\text{Ca}^{2+}$  accumulation (280). Remarkably, a similar effect could be obtained with MGO (283). It was hypothesized that the effects on the PTP could be due to formation of an imidazolone adduct at arginine site(s) that stabilize the pore in a closed conformation (283).

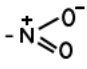
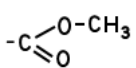
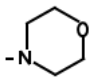
Interestingly, and in spite of its chemical reactivity that is superimposable to that of PGO, OH-PGO instead dramatically sensitized the PTP to  $\text{Ca}^{2+}$  (282). Sequential modification of RLM with OH-PGO and PGO demonstrated that the inducing or inhibitory effect depend on the order of addition, suggesting that modulation of PTP by OH-PGO and PGO occurs at the same site (282). OH-PGO readily triggers PTP opening in de-energized mitochondria even in presence of EGTA (282), showing that OH-PGO is a strong inducer that is able to activate PTP opening at low  $\Delta\psi_m$  without addition of  $\text{Ca}^{2+}$  (but in presence of mitochondrial endogenous matrix  $\text{Ca}^{2+}$ ) (126).



Many synthetic PGO derivatives have been tested for their effects on PTP opening and these experiments revealed that the derivatives containing a net negative charge or with hydrogen bonds induce the PT, while neutral adducts favor PTP closure. Positively charged amino acid residues play a key role in translating changes in membrane potential to conformational changes of ion channels, and arginine residues are common voltage-sensing elements (133,306–308). Eriksson et al. hypothesized that the target arginine may act as a voltage sensor of PTP (280–284). Previous studies have defined the PTP-modulatory effects of arginine specific reagents in RLM (280–284). Fig. 1.13 summarizes the effect of PGO derivatives on the PTP.

**Phenyglyoxal derivatives**



	R4	R3	R2	Hydrogen bond donor	Hydrogen bond acceptor	Resulting adducts
PGO	-	-	-	No	No	<div style="display: flex; align-items: center;"> <div style="border-left: 1px solid red; padding-left: 5px; margin-right: 5px;"> <p style="color: red; margin: 0;">electroneutral charge or without hydrogen bond</p> </div> <div style="text-align: center;"> <p style="color: red; font-size: 2em; margin: 0;">inhibit</p> <p style="font-size: 3em; margin: 0;">↓</p> <p style="font-size: 2em; margin: 0;">PTP</p> </div> </div>
Me-PGO	-CH <sub>3</sub>	-	-	No	No	
MeO-PGO	-O-CH <sub>3</sub>	-	-	No	Weak	
F-PGO	-F	-	-	No	No	
2,4-diF-PGO	-F	-	-F	No	No	
Cl-PGO	-Cl	-	-	No	No	<div style="display: flex; align-items: center;"> <div style="border-left: 1px solid green; padding-left: 5px; margin-right: 5px;"> <p style="color: green; margin: 0;">net negative charge or with hydrogen bond</p> </div> <div style="text-align: center;"> <p style="color: green; font-size: 2em; margin: 0;">activate</p> <p style="font-size: 2em; margin: 0;">↗</p> </div> </div>
NO-PGO		-	-	No	Yes	
OH-PGO	-O <sup>-</sup>	-	-	Yes	Yes	
CamOH-PGO	-O <sup>-</sup>		-	Yes	Yes	<div style="display: flex; align-items: center;"> <div style="margin-right: 10px;">→</div> <p style="margin: 0;">no effect</p> </div>
Mor-PGO		-	-	No	Yes	

**Fig. 1.13. Effect of phenylglyoxal derivatives on the PTP depending on the net negative charge or hydrogen bonds.** The effect of PGO derivatives on PTP depending on the overall physical-chemical properties of resulting adducts. Inhibitors: Cl-PGO, 2,4-diF-PGO, F-PGO, Me-PGO, MeO-PGO, and PGO; Inducer: CamOH-PGO, NO-PGO, and OH-PGO; No effect: Mor-PGO. The PGO derivatives that are overall electroneutral and cannot form hydrogen bonds favor the closure of PTP. The derivatives that possess a net negative charge and are able to form hydrogen bonds induce PTP opening. Mor-PGO is likely unable to react with the target arginine. This figure is set up based on the study by Eriksson and co-workers (282,284).

These previous studies focused on the structure-function relationship of GOs with different structure in RLM, rather than on the identification of the reactive residue(s). During my PhD training, I have identified species-specific effects of PGO on the PTP, and Arg 107 of yeast subunit g of F-ATP synthase as the specific residue mediating the sensitivity of the PTP to PGO in yeast.

## 1.4 Objectives and key results

- Arginine-glyoxal adducts affect the PTP with inducing or inhibitory effects that depend on the specific reagent used. I have investigated PTP modulation by PGO in different species, and I have been able to identify the unique arginine residue (Arg 107 of subunit g) conferring PTP regulation by PGO in yeast F-ATP synthase.
- Although  $\text{Ca}^{2+}$  is considered essential for PTP opening, OH-PGO, which reacts with the same arginine residues as PGO, has been reported to induce the PTP in the absence of added  $\text{Ca}^{2+}$ . I have reinvestigated the  $\text{Ca}^{2+}$ -dependence of the PTP and shown that when matrix  $\text{Ca}^{2+}$  has been depleted OH-PGO is no longer able to open the pore. Furthermore, we found that OH-PGO facilitates  $\text{Ca}^{2+}$ -dependent channel formation by purified F-ATP synthase, a finding that further supports our proposal that the PTP originates from F-ATP synthase.
- I have tested whether charged amino acids of subunits e and g are involved in the formation of F-ATP synthase dimers, which in turn determine the physiological arrangement of the enzyme in long rows of dimers located along the highly curved cristae edges. I have identified Arg 8 of subunit e as a critical residue in mediating interactions between monomers, most likely through an electrostatic bond between Arg 8 of subunit e and Glu 83 of subunit g.

## **2 MATERIALS and METHODS**

## 2.1 Reagents and cells

PGO hydrate, MGO, oligomycin, rotenone, succinic acid, pyruvate, alamethicin, BSA, Pi, ATP, ADP, EGTA, CaCl<sub>2</sub>, CuCl<sub>2</sub>, digitonin, ETH129, Trizma Base (Tris), DTT, sorbitol, mannitol, yeast extract, bacto-polypeptone, yeast synthetic drop-out medium supplements, galactose and sucrose were from Sigma (Milan, Italy). NADH was purchased from Roche. OH-PGO (4-Hydroxyphenylglyoxal hydrate), OSCP antibody (A-8) were purchased from Santa Cruz Biotechnology. CsA was purchased from Calbiochem. Ca<sup>2+</sup> Green-5N, Rhod-2 AM (1-[2-Amino-5-(3-dimethylamino-6-dimethylammonio-9-xanthenyl)phenoxy]-2-(2-amino-5-methylphenoxy)ethane-N,N,N',N'-tetraacetic acid, 1-[2-amino-5-(3-dimethylamino-6-dimethylammonio-9-xanthenyl)phenoxy]-2-(2-amino-5-methylphenoxy)ethane-N,N,N',N'-tetraacetic acid, tetraacetoxymethyl ester) and BAPTA-AM (1,2-bis(2-aminophenoxy)ethane-N,N,N',N'-tetraacetic acid tetrakis(acetoxymethyl ester)) were purchased from Invitrogen. Zymolyase 100T was purchased from US Biological. “QuikChange Lightning Site-Directed Mutagenesis Kit” was purchased from Agilent Technologies. The CellTiter 96® AQueous One Solution Cell Proliferation Assay was purchased from Promega Corporation. HEK293 cells were obtained from the American Tissue Culture Collection (ATCC) and cultured in Dulbecco’s modified Eagle’s medium (DMEM; Life Technologies) supplemented with fetal bovine serum (10%) and penicillin & streptomycin (1%) (Thermo Fisher Scientific, Waltham, MA, USA). *Drosophila* Schneider S2 cells was obtained from Dr. Michael Forte at Oregon Health and Science University. The *S. cerevisiae* strains BY4743 (4741/4742), W303 (MATa/MATα, leu2-3,112 trp1-1 can1-100 ura3-1 ade2-1 his3-11,15) as well as the  $\Delta$ TIM11 ( $\Delta e$ ) (MATa, *his3 $\Delta$ 1*, *leu2 $\Delta$ 0*, *met5 $\Delta$ 0*, *ura3 $\Delta$ 0*) and  $\Delta$ ATP20 ( $\Delta g$ ) (MATα, *his3 $\Delta$ 1*, *leu2 $\Delta$ 0*, *lys2 $\Delta$ 0*, *ura3 $\Delta$ 0*) were purchased from Thermo Scientific.  $\Delta$ TIM11 $\Delta$ ATP20 was generated as described (158). Antibodies for TIM11, ATP20 and ATP3 subunits were a kind gift of Dr. Marie-France Giraud, University of Bordeaux, France.

## 2.2 Yeast mutant generation

In order to generate  $\Delta$ ATP5 yeast expressing the human or yeast OSCP (ATP5) sequence, ATP5 gene was firstly deleted in W303 diploids by homologous recombination, i.e. by substituting the genomic sequence with the Kan cassette of pFA6a-KanMX4 vector. Then, diploids were let to sporulate in 2% potassium acetate medium, resulting tetrads were dissected, selected in G418 plates and correct clones were checked by semi-quantitative PCR using appropriate primers. Yeast ATP5 gene (yOSCP) was cloned in pFL38-URA vector after amplification using following primers that include upstream and downstream regulatory sites (endogenous promoter and termination

sequence): (Forward) 5'-  
CACGACGTTGTAAAACGACGGCCAGTGAATTCGAGCTCGGTACCCTGCCGTCGTCATA  
AAGTGGAC and (Reverse) 5'-  
TTACGCCAAGCTTGCATGCCTGCAGGTCGACTCTAGAGGATCCCCGTTTGCCTGGATAC  
ACGAAC. Cloned products were confirmed by sequence analysis. Human OSCP (hOSCP) cDNA  
(NM\_001697) was purchased from GenScript and amplified using the following primers: (Forward)  
5'-CAGTGTGCTGGAATTCAACACAATGGCTGCCCCAGCAGTGTCC and (Reverse) 5'-  
GATATCTGCAGAATTTTAGACAATCTCCCGCATAGCCCTG. To substitute with the yeast  
putative mitochondrial import sequence at the N-terminus of the OSCP gene (yhOSCP), we used  
the following forward primer: 5'-  
CAGTGTGCTGGAATTCAACACAATGTTTAATAGAGTCTTTACCAGGTCATTTGCATCAA  
GCTTAAGAGCTGCTGCTTCCAAAGCTGCTGCTCCCCCTCCTGTTTCAGGTATACGGTATT  
G, and the same reverse primer for hOSCP. PCR products were cloned in pYES2-URA previously  
digested with EcoRI-HF using In-Fusion HD Cloning Kit (Clontech) and resulting vectors were  
checked by sequencing. Yeast *ΔATP5* cells were separately transformed by standard procedure (309)  
with yOSCP pFL38-URA, hOSCP pYES2-URA or yhOSCP pYES2-URA and correct clones were  
selected.

Human cDNA *ATP5L* (subunit g) cloned into pESC-LEU vector by Sall/XhoI sites was purchased  
from GenScript. The oligonucleotide primers used for yeast *ATP20* gene (subunit g) to be cloned in  
pESC-LEU vector by Sall/XhoI sites were: (Forward) 5'-  
GGGCCCCGGGCGTCGACAACAATGCTAAGCAGGATCCAA, (Reverse) 5'-  
ACCAAGCTTACTCGATTAGTGATGTTTATATCCCAC. PCR products were cloned in pESC-  
LEU vector previously digested with Sall-HF and XhoI using In-Fusion HD Cloning Kit (Clontech)  
and resulting vectors were checked by sequencing. One-step transformation protocol (309) was  
used to transform *ATP5L* pESC-LEU or *ATP20* pESC-LEU into yeast *ΔATP20* strain, and cultured  
in the selective medium 2% galactose (Drop-out-leucine).

The oligonucleotide primers used for site-directed mutagenesis were: TIM11 R8A (Forward) 5'-  
CGACAGTTAATGTTTTGGCATACTCTGCGTTGGGTTTG and (Reverse) 5'-  
CAAACCCAACGCAGAGTATGCCAAAACATTAAGTTCG, ATP20 R107A (Forward) 5'-  
CGGTGAAATAATTGGAAGAGGCAAAAATTAGTGGGATATAAAC and (Reverse) 5'-  
GTTTATATCCCATAATTTTGCTCTTCCAATTATTTACCG, TIM11 R8E (Forward)  
CGACAGTTAATGTTTTGGAATACTCTGCGTTGGGTTTG and (Reverse)  
CAAACCCAACGCAGAGTATTCCAAAACATTAAGTTCG, ATP20 E83A (Forward)  
CATCCAAAAGAATGCACTATTAATAATATGGCGC and (Reverse)  
GCGCCATATTTTAATAGTGCATTCTTTTGGATG, ATP20 E102A (Forward)

TTATTCTGTCCGGTGCCAATAATTGGAAGAAGAAA and (Reverse)  
 TTTCTTCTTCCAATTATTGCACCGACAGAATAA, ATP20 E83K (Forward)  
 CATCCAAAAGAATAAAACTATTTAAAATATGGCGC and (Reverse)  
 GCGCCATATTTTAATAGTTTATTCTTTTGGATG, ATP20 R107E (Forward)  
 CCGTGAAATAATTGGAAGAGAAAAAATTAGTGGGATATAAAC and (Reverse)

GTTTATATCCCCTAATTTTTTCTCTTCCAATTATTTACCG. QuikChange Lightning Site-Directed Mutagenesis Kit (Agilent) was used to harvest point mutations using TIM11 and ATP20 wild-type genes cloned in pFL38 vector as template. After the mutations were confirmed by sequencing, one-step transformation protocol (309) was used to transform the plasmid into  $\Delta$ TIM11 or  $\Delta$ ATP20 *S. cerevisiae* strain, and plated on the selective medium 2% Glu (Drop-out-uracil) and incubated in 30°C.

### 2.3 Yeast mitochondria isolation

Yeast strains BY4743,  $\Delta$ TIM11,  $\Delta$ ATP20 and  $\Delta$ TIM11 $\Delta$ ATP20 were pre-cultured in YPG medium (1% yeast extract, 1% bacto-polypeptone, 2% glucose) at 30°C. TIM11 WT, TIM11 R8A, TIM11 R8E, ATP20 WT, ATP20 R107A, ATP20 E83A and ATP20 E102A mutant strains were pre-cultured in 2% glucose (Drop-out-uracil) selective medium at 30°C.  $\Delta$ ATP20 expressing ATP20 and  $\Delta$ ATP20 expressing ATP5L mutants were pre-cultured in 2% galactose (Drop-out-leucine) selective medium at 30°C. For mitochondria preparation, yeast cells were cultured with a starting OD600 0.2-0.3 in 400 ml medium containing 1% yeast extract, 1% bacto-polypeptone and 2% galactose overnight at 30°C with rotation (180 rpm), and harvested in logarithmic growth phase by centrifugation at 2000  $\times$  g for 5 min, yielding about 4.0 g of yeast cells. The cell pellet was suspended in 0.1 M Tris-SO<sub>4</sub>, pH 9.4 buffer supplemented with 10 mM DTT and incubated at 37°C for 15 min with rotation (180 rpm). The cell pellet was washed once with 1.2 M sorbitol, 20 mM Pi, pH 7.4 buffer, and incubated in the above sorbitol buffer supplemented with zymolyase 100T 0.4 mg/g pellet at 30°C for 45 min with rotation (180 rpm). The incubation was terminated by centrifugation at 2000  $\times$  g for 5 min and washed once with the above buffer at 4°C. The cell pellet was suspended in cold isolation buffer (0.6 M mannitol, 10 mM Tris-HCl, 0.1 mM EDTA, pH 7.4) and homogenized with a Potter homogenizer. The homogenate was spun for 5 min at 2000  $\times$  g and supernatant was collected and centrifuged for 10 min at 12000  $\times$  g. The mitochondrial pellet was suspended in the isolation buffer and protein concentration was determined by the absorbance at 280nm of 0.6% SDS-solubilized mitochondria (OD 0.21 corresponds to 10 mg/ml protein) (310).

## 2.4 Mouse liver mitochondria isolation

Everything was pre-chilled to 0-4°C and respiratory substrate was avoided to minimize any effect during the isolation, e.g.. mitochondrial activity and possible redox environment. All the isolation procedures were performed at 4°C or on ice with pre-chilled buffers. The liver from male C57BL6/J mice were cut into pieces in the isolation buffer (250 mM sucrose, 10 mM Tris-HCl, 0.1 mM EGTA, pH 7.4) and homogenate with a Potter homogenizer. The homogenate suspension was centrifuged at  $690 \times g$  for 10 min. The supernatant was collected and centrifuged at  $7000 \times g$  for 10 min. The pellet was suspended in the isolation buffer and centrifuged at  $9400 \times g$  for 5 min. The mitochondria pellet was suspended in about 400  $\mu$ l isolation buffer, and Biuret method was used for determining protein concentration.

## 2.5 Cell permeabilization

The culture medium of human HEK293 cell lines were discarded and cells washed once with Dulbecco's Phosphate Buffered Saline (PBS). Cells were treated with 0.25% trypsin and the reaction terminated by addition of culture medium. *Drosophila* S<sub>2</sub>R<sup>+</sup> cells were instead detached with a scraper. Cell suspensions were centrifuged at  $500 \times g$  for 5 min and washed once with medium containing 130 mM KCl, 10 mM MOPS-Tris, 1 mM Pi, 0.1 mM EGTA, pH 7.4. The cell pellet was suspended in a medium containing 130 mM KCl, 10 mM MOPS-Tris, 1 mM Pi, 1 mM EGTA, pH 7.4, supplemented with 100  $\mu$ M digitonin and incubated for 10 min on ice at a density of  $2 \times 10^7$  cells  $\times$  ml<sup>-1</sup> for HEK293 cell lines or supplemented with 150  $\mu$ M digitonin and incubated on ice for 20 min at a density of  $6 \times 10^7$  cells  $\times$  ml<sup>-1</sup> for *Drosophila* S<sub>2</sub>R<sup>+</sup> cells. Permeabilization was stopped by diluting with 15-20 ml medium containing 130 mM KCl, 10 mM MOPS-Tris, 1 mM Pi, 0.1 mM EGTA, pH 7.4 followed by centrifugation at  $500 \times g$  for 5 min at 4°C. The cell pellet was washed once with the above KCl medium, spin down again. The final pellet was suspended in the assay medium, or in 250 mM sucrose, 10 mM HEPES-KOH, 20  $\mu$ M EGTA, pH 8.0 for reaction with glyoxals as described in the following paragraph.

## 2.6 Chemical modification with glyoxals

Freshly isolated mouse liver mitochondria (MLM) or yeast mitochondria (YM) (1 mg  $\times$  ml<sup>-1</sup>) or  $2 \times 10^7 \times$  ml<sup>-1</sup> permeabilized cells were incubated with glyoxals in 250 mM sucrose, 10 mM HEPES-KOH, 20  $\mu$ M EGTA, pH 8.0, for 15 min at 25°C. The reaction was terminated by decreasing the pH to 6.8 with HEPES and cooling to 4°C. Mitochondria were precipitated by centrifugation at  $8000 \times g$  for 6 min and washed once with 250 mM sucrose, 10 mM Tris-HCl, 0.1 mM EGTA, 0.5 mg  $\times$  ml<sup>-1</sup> BSA, pH 7.4. Mitochondria or cells were finally resuspended in the assay medium.

## 2.7 Isolation of mitochondria from cells

All the isolation procedures were performed at 4°C or on ice. Cells were washed with cold PBS and detached with a scraper. The cell suspension was collected and centrifuged at  $600 \times g$  for 5 min. The pellet was suspended in the isolation buffer containing 250 mM sucrose, 10 mM Tris-HCl, 0.1 mM EGTA, pH 7.4 and homogenized with a Potter homogenizer. The homogenate suspension was centrifuged at  $600 \times g$  for 5 min. The supernatant was collected and centrifuged at  $6800 \times g$  for 15 min. Pellet was then washed with isolation buffer and spin down again at  $6800 \times g$  for 15 min. The mitochondrial pellet was suspended in the isolation buffer and quantified with the BCA method.

## 2.8 Mitochondrial Ca<sup>2+</sup> retention capacity

YM ( $0.5 \text{ mg} \times \text{ml}^{-1}$ ) were suspended in 250 mM sucrose, 10 mM Tris-MOPS, 2 mM Pi, 1 mM NADH, 20  $\mu\text{M}$  EGTA, 5  $\mu\text{M}$  ETH129, 1  $\mu\text{M}$  Calcium Green-5N, 0.5  $\text{mg} \times \text{ml}^{-1}$  BSA, pH 7.4. MLM ( $0.5 \text{ mg} \times \text{ml}^{-1}$ ) and permeabilized HEK293 or *Drosophila* S<sub>2</sub>R<sup>+</sup> cells ( $1 \times 10^7$  cells  $\times \text{ml}^{-1}$ ) were suspended in 250 mM sucrose, 10 mM Tris-MOPS, 5 mM succinate, 1 mM Pi, 10  $\mu\text{M}$  EGTA, 2  $\mu\text{M}$  rotenone, 0.5  $\mu\text{M}$  Calcium green-5N, pH 7.4. Final volume was 0.2 ml. Extramitochondrial Ca<sup>2+</sup> was monitored by Calcium Green-5N fluorescence (excitation and emission wavelengths 485 nm and 538 nm, respectively), using a Fluoroskan Ascent FL (Thermo scientific) plate reader.

## 2.9 Mitochondrial swelling assay

Unless otherwise stated, YM ( $0.5 \text{ mg} \times \text{ml}^{-1}$ ) were suspended in 250 mM sucrose, 10 mM Tris-MOPS, 2 mM Pi, 1 mM NADH, 20  $\mu\text{M}$  EGTA, 5  $\mu\text{M}$  ETH129, 0.5  $\text{mg} \times \text{ml}^{-1}$  BSA, pH 7.4 in a final volume of 2 ml. MLM ( $0.5 \text{ mg} \times \text{ml}^{-1}$ ) were suspended in the assay medium as indicated in the figure legends in a final volume of 2 ml. Mitochondrial swelling was measured as the decrease of the turbidity (apparent absorbance at 540 nm) using a Cary 100 UV-Vis Spectrophotometer (Agilent Technologies).

## 2.10 ATP hydrolysis assay

MLM or YM pre-treated by glyoxals were suspended in 30 mM sucrose, 50 mM KCl, 50 mM Tris-HCl, 2 mM EGTA, 4 mM MgCl<sub>2</sub> and 2 mM phosphoenolpyruvate, supplemented with 4 U/ml pyruvate kinase, 3 U/ml lactate dehydrogenase, 2 mM ATP and 0.3 mM NADH. Treatment with 4  $\mu\text{M}$  oligomycin was performed at 37°C for 15 min. The assay was carried out at 37°C at a protein concentration of  $40 \mu\text{g} \times \text{ml}^{-1}$  in a final volume of 0.2 ml. ATP synthesis was measured as the decrease of absorbance of NADH at 340 nm using an Infinite® 200 PRO multimode microplate reader.



## 2.11 Oxygen consumption rate assay

A Clark oxygen electrode was used to detect the oxygen consumption rate of isolated mitochondria. MLM were incubated in 250 mM sucrose, 10 mM Tris-MOPS, 10  $\mu$ M EGTA, pH 7.4 at a final concentration of 0.5 mg of protein  $\times$  ml<sup>-1</sup> in a final volume of 2 ml. Further additions were 5 mM succinate as substrate, 1 mM Pi and 0.2 mM ADP. YM were incubated in 250 mM sucrose, 10 mM Tris-MOPS, 20  $\mu$ M EGTA, 5 mM Pi, 0.5 mg/ml BSA, pH 7.4 at a final concentration of 0.25 mg of protein  $\times$  ml<sup>-1</sup> in a final volume of 2 ml. Further additions were 1 mM NADH, 0.2 mM ADP and 4  $\mu$ M oligomycin.

## 2.12 Yeast cell lysis

Yeast strains were cultured in YPG medium or 2% glucose (Drop-out-uracil) selective medium (as mentioned above) overnight at 30°C. About  $5 \times 10^7$  cells (OD<sub>600nm</sub> of 3) were harvested and wash once with 1 ml cold H<sub>2</sub>O. Cell pellet was suspended in 0.1 M NaOH and incubated at 25°C for 10 min. The incubation was stopped by centrifugation and the resulting pellet was solubilized in 50  $\mu$ l SDS-PAGE loading buffer (50 mM Tris/HCl pH 6.8, 20% v/v glycerol, 5% v/v  $\beta$ -mercaptoethanol, 2% w/v SDS and 0.04% w/v bromophenol blue). The sample was heated at 95°C for 3 min, followed by centrifugation at 12000  $\times$  g for 10 min at 4°C, and 25  $\mu$ l of the lysates was subjected to SDS-PAGE.

## 2.13 Cross-linking experiments

Isolated yeast mitochondria were suspended at a protein concentration of 1 mg  $\times$  ml<sup>-1</sup> in 250 mM sucrose, 10 mM Tris-MOPS, 2 mM Pi, 10  $\mu$ M EGTA, pH 7.4. The cross-linking reaction was carried out with the addition of 2 mM CuCl<sub>2</sub> and incubation at room temperature for 15 min. The reaction was stopped with the addition of 5 mM EDTA and 5 mM of N-ethylmaleimide (NEM) and incubation on ice for 10 min. Mitochondrial pellet was collected by centrifugation at 12000  $\times$  g for 10 min at 4°C and subjected to the BN-PAGE analysis.

## 2.14 Western blotting

Isolated mitochondria (5  $\mu$ g  $\times$   $\mu$ l<sup>-1</sup>) or yeast cell lysate were suspended in 50 mM Tris/HCl pH 6.8, 2% w/v SDS, 20% v/v glycerol, 5% v/v  $\beta$ -mercaptoethanol, and 0.04% w/v bromophenol blue at, and boiled for 5 minutes. After a centrifuge at 12000  $\times$  g for 10 min at 4°C, 25  $\mu$ l of cell lysates or 10  $\mu$ l mitochondrial lysates were loaded onto NuPAGE™ 12% Bis-Tris Protein Gels (Invitrogen), and proteins were separated by electrophoresis in MOPS SDS Running Buffer (Invitrogen) for 3 h at 20 mA at 4°C. Proteins were transferred onto nitrocellulose membranes at 30 V for 1.25 h at 4°C. The membrane was blocked with 5% (w/v) milk at room temperature for 1 h and incubated with the

antibodies against TIM11, ATP20, ATP4, ATP3 (subunit  $\gamma$ ) and OSCP overnight at 4°C. Immunoreactive bands were detected by chemiluminescence using an Uvitec Cambridge instrument.

## 2.15 Blue native gel electrophoresis

Yeast mitochondria were suspended at a protein concentration of 10 mg  $\times$  ml<sup>-1</sup> in 150 mM potassium acetate, 30 mM HEPES, 10% v/v glycerol, 1 mM phenylmethylsulfonyl fluoride (PMSF), supplemented with 1.5% (w/v) digitonin (unless otherwise stated), pH 7.4. The mitochondrial lysates were harvested by centrifugation at 100,000  $\times$  g for 25 min at 4°C with a Beckman TL-100 rotor. The supernatants were supplemented with native PAGE 5% G-250 sample additive (Invitrogen), and loaded onto NativePAGE™ 3-12% gradient Bis-Tris Protein Gels (BN-PAGE, Invitrogen). Electrophoresis was carried out in the Dark Blue cathode buffer at 150 V for 20 min and in the Light Blue cathode buffer at 250 V for 2 h. After electrophoresis, gels were stained with 0.25 mg/ml Coomassie Blue, 10% acetic acid at room temperature overnight, or used for in-gel activity staining for ATP hydrolysis of F-ATP synthase. Activity was monitored in 270 mM glycine, 35 mM Tris, pH 7.4, 8 mM ATP-Tris, pH 7.4, 15 mM MgSO<sub>4</sub>, and 2 mg/ml Pb(NO<sub>3</sub>)<sub>2</sub> at 37°C. Alternatively, gels were blotted to polyvinylidene difluoride (PVDF) membranes for Western Blot analysis, or excised to obtain bands of F-ATP synthase dimers and monomers. These protein complexes were eluted from gels by an overnight incubation at 4°C in 25 mM Tricine, 10 mM MgSO<sub>4</sub>, 8 mM ATP, 7.5 mM Bis-Tris, 1% (w/v) n-heptyl  $\beta$ -D-thioglucopyranoside, pH 7.0. Samples were then centrifuged at 20,000  $\times$  g for 10 min at 4°C and supernatants were used either for Western Blotting, silver staining or for bilayer experiments as described in next paragraphs.

## 2.16 Silver staining

F-ATP synthase dimers and monomers eluted from BN-PAGE as described above were processed for silver staining analysis. Briefly, protein was denatured and separated by SDS-PAGE as detailed in “Western Blotting” section. After SDS-PAGE electrophoresis, gels were fixed in 50% methanol, 12% acetic acid, 0.05% formalin (37% Formaldehyde) for 3 h, then washed twice with 50% ethanol for 20 min. The gels were treated with 0.02% Na<sub>2</sub>S<sub>2</sub>O<sub>3</sub> for 1 min, followed by incubation with silver staining buffer containing 0.2% AgNO<sub>3</sub>, 0.076% formalin (35% Formaldehyde) for 20 min, and washed twice with H<sub>2</sub>O. The gels were incubated in 6% Na<sub>2</sub>CO<sub>3</sub>, 0.05% formalin (35% Formaldehyde) and 0.0004% Na<sub>2</sub>S<sub>2</sub>O<sub>3</sub> until the bands were clearly visible and then washed twice with H<sub>2</sub>O. The developing reaction was blocked in 50% methanol, 12% acetic acid for  $\geq$  10 min, and the gels finally washed with 50% methanol for  $\geq$  20 min.

## 2.17 Electrophysiology

Eluted dimers of F-ATP synthase from BN-PAGE gels were used for planar lipid bilayer experiments. Electrophysiological properties of F-ATP synthase were assessed by means of multisite single channel recording following protein insertion into artificial planar lipid bilayer. Multiple electrophysiological recordings were assessed at the same time from the same sample exploiting a Orbit mini bilayer workstation (Nanion Technologies, Munich, Germany) enabling the simultaneous recording of up to four artificial lipid bilayers. Membranes were prepared by painting a solution (10 mg/ml in octane) of soybean asolectin (Sigma) across four microcavities (150  $\mu\text{m}$  in diameter) on standard Multielectrode Cavity Array (Meca) 4 chips (IonEra, Freiburg, Germany), set on the bottom of the Orbit mini recording chamber. The cavities and the whole recording chamber were filled with a recording solution (150 mM KCl, 10 mM HEPES, pH 7.5), before membrane painting. The microcavities of the chip constituted the *cis* compartment, to which all voltages reported refer, zero being assigned by convention to the *trans* (grounded) side. Currents were considered as positive when carried by cations flowing from the *cis* to the *trans* compartment, and vice versa. Currents were elicited after bulk loading of the protein into the recording chamber and addition of 3 mM  $\text{CaCl}_2$ , 100  $\mu\text{M}$  PhAsO, and 5  $\mu\text{M}$   $\text{Cu}(\text{OP})_2$ . Membrane capacity ranged from 10 to 80 pF (average 50 pF) and no current leakage was detectable. Control recordings from empty membrane showed no currents occurrence during the whole recording time, up to 30 minutes. Data were acquired at 5 KHz, filtered at 500 Hz using a low-pass 4-pole Bessel filter, digitalized, and stored on a computer by a dedicated software (EDR, Elements s.r.l, Italy); data were analyzed offline using MATLAB 2007b (MathWorks). The power spectrum for each current signal was calculated by means of the Fast Fourier transform; frequencies lower than 5 Hz (baseline drifts) and higher than 500 Hz were not included in the analysis. The area under the power spectrum curve, referred for brevity as  $|P(f)|$ , as well as mean currents for non-zero values, and maximal currents, were calculated for each condition, taking advantage of a home-made algorithm developed on MATLAB. Averaged  $|P(f)|$  values were normalized for the WT value. Results are normally distributed by the Shapiro-Wilk test, and data are represented as mean  $\pm$  s.e.m. Statistical comparison of data was assessed with ANOVA analysis.

## 2.18 Serial-dilution spotting assay

Overnight cultures of yeast different genotypes in appropriate selective mediums were diluted with sterile  $\text{H}_2\text{O}$  to an  $\text{OD}_{600\text{nm}}$  of 0.1 and four serial dilutions (1:10) were prepared in sterile  $\text{H}_2\text{O}$ . Cell suspensions were transferred onto plates containing 2% Glucose, glycerol and 2% Glucose (-uracil) selective medium using a multi-channel pipette. Plates were analyzed after one to three days of incubation at 30°C.

## **2.19 Fluorescence dye rhod-2 loading**

MLM ( $25 \text{ mg} \times \text{ml}^{-1}$ ) were pre-incubated with  $10 \text{ }\mu\text{M}$  Rhod-2 AM in the mitochondrial isolation buffer ( $250 \text{ mM}$  sucrose,  $10 \text{ mM}$  Tris-HCl,  $0.1 \text{ mM}$  EGTA, pH 7.4) for 20 min at  $25^\circ\text{C}$ . Mitochondria were collected by centrifugation at  $15,300 \times g$  for 6 min, washed once and finally suspended in the isolation buffer at a concentration of  $25 \text{ mg} \times \text{ml}^{-1}$ . Change of fluorescence was followed with a Perkin Elmer luminescence spectrometer at excitation 552 nm and emission 581 nm.

## **2.20 BAPTA-AM mitochondria loading**

MLM ( $1 \text{ mg} \times \text{ml}^{-1}$ ) were suspended in the isolation buffer ( $250 \text{ mM}$  sucrose,  $10 \text{ mM}$  Tris-HCl,  $0.1 \text{ mM}$  EGTA, pH 7.4) in the presence of  $0.2 \text{ mM}$  BAPTA-AM for 20 min at  $25^\circ\text{C}$ . Mitochondria were harvested by centrifugation at  $15,300 \times g$  for 6 min and resuspended at  $10 \text{ mg/ml}$  in the isolation buffer at  $4^\circ\text{C}$ . Mitochondria not loaded with BAPTA-AM were subjected to the same procedure after the addition of equivalent vehicle (DMSO)

# **3 RESULTS and DISCUSSION**

### 3.1 OH-PGO is able to generate channel activity comparable to MMC in purified F-ATP synthase

Modification with arginine-specific glyoxals modulates the PTP with inhibitory or inducing effects, depending on the net charge of the adduct(s) (281–284). Consistent with the effect of OH-PGO on the PTP of RLM, OH-PGO sensitized the PTP to  $\text{Ca}^{2+}$  in MLM, as well as in permeabilized human HEK293 cells (data not shown). We then tested whether OH-PGO was able to generate channels in purified F-ATP synthase.

We found that purified bovine F-ATP synthase reconstituted into planar lipid bilayers displayed channel activity after the addition OH-PGO in presence of  $\text{Ca}^{2+}$ , even in the absence of Bz-423 and of oxidants, which were previously shown to potentiate  $\text{Ca}^{2+}$ -induced activation of the channel (Fig. 3.1). OH-PGO is thus a strong inducer of PTP, and these results indicate that reactive arginine(s) are located in the F-ATP synthase.

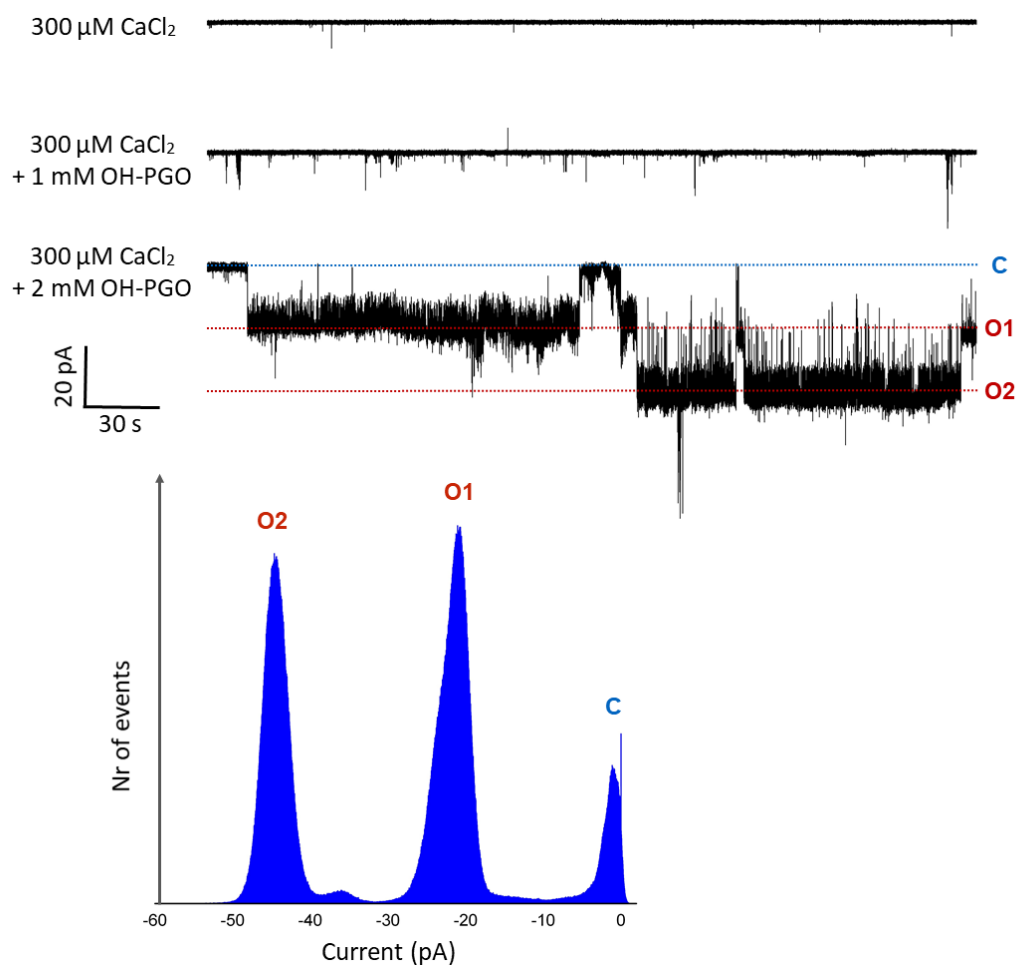


**Fig. 3.1. OH-PGO is able to trigger PTP opening in planar lipid bilayer in the presence of Ca<sup>2+</sup>.** *Upper*, representative current traces recorded at -60 mV holding potential in symmetrical 150 mM KCl. 300  $\mu$ M Ca<sup>2+</sup> was added upon incorporation of purified F-ATP synthase following the addition of OH-PGO as indicated. *Lower*, corresponding current amplitude histograms were obtained from at least three independent experiments. The purified bovine F-ATP synthase could form a 350-pS channel after the addition of 2 mM OH-PGO together with 300  $\mu$ M Ca<sup>2+</sup>. The F-ATP synthase was purified from bovine heart mitochondria by Christoph Gerle(266). The bilayer experiments were performed with Andrea Urbani.

### **3.2 Matrix Ca<sup>2+</sup> is an essential permissive factor for opening of the PTP**

Consistent with a strict Ca<sup>2+</sup> requirement for channel activity is the finding that MMC opening at the patch-clamp has never been observed unless Ca<sup>2+</sup> was added (81). In isolated mitochondria PTP opening is usually triggered by matrix Ca<sup>2+</sup> accumulation in the presence of one of a variety of inducers (311). Yet, as already mentioned conditions have been described under which PTP opening takes place in the absence of Ca<sup>2+</sup> accumulation. These conditions include treatment with the SH reagent PhAsO (312), the wasp venom peptide mastoparan (313,314), the thiol oxidant Cu(OP)<sub>2</sub> (312), cyanine dyes (315) and the arginine reagent OH-PGO(282). The addition of OH-PGO readily induced mitochondrial swelling in de-energized mitochondria even in presence of EGTA, indicating the matrix Ca<sup>2+</sup> was thus sufficient for PTP opening triggered by OH-PGO at low  $\Delta\psi_m$  (282).

Establishing whether pore opening can occur in the absence of Ca<sup>2+</sup> is an important issue because it represents a test for the hypothesis that Ca<sup>2+</sup> binding to the  $\beta$  subunit of F-ATP synthase triggers PTP opening. Given that the presence of adventitious and/or matrix Ca<sup>2+</sup> has not been addressed in the above-mentioned studies, we have reinvestigated the problem of whether PhAsO and OH-PGO can induce a Ca<sup>2+</sup>-insensitive permeability transition.

In the absence of EGTA, energized mitochondria take up the adventitious or contaminating Ca<sup>2+</sup>, which may lead to PTP, which was potentiated by relatively low amounts of PhAsO and OH-PGO, prevented by EGTA and potentiated by added Ca<sup>2+</sup> (Fig. 3.2.1).

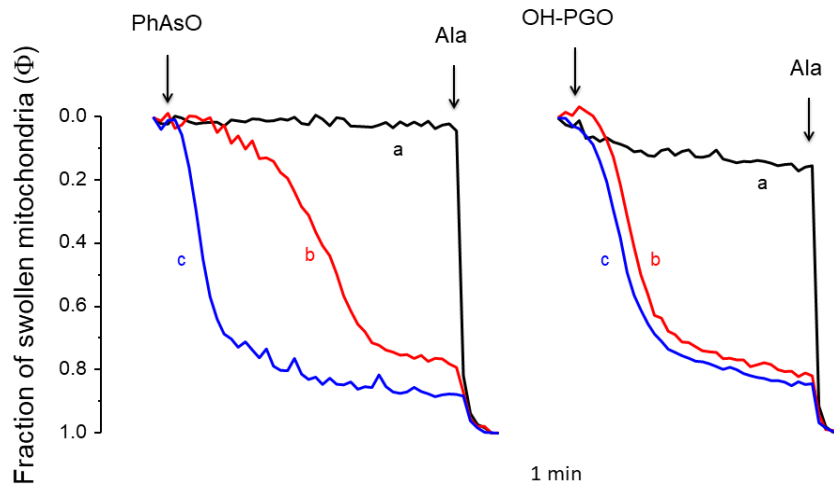


**Fig. 3.2.1. Differential permeability induced by PhAsO and OH-PGO in absence and presence of EGTA.** MLM were added to 0.1 M KCl, 10 mM Tris-MOPS, 1 mM Pi, 2  $\mu$ M rotenone, 5 mM succinate, pH 7.4 at 0.5 mg/ml. In trace a (black), 1 mM EGTA was added before the addition of mitochondria. In trace c (blue), 50  $\mu$ M  $\text{Ca}^{2+}$  was added before the addition of mitochondria. 5  $\mu$ M PhAsO, 20  $\mu$ M OH-PGO, 5  $\mu$ M alamethicin (Ala) were added as indicated by arrows.

To test the role of matrix  $\text{Ca}^{2+}$  in PTP opening we devised protocols to deplete or chelate matrix  $\text{Ca}^{2+}$ . Mitochondria were loaded with Rhod-2 AM, which generates the  $\text{Ca}^{2+}$  indicator Rhod-2 in the matrix giving rise to a detectable fluorescence signal (Fig. 3.2.2). Addition of A23187 (allowing release of matrix  $\text{Ca}^{2+}$ , which is then chelated by EGTA, panel A) or treatment with BAPTA-AM (which generates the  $\text{Ca}^{2+}$  chelator BAPTA in the matrix, panel B) resulted in the decrease of the fluorescence signal (Fig. 3.2.2).

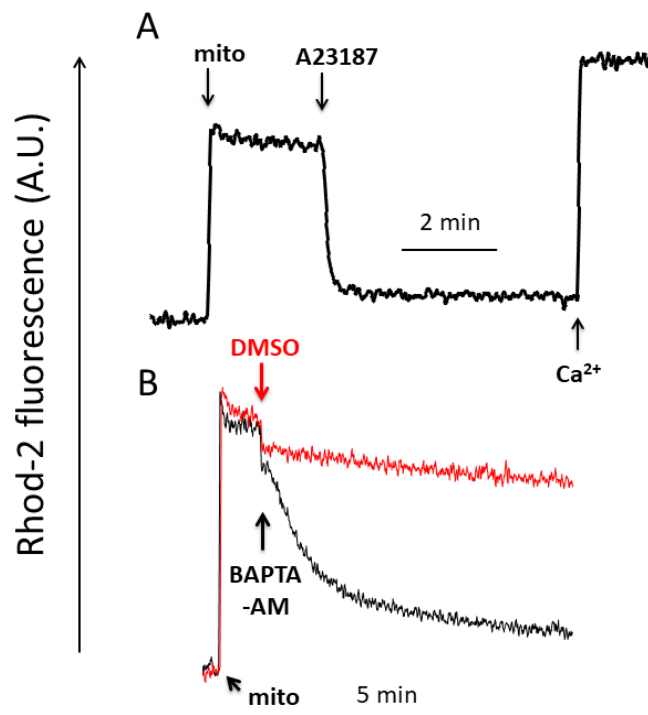




**Fig. 3.2.2. Effect of A23187 and BAPTA-AM on intramitochondrial  $\text{Ca}^{2+}$  level monitored by Rhod-2 fluorescence.** MLM (mito) were pre-treated by Rhod-2 AM as described in "Materials and Methods". **A**, the pre-treated MLM were added to a medium containing 0.1 M KCl, 10 mM Tris-MOPS, 2  $\mu\text{M}$  Rotenone, 1 mM  $\text{Mg}^{2+}$ , 1 mM EGTA, pH 7.4 at 0.5 mg/ml, followed by additions of 1  $\mu\text{M}$  A23187 and 1 mM  $\text{Ca}^{2+}$ . **B**, the pre-treated MLM were added to a buffer containing 250 mM sucrose, 10 mM Tris-HCl, 0.1 mM EGTA, pH 7.4 at 1 mg/ml, followed by additions of equivalent amount of DMSO (red trace) or 200  $\mu\text{M}$  BAPTA-AM (black trace).

We next used these protocols to test whether PTP opening by PhAsO and OH-PGO, which occurs even in the presence of EGTA (282,312), was inhibited by depletion of matrix  $\text{Ca}^{2+}$ . It should be recalled that a high membrane potential tends to prevent PTP opening (132); and that, due to operation of the  $\text{K}^+/\text{H}^+$  exchanger, incubation of deenergized mitochondria in sucrose-based media causes matrix acidification, which in turn inhibits the PTP (316).

In order to observe a reproducible induction of the permeability transition in the absence of  $\text{Ca}^{2+}$  uptake, we therefore incubated mitochondria in the absence of oxidizable substrates in an isotonic, KCl-based medium in the presence of EGTA. In the absence of further additions mitochondria maintained a constant volume, as indicated by readings of apparent absorbance (Fig. 3.2.3A, trace a in both panels). Addition of PhAsO (upper panel) or of OH-PGO (lower panel) was readily followed by a process of absorbance decrease (Fig. 3.2.3A, traces b), which was blunted by treatment with CsA (Fig. 3.2.3A, traces c), A23187 (Fig. 3.2.3A, traces d), or their combination (Fig. 3.2.3A, traces e). The results were highly significant both for treatment with PhAsO and with OH-PGO (Fig. 3.2.3B).

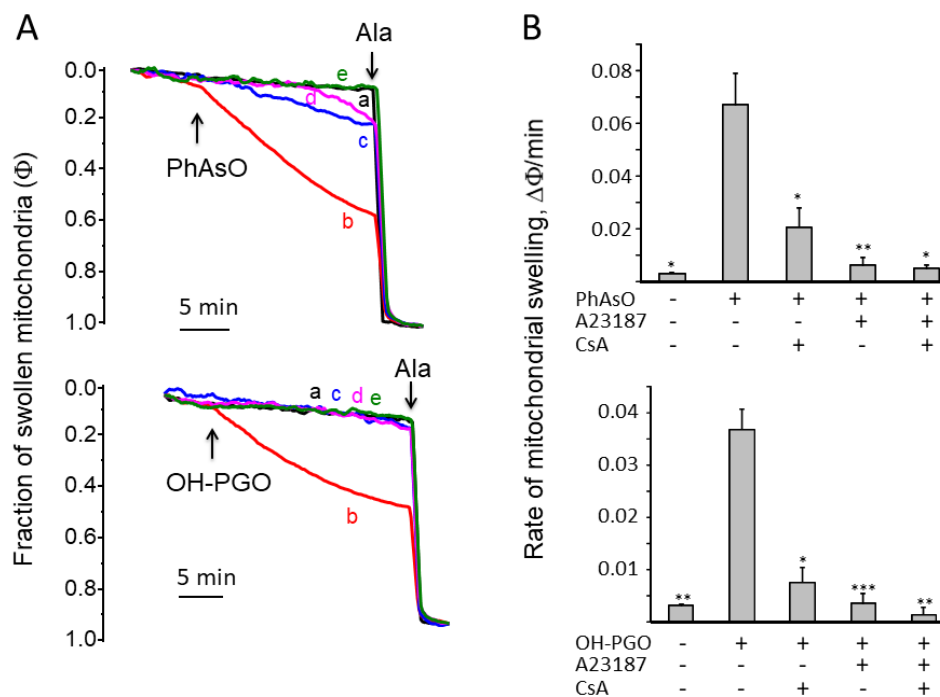


**Fig. 3.2.3. Depletion of matrix  $\text{Ca}^{2+}$  by A23187 inhibits the PTP induction by PhAsO and OH-PGO.** MLM were incubated in a KCl based medium containing 0.1 M KCl, 10 mM Tris-MOPS, 1 mM  $\text{Mg}^{2+}$ , 1 mM EGTA, 2  $\mu\text{M}$  rotenone, pH 7.4 at 0.5 mg/ml.  $\text{Mg}^{2+}$  was added to avoid the loss of matrix  $\text{Mg}^{2+}$  via A23187. **A**, in trace a (black), there was no addition of PhAsO or OH-PGO. In trace b (control, red), the assay medium was supplemented with equivalent amount of DMSO. In trace c (blue), the assay medium was supplemented with 1

$\mu\text{M}$  CsA. In trace d (purple), mitochondria were incubated with  $1 \mu\text{M}$  A23187 for 15 min. In trace e (green), the assay medium was supplemented with  $1 \mu\text{M}$  A23187 and  $1 \mu\text{M}$  CsA.  $50 \mu\text{M}$  PhAsO,  $2 \text{ mM}$  OH-PGO and  $5 \mu\text{M}$  Ala were added as the arrow indicated. **B**, rate of mitochondrial swelling was expressed as the fraction of swollen mitochondria per minute. Results are mean  $\pm$  S.E. of three independent experiments. \* $P < 0.05$  vs control, \*\* $P < 0.01$  vs control, \*\*\* $P < 0.001$  vs control. Student's t test.

A titration was also performed, which confirmed that swelling (i.e. spreading of PTP opening throughout the mitochondrial populations (317)) was observed in the presence of EGTA (black squares), indicating that endogenous  $\text{Ca}^{2+}$  is sufficient to allow pore opening upon addition of the inducer. The rate of swelling was stimulated by added  $\text{Ca}^{2+}$  (green diamonds) and inhibited by both treatment with BAPTA-AM (red circles) and with the novel diarylisoxazole PTP inhibitor 63 (318) (purple triangles) (Fig. 3.2.4).

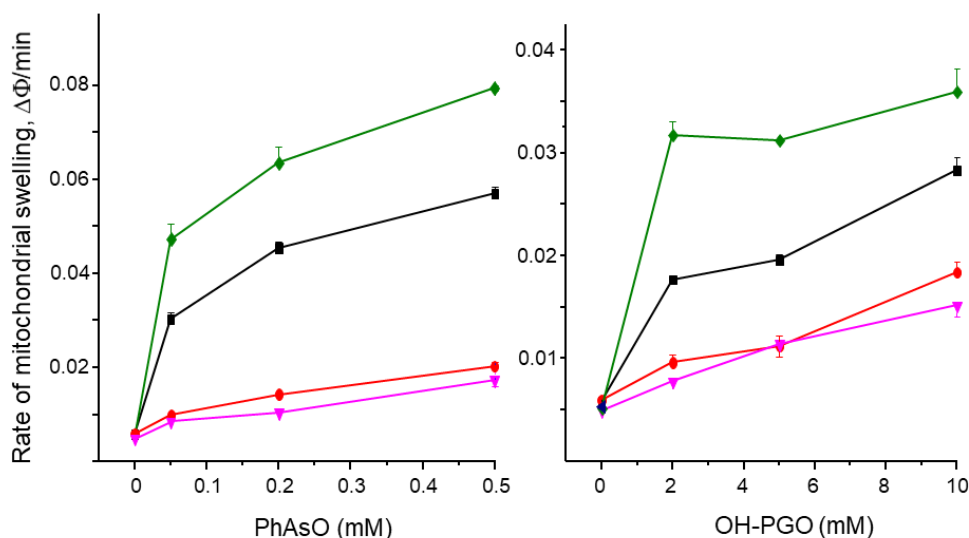


**Fig. 3.2.4. Mitochondrial BAPTA loading inhibits the PTP induction by different concentrations of PhAsO and OH-PGO.** MLM were added to a medium containing  $0.1 \text{ M}$  KCl,  $10 \text{ mM}$  Tris-MOPS,  $1 \text{ mM}$  Pi,  $2 \mu\text{M}$  rotenone, pH 7.4 at  $0.5 \text{ mg/ml}$  and rate of mitochondrial swelling (fraction of swollen mitochondria per minute) was measured in presence of indicated concentrations of PhAsO and OH-PGO. In traces colored in black, red and purple, the assay medium supplemented with  $1 \text{ mM}$  EGTA. In red trace, MLM were pre-treated with BAPTA-AM. In purple trace, the assay medium supplemented with  $1 \mu\text{M}$  a N-phenylbenzamide compound (a novel diarylisoxazole PTP inhibitor 63) (318). In green trace, EGTA was omitted and  $50 \mu\text{M}$   $\text{Ca}^{2+}$  was added before the addition of mitochondria.

Taken together, these results demonstrate that PTP opening can occur in the absence of added  $\text{Ca}^{2+}$  after treatment of isolated mitochondria with the dithiol reagent PhAsO or the arginine reagent OH-PGO, two very effective PTP inducers. The inducing effect was inhibited by treatment with the ionophore A23187 (which depletes matrix divalent cations) or with BAPTA-AM (which chelates matrix  $\text{Ca}^{2+}$ ). We conclude that matrix  $\text{Ca}^{2+}$  is an essential permissive factor for PTP opening. This is consistent with the hypothesis that the permeability transition requires  $\text{Ca}^{2+}$  binding, possibly to the  $\beta$  subunit of F-ATP synthase (275).

### 3.3 Species-specificity of the PTP regulation by arginine residue(s)

#### 3.3.1 The species-specific effects of PGO on the PTP

Previous studies had defined the PTP-modulatory effects of arginine-selective reagents. The outcome was dependent on the specific glyoxal used, with PTP inhibition by MGO or PGO and PTP activation by OH-PGO (281–284). However, these previous studies had focused on the effect of the reagents in RLM while whether the arginine-glyoxal adducts can modulate PTP in other species had not been investigated.

Consistent with the effect of PGO on the PTP of RLM, PGO desensitized the PTP to  $\text{Ca}^{2+}$  in MLM (Fig. 1A) as well as in mitochondria from *Saccharomyces cerevisiae* in the presence of ETH129, a selective ionophore that allows  $\text{Ca}^{2+}$  equilibration across the inner membrane in yeast mitochondria (Fig. 3.3.1B). In either case, the desensitizing effect can be appreciated from the increased CRC of PGO-treated mitochondria (Fig. 3.3.1A,B). Unexpectedly, PGO caused instead sensitization of the pore to  $\text{Ca}^{2+}$  in permeabilized human HEK293 (Fig. 3.3.1C) and *Drosophila*  $\text{S}_2\text{R}^+$  cells (Fig. 3.3.1D). Sensitization of PTP opening by PGO in human and *Drosophila* cells was not due to digitonin permeabilization, as it was also observed in mitochondria isolated from these cells (results not shown). These findings indicate that the ability to modulate the PTP by PGO has been conserved although the effect (induction or inhibition) differs between species.

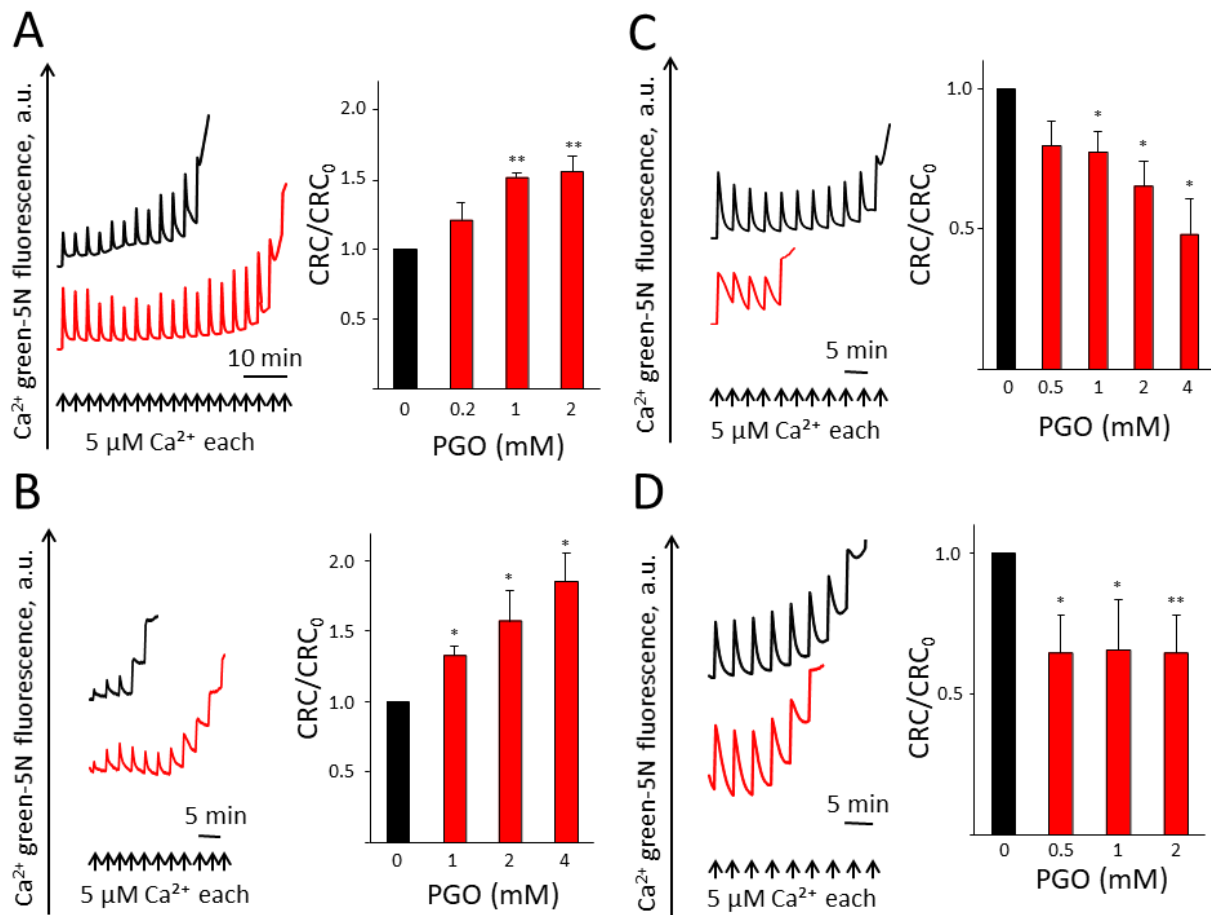


**Fig. 3.3.1. The effects of PGO on the PTP have been conserved but differ between species.** Isolated mitochondria or permeabilized cells were pre-treated with vehicle (DMSO) or PGO and resuspended in the CRC assay buffer as described in “Materials and Methods”. **A**, CRC of MLM pretreated with DMSO (black trace) or 1 mM PGO (red trace). **B**, CRC of isolated yeast mitochondria pretreated with DMSO (black trace) or 4 mM PGO (red trace). **C**, CRC of permeabilized HEK293 cells pretreated with DMSO (black trace) or 4 mM PGO (red trace). **D**, CRC of permeabilized *Drosophila* S<sub>2</sub>R<sup>+</sup> cells pretreated with DMSO (black trace) or 1 mM PGO (red trace). Representative traces are shown. Bars represent the CRC of DMSO- (black) or PGO-pretreated (red) isolated mitochondria or permeabilized cells. CRC of DMSO-treated mitochondria was set as one unit. Results are mean ± s.e.m. of at least three independent experiments. \**P*<0.05 vs vehicle, \*\**P*<0.01 vs vehicle. One-way ANOVA was used for statistical analysis.

Subunit	Total Nr.	Position in <i>S. cerevisiae</i>	Position in <i>H. sapiens (M. musculus)</i>
$\alpha$	26	4, 9, 67, 77, 127, 143, 163, 165, 176, 198, 201, 208, 225, 247, 295, 316, 323, 324, 328, 341, 345, 399, 410, 435, 457, 460	5, 12, 73, 83, 133, 149, 169, 171, 182, 204, 207, 214, 231, 253, 301, 322, 329, 330, 334, 347, 351, 405, 416, 441, 463, 466
$\beta$	17	93, 105, 127, 139, 223, 225, 262, 264, 277, 293, 307, 328, 370, 389, 439, 441, 445	109, 121, 143, 155, 239, 241, 279, 281, 294, 310, 324, 345, 387, 406, 456, 458, 462
$\gamma$	7	4, 31, 42, 153, 266, 290, 292	4, 23, 34, 143, 253, 277, 279
a	1	186	159
c	1	39	c1:99, c2:104(109), c3:105(104)
$\epsilon$	2	5, 23	6, 24
OSCP	2	8, 114	14, 117
b	1	200	208
f	1	56	50 (44)
e	1	8	15
g	1	107	96
<b>TOTAL</b>	<b>60</b>	<b>60</b>	<b>60</b>

**Table 3. Number and position of arginine residues conserved between F-ATP synthase of *S. cerevisiae*, *H. sapiens* and *M. musculus* (in parentheses when different).**

Under the assumptions (i) that the observed differences depend on specific features of the PTP rather than on the existence of species-specific reactive sites and (ii) that these sites are located on the F-ATP synthase, we narrowed the search of the reactive arginine(s) from 135 (yeast) to 60 arginines that are conserved between F-ATP synthases of *S. cerevisiae*, *H. sapiens*, *M. musculus* and *D. melanogaster* (the position of these residues in the yeast, human, and mouse enzymes are reported in Table 3). After ruling out a major role for the arginine residues of the  $\alpha$ ,  $\beta$ ,  $\gamma$ ,  $\epsilon$ , a and c subunits because PGO treatment did not affect the catalytic activity of the enzyme, we were able to identify a key role for the g subunit Arg 107 in a study that is reported in full in the Appendix as Publication 1. The key findings are reported below for the reader's convenience.

### 3.3.2 The role of subunit g in conferring this species-specificity

Taking advantage of the yeast model and of the species-specific response to PGO, we have replaced yeast subunit g (encoded by *ATP20* gene) with its human counterpart (encoded by *ATP5L* gene). PGO desensitizes the yeast PTP to  $\text{Ca}^{2+}$  (thus increasing the CRC) while it sensitizes it in human HEK293 cells (thus decreasing the CRC, see Fig. 3.3.1). We exploited this phenotypic difference to test whether expression of human subunit g is able to switch the inhibitory effect of PGO in yeast

mitochondria to the inducing effect seen in human mitochondria. Deletion of the *ATP20* gene encoding for yeast subunit g prevented dimerization of F-ATP synthase, which could be rescued by both expression of *ATP20* and of *ATP5L* (which encodes human subunit g) (Fig. 3.3.2A). As for wild-type yeast (compare with Fig. 3.3.1), PGO increased the CRC of  $\Delta$ *ATP20* mitochondria reexpressing *ATP20*, while replacement with *ATP5L* totally prevented the desensitizing effects of PGO, which rather decreased the CRC (Fig. 3.3.2B) as also seen in permeabilized HEK293 cells. These results suggest that subunit g confers species-specificity to the effects of PGO on the PTP.

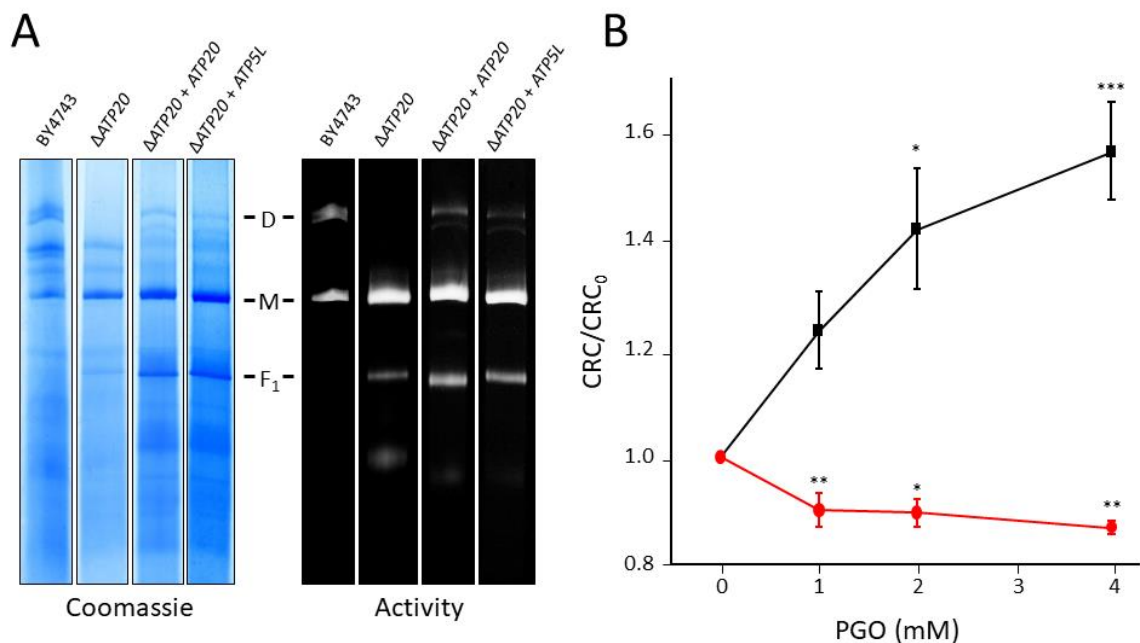


**Fig. 3.3.2. Expression of human subunit g in yeast prevents the inhibitory effect of PGO.** **A**, yeast mitochondrial proteins of the indicated genotypes were separated by BN-PAGE as described in “Materials and Methods” and revealed with Coomassie blue and in-gel activity staining for ATP hydrolysis to identify dimers (D), monomers (M) and F<sub>1</sub> sector of F-ATP synthase. **B**, CRC of YM from  $\Delta$ *ATP20* + *ATP20* (black trace) and  $\Delta$ *ATP20* + *ATP5L* (red trace) pretreated with the indicated concentrations of PGO. Data are expressed as CRC/CRC<sub>0</sub> ratio, in which CRC<sub>0</sub> refers to the CRC of DMSO-treated mitochondria. Results are mean  $\pm$  s.e.m. of at least three independent experiments. \**P*<0.05 vs vehicle, \*\**P*<0.01 vs vehicle, \*\*\**P*<0.001 vs vehicle. One-way ANOVA was used for statistical analysis. All sets of lanes in panel A are from the same gels.

### 3.4 Arginine 107 of yeast subunit g mediates the sensitivity of PTP to PGO

Subunits e and g are essential for dimerization of yeast F-ATP synthase and cristae generation, and deletion of either subunit leads to dimer and cristae disruption (254,259,262–264,267,269). The e and g subunits are also important for regulation of the Ca<sup>2+</sup> sensitivity of yeast PTP, which undergoes desensitization after their genetic ablation (158). The fact that their contribution has been so far addressed in null mutants inevitably limits our understanding of their putative function in PTP formation. Conversely, site-directed mutagenesis of specific residues that does not alter

assembly, subunit composition and activity of the enzyme allows to interrogate their role in PTP formation and regulation.

Both subunit e and g possess a single conserved arginine residue (R8 and R107 in the yeast sequence, respectively). To test whether these residues are involved in PTP modulation by PGO, we first analyzed deletion mutants of subunit g ( $\Delta ATP20$ ) and of subunit e ( $\Delta TIM11$ ). The effect of PGO was completely abolished in the  $\Delta ATP20$  deletion mutant lacking subunit g (Fig. 3.4A) and a similar, albeit somewhat smaller effect, was observed with the  $\Delta TIM11$  mutant lacking subunit e (Fig. 3.4B). In order to explore the role of individual arginines, we generated specific point mutants and tested their CRC. Remarkably, the R107A mutation in subunit g dramatically blunted the effect of PGO (Fig. 3.4C) while the R8A mutation in subunit e was ineffective, with an identical sensitivity to PGO as the wild-type species (Fig. 3.4D). This result was puzzling because subunit e only has one conserved arginine in position 8 and therefore, we would have expected the same result following either deletion of the subunit e gene or the R8A mutation. This apparent contradiction was resolved by analysis of the expression of the e and g subunits in the  $\Delta ATP20$  and  $\Delta TIM11$  mutants. Indeed, deletion of the *ATP20* gene led to the expected disappearance of subunit g only,

while deletion of the *TIM11* gene caused the disappearance of both subunit e and g (Fig. 3.4E). Both R8 and R107 are located next to the GxxxG dimerization domains (Figs. 3.4F), and we suspect that this is the region where the PTP forms.

Previous studies have focused on the structure-function relationship of glyoxals of different structure (281–284) rather than on the identification of the reactive residue(s). Here we had been able to identify R107 of subunit g as the unique target of PGO in yeast.

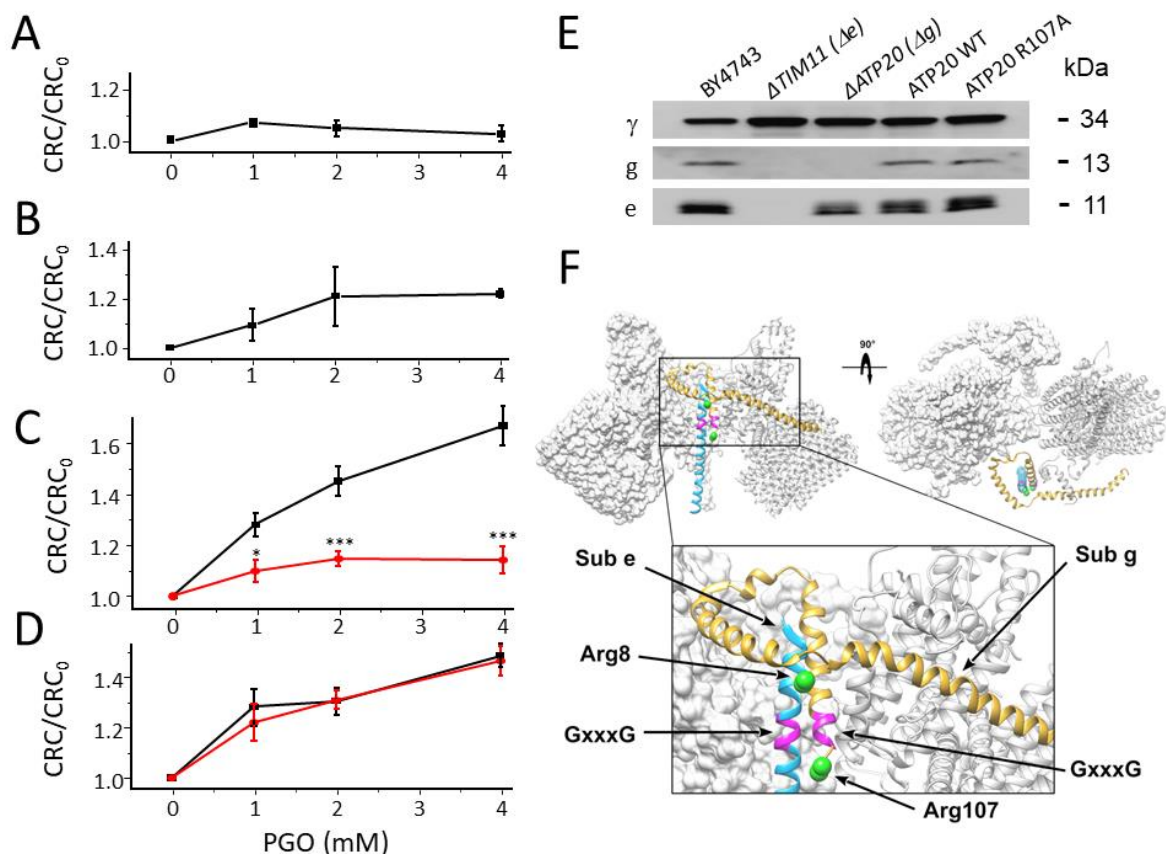


**Fig. 3.4. R107 of yeast F-ATP synthase subunit g mediates the effects of PGO on the CRC.** Experimental conditions were as in Fig. 3.3.1B. **A**, CRC of YM from  $\Delta$ ATP20 pretreated with the indicated concentrations of PGO. **B**, CRC of YM from  $\Delta$ TIM11 pretreated with the indicated concentrations of PGO. **C**, CRC of YM from ATP20 WT control (black trace) and ATP20 R107A (red trace) pretreated with the indicated concentrations of PGO. \* $P < 0.05$  vs ATP20 WT, \*\*\* $P < 0.001$  vs ATP20 WT. Two-way ANOVA was used for statistical analysis. One-way ANOVA had been used for the statistical analysis, revealing that PGO did show any significance at all indicated concentration treatment comparing to vehicle treatment in YM from ATP20 R107A. **D**, CRC of YM from TIM11 WT control (black trace) and TIM11 R8A (red trace) pretreated with the indicated concentrations of PGO. In **A-D**, data are expressed as ratio to DMSO-treated mitochondria. Means  $\pm$  s.e.m. of at least three independent experiments are shown. **E**, isolated yeast mitochondria of the indicated genotypes were evaluated by western blotting for  $\gamma$ , *TIM11* and *ATP20* subunit content after SDS-PAGE separation of 50  $\mu$ g of protein per lane. **F**, overview of F-ATP synthase F<sub>0</sub> dimer (PDB code 6B2Z) with frontal and top views highlighting the relative position of subunits g (yellow) and e (light blue) (with help of Giovanni Minervini). Putative GxxxG dimerization motifs is represented in purple. The structure is shown in standard view (front) and after a 90° rotation around the z-axis and two F<sub>0</sub> monomers are presented. The boxed region is expanded in the lower part of the panel. Green spheres represent the position of R8 of subunit e and R117 of subunit g, which are predicted to localize at the border of the GxxxG domains. These positions were derived by comparing data from 3D structure (PDB: 6B2Z) with secondary structure predictions.



### **3.5 Arginine 8 of yeast subunit e is required for dimerization of F-ATP synthase**

Subunits e and g of yeast F-ATP synthase are not essential for mitochondrial respiratory competence while they are necessary for the formation of F-ATP synthase dimers and maintenance of cristae morphology (228–230,254,262–265). In yeast  $\Delta TIM11$  mutant, *ATP20* is unable to be detected, while the subunit e is present in  $\Delta ATP20$  (262,319). We propose the charged amino acids may play a role in the interactions between subunits that favor their stability.

#### **3.5.1 Substitution of Arg 8 in subunit e affects dimerization of the F-ATP synthase complex**

Arg 8 (R8) of subunit e, encoded by yeast *TIM11* gene, is the only one positively charged arginine conserved across species. We substituted *TIM11* R8 with alanine (A) or glutamic acid (E) using site-directed mutagenesis. Mitochondria from *TIM11* R8A and *TIM11* R8E mutants were assessed for F-ATP synthase supramolecular structure and compared to the  $\Delta TIM11$  mutant lacking subunit e. The presence of monomers and dimers was examined in the mitochondrial extracts, which were obtained with increasing digitonin-to protein ratios and were subjected to blue native electrophoresis (BN-PAGE), then stained by Coomassie blue or tested for in-gel ATPase activity. As expected, the null mutant  $\Delta TIM11$  displayed only monomers whatever the digitonin-to protein ratio used, while in the *S. cerevisiae* wild type strain BY4743 and in  $\Delta TIM11$  re-expressing wild-type *TIM11* genotype dimers were well detectable along with monomers at all digitonin concentrations. Conversely, in the mitochondrial extracts from *TIM11* R8A and *TIM11* R8E mutants the dimers were evident only at low, but not at high digitonin-to protein ratios, which favor dimer dissociation into monomers after the separation by BN-PAGE (Fig. 3.5.1A,B). In Panel C the dimer/monomer ratio of the different genotypes is reported, demonstrating that in the *TIM11* R8A and *TIM11* R8E mutants dimerization status was dramatically affected. In these mutants, like in the wild-type genotype, subunit e was found mainly associated to the dimers, as assessed by 2D-SDS-PAGE and Western blotting of monomers and dimers cut out from BN gel (Fig. 3.5.1D). This finding further supports the interpretation that the low dimer/monomer ratio found in the *TIM11* R8A and *TIM11* R8E mutants arose from an increased tendency of the dimers to dissociate when extracted with detergents and/or run in BN gels, rather than from a defect in assembly of the

mutated subunit e. All together these results show that the single amino acid substitutions of Arg 8 of yeast subunit e affected dimerization of the F-ATP synthase complex.

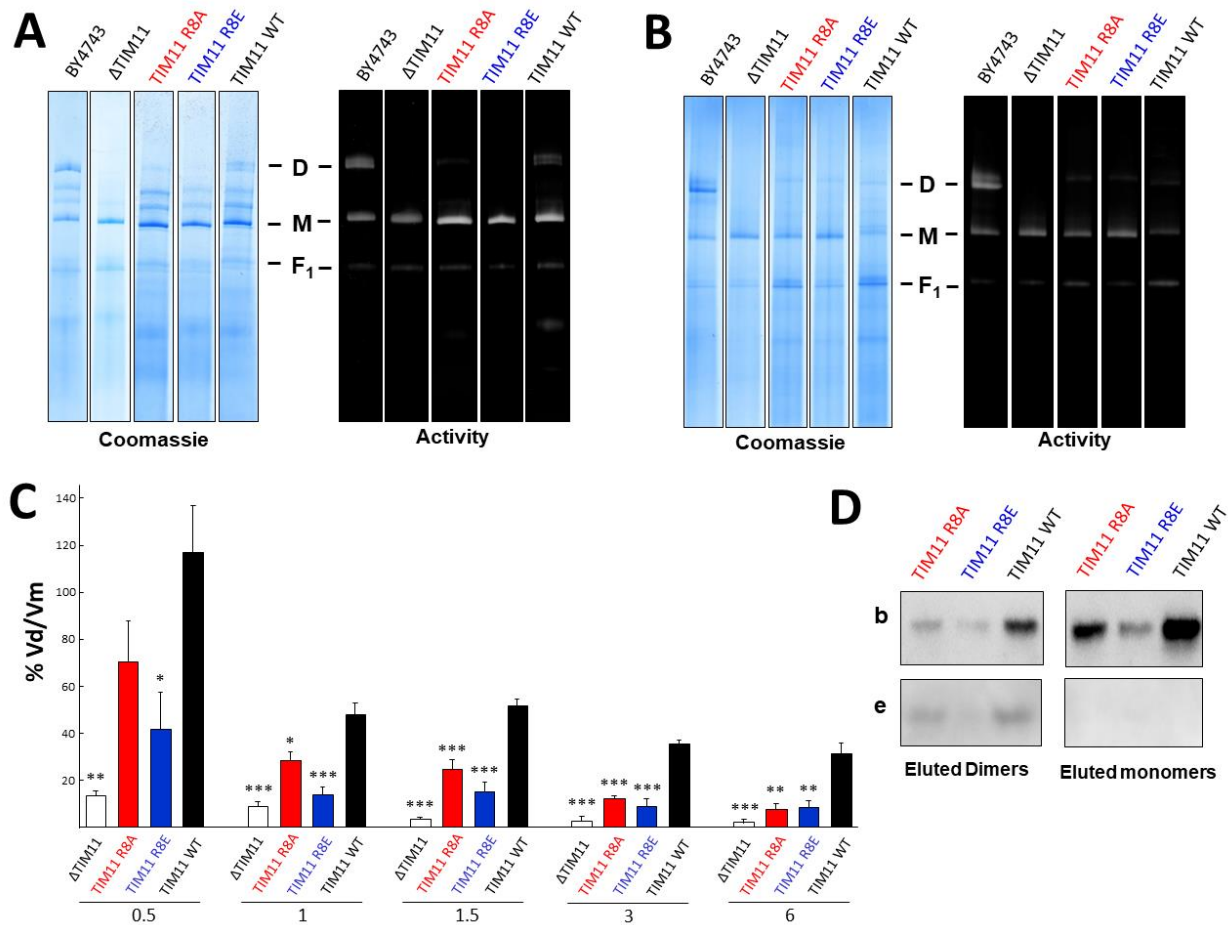


**Fig. 3.5.1. Single amino acid substitutions of Arg 8 of yeast subunit e affect F-ATP synthase dimerization.** **A-B**, mitochondrial protein extracts with 1.5 g/g or 0.5 g/g (digitonin/protein), respectively, from the indicated genotypes were subjected to BN-PAGE to separate the dimers (D), monomers (M) and F<sub>1</sub> sector of F-ATP synthase identified by Coomassie blue staining and in-gel activity staining. **C**, histograms refer to dimer/monomer ratios (expressed in %) obtained by densitometry analysis of gel activity staining after indicated digitonin extraction and BN-PAGE separation. Data are an average  $\pm$  S.E.M. of at least three independent experiments. \* $p < 0.05$  vs TIM11WT, \*\* $p < 0.01$  vs TIM11WT, \*\*\* $p < 0.001$  vs TIM11WT. One-way ANOVA were used for statistical analysis. **D**, monomers and dimers separated from the 0.5g/g digitonin extracts were cut out from BN gel and eluted. The elution was subjected to 2D SDS-PAGE and Western blotting against subunit e. Plots are representative of three independent experiments.

### 3.5.2 Ablation or loss of subunit g affects accommodation of subunit e in the F-ATP synthase dimers

As already mentioned in the Introduction, CuCl<sub>2</sub> treatment leads to dimer formation even in the null mutants lacking subunit e ( $\Delta TIM1$ ) or subunit g ( $\Delta ATP20$ ), by stabilizing pre-existing dimers through copper cross-linking, which is resistant to digitonin extraction and detectable in BN gels (158,253,257,260). Consistently, after cross-linking with copper dimer/monomer ratios similar to those of the wild-type genotypes were observed in the null mutants  $\Delta TIM11$  and  $\Delta ATP20$ , as well

as in TIM11 R8A and TIM11 R8E mutants (Fig. 3.5.2A). To assess the abundance of subunit e in the monomers and dimers after CuCl<sub>2</sub> treatment, the BN gels were directly subjected to immunoblotting against subunit e or  $\gamma$  (Fig. 3.5.2B). The levels of subunit  $\gamma$  were consistent with the protein abundance detected in BN gels, but not those of subunit e. As expected, in the wild type strain BY4743 and in the  $\Delta$ TIM11 re-expressing wild type subunit e, subunit e was only present in the dimers, while in the null mutant  $\Delta$ TIM11 subunit e was not detectable both in monomers and dimers. Interestingly, in the mutants TIM11 R8A and TIM11 R8E appreciable quantity of subunit e was found in the dimers, but also in the monomers, while in the null mutant  $\Delta$ ATP20 almost all subunit e was only observed in the monomers. These findings exclude that Cu<sup>2+</sup> treatment forms F-ATP synthase dimers by subunit e homodimers in all genotypes, in accordance with the recent genetic evidence that Cys23 of subunit a is responsible for Cu<sup>2+</sup>-dependent dimer formation in yeast (320). Moreover, our results demonstrate that deletion of ATP20 affects the proper assembly of subunit e, which remains associated to the F-ATP synthase monomers even after Cu<sup>2+</sup> cross-linking. The presence of subunit e in monomers of the mutants TIM11 R8A and TIM11 R8E may be due to a partial loss of subunit g, which is essential for properly accommodate subunit e in the F-ATP synthase complex.

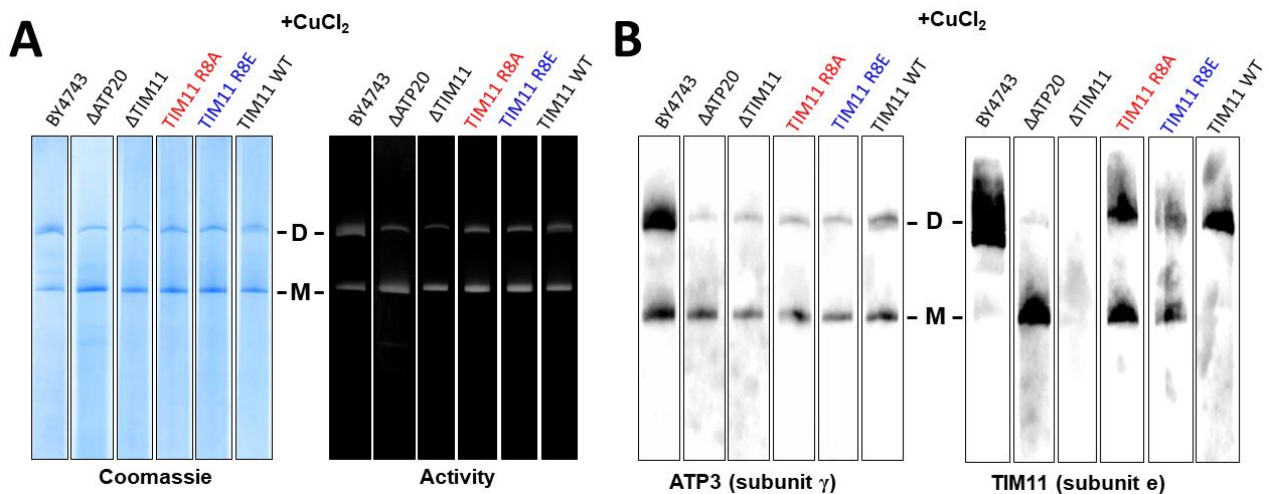


**Fig. 3.5.2. Ablation or loss of subunit g affects accommodation of subunit e in F-ATP synthase dimers.** **A**, after pre-treatment with CuCl<sub>2</sub> as described in “Materials and Methods”, mitochondrial protein extracts with 1.5 g/1 g (digitonin/protein) from the indicated genotypes were separated by BN-PAGE and stained with Coomassie blue or identified by in-gel activity staining. **B**, BN-PAGE gels as described in panel A were subjected to immunoblotting to assess the abundance of  $\gamma$  or e subunit in dimers (D) and monomers (M).

### 3.5.3 Glu 83 of subunit g interacts with Arg 8 of subunit e

Subunit g possesses two glutamic acids that are the only two negatively charged amino acids well conserved in the subunit g (Fig. 3.5.3A). The predicted positions of TIM11 R8 and ATP20 E83 or

E102 are reported in Fig. 3.5.3B. To investigate the putative glutamic residues of subunit g interacting with TIM11 R8, we generated the point mutants in the position of E83 and E102 of subunit g. We found that dimer/monomer ratio detected by digitonin extraction and BN gels in mitochondria from the mutant ATP20 E83A was significantly decreased, while the mutation of ATP20 R102A was ineffective (Fig. 3.5.4A-C). Remarkably, re-expression of TIM11 R8E and ATP20 E83K in  $\Delta TIM11 \Delta ATP20$  mutant was able to rescue the dimer formation, as re-expression of TIM11 WT and ATP20 WT in  $\Delta TIM11 \Delta ATP20$  mutant (Fig. 3.5.4D). These data indicate that ATP20 E83 participates in the interaction with TIM11 R8, which favors their incorporation into F-ATP synthase and the dimerization of F-ATP synthase.

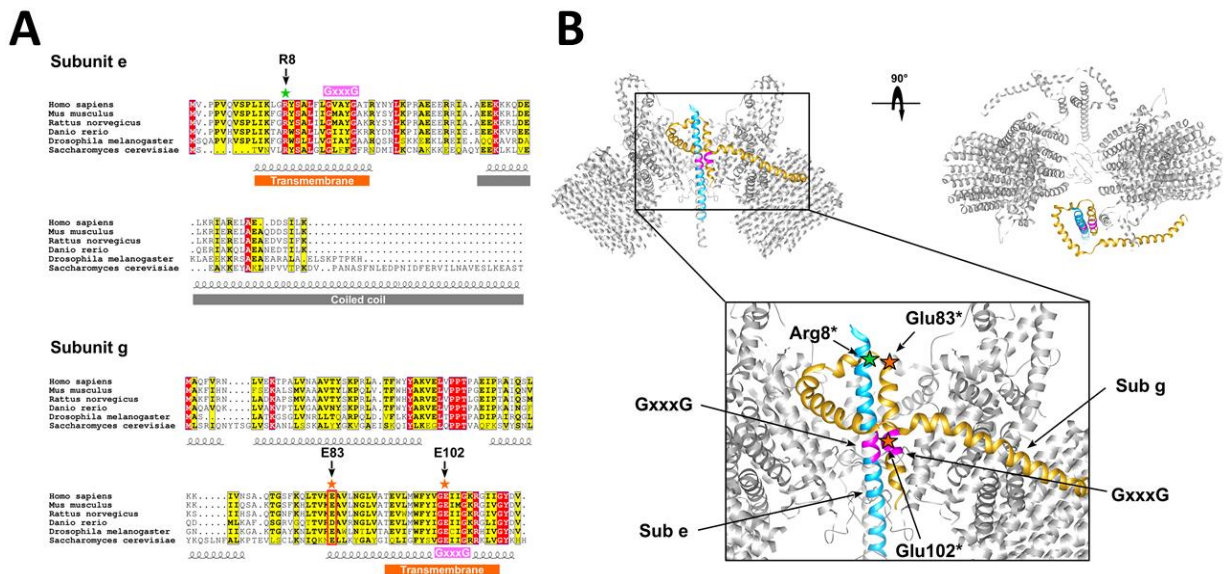


**Fig. 3.5.3. Sequence and structure of yeast subunit e and g.** **A**, amino acid sequence comparison of F-ATP synthase subunit e and subunit g across species. **B**, overview of F-ATP synthase  $F_0$  dimer (PDB code 6B2Z) frontal and top views highlighting the relative position of subunits g (yellow) and e (light blue). Putative GxxxG dimerization motifs is marked in purple. Stars represent putative positions of Arg 8 of subunit e, Glu 83 and Glu 102 of subunit g in the zoomed view. These positions were kindly provided by Dr. Giovanni Minervini (University of Padova).

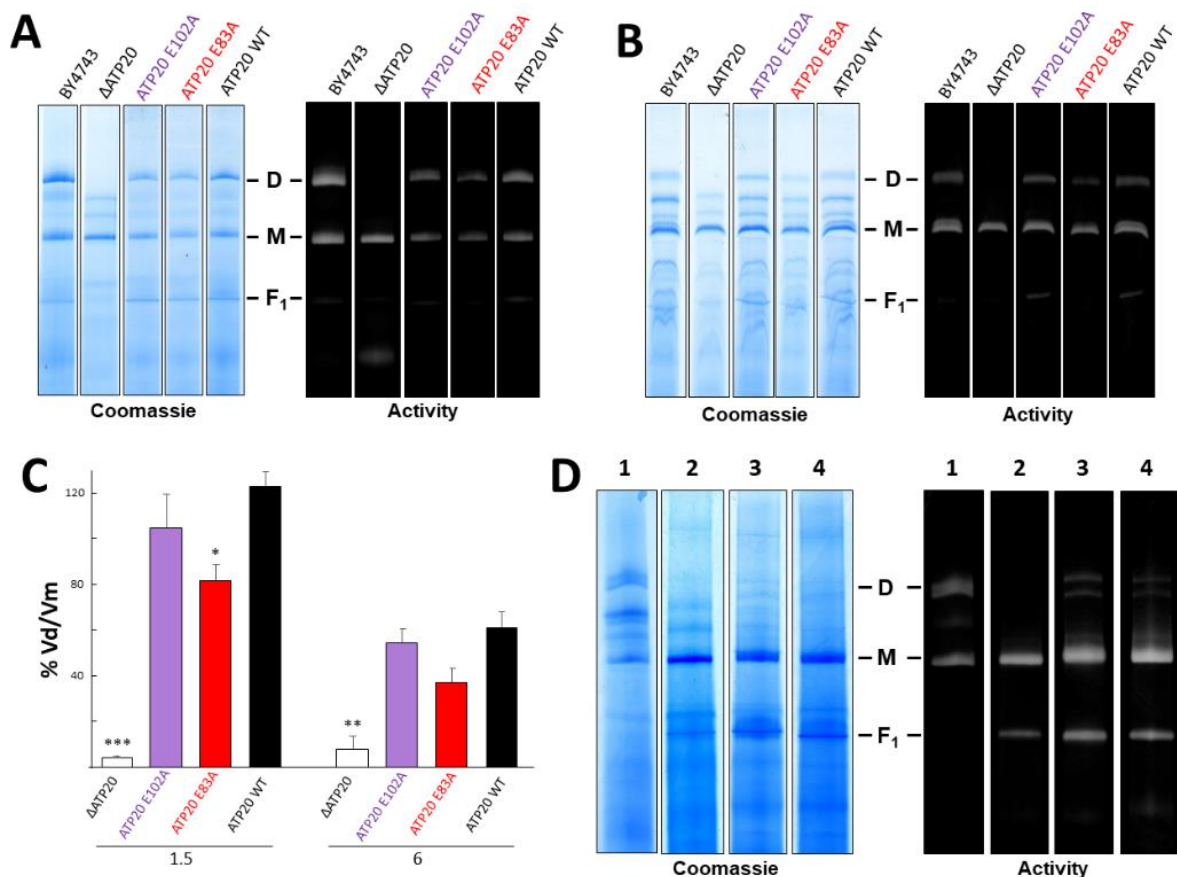


**Fig. 3.5.4. Glu 83 of subunit g interacts with Arg 8 of subunit e favoring F-ATP synthase dimerization.** A-B, mitochondrial protein extracts with 1.5 g/g (A) or 6 g/g (B) (digitonin/protein), respectively, from the indicated genotypes were subjected to BN-PAGE to separate the dimers (D), monomers (M) and F<sub>1</sub> sector of F-ATP synthase identified by Coomassie blue staining and in-gel activity staining. C, histograms refer to dimer/monomer ratios (expressed in %) of indicated genotypes obtained by densitometry of in-gel activity staining after indicated digitonin extraction and BN-PAGE separation. Data are an average  $\pm$  S.E.M. of at least three independent experiments. \* $p < 0.05$  vs ATP20WT, \*\* $p < 0.01$  vs ATP20WT, \*\*\* $p < 0.001$  vs ATP20WT. One-way ANOVA were used for statistical analysis. D, experimental conditions were as described in Fig. 1A. Lanes 1-4 represent the genotypes BY4743,  $\Delta$ TIM11 $\Delta$ ATP20 mutant (DKO),  $\Delta$ TIM11 $\Delta$ ATP20 mutant re-expressing TIM11 R8E and ATP20 E83K (DKO+TIM11 R8E +ATP20 E83K),  $\Delta$ TIM11 $\Delta$ ATP20 mutant re-expressing TIM11 WT and ATP20 WT (DKO+TIM11 WT +ATP20 WT), respectively. Plots are representative of at least three independent experiments.

### 3.5.4 Expression level of subunits e and g in the mutants

We next examined the abundance of several F-ATP synthase subunits by Western blotting in cell lysates and mitochondria from all genotypes. The analyses of cells lysates revealed that the mutants TIM11 R8A and TIM11 R8E, as well as the mutants ATP20 E83A and ATP20 E102A retained the expression levels of subunits g and e, as compared to subunit b and taken as control. These results indicated that the significant reduction in the levels of dimeric F-ATP synthase complexes observed in these mutants did not significantly alter the expression levels of subunits e and g in cells and mitochondrial lysates (Fig. 3.5.5).

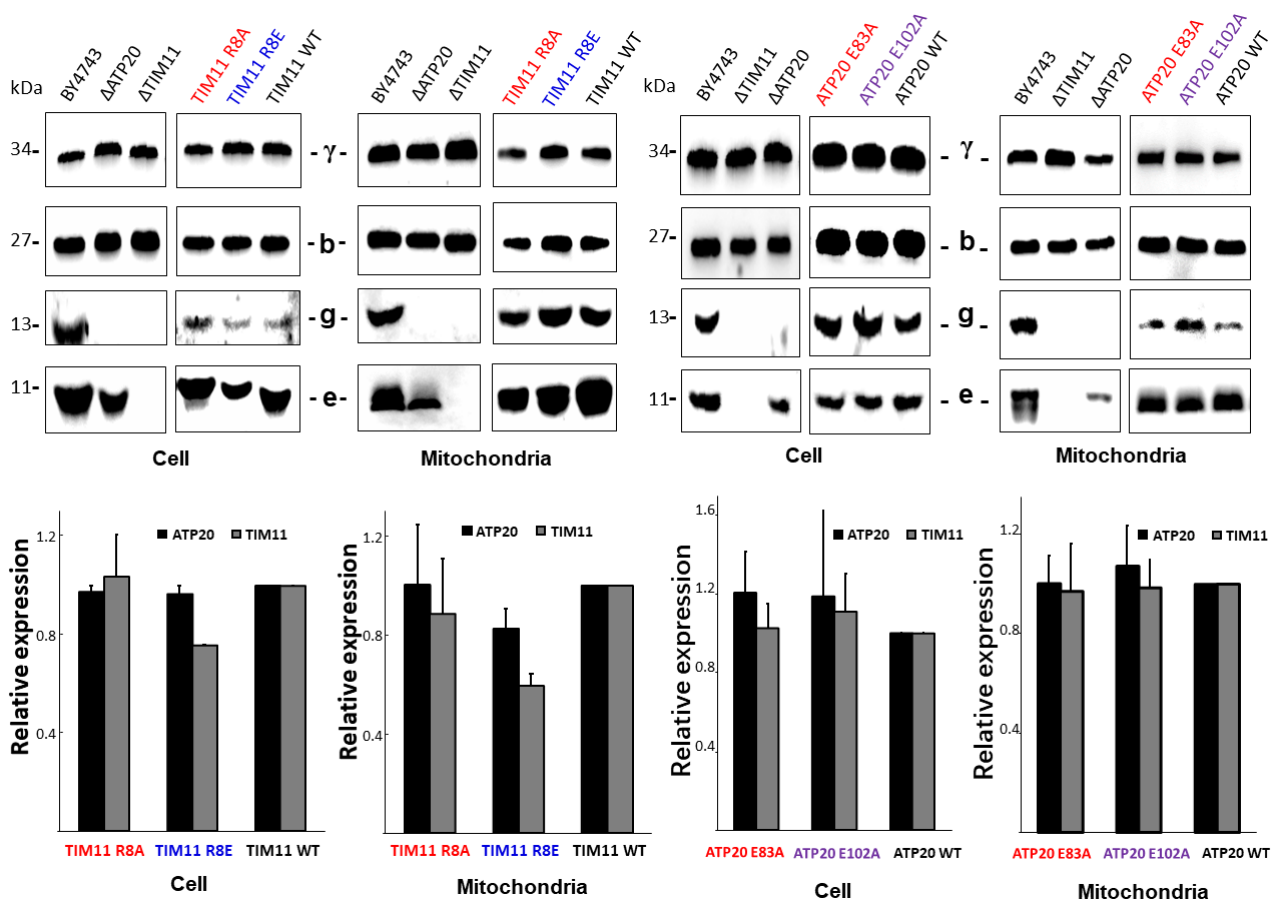


**Fig. 3.5.5. Expression level of subunits e and g in the mutants.** Total or mitochondrial proteins from indicated genotypes were separated by SDS-PAGE and analyzed by Western blotting. Plots are representative of at least three independent experiments. Graphs show the mean  $\pm$  s.e.m. of at least three independent experiments. Values refer to the relative densitometry values of TIM11 or ATP20 respect to subunit b and normalized to those of BY4743. \* $p < 0.05$  vs TIM11WT, \*\* $p < 0.01$  vs TIM11WT, \*\*\* $p < 0.001$  vs TIM11WT; \* $p < 0.05$  vs ATP20WT, \*\* $p < 0.01$  vs ATP20WT. One-way ANOVA were used for statistical analysis.

### 3.5.5 Substitutions of Arg 8 of subunit e affect the channel features

We finally assessed the channel properties of TIM11 R8A and TIM11 R8E. Dimers cut out from BN-PAGE were eluted, and reconstituted into planar lipid bilayers followed by detection of their electrophysiological properties. Compared to the enzyme from WT mitochondria, dimers from the TIM11 R8A and TIM11 R8E mutants displayed strikingly smaller channel activities with a decrease of both the relative  $|P(f)|$  area (curve under the power spectrum) and of the mean currents (Fig. 3.5.6). These results suggest that Arg 8 of subunit e might participate in generating the full conductance channel, probably through the interaction with neighbor subunit(s) like subunit g.

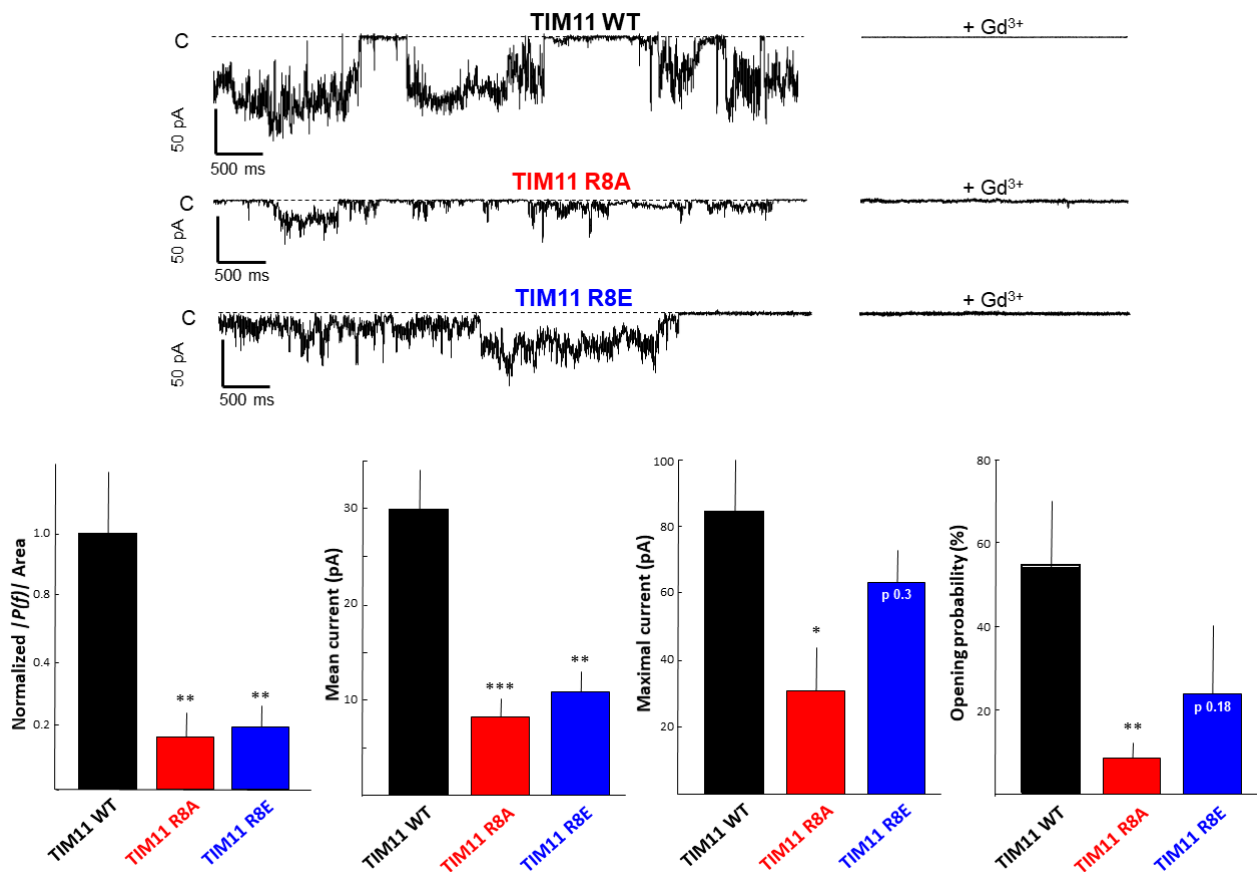


**Fig. 3.5.6. Substitutions of Arg 8 of subunit e affects channel features of the PTP in planar lipid bilayers.** **A**, dimers and monomers from BN-PAGE gels as described in Fig. 1B were cut and eluted. The elution was subjected to Western blotting. Plots are representative of three independent experiments. **B**, electrophysiological characterizations of F-ATP synthase dimers reconstituted in planar lipid bilayers. Dimers from BN-PAGE gels as described in Fig. 1B were cut and eluted for planar lipid bilayers. *Upper panels*, representative current traces elicited after insertion of purified dimeric F-ATP synthase from TIM11 WT, TIM11 R8A, and TIM11 R8E into planar lipid bilayer following the additions of 3 mM  $\text{Ca}^{2+}$  (to the *trans* side), plus 100  $\mu\text{M}$  PhAsO and 5  $\mu\text{M}$   $\text{Cu}(\text{OP})_2$  (to both sides). Channel activity was abolished by the addition of 1 mM  $\text{Gd}^{3+}$ .  $V_{\text{hold}} = -60$  mV. Dotted lines indicate the closed state of the channel (0 pA). *Lower panels*, Average relative  $|P(f)|$  area, mean current, maximal current and open probability of the indicated genotypes. Data are mean  $\pm$  s.e.m. of at least three independent experiments. \* $P < 0.05$  vs TIM11WT, \*\* $P < 0.01$  vs TIM11WT, \*\*\* $P < 0.001$  vs TIM11WT. Statistical analysis was performed with ANOVA. With the help of Andrea Carrer.

Taken together, these observations suggest that Arg 8 of TIM11 favors the dimerization of F-ATP synthase, most likely through the electrostatic interaction with Glu 83 of ATP20.

## **4 ACKNOWLEDGMENT**

I would like to thank all the members of the Bernardi lab for their help and support during my PhD program. Special thanks to Michela Carraro for her guidance and training into the fascinating world of yeast and its use to unravel the mysteries of the PTP. And thanks to my supervisor Prof. Bernardi for the opportunity to study mitochondria and the PTP and all the advice for my PhD training. Thanks to all the people who have kindly helped me.



# 5 APPENDIX

## 5.1 Publication 1

**Guo, L.**, Carraro, M., Sartori, G., Minervini, G., Eriksson, O., Petronilli, V., Bernardi, P. Arginine 107 of yeast ATP synthase subunit g mediates sensitivity of the mitochondrial permeability transition to phenylglyoxal. *J. Biol. Chem.* 293, 14632–14645 (2018).



## 5.2 Publication 2

Giorgio, V.\*, **Guo, L.\***, Bassot, C., Petronilli, V. & Bernardi, P. Calcium and regulation of the mitochondrial permeability transition. *Cell Calcium.* 70, 56–63 (2018). (\*Co-first author).



# Arginine 107 of yeast ATP synthase subunit g mediates sensitivity of the mitochondrial permeability transition to phenylglyoxal

Received for publication, June 16, 2018, and in revised form, July 27, 2018. Published, Papers in Press, August 9, 2018, DOI 10.1074/jbc.RA118.004495

Lishu Guo<sup>†1</sup>, Michela Carraro<sup>‡</sup>, Geppo Sartori<sup>‡</sup>, Giovanni Minervini<sup>‡</sup>,  Ove Eriksson<sup>§</sup>,  Valeria Petronilli<sup>‡</sup>, and  Paolo Bernardi<sup>‡2</sup>

From the <sup>†</sup>Consiglio Nazionale delle Ricerche Institute of Neuroscience and Department of Biomedical Sciences, University of Padova, Padova 35131, Italy and the <sup>§</sup>Department of Biochemistry and Developmental Biology, Faculty of Medicine, University of Helsinki, Helsinki 00290, Finland

Edited by John M. Denu

Modification with arginine-specific glyoxals modulates the permeability transition (PT) of rat liver mitochondria, with inhibitory or inducing effects that depend on the net charge of the adduct(s). Here, we show that phenylglyoxal (PGO) affects the PT in a species-specific manner (inhibition in mouse and yeast, induction in human and *Drosophila* mitochondria). Following the hypotheses (i) that the effects are mediated by conserved arginine(s) and (ii) that the PT is mediated by the F-ATP synthase, we have narrowed the search to 60 arginines. Most of these residues are located in subunits  $\alpha$ ,  $\beta$ ,  $\gamma$ ,  $\epsilon$ ,  $a$ , and  $c$  and were excluded because PGO modification did not significantly affect enzyme catalysis. On the other hand, yeast mitochondria lacking subunit  $g$  or bearing a subunit  $g$  R107A mutation were totally resistant to PT inhibition by PGO. Thus, the effect of PGO on the PT is specifically mediated by Arg-107, the only subunit  $g$  arginine that has been conserved across species. These findings are evidence that the PT is mediated by F-ATP synthase.

The mitochondrial PT<sup>3</sup> is a Ca<sup>2+</sup>-dependent permeability increase of the inner membrane (1). The PT is mediated by opening of a regulated channel, the permeability transition pore (PTP), which coincides with the mitochondrial megachannel (MMC) identified by electrophysiology (2, 3). The mammalian PTP/MMC displays a range of conductance states, which can be as high as 1.2 nanosiemens, corresponding to a pore with a diameter of about 2 nm. The channel also visits lower conductance states that may be the basis for selective permeation of

small solutes (4). Depending on open time and channel size, the PTP/MMC can participate in Ca<sup>2+</sup> homeostasis (short-term and/or low-conductance openings that provide a pathway for fast Ca<sup>2+</sup> release) (5) or cell death (long-lasting and/or high-conductance openings that cause energy dissipation, membrane permeabilization to solutes, matrix swelling, and outer membrane rupture with release of proapoptotic proteins) (6). The mammalian PTP is modulated by binding of cyclophilin D (CyPD), which favors pore opening after matrix accumulation of Ca<sup>2+</sup>, an essential permissive factor (7). Regulation of the PTP is complex; opening is favored by CyPD, P<sub>i</sub>, and oxidative stress, whereas it is inhibited by matrix H<sup>+</sup>, Mg<sup>2+</sup>, adenine nucleotides, and cyclosporin A, which displaces CyPD and desensitizes the pore to Ca<sup>2+</sup> (8). Although the molecular components of the PTP were unknown, a few discrete regulatory sites have been defined in the 1990s through the use of modifiers of SH groups and of relatively specific histidine and arginine reagents (9–15).

The most recent hypothesis about the molecular nature of the PTP/MMC is that it originates from a conformational change occurring on F-ATP synthase when Mg<sup>2+</sup> is replaced by Ca<sup>2+</sup> at the catalytic site. The conformational change would be transmitted to the inner membrane by the peripheral stalk, causing pore formation at the interface between enzyme monomers (7). Whether and how the F-ATP synthase can form channels is the matter of controversy. The hypothesis is supported by genetic manipulation of F-ATP synthase (16, 17); by electrophysiological measurements of the bovine, human, yeast, and *Drosophila* enzymes (17–20); and by site-directed mutagenesis of specific F-ATP synthase residues (21, 22), whereas it has been questioned by studies based on genetic ablation of subunits  $c$ ,  $b$ , and OSCP (23, 24) (see Bernardi and Lippe (25) for a recent discussion that covers this controversy and offers an explanation for the apparent discrepancies).

The PTP response to Ca<sup>2+</sup> is modulated by arginine residues, which upon modification with glyoxals can cause PTP sensitization or desensitization, depending on the specific reagent (12–15). Previous studies have focused on the structure–function relationship of glyoxals of different structure rather than on the identification of the reactive residue(s) (12–15). Here, we have found that the effect of phenylglyoxal (PGO) on the PTP differs between species and used sequence comparison

This work was supported by AIRC Grant IG17067 (to P.B.) and Fondazione Leducq Grant 16CVD04 (to P.B.). The authors declare that they have no conflicts of interest with the contents of this article.

<sup>1</sup> Supported by a fellowship from the China Scholarship Council. This work is in partial fulfillment of the requirements for the Ph.D. for this author at the Department of Biomedical Sciences, University of Padova.

<sup>2</sup> To whom correspondence should be addressed. Tel.: 39-049-827-6365; Fax: 39-049-827-6049; E-mail: [bernardi@bio.unipd.it](mailto:bernardi@bio.unipd.it).

<sup>3</sup> The abbreviations used are: PT, mitochondrial permeability transition; AGE, advanced glycation end-products; CRC, Ca<sup>2+</sup> retention capacity; CyPD, cyclophilin D; MGO, methylglyoxal; MLM, mouse liver mitochondria; MMC, mitochondrial megachannel; PGO, phenylglyoxal; PTP, permeability transition pore; YM, yeast mitochondria; MGO, methylglyoxal; BisTris, 2-[bis(2-hydroxyethyl)amino]-2-(hydroxymethyl)propane-1,3-diol; ANOVA, analysis of variance.

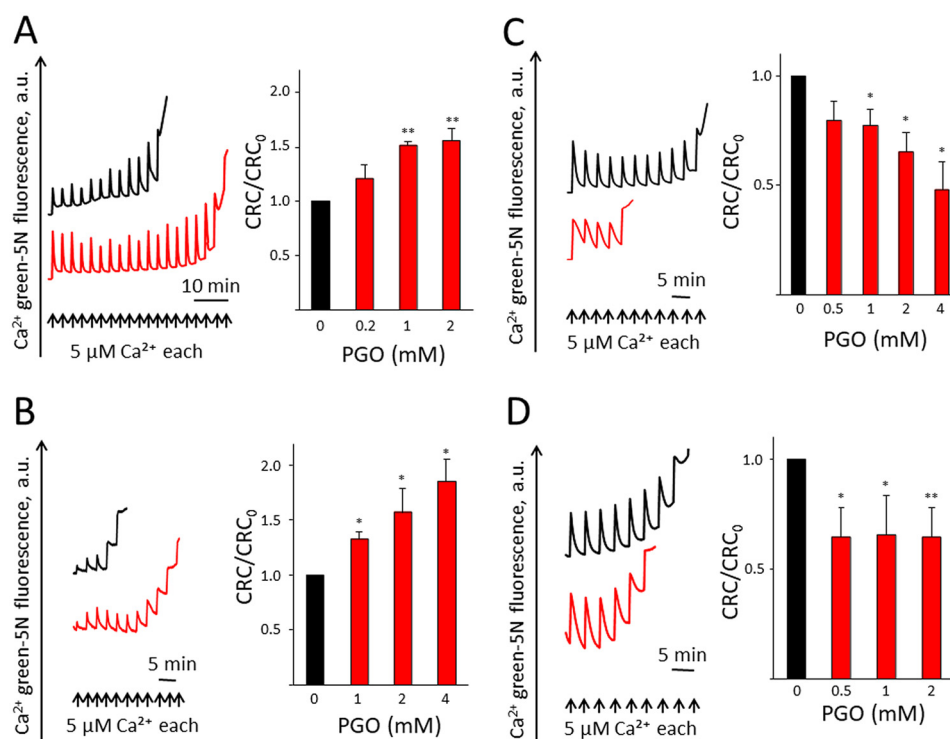


**Figure 1. The sensitivity of PTP to PGO is conserved across species.** Isolated mitochondria or permeabilized cells were pretreated with vehicle (DMSO) or PGO and resuspended in the CRC assay buffer as described under "Experimental Procedures." A, CRC of MLM pretreated with DMSO (black trace) or 1 mM PGO (red trace). B, CRC of isolated yeast mitochondria pretreated with DMSO (black trace) or 4 mM PGO (red trace). C, CRC of permeabilized HEK293 cells pretreated with DMSO (black trace) or 4 mM PGO (red trace). D, CRC of permeabilized *Drosophila* S<sub>2</sub>R<sup>+</sup> cells pretreated with DMSO (black) or 1 mM PGO (red trace). Representative traces are shown. Bars, CRC of DMSO- (black) or PGO-pretreated (red) isolated mitochondria or permeabilized cells. CRC of DMSO-treated mitochondria was set as 1 unit. Results are mean  $\pm$  S.E. (error bars) of at least three independent experiments. \*,  $p < 0.05$  versus vehicle; \*\*,  $p < 0.01$  versus vehicle. One-way ANOVA was used for statistical analysis.

and mutagenesis to identify the unique arginine of F-ATP synthase subunit g (of a total of 60 conserved residues) that mediates the PTP-modulating effect of PGO in yeast. This finding is a step forward in the molecular understanding of PTP regulation and further supports the hypothesis that the PTP forms from F-ATP synthase.

## Results

### The effects of PGO on the PTP have been conserved but differ between species

Consistent with the effect of PGO on the PTP of rat liver mitochondria, PGO desensitized the PTP to Ca<sup>2+</sup> in mouse liver mitochondria (MLM) (Fig. 1A) as well as in mitochondria from *Saccharomyces cerevisiae* in the presence of ETH129, a selective ionophore that allows Ca<sup>2+</sup> equilibration across the inner membrane in yeast mitochondria (Fig. 1B). In either case, the desensitizing effect can be appreciated from the increased Ca<sup>2+</sup> retention capacity (CRC) of PGO-treated mitochondria (Fig. 1, A and B). Unexpectedly, PGO caused instead sensitization of the pore to Ca<sup>2+</sup> in permeabilized human HEK293 (Fig. 1C) and *Drosophila* S<sub>2</sub>R<sup>+</sup> cells (Fig. 1D). Sensitization of PTP opening by PGO in human and *Drosophila* cells was not due to digitonin permeabilization, as it was also observed in mitochondria isolated from these cells (results not shown). These findings indicate that the ability to modulate the PTP by PGO has been conserved across species. Under the assumptions (i) that the observed differences depend on specific

features of the PTP rather than on the existence of species-specific reactive sites and (ii) that these sites are located on the F-ATP synthase, we narrowed the search of the reactive arginine(s) from 135 (yeast) to 60 arginines that are conserved between F-ATP synthases of *S. cerevisiae*, *Homo sapiens*, *Mus musculus*, and *Drosophila melanogaster* (the positions of these residues in the yeast, human, and mouse enzymes are reported in Table 1).

### Chemical modification by PGO does not affect catalytic activity, oligomycin sensitivity, assembly, and subunit composition of F-ATP synthase

Due to the large number of arginine residues and their specific relevance to enzymatic activity of F-ATP synthase, we assessed whether treatment with PGO affects the catalytic properties of the enzyme in MLM and yeast mitochondria (YM). In MLM, a trend toward a slight inhibition of ATP hydrolysis was observed (but this did not reach statistical significance), and the catalytic activity maintained its sensitivity to oligomycin (Fig. 2A), and respiratory stimulation by ADP was not affected (Fig. 2B). Similarly, in YM, both ATP hydrolytic activity and respiratory stimulation by ADP were unaffected by PGO (Fig. 2, C and D). Blue native gel separation and in-gel activity staining after digitonin extraction did not reveal any major effect of PGO on F-ATP synthase oligomeric state in MLM (Fig. 2E). In these experiments, we used MLM because they are easy to purify and because the mouse enzyme is virtu-

## Subunit g Arg-107 of F-ATPase regulates PTP

**Table 1**

Number and positions of arginine residues conserved between F-ATP synthase of *S. cerevisiae*, *H. sapiens*, and *M. musculus* (in parentheses when different)

Subunit	Total number	Positions in <i>S. cerevisiae</i>	Positions in <i>H. sapiens</i> ( <i>M. musculus</i> )
$\alpha$	26	4, 9, 67, 77, 127, 143, 163, 165, 176, 198, 201, 208, 225, 247, 295, 316, 323, 324, 328, 341, 345, 399, 410, 435, 457, 460	5, 12, 73, 83, 133, 149, 169, 171, 182, 204, 207, 214, 231, 253, 301, 322, 329, 330, 334, 347, 351, 405, 416, 441, 463, 466
$\beta$	17	93, 105, 127, 139, 223, 225, 262, 264, 277, 293, 307, 328, 370, 389, 439, 441, 445	109, 121, 143, 155, 239, 241, 279, 281, 294, 310, 324, 345, 387, 406, 456, 458, 462
$\gamma$	7	4, 31, 42, 153, 266, 290, 292	4, 23, 34, 143, 253, 277, 279
a	1	186	159
c	1	39	c1: 99, c2: 104 (109), c3: 105 (104)
$\epsilon$	2	5, 23	6, 24
OSCP	2	8, 114	14, 117
b	1	200	208
f	1	56	50 (44)
e	1	8	15
g	1	107	96
Total	60	60	60

ally identical to the human and yeast species for composition of conserved arginines (Table 1). Analysis of dimers and monomers resolved by SDS-PAGE and silver staining demonstrated that treatment with PGO did not alter the pattern and relative abundance of F-ATP synthase subunits (Fig. 2F). Based on these results, the arginine residues of the  $F_1$  sector, subunit a, and c-ring were not investigated further. Taking advantage of the yeast model and of the species-specific response to PGO, we performed a set of mutagenesis experiments in yeast cells to identify the arginine residue(s) conferring the modulatory effect to PGO.

### OSCP does not confer sensitivity to the effects of PGO

We first investigated whether OSCP, which contains two conserved arginine residues (Table 1), could be involved in conferring the species specificity to the effects of PGO, which are opposite in human and yeast mitochondria (Fig. 1). Deletion of the *ATP5* gene encoding for OSCP ( $\Delta ATP5$ ) prevented F-ATP synthase assembly and growth on glycerol, both features being rescued by reexpression of the WT yeast gene ( $\Delta ATP5 + yOSCP$ ) (Fig. 3, A–C). Replacement with the human OSCP gene ( $\Delta ATP5 + hOSCP$ ) was instead essentially unable to rescue F-ATP synthase assembly unless the yeast mitochondrial targeting sequence replaced the human sequence in the construct ( $\Delta ATP5 + yhOSCP$ ). Indeed, only the chimeric protein allowed assembly of a functional F-ATP synthase complex, which grew normally on glycerol (Fig. 3, A–C). The rescued mutant displayed an increased CRC in response to PGO (*i.e.* the same response of WT yeast mitochondria) (Fig. 3D). Thus, OSCP does not confer species specificity to the effects of PGO on the PTP.

### Arginine 107 of yeast F-ATP synthase subunit g mediates the effect of PGO on the mitochondrial permeability transition

Both subunit e and g possess a conserved arginine residue (Arg-8 and Arg-107 in the yeast sequence, respectively, Fig. 4). These residues correspond to Arg-15 and Arg-96, respectively, in the human sequence (Table 1). To test whether these resi-

dues are involved in PTP modulation by PGO, we first analyzed deletion mutants of subunit g ( $\Delta ATP20$ ) and of subunit e ( $\Delta TIM11$ ). The effect of PGO was completely abolished in the  $\Delta ATP20$  deletion mutant lacking subunit g (Fig. 5A), and a similar, albeit somewhat smaller, effect was observed with the  $\Delta TIM11$  mutant lacking subunit e (Fig. 5B). To explore the role of individual arginines, we generated specific point mutants and tested their CRC. Remarkably, the R107A mutation in subunit g dramatically blunted the effect of PGO (Fig. 5C), whereas the R8A mutation in subunit e was ineffective, with an identical sensitivity to PGO as the WT species (Fig. 5D). This result was puzzling because subunit e only has one conserved arginine in position 8, and therefore we would have expected the same result following either deletion of the subunit e gene or the R8A mutation. This apparent contradiction was resolved by analysis of the expression of the e and g subunits in the  $\Delta ATP20$  and  $\Delta TIM11$  mutants. Indeed, deletion of the *ATP20* gene led to the expected disappearance of subunit g only, whereas deletion of the *TIM11* gene caused the disappearance of both subunit e and g (Fig. 5E). Both Arg-8 and Arg-107 are located next to the GXXXG dimerization domains (Figs. 4 and 5F), and we suspect that this is the region where the PTP forms.

### The ATP20 Arg-107 mutation does not affect growth properties, dimerization, and subunit composition of F-ATP synthase

Given the importance of subunits e and g in both F-ATP synthase dimerization and PTP formation in yeast (19), we characterized the key features of the R107A mutants. Yeast cells can grow by fermentation in glucose-rich medium, whereas they need ATP generated from oxidative phosphorylation in glycerol medium. The *ATP20* R107A mutant grew both on the glucose and glycerol (Fig. 6A), indicating that the mutation did not influence the function of F-ATP synthase. The  $\Delta TIM11$  and  $\Delta ATP20$  mutants expectedly did not display dimers after digitonin extraction and blue native PAGE (Fig. 6B). Mitochondria

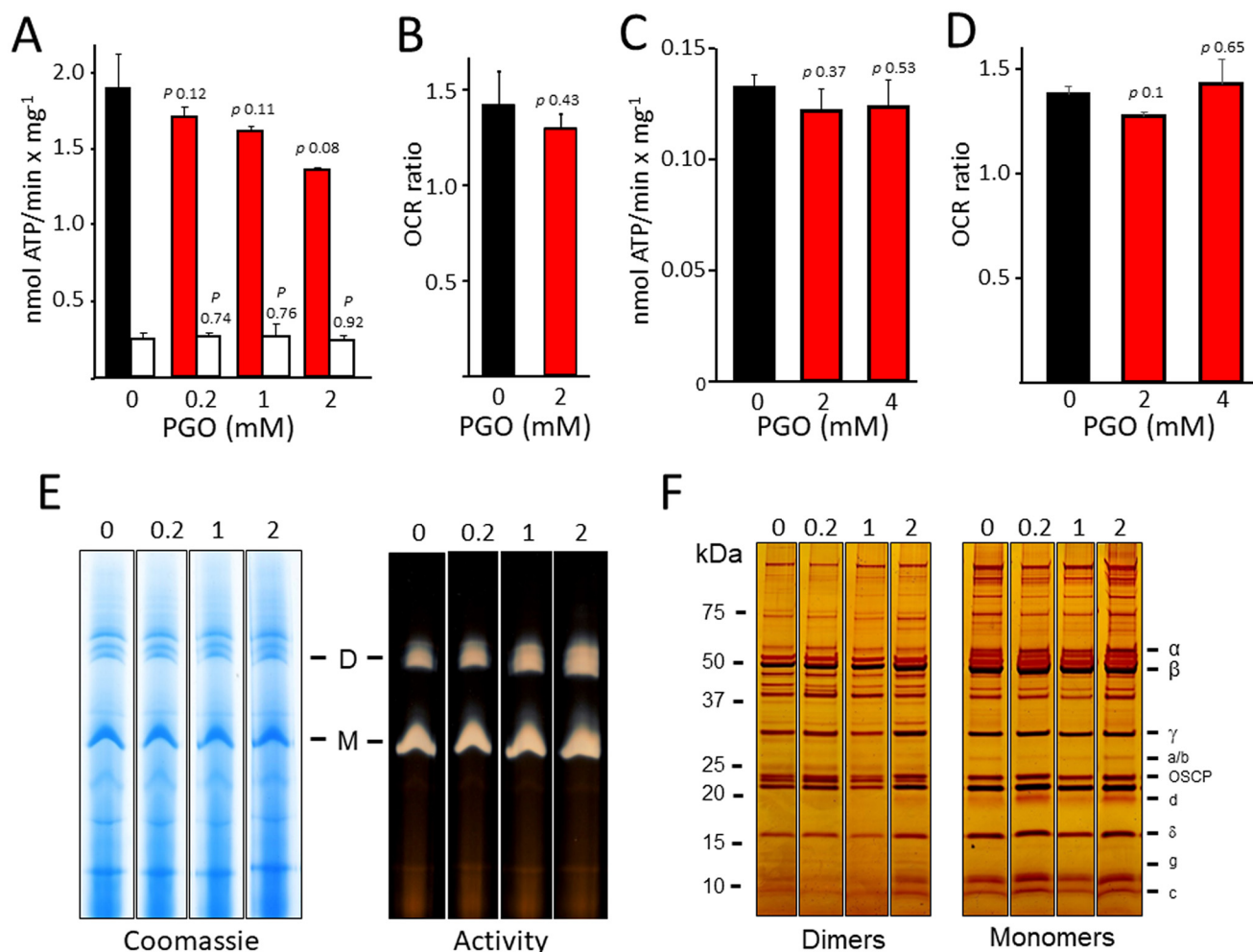


**Figure 2. Chemical modification of arginine residue(s) by PGO does not significantly affect activity, dimerization, and assembly of F-ATP synthase.** Experimental conditions were as described under "Experimental procedures." *A*, ATP hydrolysis rate of MLM pretreated with DMSO (black bar) or with the indicated concentrations of PGO (red bars). Closed bars, values subtracted for the oligomycin-insensitive fraction and expressed as nmol of ATP/mg/min. Open bars, ATP hydrolysis in the presence of 4  $\mu$ M oligomycin. Results are mean  $\pm$  S.E. (error bars) of three independent experiments. *B*, oxygen consumption rate of DMSO- or 2 mM PGO-pretreated MLM in presence of succinate (state 4) and ADP + P<sub>i</sub> (state 3). Values refer to state 3/state 4 ratio and are expressed as mean  $\pm$  S.E. of three independent experiments. *C*, ATP hydrolysis rate of YM isolated from WT strain BY4743 pretreated with DMSO (black bar) or with the indicated concentrations of PGO (red bars). Values have been subtracted for the oligomycin-insensitive fraction and expressed as nmol of ATP/mg/min. Results are mean  $\pm$  S.E. of at least three independent experiments. *D*, oxygen consumption rate of YM isolated from WT strain BY4743 pretreated with DMSO (black bar) or with the indicated concentrations of PGO (red bars) in the presence of NADH and ADP. Values refer to the ratio of OCR (ADP) and OCR (NADH) and are expressed as mean  $\pm$  S.E. of three independent experiments. *E*, isolated MLM pretreated with the concentrations of PGO labeling each lane were separated by BN-PAGE as described under "Experimental procedures" and revealed with Coomassie Blue and in-gel activity staining for ATP hydrolysis to identify dimers (*D*), monomers (*M*), and F<sub>1</sub> sector of F-ATP synthase. *F*, dimers and monomers were cut out from BN-PAGE gels and subjected to SDS-PAGE and silver-stained. All sets of lanes in *E* and *F* are from the same gels.

reexpressing either WT or R107A subunit g had functional dimers indistinguishable from those of WT BY4743 cells (Fig. 6B) with identical subunit composition, as judged from SDS-PAGE and silver staining (Fig. 6C). Thus, the R107A replacement in subunit g did not influence the assembly, activity, and stability of F-ATP synthase.

#### PGO reacts with Arg-107 of subunit g and affects the pore only in mitochondria with the WT subunit

We next tested whether the PGO adduct affects the properties of the PTP. One emerging issue is pore size, which is affected by the deletion of lateral stalk subunits OSCP and b even when the CRC is apparently unaffected (24). We therefore measured Ca<sup>2+</sup>-induced swelling in yeast mitochondria in the presence of ETH129 to allow electrophoretic Ca<sup>2+</sup> uptake. The

swelling rate was significantly inhibited by PGO in mitochondria reexpressing WT subunit g but not the R107A mutant, which displayed a lower rate of swelling (Fig. 7, A–C). Because yeast subunit g also contains an arginine residue at position 106, we employed synthetic test peptides corresponding to the 88–114 amino acid segment of WT or containing the R106A replacement. Following reaction with PGO, the peptides were analyzed by MALDI-TOF MS. The results revealed that one adduct with a molecular mass of 116 Da was formed on both the WT and the R106A modified peptide (Fig. 7D). This molecular mass corresponds to one molecule of PGO covalently attached to the guanidine moiety of arginine. Formation of one single adduct in the WT peptide carrying two adjacent arginines suggests that reaction of Arg-107 with PGO may reduce the reactivity of Arg-106.

## Subunit g Arg-107 of F-ATPase regulates PTP

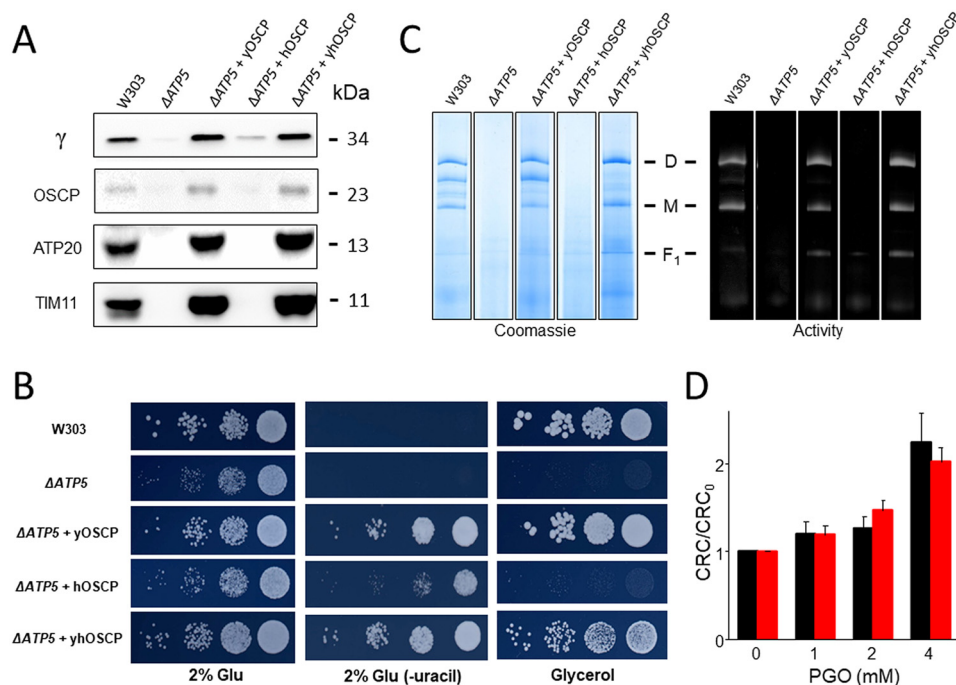


**Figure 3. Expression of human OSCP does not alter the inhibitory effect of PGO on yeast PTP.** *A*, isolated yeast mitochondria of the indicated genotypes (50  $\mu$ g of protein/lane) were evaluated by Western blotting for  $\gamma$ , OSCP, *TIM11*, and *ATP20* subunits. *B*, serial dilution spotting assay of the indicated genotypes. Cell suspensions were grown to  $A_{600\text{ nm}} = 1$ ; serially diluted; plated on medium containing 2% glucose (*Glu*), 2% *Glu* drop-out uracil (*-uracil*), and 2% glycerol; and incubated at 30  $^{\circ}$ C. Pictures were taken after 1–2 days. *C*, yeast mitochondrial proteins of the indicated genotypes were separated by BN-PAGE as described under “Experimental procedures,” and revealed with Coomassie Blue and in-gel activity staining for ATP hydrolysis to identify dimers (*D*), monomers (*M*), and  $F_1$  sector of F-ATP synthase. *D*, CRC of yeast mitochondria from  $\Delta$ *ATP5* + *yOSCP* (black bars) and  $\Delta$ *ATP5* + *yhOSCP* (red bars) pretreated with the indicated concentrations of PGO. Data are expressed as CRC/CRC<sub>0</sub> ratio, in which CRC<sub>0</sub> refers to the CRC of DMSO-treated mitochondria. Results are mean  $\pm$  S.E. (error bars) of at least three independent experiments. All sets of lanes in *A* and *C* are from the same gels.

### Expression of human subunit g in yeast prevents PGO-dependent desensitization of PTP

PGO desensitizes the yeast PTP to  $\text{Ca}^{2+}$  (thus increasing the CRC), whereas it sensitizes it in human HEK293 cells (thus decreasing the CRC; see Fig. 1). We exploited this phenotypic difference to test whether expression of human subunit g is able to switch the inhibitory effect of PGO in yeast mitochondria to the inducing effect seen in human mitochondria. Deletion of the *ATP20* gene encoding for yeast subunit g prevented dimerization of F-ATP synthase, which could be rescued by both expression of *ATP20* and of *ATP5L* (which encodes human subunit g) (Fig. 8A). As for WT yeast (compare with Fig. 1), PGO increased the CRC of  $\Delta$ *ATP20* mitochondria reexpressing *ATP20*, whereas replacement with *ATP5L* totally prevented the desensitizing effects of PGO, which rather decreased the CRC (Fig. 8B), as also seen in permeabilized HEK293 cells. These results suggest that subunit g confers species specificity to the effects of PGO on the PTP.

### Arg-107 of subunit g is a target for modification by high glucose, phenylglyoxal, and methylglyoxal

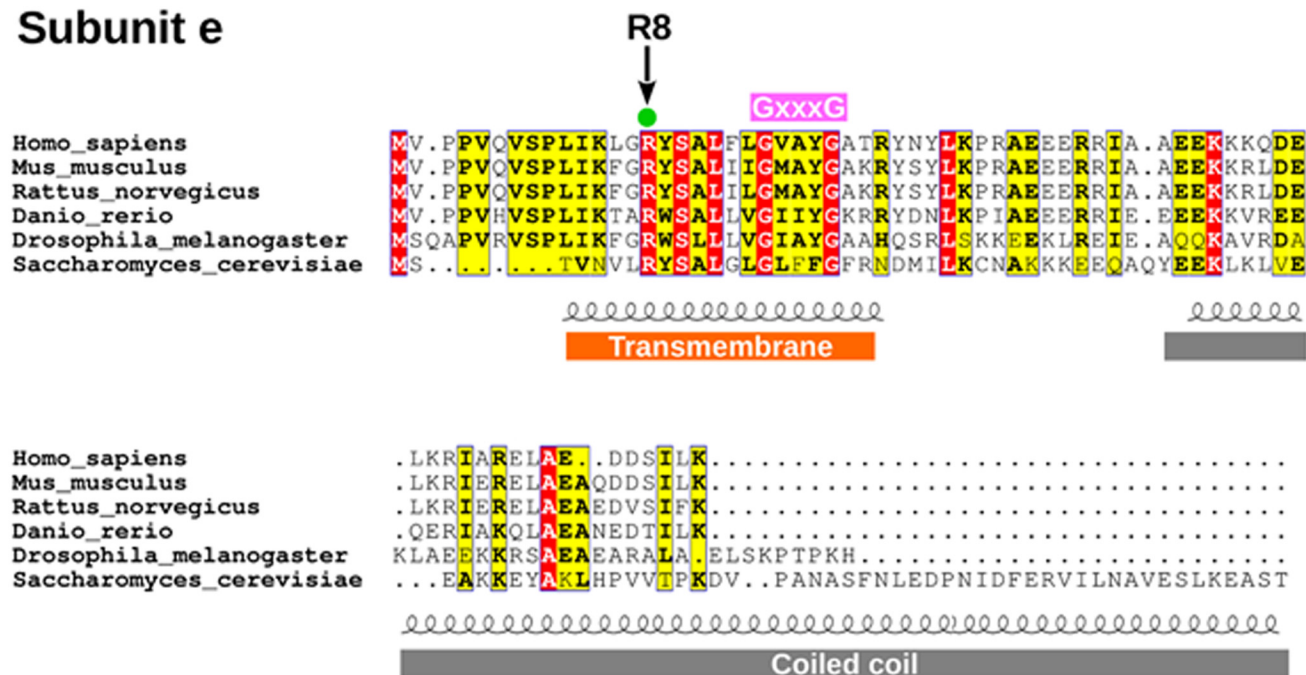
Advanced glycation end-products (AGE) originate from nonenzymatic modification of lysine and arginine residues that takes place after long-term exposure to high concentrations of glucose or to reactive compounds like methylglyoxal (MGO), a byproduct of glycolysis that alters protein structure, stability, and function (26–28). Yeast cells grown at high glucose concentration undergo protein glycation largely due to generation

of high levels of MGO (29), with a relevant increase in argpyrimidine-modified proteins (30, 31). Arginine residues are frequently found in enzyme sites involved in substrate binding and catalysis, and their modification by MGO results in the formation of AGE (28). Consistent with these toxic effects, the growth rate of yeast cells was slowed down in high-glucose medium (Fig. 9A). At normal concentrations of glucose, toxicity was mimicked by PGO and MGO (Fig. 9A). Remarkably, yeast strains lacking subunit g or harboring the subunit g R107A mutation were significantly more resistant to PGO toxicity (Fig. 9B).

### Discussion

The molecular nature of the PTP is a long-standing mystery of mitochondrial biology. In the past, we have used relatively selective sulfhydryl, histidine, and arginine reagents to define the properties of discrete sites conferring PTP regulation by the proton electrochemical gradient, divalent cations, quinones, and oxidative stress (8). The recent hypothesis that the PTP may originate from a specific,  $\text{Ca}^{2+}$ -induced conformation of F-ATP synthase (16–19) provides a unique opportunity to identify these sites in molecular terms. Indeed, mutagenesis of specific residues or deletion of specific subunits of F-ATP synthase should modify predictably the properties of the PTP and/or the effect of reagents acting at these sites. This is a formidable challenge because F-ATP synthase is a complex multi-subunit enzyme (32–37) whose assembly is affected by deletion of specific subunits (23, 24). The present study is part of our

## Subunit e



## Subunit g

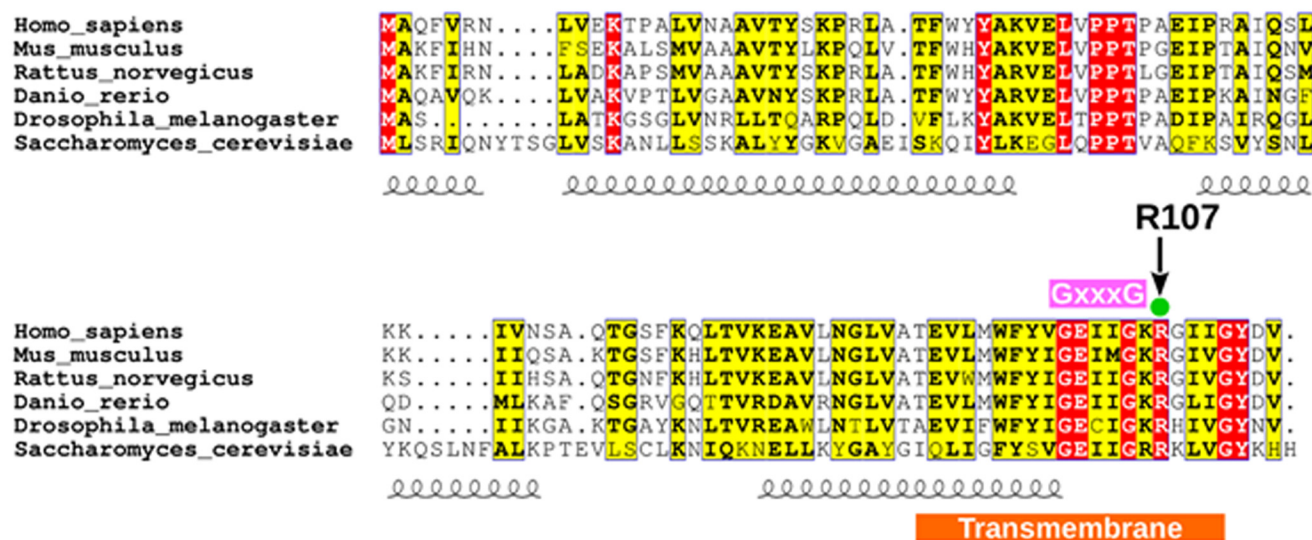
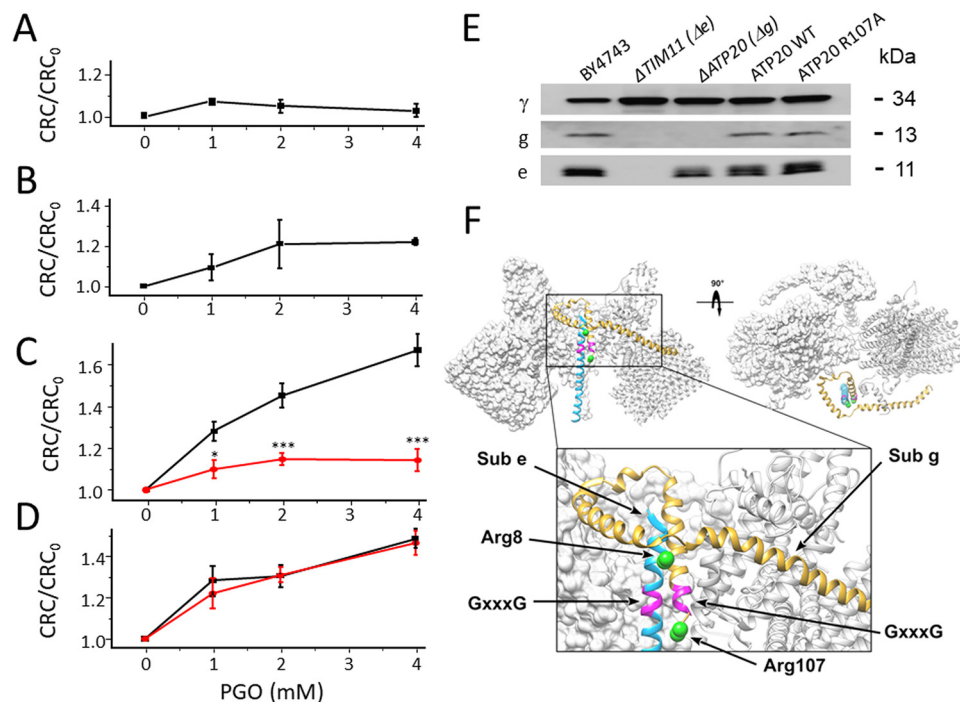


Figure 4. Amino acid sequence comparison of F-ATP synthase subunits e and g.

efforts at identifying such regulatory sites and, as a corollary, at (dis)proving the general hypothesis that the PTP originates from F-ATP synthase. So far, we have provided evidence (i) that  $\text{Ca}^{2+}$  triggers the PTP by substituting  $\text{Mg}^{2+}$  at the catalytic site, causing a conformational change that is transmitted through OSCP to the lateral stalk and eventually to the inner membrane (21), and (ii) that PTP blockade by matrix  $\text{H}^+$  is mediated by the unique, highly conserved histidine residue of OSCP subunit (22). Here, we have been able to identify a unique arginine residue that mediates the effects of PGO on the  $\text{Ca}^{2+}$  sensitivity of the PTP in yeast mitochondria.

Our previous studies had defined the PTP-modulatory effects of arginine-selective reagents like glyoxals and 2,3-butanedione (12–15). Although glyoxals can also react with other residues (such as lysines and cysteines) (38), it has been possible to trace their effects on the PT to modification of arginines with reasonable certainty (12–15). In rat liver mitochondria, the outcome depended on the specific glyoxal used, with PTP inhibition by MGO or PGO and PTP activation by OH-PGO (12–15). Studies with a variety of compounds with similar reactivity but different overall physical-chemical properties led to the conclusion that glyoxals react with the same arginine residue(s) and

## Subunit g Arg-107 of F-ATPase regulates PTP



**Figure 5. Arg-107 of yeast F-ATP synthase subunit g mediates the effects of PGO on the CRC.** Experimental conditions were as in Fig. 1B. *A*, CRC of  $\Delta$ ATP20 yeast mitochondria pretreated with the indicated concentrations of PGO. *B*, CRC of  $\Delta$ TIM11 yeast mitochondria pretreated with the indicated concentrations of PGO. *C*, CRC of yeast mitochondria from ATP20 WT control (black trace) and ATP20 R107A (red trace) pretreated with the indicated concentrations of PGO. \*,  $p < 0.05$  versus ATP20 WT; \*\*\*,  $p < 0.001$  versus ATP20 WT. Two-way ANOVA was used for statistical analysis. *D*, CRC of yeast mitochondria from TIM11 WT control (black trace) and TIM11 R8A (red trace) pretreated with the indicated concentrations of PGO. In *A–D*, data are expressed as ratio to DMSO-treated mitochondria. Means  $\pm$  S.E. (error bars) of at least three independent experiments are shown. *E*, isolated yeast mitochondria of the indicated genotypes were evaluated by Western blotting for  $\gamma$ , TIM11, and ATP20 subunit content after SDS-PAGE separation of 50  $\mu$ g of protein per lane. *F*, overview of ATP synthase  $F_0$  dimer (Protein Data Bank code 6B2Z) with frontal and top views highlighting the relative position of subunits g (yellow) and e (light blue). Putative GXXXG dimerization motifs are represented in purple. The structure is shown in standard view (front) and after a 90° rotation around the z axis, and two  $F_0$  monomers are presented. The boxed region is expanded in the bottom part of the panel. Green spheres represent the position of Arg-8 of subunit e and Arg-107 of subunit g, which are predicted to localize at the border of the GXXXG domains. These positions were derived by comparing data from the three-dimensional structure (Protein Data Bank code 6B2Z) with secondary structure predictions.

that the main determinants for the effects on the PTP are charge and hydrogen-bonding capacity of the adducts (12–15). Here, we have added the very relevant piece of information that PGO has species-specific effects on the PTP. Having identified Arg-107 of subunit g as the unique target of PGO in yeast, we suspect that the species-specific effects may depend on differences in the primary structure of F-ATP synthase, which appear to be particularly prominent in subunits e and g (Fig. 4).

A large fraction of the 60 conserved arginines of F-ATP synthase is located in the catalytic sector (26 in subunit  $\alpha$  and 17 in subunit  $\beta$ ) and in the  $F_0$  subunits  $\gamma$ ,  $\epsilon$ , c, and a (11 residues). The membrane extrinsic region ( $F_1$  sector) of the F-ATP synthase complex is composed of  $3\alpha$  and  $3\beta$  and of one each of the  $\gamma$ ,  $\delta$ , and  $\epsilon$  subunits. The  $3\alpha 3\beta$  hexamer contains the catalytic sites responsible for ATP synthesis or hydrolysis (32) and associates through the  $\gamma$ ,  $\delta$ , and  $\epsilon$  subunits with a ring of hydrophobic c subunits (the c-ring) in the membrane domain. The rotating c-ring is in contact with the static a subunit, which maintains a specific pathway for translocation of protons through the membrane (34). A conserved arginine residue of subunit a plays a critical role in blocking a futile proton shortcut and in facilitating proton transfer at the a/c-ring interface via a carboxylic group in the c-ring (39). Our data do not reveal whether the arginine residues of the catalytic sector react with glyoxals, but they do indicate that, if present, these adducts do not play a direct role in PTP modulation.

OSCP plays a critical role in the assembly and function of F-ATP synthase (40, 41) and has a well-characterized regulatory role in PTP modulation in mammals by providing a site for CyPD binding, which results in sensitization of the PTP to  $Ca^{2+}$  (17, 42, 43). Replacement of yeast with human OSCP did not reverse PTP sensitization to  $Ca^{2+}$  by PGO, however, suggesting that also OSCP arginines are not critical for PTP modulation by glyoxals.

F-ATP synthase complexes associate into dimers, which are essential for the formation of oligomers and generation of the cristae (44–46). Subunits e and g are essential for this process, and deletion of either subunit leads to dimer and cristae disruption (46–52). The e and g subunits are also important for regulation of the  $Ca^{2+}$  sensitivity of yeast PTP, which undergoes desensitization after their genetic ablation (19). The fact that their contribution has been so far addressed in null mutants inevitably limits our understanding of their putative function in PTP formation. Conversely, site-directed mutagenesis of specific residues that does not alter assembly, subunit composition, and enzymatic activity of the enzyme allows interrogation of their role in PTP formation and regulation.

The yeast R107A mutant of subunit g described here shows F-ATP synthase dimers with normal hydrolytic activity, yet it displays a PTP that is desensitized to  $Ca^{2+}$  (data not shown) and insensitive to PGO and a decreased swelling rate in sucrose. This last finding suggests that Arg-107 of subunit g may be



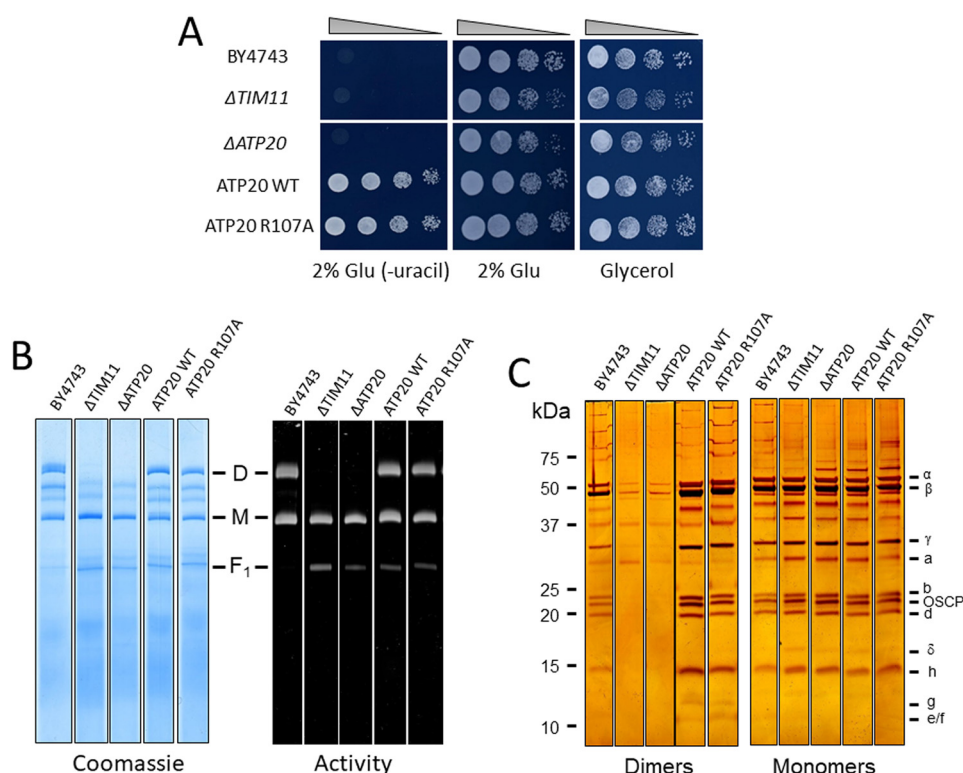


**Figure 6. The ATP20 R107A mutation does not affect dimerization, assembly, and function of F-ATP synthase.** *A*, serial dilution spotting assay of BY4743,  $\Delta$ TIM11,  $\Delta$ ATP20, ATP20 WT, ATP20 R107A strains. Cell suspensions were grown to  $A_{600\text{ nm}} = 1$ ; serially diluted; plated on medium containing 2% Glu, 2% Glu drop-out uracil (*-uracil*), and 2% glycerol; and incubated at 30 °C. Pictures were taken after 1–3 days. *B*, yeast mitochondrial proteins of the indicated genotypes were separated by BN-PAGE as described under “Experimental procedures” and revealed with Coomassie Blue and in-gel activity staining for ATP hydrolysis to identify dimers (*D*), monomers (*M*), and the  $F_1$  sector of F-ATP synthase. *C*, dimers and monomers were cut out from BN-PAGE, subjected to two-dimensional SDS-PAGE, and revealed by silver staining. All sets of lanes in *B* and *C* are from the same gels.

important for solute permeation through the PTP, providing a further clue as to a possible site where the pore forms. Of note, replacement of yeast subunit g with its human counterpart confers the “human” phenotype to yeast, suggesting that the species-specific effect of PGO is more likely to depend on structural differences between the yeast and human F-ATP synthase than on the Arg-107–PGO adduct as such.

In mammals, dysregulated PTP opening is a primary cause of cell death initiated via matrix swelling and rupture of the outer membrane followed by release of proapoptotic factors (cytochrome *c*), whereas its inhibition appears often to be protective (8). Whether the pore plays a similar role in yeast is still a matter of debate. Yeast does not possess a mitochondrial  $\text{Ca}^{2+}$  uniporter to mediate rapid  $\text{Ca}^{2+}$  overload; nor does it form the apoptosome complex required for the activation of effector caspases. However, yeast mitochondria can undergo membrane permeabilization in response to  $\text{Ca}^{2+}$  and oxidative stress (53, 54), leading to the release of cytochrome *c*, which certainly causes decreased respiration and ATP production. These events, together with the activation of the yeast metacaspase Ycalp, are proximal events in yeast programmed cell death (54). Thus, as for mammals, PTP opening might represent an important cell death pathway also for yeast, which can undergo apoptosis and aging (55).

AGE arising from carbonyl stress contribute to many pathological states, such as diabetes and age-related diseases (26–28). It is apparent that adducts form at many sites other than subunit g, yet our findings suggest that altered PTP features may

play a role in glucose-dependent toxicity also in human cells, as was already suggested (56). Whether additional arginine residues mediate the glyoxal-specific effects described in rat mitochondria and human cells (12–15) remains to be established. However, the demonstration that a single conserved arginine residue of subunit g mediates the effects of PGO on the PTP in yeast is another step toward a molecular understanding of PTP regulation and evidence that the latter forms from a specific conformation of the F-ATP synthase.

## Experimental procedures

### Reagents and cells

PGO hydrate, MGO, oligomycin, rotenone, succinic acid, pyruvate, alamethicin, ATP, ADP, EGTA,  $\text{CaCl}_2$ , digitonin, NADH, ETH129, galactose, and sucrose were from Sigma (Milan, Italy). Cyclosporin A was purchased from Calbiochem.  $\text{Ca}^{2+}$  Green-5N was from Invitrogen (Milan, Italy). HEK293T were obtained from the American Tissue Culture Collection (ATCC) and cultured in Dulbecco’s modified Eagle’s medium (Lonza, Basel, Switzerland) supplemented with fetal bovine serum (10%) and penicillin and streptomycin (1%) (Thermo Fisher Scientific). *Drosophila* Schneider S2 cells were obtained from Dr. Michael Forte (Oregon Health and Science University) and cultured as described (57). The *Saccharomyces cerevisiae* strains BY4743,  $\Delta$ TIM11, and  $\Delta$ ATP20 were purchased from Thermo Scientific, and mitochondria were isolated as described (19). Antibodies for TIM11, ATP20, and  $\gamma$  subunits

## Subunit g Arg-107 of F-ATPase regulates PTP

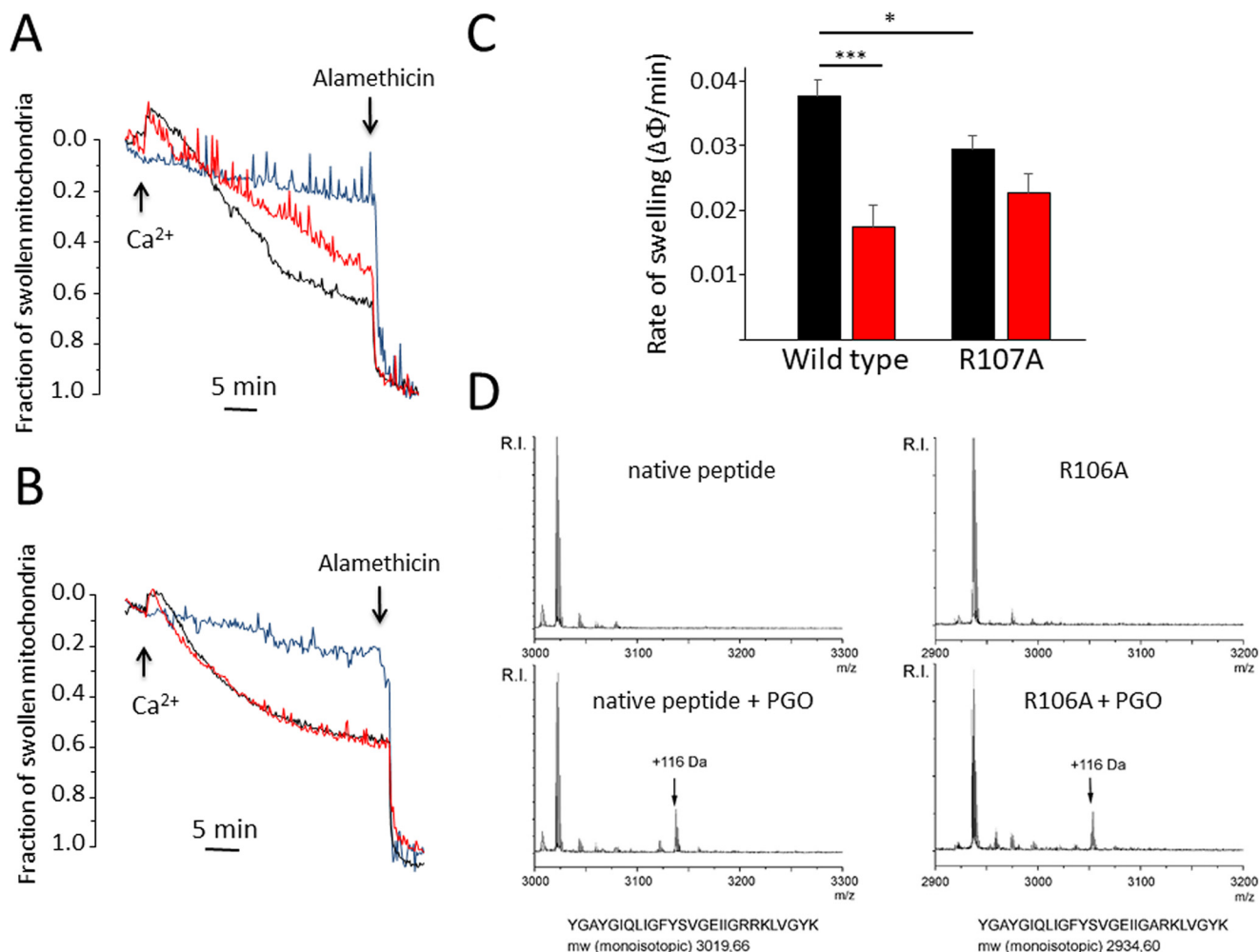


**Figure 7. Arg-107 of yeast F-ATPase subunit g mediates inhibition of mitochondrial permeability transition by PGO.** Experimental conditions were as in Fig. 1B except that  $\text{Ca}^{2+}$  green-5N was omitted. A and B, PTP-dependent mitochondrial swelling was evaluated as the decrease of absorbance at 540 nm, and the fraction of mitochondria that underwent the PT was assessed as described by Petronilli *et al.* (63). Additions of  $50 \mu\text{M}$   $\text{Ca}^{2+}$  and  $5 \mu\text{M}$  alamethicin are indicated by arrows.  $\text{Ca}^{2+}$  was omitted in the light blue traces. Mitochondria isolated from ATP20 WT (A) and ATP20 R107A yeast (B) were treated with DMSO (black traces) or 4 mM PGO in DMSO (red traces). Representative traces of at least three independent experiments are shown. C, rate of mitochondrial swelling triggered by  $50 \mu\text{M}$   $\text{Ca}^{2+}$ . ATP20 WT or ATP20 R107A mitochondria were pretreated with DMSO (black bars) or 4 mM PGO (red bars). The rate of mitochondrial swelling is expressed as the fraction of swollen mitochondria/min. Data are mean  $\pm$  S.E. (error bars) of at least three independent experiments. \*,  $p < 0.05$  versus WT (ATP20 WT); \*\*\*,  $p < 0.001$  versus vehicle. One-way ANOVA was used for statistical analysis. D, MALDI-TOF mass spectra of synthetic peptides of the amino acid segment comprising Arg-107. The mass spectra of the parent peptides are shown in the top windows, and that of the PGO-modified peptides is shown in the bottom window. Masses in the spectra are  $M + \text{H}^+$ . The 116-Da adducts are marked with arrows.

were a kind gift of Dr. Marie-France Giraud (University of Bordeaux, France). Antibody for the OSCP subunit was purchased from Santa Cruz Biotechnology, Inc. (sc-365162).

### Yeast mutant generation

To generate  $\Delta\text{ATP5}$  yeast expressing the human or yeast OSCP (*ATP5*) sequence, the *ATP5* gene was first deleted in W303 diploids by substituting the genomic sequence with the Kan cassette of pFA6a-KanMX4 vector. Then diploids were allowed to sporulate in 2% potassium acetate medium, resulting tetrads were dissected, and correct clones were checked by semiquantitative PCR using appropriate primers. Yeast *ATP5* gene (yOSCP) was cloned in pFL38-URA vector after amplification using the following primers that include upstream and downstream regulatory sites (endogenous promoter and termination sequence): 5'-CACGACGTTGTAAAACGACGGCCAGTGAATTCGAGCTCGGTACCCTGCCGTCGCATAA-

AGTGGAC (forward) and 5'-TTACGCCAAGCTTGCATGCTGCAGGTCGACTCTAGAGGATCCCCGTTTGCCTGGATACACGAAC (reverse). Cloned products were confirmed by sequence analysis. Human OSCP (hOSCP) cDNA (NM\_001697) was purchased from GenScript and amplified using the following primers: 5'-CAGTGTGCTGGAATTCAACACAATGGCTGCCCGCAGCAGTGTCC (forward) and 5'-GATA-TCTGCAGAATTTTAGACAATCTCCCGCATAGCCCTG (reverse). To substitute with the yeast putative mitochondrial import sequence at the N terminus of the OSCP gene (yOSCP), we used the forward primer 5'-CAGTGTGCTGGAATTCAACACAATGTTTAATAGAGTCTTTACCAGGT-CATTTGCATCAAGCTTAAGAGCTGCTGCTTCCAAAGCTGCTGCTCCCCCTCCTGTTTACGGTATACGGTATTG and the same reverse primer as for hOSCP. PCR products were cloned in pYES2-URA previously digested with EcoRI-HF using the In-Fusion HD cloning kit (Clontech), and resulting

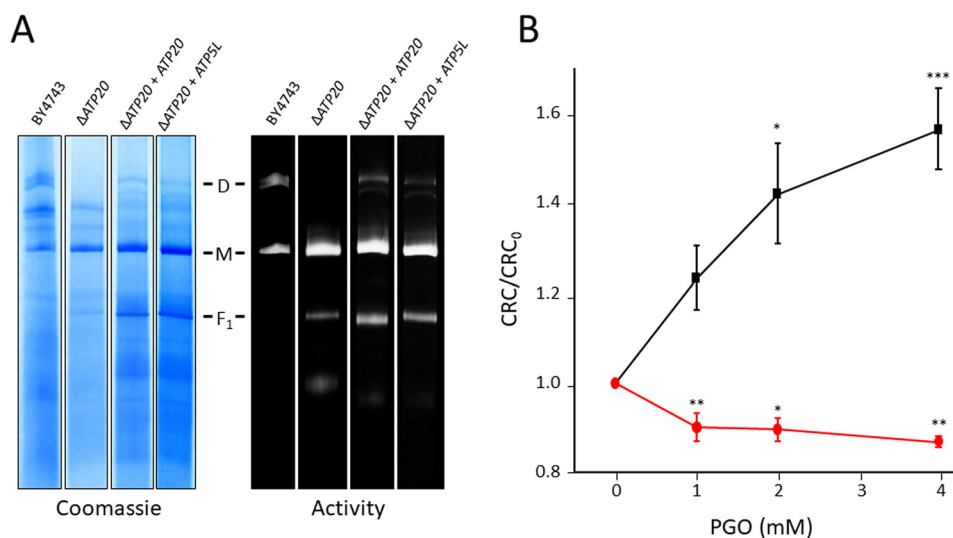


**Figure 8. Expression of human subunit g in yeast prevents the inhibitory effect of PGO.** *A*, yeast mitochondrial proteins of the indicated genotypes were separated by BN-PAGE as described under “Experimental Procedures” and revealed with Coomassie Blue and in-gel activity staining for ATP hydrolysis to identify dimers (*D*), monomers (*M*), and  $F_1$  sector of F-ATP synthase. *B*, CRC of yeast mitochondria from  $\Delta ATP20 + ATP20$  (black trace) and  $\Delta ATP20 + ATP5L$  (red trace) pretreated with the indicated concentrations of PGO. Data are expressed as CRC/CRC<sub>0</sub> ratio, in which CRC<sub>0</sub> refers to the CRC of DMSO-treated mitochondria. Results are mean  $\pm$  S.E. (error bars) of at least three independent experiments. \*,  $p < 0.05$  versus vehicle; \*\*,  $p < 0.01$  versus vehicle; \*\*\*,  $p < 0.001$  versus vehicle. One-way ANOVA was used for statistical analysis.

vectors were checked by sequencing. Yeast  $\Delta ATP5$  cells were separately transformed by a standard procedure (58) with yOSCP pFL38-URA, hOSCP pYES2-URA, or yHOSCP pYES2-URA, and correct clones were selected. Human cDNA *ATP5L* cloned into pESC-LEU vector by Sali/XhoI sites was purchased from GenScript. The oligonucleotide primers used for the yeast *ATP20* gene to be cloned in pESC-LEU vector by Sali/XhoI sites were 5'-GGGCCCGGGCGTCGACAACACAATGCTAAGC-AGGATCCAA (forward) and 5'-ACCAAGCTTACTCGATT-AGTGATGTTTATATCCCAC (reverse). PCR products were cloned in pESC-LEU vector previously digested with Sali-HF and XhoI using the In-Fusion HD cloning kit (Clontech), and resulting vectors were checked by sequencing. A one-step transformation protocol (58) was used to transform *ATP5L* pESC-LEU or *ATP20* pESC-LEU into yeast  $\Delta ATP20$  strain and cultured in the selective medium 2% galactose (drop-out leucine). The oligonucleotide primers used for TIM11 R8A and *ATP20* R107A site-directed mutagenesis were as follows: TIM11 R8A, 5'-CGACAGTTAATGTTTTGGCATACTCTG-CGTTGGGTTT (forward) and 5'-CAAACCAACGCAG-AGTATGCCAAAACATTAAGTCTGTCG (reverse); *ATP20* R107A, 5'-CGGTGAAATAATTGGAAGAGCAAAAATTAG-TGGGATATAAAC (forward) and 5'-GTTTATATCCCCT-AATTTTGGCTCTTCCAATTATTTACCG (reverse).

The QuikChange Lightning site-directed mutagenesis kit (Agilent) was used to harvest the mutants, and the dsDNA templates we used were *TIM11* and *ATP20* WT genes created in pFL38 plasmid. After the mutations were confirmed by sequencing, a one-step transformation protocol (58) was used to transform the plasmid into  $\Delta TIM11$  or  $\Delta ATP20$  *S. cerevisiae* strain and plated on the selective medium 2% Glu (drop-out uracil) and incubated in 30 °C for 2 days.

#### Mouse liver mitochondria preparation

All of the isolation procedures were performed at 4 °C or on ice. Mouse livers were cut into pieces in the isolation

buffer containing 250 mM sucrose, 10 mM Tris-HCl, 0.1 mM EGTA, pH 7.4. The homogenate suspension was centrifuged at  $690 \times g$  for 10 min. The supernatant was collected and centrifuged at  $7000 \times g$  for 10 min. The pellet was suspended in the isolation buffer and centrifuged at  $9400 \times g$  for 5 min. The mitochondria pellet was resuspended in about 400  $\mu$ l of isolation buffer. The biuret test was used for determining protein concentration.

#### Yeast mitochondria isolation

Yeast mitochondria were isolated as described previously (19). Briefly, yeast cells were cultured in 400 ml of medium containing 1% yeast extract, 1% bacto-polypeptone, and 2% galactose overnight at 30 °C. Yeast cells were harvested by centrifugation at  $2000 \times g$  for 5 min at room temperature. The cell pellet was incubated in 0.1 M Tris-SO<sub>4</sub>, pH 9.4, buffer, supplemented with 10 mM DTT for 15 min at 37 °C. The incubation was terminated by centrifugation at  $2000 \times g$  for 5 min and washed once with 1.2 M sorbitol, 20 mM P<sub>i</sub>, pH 7.4, buffer. The cell pellet was resuspended in the above sorbitol buffer supplemented with zymolyase (0.4 mg/g pellet) and then incubated for 45 min at 30 °C. The incubation was terminated by centrifugation at  $2000 \times g$  for 5 min at 4 °C and washed once with sorbitol buffer. The cell pellet was resuspended in cold buffer containing 0.6 M mannitol, 10 mM Tris-HCl, 0.1 mM EDTA, pH 7.4, and homogenized with a Potter homogenizer. The supernatant was collected and centrifuged at  $2000 \times g$  for 5 min at 4 °C, and then the supernatant was centrifuged at  $12,000 \times g$  for 10 min at 4 °C. The mitochondrial pellet was harvested in mannitol medium. Protein concentration was quantified by the A<sub>280</sub> of 0.6% SDS-solubilized mitochondria.

#### Cell permeabilization

The culture medium of human HEK293 cells was discarded, and cells were washed once with Dulbecco's PBS. Cells were

## Subunit g Arg-107 of F-ATPase regulates PTP

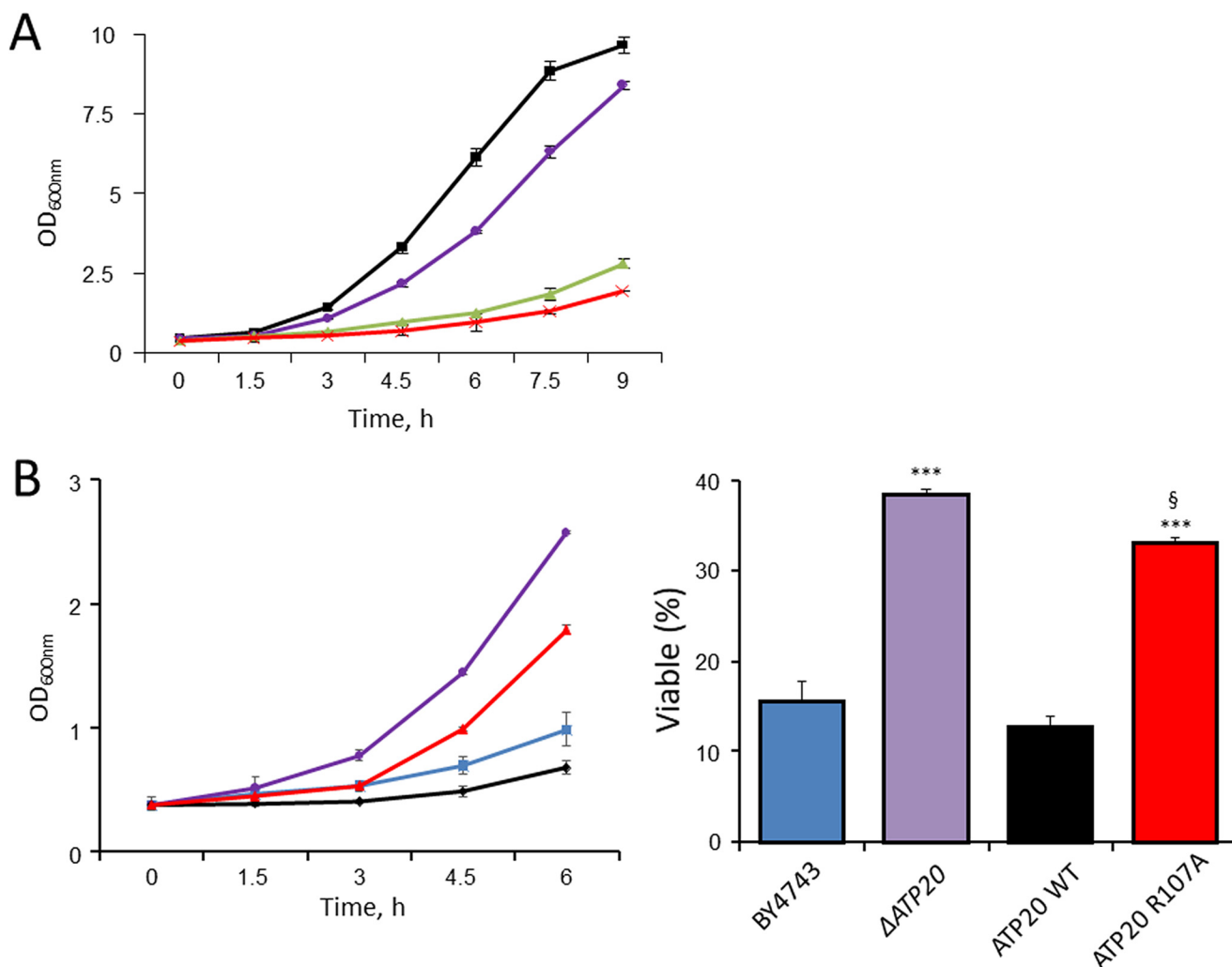


**Figure 9. The ATP20 R107A yeast mutant is partially resistant to PGO toxicity.** A,  $A_{600\text{ nm}}$  values of WT strain BY4743 cultured in 2% glucose (black trace), 20% glucose (purple trace), 2% glucose with the addition of 16 mM MGO (green trace), or 2% glucose with the addition of 0.5 mM PGO (red trace) at the indicated time points. B (left),  $A_{600\text{ nm}}$  value of yeast WT strain BY4743 (blue trace),  $\Delta$ ATP20 mutant (purple trace), ATP20 WT control (black trace), or ATP20 R107A (red trace) cultured in 2% glucose with the addition of 0.5 mM PGO. Right, survival of yeast cells incubated with 0.5 mM PGO at 30 °C for 6 h normalized to untreated cultures. Data are mean  $\pm$  S.E. (error bars) of three independent experiments. \*\*\*,  $p < 0.001$  versus BY4743; §,  $p < 0.001$  versus ATP20 WT. One-way ANOVA was used for statistical analysis.

treated with 0.25% trypsin, and the reaction was terminated by the addition of culture medium. *Drosophila*  $S_2R^+$  cells were detached with a scraper. Cell suspensions were centrifuged at  $500 \times g$  for 5 min and washed once with medium containing 130 mM KCl, 10 mM MOPS-Tris, 1 mM  $P_i$ , 0.1 mM EGTA, pH 7.4. The cell pellet was resuspended in a medium containing 130 mM KCl, 10 mM MOPS-Tris, 1 mM  $P_i$ , 1 mM EGTA, pH 7.4, and supplemented with 100  $\mu$ M digitonin and incubated for 10 min on ice at a density of  $2 \times 10^7$  cells/ml (HEK293 cells) or supplemented with 150  $\mu$ M digitonin and incubated on ice for 20 min at a density of  $6 \times 10^7$  cells/ml (*Drosophila*  $S_2R^+$  cells). The incubations were terminated by dilution with 15–20 ml of medium containing 130 mM KCl, 10 mM MOPS-Tris, 1 mM  $P_i$ , 0.1 mM EGTA, pH 7.4, followed by centrifugation at  $500 \times g$  for 5 min at 4 °C. The cell pellet was washed once with 5 ml of the above KCl medium at 4 °C. The final pellet was resuspended in 250 mM sucrose, 20  $\mu$ M EGTA, 10 mM HEPES-KOH, pH 8.0, for reaction with PGO.

### Chemical modification with PGO

Freshly isolated mouse liver or yeast mitochondria (1 mg/ml) or  $2 \times 10^7$ /ml permeabilized cells were incubated with PGO in 250 mM sucrose, 20  $\mu$ M EGTA, 10 mM HEPES-KOH, pH 8.0, for 15 min at 25 °C. The reaction was terminated by decreasing the pH to 6.8 with HEPES and cooling to 4 °C. Mitochondria were precipitated by centrifugation at  $8000 \times g$  for 6 min and washed once with 250 mM sucrose, 0.1 mM EGTA, 0.5 mg/ml BSA, 10 mM Tris-HCl, pH 7.4. Mitochondria or cells were finally resuspended in the assay medium.

### Mitochondrial $Ca^{2+}$ retention capacity

Yeast mitochondria (0.5 mg of protein/ml) were suspended in 250 mM sucrose, 10 mM Tris-MOPS, 20  $\mu$ M EGTA, 1 mM NADH, 5  $\mu$ M ETH129, 2 mM  $P_i$ , 1  $\mu$ M Calcium Green-5N, 0.5 mg/ml BSA, pH 7.4. MLM (0.5 mg of protein/ml) and permeabilized HEK293 or *Drosophila*  $S_2R^+$  cells ( $1 \times 10^7$  cells/ml) were suspended in 250 mM sucrose, 10 mM Tris-MOPS, 10  $\mu$ M

EGTA, 1 mM P<sub>i</sub>, 0.5 μM Calcium Green-5N, 5 mM succinate, 2 μM rotenone, pH 7.4. Final volume was 0.2 ml. External Ca<sup>2+</sup> concentration was monitored by Calcium Green-5N fluorescence (excitation and emission wavelengths 485 and 538 nm, respectively) using a Fluoroskan Ascent FL (Thermo Scientific) plate reader.

### Mitochondrial swelling assay

Isolated yeast mitochondria were suspended in 250 mM sucrose, 10 mM Tris-MOPS, 20 μM EGTA, 1 mM NADH, 5 μM ETH129, 0.5 mg/ml BSA, 2 mM P<sub>i</sub>, pH 7.4, at a concentration of 0.5 mg of protein/ml in a final volume of 2 ml. Mitochondrial swelling was measured as the decrease of the turbidity (apparent absorbance at 540 nm) using a Cary 100 UV-visible spectrophotometer from Agilent Technologies.

### Western blotting

Isolated mitochondria were lysed in 150 mM NaCl, 50 mM Tris-HCl, pH 7.4, 2 mM EDTA, 2 mM EGTA, 1% Triton X-100, 10 mM β-mercaptoethanol, 10% glycerol, 0.3% Nonidet P-40, 0.04% bromphenol blue, supplemented with protease inhibitor mixture (Sigma) at 2.5 μg of protein/μl and boiled for 5 min. The above lysates were loaded onto NuPAGE™ 12% BisTris protein gels (Invitrogen), and proteins were separated by electrophoresis in NuPAGE™ MOPS SDS running buffer (Invitrogen) for 3 h at 20 mA at 4 °C. Resolved proteins were transferred to nitrocellulose membranes in NuPAGE™ transfer buffer for 1.25 h at 30 V at 4 °C, followed by membrane blocking with 5% (w/v) dry milk. The membrane was incubated overnight with the antibodies for *TIM11*, *ATP20*, and γ subunits overnight at 4 °C. Immunoreactive bands were detected by chemiluminescence using an Uvitec Cambridge instrument.

### Blue native gel electrophoresis

Isolated yeast mitochondria were suspended in 150 mM potassium acetate, 30 mM HEPES, 10% glycerol, 1 mM phenylmethylsulfonyl fluoride, supplemented with 1.5% (w/v) digitonin, pH 7.4, at 10 mg/ml, followed by centrifugation at 100,000 × *g* for 25 min at 4 °C with a Beckman TL-100 rotor. Supernatants were collected and supplemented with native PAGE 5% G-250 sample additive (Invitrogen) and then rapidly applied onto NativePAGE™ Novex™ 3–12% BisTris protein gels (Invitrogen). Electrophoresis was carried out in the Dark Blue cathode buffer at 150 V for 20 min and in the Light Blue cathode buffer at 250 V for 2 h. After electrophoresis, gels were stained with Coomassie Blue or used for in-gel activity staining of F-ATP synthase as described previously (19).

### ATP hydrolysis assay

MLM or YM pretreated by PGO were suspended in 30 mM sucrose, 50 mM KCl, 50 mM Tris-HCl, 2 mM EGTA, 4 mM MgCl<sub>2</sub> and 2 mM phosphoenolpyruvate, supplemented with 4 units/ml pyruvate kinase, 3 units/ml lactate dehydrogenase, 2 mM ATP, and 0.3 mM NADH. Treatment with 4 μM oligomycin was performed at 37 °C for 15 min. The assay was carried out at 37 °C at a protein concentration of 40 μg × ml<sup>-1</sup> in a final volume of 0.2 ml. ATP synthesis was measured as the decrease of absorbance

of NADH at 340 nm using an Infinite® 200 PRO multimode microplate reader.

### Oxygen consumption rate

A Clark oxygen electrode was used to detect the oxygen consumption rate of isolated mitochondria. MLM were incubated in 250 mM sucrose, 10 mM Tris-MOPS, 10 μM EGTA, pH 7.4, at a final concentration of 0.5 mg of protein/ml in a final volume of 2 ml. Further additions were 5 mM succinate as substrate, 1 mM P<sub>i</sub>, and 0.2 mM ADP. YM were incubated in 250 mM sucrose, 10 mM Tris-MOPS, 20 μM EGTA, 5 mM P<sub>i</sub>, 0.5 mg/ml BSA, pH 7.4, at a final concentration of 0.25 mg of protein/ml in a final volume of 2 ml. Further additions were 1 mM NADH, 0.2 mM ADP, and 4 μM oligomycin.

### Mass spectrometry of g subunit peptides

Peptides (amino acids 88–114 of subunit g) modeled on the native sequence or containing alanine at position 106 were purchased from Caslo ApS (Kongens Lyngby, Denmark). Peptides were dissolved at a concentration of 100 μM in 10 mM Hepes-K<sup>+</sup>, pH 8.0, and allowed to react with 2 mM PGO at room temperature for 60 min. The reaction was stopped by the addition of 0.5% TFA. The peptides were separated from the reaction mixture by reverse phase chromatography using C18 ZipTips (Millipore) pre-equilibrated with 0.5% TFA. Bound peptides were eluted with 10 μl of 60% acetonitrile and 0.5% TFA. The eluate was concentrated to 1 μl under a stream of nitrogen, mixed with 1 μl of a saturated solution of α-cyano-4-hydroxycinnamic acid, and applied to the MALDI target plate. MALDI-TOF was performed on a Bruker Ultraflextreme (Bremen, Germany) mass spectrometer operating in positive reflectron mode. Calibration of the instrument was performed using peptides of known mass.

### Secondary structure assignment

This was performed pairing predictions from PSIPRED (59) and FIELDS (60), whereas transmembrane regions were predicted with TMHMM (61). Default parameters were selected. The three-dimensional structure was visualized with Chimera (62).

---

*Author contributions*—L. G., M. C., and P. B. conceptualization; L. G. and P. B. data curation; L. G. and M. C. formal analysis; L. G., M. C., and O. E. investigation; L. G. and P. B. writing-original draft; M. C., G. S., V. P., and P. B. supervision; M. C. validation; M. C. and G. S. methodology; P. B. funding acquisition; P. B. writing-review and editing; G. M. bioinformatics analysis.

---

### References

- Hunter, D. R., Haworth, R. A., and Southard, J. H. (1976) Relationship between configuration, function, and permeability in calcium-treated mitochondria. *J. Biol. Chem.* **251**, 5069–5077 [Medline](#)
- Kinnally, K. W., Campo, M. L., and Tedeschi, H. (1989) Mitochondrial channel activity studied by patch-clamping mitoplasts. *J. Bioenerg. Biomembr.* **21**, 497–506 [CrossRef Medline](#)
- Petronilli, V., Szabò, I., and Zoratti, M. (1989) The inner mitochondrial membrane contains ion-conducting channels similar to those found in bacteria. *FEBS Lett.* **259**, 137–143 [CrossRef Medline](#)

## Subunit g Arg-107 of F-ATPase regulates PTP

- Szabo, I., and Zoratti, M. (2014) Mitochondrial channels: ion fluxes and more. *Physiol. Rev.* **94**, 519–608 [CrossRef Medline](#)
- Bernardi, P., and von Stockum, S. (2012) The permeability transition pore as a Ca<sup>2+</sup> release channel: new answers to an old question. *Cell Calcium* **52**, 22–27 [CrossRef Medline](#)
- Petronilli, V., Penzo, D., Scorrano, L., Bernardi, P., and Di Lisa, F. (2001) The mitochondrial permeability transition, release of cytochrome *c* and cell death: correlation with the duration of pore openings *in situ*. *J. Biol. Chem.* **276**, 12030–12034 [CrossRef Medline](#)
- Giorgio, V., Guo, L., Bassot, C., Petronilli, V., and Bernardi, P. (2018) Calcium and regulation of the mitochondrial permeability transition. *Cell Calcium* **70**, 56–63 [CrossRef Medline](#)
- Bernardi, P., Rasola, A., Forte, M., and Lippe, G. (2015) The mitochondrial permeability transition pore: channel formation by F-ATP synthase, integration in signal transduction, and role in pathophysiology. *Physiol. Rev.* **95**, 1111–1155 [CrossRef Medline](#)
- Nicolli, A., Petronilli, V., and Bernardi, P. (1993) Modulation of the mitochondrial cyclosporin A-sensitive permeability transition pore by matrix pH: evidence that the pore open-closed probability is regulated by reversible histidine protonation. *Biochemistry* **32**, 4461–4465 [CrossRef Medline](#)
- Petronilli, V., Costantini, P., Scorrano, L., Colonna, R., Passamonti, S., and Bernardi, P. (1994) The voltage sensor of the mitochondrial permeability transition pore is tuned by the oxidation-reduction state of vicinal thiols: increase of the gating potential by oxidants and its reversal by reducing agents. *J. Biol. Chem.* **269**, 16638–16642 [Medline](#)
- Costantini, P., Chernyak, B. V., Petronilli, V., and Bernardi, P. (1996) Modulation of the mitochondrial permeability transition pore by pyridine nucleotides and dithiol oxidation at two separate sites. *J. Biol. Chem.* **271**, 6746–6751 [CrossRef Medline](#)
- Eriksson, O., Fontaine, E., and Bernardi, P. (1998) Chemical modification of arginines by 2,3-butanedione and phenylglyoxal causes closure of the mitochondrial permeability transition pore. *J. Biol. Chem.* **273**, 12669–12674 [CrossRef Medline](#)
- Linder, M. D., Morkunaite-Haimi, S., Kinnunen, P. K. J., Bernardi, P., and Eriksson, O. (2002) Ligand-selective modulation of the permeability transition pore by arginine modification: opposing effects of *p*-hydroxyphenylglyoxal and phenylglyoxal. *J. Biol. Chem.* **277**, 937–942 [CrossRef Medline](#)
- Speer, O., Morkunaite-Haimi, S., Liobikas, J., Franck, M., Hensbo, L., Linder, M. D., Kinnunen, P. K. J., Wallimann, T., and Eriksson, O. (2003) Rapid suppression of mitochondrial permeability transition by methylglyoxal: role of reversible arginine modification. *J. Biol. Chem.* **278**, 34757–34763 [CrossRef Medline](#)
- Johans, M., Milanese, E., Franck, M., Johans, C., Liobikas, J., Panagiotaki, M., Greci, L., Principato, G., Kinnunen, P. K. J., Bernardi, P., Costantini, P., and Eriksson, O. (2005) Modification of permeability transition pore arginine(s) by phenylglyoxal derivatives in isolated mitochondria and mammalian cells: structure-function relationship of arginine ligands. *J. Biol. Chem.* **280**, 12130–12136 [CrossRef Medline](#)
- Bonora, M., Bononi, A., De Marchi, E., Giorgi, C., Lebedzinska, M., Marchi, S., Patergnani, S., Rimessi, A., Suski, J. M., Wojtala, A., Wieckowski, M. R., Kroemer, G., Galluzzi, L., and Pinton, P. (2013) Role of the c subunit of the F<sub>0</sub> ATP synthase in mitochondrial permeability transition. *Cell Cycle* **12**, 674–683 [CrossRef Medline](#)
- Giorgio, V., von Stockum, S., Antoniel, M., Fabbro, A., Fogolari, F., Forte, M., Glick, G. D., Petronilli, V., Zoratti, M., Szabó, I., Lippe, G., and Bernardi, P. (2013) Dimers of mitochondrial ATP synthase form the permeability transition pore. *Proc. Natl. Acad. Sci. U.S.A.* **110**, 5887–5892 [CrossRef Medline](#)
- Alavian, K. N., Beutner, G., Lazrove, E., Sacchetti, S., Park, H. A., Licznarski, P., Li, H., Nabili, P., Hockensmith, K., Graham, M., Porter, G. A., Jr., and Jonas, E. A. (2014) An uncoupling channel within the c-subunit ring of the F<sub>1</sub>F<sub>0</sub> ATP synthase is the mitochondrial permeability transition pore. *Proc. Natl. Acad. Sci. U.S.A.* **111**, 10580–10585 [CrossRef Medline](#)
- Carraro, M., Giorgio, V., Šileikyte, S., Sartori, G., Forte, M., Lippe, G., Zoratti, M., Szabó, I., and Bernardi, P. (2014) Channel formation by yeast F-ATP synthase and the role of dimerization in the mitochondrial permeability transition. *J. Biol. Chem.* **289**, 15980–15985 [CrossRef Medline](#)
- von Stockum, S., Giorgio, V., Trevisan, E., Lippe, G., Glick, G. D., Forte, M. A., Da-Rè, C., Checchetto, V., Mazzotta, G., Costa, R., Szabó, I., and Bernardi, P. (2015) F-ATPase of *D. melanogaster* forms 53 picosiemens (53-pS) channels responsible for mitochondrial Ca<sup>2+</sup>-induced Ca<sup>2+</sup> release. *J. Biol. Chem.* **290**, 4537–4544 [CrossRef Medline](#)
- Giorgio, V., Burchell, V., Schiavone, M., Bassot, C., Minervini, G., Petronilli, V., Argenton, F., Forte, M., Tosatto, S., Lippe, G., and Bernardi, P. (2017) Ca<sup>2+</sup> binding to F-ATP synthase  $\beta$  subunit triggers the mitochondrial permeability transition. *EMBO Rep.* **18**, 1065–1076 [CrossRef Medline](#)
- Antoniel, M., Jones, K., Antonucci, S., Spolaore, B., Fogolari, F., Petronilli, V., Giorgio, V., Carraro, M., Di Lisa, F., Forte, M., Szabó, I., Lippe, G., and Bernardi, P. (2018) The unique histidine in OSCP subunit of F-ATP synthase mediates inhibition of the permeability transition pore by acidic pH. *EMBO Rep.* **19**, 257–268 [CrossRef Medline](#)
- He, J., Ford, H. C., Carroll, J., Ding, S., Fearnley, I. M., and Walker, J. E. (2017) Persistence of the mitochondrial permeability transition in the absence of subunit c of human ATP synthase. *Proc. Natl. Acad. Sci. U.S.A.* **114**, 3409–3414 [CrossRef Medline](#)
- He, J., Carroll, J., Ding, S., Fearnley, I. M., and Walker, J. E. (2017) Permeability transition in human mitochondria persists in the absence of peripheral stalk subunits of ATP synthase. *Proc. Natl. Acad. Sci. U.S.A.* **114**, 9086–9091 [CrossRef Medline](#)
- Bernardi, P., and Lippe, G. (2018) Channel formation by F-ATP synthase and the permeability transition pore: an update. *Curr. Opin. Physiol.* **3**, 1–5 [CrossRef](#)
- Oya, T., Hattori, N., Mizuno, Y., Miyata, S., Maeda, S., Osawa, T., and Uchida, K. (1999) Methylglyoxal modification of protein: chemical and immunochemical characterization of methylglyoxal-arginine adducts. *J. Biol. Chem.* **274**, 18492–18502 [CrossRef Medline](#)
- Ellis, E. M. (2007) Reactive carbonyls and oxidative stress: potential for therapeutic intervention. *Pharmacol. Ther.* **115**, 13–24 [CrossRef Medline](#)
- Maessen, D. E., Stehouwer, C. D., and Schalkwijk, C. G. (2015) The role of methylglyoxal and the glyoxalase system in diabetes and other age-related diseases. *Clin. Sci.* **128**, 839–861 [CrossRef Medline](#)
- Martins, A. M., Cordeiro, C. A., and Ponces Freire, A. M. (2001) *In situ* analysis of methylglyoxal metabolism in *Saccharomyces cerevisiae*. *FEBS Lett.* **499**, 41–44 [CrossRef Medline](#)
- Gomes, R. A., Sousa Silva, M., Vicente Miranda, H., Ferreira, A. E., Cordeiro, C. A., and Freire, A. P. (2005) Protein glycation in *Saccharomyces cerevisiae*: argpyrimidine formation and methylglyoxal catabolism. *FEBS J.* **272**, 4521–4531 [CrossRef Medline](#)
- Gomes, R. A., Vicente Miranda, H., Sousa Silva, M., Graça, G., Coelho, A. V., do Nascimento Ferreira, A. E., Cordeiro, C., and Freire, A. P. (2008) Protein glycation and methylglyoxal metabolism in yeast: finding peptide needles in protein haystacks. *FEMS Yeast Res.* **8**, 174–181 [CrossRef Medline](#)
- Baker, L. A., Watt, I. N., Runswick, M. J., Walker, J. E., and Rubinstein, J. L. (2012) Arrangement of subunits in intact mammalian mitochondrial ATP synthase determined by cryo-EM. *Proc. Natl. Acad. Sci. U.S.A.* **109**, 11675–11680 [CrossRef Medline](#)
- Davies, K. M., Anselmi, C., Wittig, I., Faraldo-Gómez, J. D., and Kühlbrandt, W. (2012) Structure of the yeast F<sub>1</sub>F<sub>0</sub>-ATP synthase dimer and its role in shaping the mitochondrial cristae. *Proc. Natl. Acad. Sci. U.S.A.* **109**, 13602–13607 [CrossRef Medline](#)
- Allegretti, M., Klusch, N., Mills, D. J., Vonck, J., Kühlbrandt, W., and Davies, K. M. (2015) Horizontal membrane-intrinsic  $\alpha$ -helices in the stator a-subunit of an F-type ATP synthase. *Nature* **521**, 237–240 [CrossRef Medline](#)
- Hahn, A., Parey, K., Bublitz, M., Mills, D. J., Zickermann, V., Vonck, J., Kühlbrandt, W., and Meier, T. (2016) Structure of a complete ATP synthase dimer reveals the molecular basis of inner mitochondrial membrane morphology. *Mol. Cell* **63**, 445–456 [CrossRef Medline](#)
- Guo, H., Bueler, S. A., and Rubinstein, J. L. (2017) Atomic model for the dimeric F<sub>0</sub> region of mitochondrial ATP synthase. *Science* **358**, 936–940 [CrossRef Medline](#)
- He, J., Ford, H. C., Carroll, J., Douglas, C., Gonzales, E., Ding, S., Fearnley, I. M., and Walker, J. E. (2018) Assembly of the membrane domain of ATP

- synthase in human mitochondria. *Proc. Natl. Acad. Sci. U.S.A.* **115**, 2988–2993 [CrossRef Medline](#)
38. Zeng, J., and Davies, M. J. (2005) Evidence for the formation of adducts and S-(carboxymethyl)cysteine on reaction of  $\alpha$ -dicarbonyl compounds with thiol groups on amino acids, peptides, and proteins. *Chem. Res. Toxicol.* **18**, 1232–1241 [CrossRef Medline](#)
  39. Mitome, N., Ono, S., Sato, H., Suzuki, T., Sone, N., and Yoshida, M. (2010) Essential arginine residue of the F<sub>o</sub>: a subunit in F<sub>o</sub>F<sub>1</sub>-ATP synthase has a role to prevent the proton shortcut without c-ring rotation in the F<sub>o</sub> proton channel. *Biochem. J.* **430**, 171–177 [CrossRef Medline](#)
  40. Uh, M., Jones, D., and Mueller, D. M. (1990) The gene coding for the yeast oligomycin sensitivity-conferring protein. *J. Biol. Chem.* **265**, 19047–19052 [Medline](#)
  41. Prescott, M., Bush, N. C., Nagley, P., and Devenish, R. J. (1994) Properties of yeast cells depleted of the OSCP subunit of mitochondrial ATP synthase by regulated expression of the ATP5 gene. *Biochem. Mol. Biol. Int.* **34**, 789–799 [Medline](#)
  42. Lee, C. F., Chavez, J. D., Garcia-Menendez, L., Choi, Y., Roe, N. D., Chiao, Y. A., Edgar, J. S., Goo, Y. A., Goodlett, D. R., Bruce, J. E., and Tian, R. (2016) Normalization of NAD<sup>+</sup> redox balance as a therapy for heart failure. *Circulation* **134**, 883–894 [CrossRef Medline](#)
  43. Burstein, S. R., Kim, H. J., Fels, J. A., Qian, L., Zhang, S., Zhou, P., Starkov, A. A., Iadecola, C., and Manfredi, G. (2018) Estrogen receptor  $\beta$  modulates permeability transition in brain mitochondria. *Biochim. Biophys. Acta* **1859**, 423–433 [CrossRef Medline](#)
  44. Allen, R. D. (1995) Membrane tubulation and proton pumps. *Protoplasma* **189**, 1–8 [CrossRef](#)
  45. Dudkina, N. V., Sunderhaus, S., Braun, H. P., and Boekema, E. J. (2006) Characterization of dimeric ATP synthase and cristae membrane ultrastructure from *Saccharomyces* and *Polytomella* mitochondria. *FEBS Lett.* **580**, 3427–3432 [CrossRef Medline](#)
  46. Paumard, P., Vaillier, J., Couly, B., Schaeffer, J., Soubannier, V., Mueller, D. M., Brèthes, D., di Rago, J. P., and Velours, J. (2002) The ATP synthase is involved in generating mitochondrial cristae morphology. *EMBO J.* **21**, 221–230 [CrossRef Medline](#)
  47. Arnold, I., Pfeiffer, K., Neupert, W., Stuart, R. A., and Schægger, H. (1998) Yeast mitochondrial F<sub>1</sub>F<sub>o</sub>-ATP synthase exists as a dimer: identification of three dimer-specific subunits. *EMBO J.* **17**, 7170–7178 [CrossRef Medline](#)
  48. Arselin, G., Giraud, M. F., Dautant, A., Vaillier, J., Brèthes, D., Couly, B., Schaeffer, J., and Velours, J. (2003) The GxxxG motif of the transmembrane domain of subunit e is involved in the dimerization/oligomerization of the yeast ATP synthase complex in the mitochondrial membrane. *Eur. J. Biochem.* **270**, 1875–1884 [CrossRef Medline](#)
  49. Arselin, G., Vaillier, J., Salin, B., Schaeffer, J., Giraud, M. F., Dautant, A., Brèthes, D., and Velours, J. (2004) The modulation in subunits e and g amounts of yeast ATP synthase modifies mitochondrial cristae morphology. *J. Biol. Chem.* **279**, 40392–40399 [CrossRef Medline](#)
  50. Strauss, M., Hofhaus, G., Schröder, R. R., and Kühlbrandt, W. (2008) Dimer ribbons of ATP synthase shape the inner mitochondrial membrane. *EMBO J.* **27**, 1154–1160 [CrossRef Medline](#)
  51. Wittig, I., Velours, J., Stuart, R., and Schægger, H. (2008) Characterization of domain interfaces in monomeric and dimeric ATP synthase. *Mol. Cell. Proteomics* **7**, 995–1004 [CrossRef Medline](#)
  52. Habersetzer, J., Ziani, W., Larriue, I., Stines-Chaumeil, C., Giraud, M. F., Brèthes, D., Dautant, A., and Paumard, P. (2013) ATP synthase oligomerization: from the enzyme models to the mitochondrial morphology. *Int. J. Biochem. Cell Biol.* **45**, 99–105 [CrossRef Medline](#)
  53. Madeo, F., Fröhlich, E., Ligr, M., Grey, M., Sigrist, S. J., Wolf, D. H., and Fröhlich, K. U. (1999) Oxygen stress: a regulator of apoptosis in yeast. *J. Cell Biol.* **145**, 757–767 [CrossRef Medline](#)
  54. Carraro, M., and Bernardi, P. (2016) Calcium and reactive oxygen species in regulation of the mitochondrial permeability transition and of programmed cell death in yeast. *Cell Calcium* **60**, 102–107 [CrossRef Medline](#)
  55. Laun, P., Büttner, S., Rinnerthaler, M., Burhans, W. C., and Breitenbach, M. (2012) Yeast aging and apoptosis. *Subcell. Biochem.* **57**, 207–232 [Medline](#)
  56. Lindblom, R., Higgins, G., Coughlan, M., and de Haan, J. B. (2015) Targeting mitochondria and reactive oxygen species-driven pathogenesis in diabetic nephropathy. *Rev. Diabet. Stud.* **12**, 134–156 [CrossRef Medline](#)
  57. von Stockum, S., Basso, E., Petronilli, V., Sabatelli, P., Forte, M. A., and Bernardi, P. (2011) Properties of Ca<sup>2+</sup> transport in mitochondria of *Drosophila melanogaster*. *J. Biol. Chem.* **286**, 41163–41170 [CrossRef Medline](#)
  58. Chen, D. C., Yang, B. C., and Kuo, T. T. (1992) One-step transformation of yeast in stationary phase. *Curr. Genet.* **21**, 83–84 [CrossRef Medline](#)
  59. Buchan, D. W., Minneci, F., Nugent, T. C., Bryson, K., and Jones, D. T. (2013) Scalable web services for the PSIPRED Protein Analysis Workbench. *Nucleic Acids Res.* **41**, W349–W357 [CrossRef Medline](#)
  60. Piovesan, D., Walsh, I., Minervini, G., and Tosatto, S. C. E. (2017) FIELDS: fast estimator of latent local structure. *Bioinformatics* **33**, 1889–1891 [CrossRef Medline](#)
  61. Krogh, A., Larsson, B., von Heijne, G., and Sonnhammer, E. L. (2001) Predicting transmembrane protein topology with a hidden Markov model: application to complete genomes. *J. Mol. Biol.* **305**, 567–580 [CrossRef Medline](#)
  62. Pettersen, E. F., Goddard, T. D., Huang, C. C., Couch, G. S., Greenblatt, D. M., Meng, E. C., and Ferrin, T. E. (2004) UCSF Chimera: a visualization system for exploratory research and analysis. *J. Comput. Chem.* **25**, 1605–1612 [CrossRef Medline](#)
  63. Petronilli, V., Cola, C., Massari, S., Colonna, R., and Bernardi, P. (1993) Physiological effectors modify voltage sensing by the cyclosporin A-sensitive permeability transition pore of mitochondria. *J. Biol. Chem.* **268**, 21939–21945 [Medline](#)

**Arginine 107 of yeast ATP synthase subunit g mediates sensitivity of the mitochondrial permeability transition to phenylglyoxal**  
Lishu Guo, Michela Carraro, Geppo Sartori, Giovanni Minervini, Ove Eriksson, Valeria Petronilli and Paolo Bernardi

*J. Biol. Chem.* 2018, 293:14632-14645.

doi: 10.1074/jbc.RA118.004495 originally published online August 9, 2018

---

Access the most updated version of this article at doi: [10.1074/jbc.RA118.004495](https://doi.org/10.1074/jbc.RA118.004495)

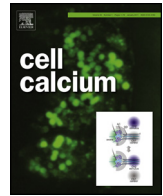
Alerts:

- [When this article is cited](#)
- [When a correction for this article is posted](#)

[Click here](#) to choose from all of JBC's e-mail alerts

This article cites 63 references, 32 of which can be accessed free at <http://www.jbc.org/content/293/38/14632.full.html#ref-list-1>





## Review

## Calcium and regulation of the mitochondrial permeability transition

Valentina Giorgio<sup>1</sup>, Lishu Guo<sup>1</sup>, Claudio Bassot, Valeria Petronilli, Paolo Bernardi\*

Department of Biomedical Sciences and CNR Neuroscience Institute, University of Padova, Italy

## ARTICLE INFO

## Article history:

Received 13 April 2017

Received in revised form 5 May 2017

Accepted 5 May 2017

Available online 10 May 2017

## Keywords:

Ca<sup>2+</sup>

Permeability transition

Mitochondria

F-ATP synthase

Channels

## ABSTRACT

Recent years have seen renewed interest in the permeability transition pore, a high conductance channel responsible for permeabilization of the inner mitochondrial membrane, a process that leads to depolarization and Ca<sup>2+</sup> release. Transient openings may be involved in physiological Ca<sup>2+</sup> homeostasis while long-lasting openings may trigger and/or execute cell death. In this review we specifically focus (i) on the hypothesis that the PTP forms from the F-ATP synthase and (ii) on the mechanisms through which Ca<sup>2+</sup> can reversibly switch this energy-conserving nanomachine into an energy-dissipating device.

© 2017 Elsevier Ltd. All rights reserved.

## Contents

1. Introduction.....	56
2. F <sub>1</sub> F <sub>0</sub> ATP synthase and the PTP.....	57
2.1. The mitochondrial F-ATP synthase.....	57
2.2. Mechanism of PTP formation from F-ATP synthase – the c ring hypothesis.....	58
2.3. Mechanism of PTP formation from F-ATP synthase – the peripheral stalk/dimer hypothesis.....	58
3. Is Ca <sup>2+</sup> a permissive factor for PTP opening?.....	59
4. Conclusions.....	60
Acknowledgements.....	60
References.....	60

## 1. Introduction

The permeability transition (PT) is an increased permeability of the mitochondrial inner membrane caused by opening of the PT pore (PTP), a channel whose prolonged opening leads to depolarization, loss of ionic homeostasis with Ca<sup>2+</sup> release, and cessation of mitochondrial ATP synthesis. If an osmotic imbalance between

*Abbreviations:* BAPTA-AM, N,N'-[1,2-ethanediybis(oxy-2,1-phenylene)]bis[N-2-[(acetyloxy)methoxy]-2-oxoethyl]]- bis[(acetyloxy)methyl] ester; CyP, cyclophilin; CsA, cyclosporin A; MMC, mitochondrial megachannel; OH-PGO, *p*-hydroxyphenylglyoxal; PhAsO, phenylarsine oxide; Pi, inorganic phosphate; PT, permeability transition; PTP, permeability transition pore.

\* Corresponding author. Department of Biomedical Sciences, University of Padova, Via Ugo Bassi 58/B, I-35121 Padova, Italy.

E-mail address: [bernardi@bio.unipd.it](mailto:bernardi@bio.unipd.it) (P. Bernardi).

<sup>1</sup> Equal contribution.

<https://doi.org/10.1016/j.ceca.2017.05.004>

0143-4160/© 2017 Elsevier Ltd. All rights reserved.

the matrix and the surrounding medium is generated and the channel has an appropriate size, mitochondrial swelling, rupture of the outer membrane and release of proapoptotic proteins may eventually take place [1]. Occurrence of a permeability increase (including inhibition by Mg<sup>2+</sup> and adenine nucleotides) in isolated mitochondria was recognized quite early [2,3] and its key functional features fully established in the 1970s [1]. The permeability change was defined “permeability transition” by Hunter and Haworth, who carried out a systematic characterization of inducers and inhibitors. They were the first to clearly propose that it resulted from opening of a regulated channel [4–6] whose molecular nature has long remained a mystery. The channel hypothesis of the PT was greatly consolidated by the discovery that the inner mitochondrial membrane possesses ion channels [7] and that one of them, the mitochondrial megachannel (MMC), has all the features of the

PTP including activation by  $\text{Ca}^{2+}$  and thiol oxidants, inhibition by  $\text{Mg}^{2+}/\text{ADP}$ , CsA and  $\text{H}^+$  [8–11] (see Ref. [12] for a thorough review).

A long-standing hypothesis proposed that the PTP forms at contact sites between the outer and inner mitochondrial membranes, and that the channel is composed by the adenine nucleotide translocator and/or the phosphate (Pi) carrier in the inner membrane and VDAC in the outer membrane, in association with a variety of regulatory proteins including the peripheral benzodiazepine receptor and cyclophilin (CyPD) [13]. This hypothesis has been conclusively disproved by genetic elimination of each candidate protein [14–18] with the exception of CyPD [19–22]. CyPD, the target of the inhibitor cyclosporin A (CsA), is a matrix peptidyl prolyl *cis-trans* isomerase that favors PTP opening but is not a structural pore component. We refer the reader to a comprehensive review for these earlier aspects of research on the PTP [1].

A recent study based on a phenotypic screen with siRNAs has proposed that the PTP forms from a complex of inner membrane SPG7 and outer membrane VDAC1 [23]. SPG7 and AFG3L are *m*-AAA proteases that associate to perform mitochondrial quality control [24]. Mutations of the corresponding genes are at the basis of hereditary spastic paraplegia [25] and spinocerebellar ataxia [26,27], respectively, and of other neurological syndromes [28]. As discussed in some detail elsewhere [29,30] we disagree with the Authors' conclusions because an essential role of VDAC1 has been conclusively ruled out by genetic experiments [15] and because PTP opening was still seen in the absence of SPG7 [23], proving that this protein is not essential for PTP formation. A subsequent study from the Langer laboratory reported that lack of SPG7 and/or AFG3L increased rather than decreased sensitivity to  $\text{Ca}^{2+}$ -induced PTP opening, a possible consequence of abnormal processing of the EMRE component of the mitochondrial  $\text{Ca}^{2+}$  uniporter complex generating excessive mitochondrial  $\text{Ca}^{2+}$  uptake [31]. While the basis for this discrepancy remains to be solved, we note that in diseases caused by SPG7 and AFG3L gene mutations the neuropathological findings include the prominent presence of abnormal, often swollen mitochondria [25–27,32,33], which is the expected outcome of PTP opening [1].

The PTP has been the subject of a very large number of studies. Its potential role in cell death was proposed in the early 1990s [34–38] and extensively addressed in a variety of paradigms that developed as the mitochondrial pathways to cell death were being unraveled, particularly after the discovery that release of cytochrome *c* is a key determinant in caspase 9 activation and induction of apoptosis [39]. Largely through the use of CsA and of its non-immunosuppressive derivatives (and later by elimination of the gene encoding CyPD), the role of the PTP could be also addressed in organ and whole animal studies, which yielded convincing results particularly in ischemia-reperfusion injury of the heart [19,21,40], in brain disease models [22,41–48] and in muscular dystrophies [49]. While long-lasting openings of the PTP are associated to cytochrome *c* release and cell death [50], transient openings have been documented *in situ* [51] that could serve the purpose of allowing fast mitochondrial  $\text{Ca}^{2+}$  release [52], as now supported by increasing experimental evidence [53–56]. These pathophysiological aspects have been addressed in a comprehensive review [1] and will not be further discussed here, where we will rather cover recent work on the nature of the PTP and the mechanism of its  $\text{Ca}^{2+}$ -dependence.

## 2. $\text{F}_1\text{F}_0$ ATP synthase and the PTP

By following its interactions with other mitochondrial proteins through an unbiased approach, we found that CyPD associates with the  $\text{F}_1\text{F}_0$  (F)-ATP synthase under conditions of mild detergent extraction. Binding was favored by Pi and prevented by CsA, and led to a partial (~30%) inhibition of enzymatic activity which could

be reactivated by CsA [57]. These findings are reminiscent of the effects of CyPD on the PTP, i.e. Pi and CyPD binding favor opening while CsA favors PTP closure through CyPD unbinding [58–60] and represent the first indication in the literature that the F-ATP synthase may be related to the PTP [57]. Following this lead, we showed that gel-purified dimers of F-ATP synthase from bovine heart mitochondria form  $\text{Ca}^{2+}$ -activated high conductance channels in lipid bilayers, and that these channels have all the key features of the MMC [61]. Channel formation was then demonstrated in preparations from yeast [62], drosophila [63] and human mitochondria [64], and in each case the electrophysiological features matched those of the corresponding PTPs [1]. Involvement of the F-ATP synthase is also supported by an independent study where treatment with siRNA against the *c* subunit of F-ATP synthase decreased PTP opening in response to several death stimuli [65]. The key question then became defining the mechanism(s) through which the energy-conserving F-ATP synthase can be turned into the energy-dissipating PTP, an issue that is the subject of intense research and considerable controversy [1].

### 2.1. The mitochondrial F-ATP synthase

F-ATP synthase is a large multisubunit complex of about 600 kDa organized into a catalytic ( $\text{F}_1$ ) and a membrane sector ( $\text{F}_0$ ) linked by central and peripheral stalks. The enzyme is located in the inner membrane, where under aerobic conditions it catalyzes the synthesis of ATP at the expense of the protonmotive force generated by the respiratory chain [66,67] whereas under anoxic conditions it works in the direction of ATP hydrolysis, a process that is limited by binding of inhibitory factor 1 [68–70]. Diffusion of  $\text{H}^+$  down their electrochemical gradient drives the rotation of a ring of *c* subunits within  $\text{F}_0$  and the co-rotation of the central stalk (comprising the  $\text{F}_1$   $\gamma$ ,  $\delta$  and  $\epsilon$  subunits) inside the catalytic  $\alpha_3\beta_3$  domain of the  $\text{F}_1$  sector, which is responsible for ATP synthesis [71]. *Vice versa*, ATP hydrolysis drives central stalk rotation in the opposite direction, with  $\text{H}^+$  translocation to the intermembrane space and formation of the protonmotive force. In either case the peripheral stalk is thought to act as a stator that counters the tendency of the  $\alpha_3\beta_3$  subcomplex to rotate with the central stalk [72]. In the  $\text{F}_0$  sector, subunits OSCP, b, d, F6, DAPIT and 6.8PL form the peripheral stalk, which extends from the top of  $\text{F}_1$  in the matrix along its external surface down into the membrane making contacts with the so-called accessory subunits e, f, g, and A6L, which also extend within the inner membrane [73–77]. Recently the regions of interaction between peripheral stalk and  $\text{F}_1$  catalytic domain have been characterized in *Yarrowia lipolytica* [77] and *Pichia angusta* [78]. These new findings suggest a general mechanism through which conformational changes occurring in  $\text{F}_1$  during catalysis may be propagated to the peripheral stalk. The binding site for CyPD is subunit OSCP [57,61,79], which is located on top of  $\text{F}_1$  and connects with the lateral stalk subunits b and d. F-ATP synthase is commonly isolated as a functional monomer, but this appears not to be the physiological state in the membrane. Indeed, high resolution cryo-electron microscopy of native mitochondrial membranes from yeast, algae, fungi, plants and mammals demonstrated that F-ATP synthase is organized in dimers, which then associate to form long rows of oligomers that help shape the cristae [80–85].

Essentially two hypotheses have been put forward to explain PTP formation from F-ATP synthase (see [86] for a specific review). The first suggests that the channel forms within the *c* ring after a  $\text{Ca}^{2+}$ -dependent modification leading to partial or total dissociation of the  $\text{F}_1$  sector from  $\text{F}_0$  [64,65]; the second proposes that the channel forms at the interface between monomers within the dimers [61]. Either model must account for activation by  $\text{Ca}^{2+}$  and ROS, inhibition by  $\text{Mg}^{2+}$ /adenine nucleotides, and for the effects of

CyPD, CsA and of a variety of PTP modulators like the membrane potential and matrix pH [1,87].

## 2.2. Mechanism of PTP formation from F-ATP synthase – the c ring hypothesis

To the best of our knowledge, evidence that the  $F_0$  sector of F-ATP synthase can form channels was first provided by Sorgato et al. in 1989, but the activity was insensitive to  $Ca^{2+}$  and pH and the Authors therefore concluded that the PTP was not involved [88]. Subsequent patch-clamp studies were carried out using highly purified c subunits, which assemble spontaneously into annular structures [89,90], and cGMP-activated channels were detected. At variance from the MMC and the PTP, however, these channels were inhibited rather than activated by  $Ca^{2+}$  [91–93]. A possible link between subunits c and PTP formation/regulation was suggested by PT induction by a phosphorylated peptide derived from subunit c as well as by subunit c itself [94,95]. Renewed interest in the c ring in the context of PTP formation was recently provided by two independent studies [64,65].

In the protocols of Bonora et al., HeLa cells were treated with siRNA against the c subunit or subjected to overexpression of a Myc-tagged c subunit, and the propensity of the PTP to open tested in several paradigms. The appropriate response was observed, with decreased PTP opening and cell death after suppression of the c subunit and increased PTP opening with matching increase in cell death after overexpression of the c subunit [65]. As also noted by Halestrap [96], these experiments are consistent with a role of the F-ATP synthase in PTP regulation but cannot reveal whether the c ring is directly involved or whether the results are rather a consequence of altered ATP production or of a misfolded protein response to the overexpressed construct. Furthermore, downregulation of the c subunit could have affected the biogenesis of the whole F-ATP synthase.

Alavian et al. have reconstituted the c subunit and the F-ATP synthase from human cells in liposomes and measured the presence of  $Ca^{2+}$ -activated channels [64] whose features resemble those we described for the purified bovine dimers [61]. They have suggested that the PTP channel forms within the c ring itself after  $Ca^{2+}$ -dependent extrusion of  $F_1$ , i.e. of the  $\gamma/\delta/\epsilon$  subunits [64]. In these experiments the channel could be closed by F-ATP synthase subunit  $\beta$  but not by its natural partners  $\gamma$ ,  $\delta$  or  $\epsilon$  [64]. We have already noted that the physical dissociation of  $F_1$  from  $F_0$  requires quite drastic conditions such as treatment with 2 M urea [97,98]. We also find it hard to envision a plausible mechanism through which matrix  $Ca^{2+}$  would cause release of  $F_1$  generating a channel that cannot be closed by  $F_1$  itself [64], while it is known that PTP-dependent swelling in saline media is a fully reversible process where pore closure is followed by shrinkage and complete recovery of inner membrane structure and function [99].

Solid evidence that the MMC/PTP channel does not form within the c ring comes from two recent studies. The Walker laboratory obtained from HAP1 human cells a clone where the *ATPG1*, *ATPG2*, and *ATPG3* genes encoding for subunit c were genetically disrupted, generating a vestigial F-ATP synthase which lacked the c subunit and additionally was devoid of subunits ATP6 and DAPIT [100]. These cells had  $Ca^{2+}$ -activated, CsA-sensitive PTP opening that was indistinguishable from what displayed by the parental, c ring-competent HAP1 line both in permeabilized and in intact cells [100]. The Faraldo-Gomez laboratory took a different approach and generated an atomistic simulation study on a variety of c rings. The results indicate that the lumen of the c ring cannot be occupied by water, which is an obvious prerequisite for ion conductivity, leading the Authors to conclude that the PTP channel cannot form within the c ring [101].

## 2.3. Mechanism of PTP formation from F-ATP synthase – the peripheral stalk/dimer hypothesis

Selective inhibitors of the PTP exist that do not compromise the catalytic activity of F-ATP synthase and *vice versa* [1], suggesting that catalytic activity and channel formation occur at different regions of the enzyme complex. Since gel-excised dimers but not monomers of F-ATP synthase rapidly gave rise to PTP-like channels in lipid bilayers [61–63] we proposed that channel formation does not involve the c ring (which participates in catalysis) but rather occurs at the interface of two adjacent monomers in the dimers [61]. This idea is also supported by a study in yeast, where ablation of subunits e and g (which are located at the monomer–monomer interface and stabilize the dimers) results in desensitization of the pore to  $Ca^{2+}$  [62]. Our working hypothesis [61], which is now supported by novel evidence [102], is that opening of the PTP is the indirect consequence of  $Ca^{2+}$  binding to the metal binding site of the  $\beta$  subunit within  $F_1$  [102], which in turn causes a conformational change that is propagated to the inner membrane by the peripheral stalk via OSCP (Fig. 1).

The  $F_1$  sector contains two binding sites for divalent metals ( $Me^{2+}$ ), a low affinity binding site in a peripheral loop [103] and the nucleotide binding pocket, which is exposed to the matrix in the  $\alpha\beta$  cleft with the majority of coordinating residues contributed by the  $\beta$  subunit [104]. The coordinating  $Me^{2+}$  is usually  $Mg^{2+}$ , but under conditions of high matrix  $Ca^{2+}$  the same site can be occupied by the latter cation [105] (Fig. 1). In the proteobacterium *Rhodospirillum rubrum* a single Thr to Ser mutation at position 159 of the  $\beta$  subunit abolished the hydrolysis of  $Ca^{2+}$ -ATP and increased the rate of hydrolysis of  $Mg^{2+}$ -ATP [106,107]. This same residue (Thr163 in the bovine enzyme) was also shown to play a key role in coordinating the  $Me^{2+}$  in the catalytic site of the bovine enzyme during ATP hydrolysis [104], suggesting that it may modulate the relative affinity for  $Me^{2+}$  also in the  $\beta$  subunit of mammals. Interestingly,  $Ca^{2+}$  binding has major functional consequences in the sense that  $Ca^{2+}$ -ATP hydrolysis occurs, but this is not matched by the buildup of a  $H^+$  gradient, suggesting that  $Ca^{2+}$  causes a conformational change in the enzyme complex that impairs energy conservation [108]. Such a conformational change could be PTP opening, as our recent data suggest [102]. We therefore investigated whether Thr163 is responsible for PTP modulation in human HeLa cells. Like in *Rhodospirillum rubrum* the Thr163Ser mutation in the human F-ATP synthase  $\beta$  subunit affected the catalytic activity, with inhibition of  $Ca^{2+}$ -ATP hydrolysis and increase of  $Mg^{2+}$ -ATP hydrolysis. At the same time, it desensitized  $Ca^{2+}$ -dependent PTP opening resulting in increased resistance to cell death in human cells as well as in developing zebrafish embryos [102]. Molecular dynamics simulations in the presence of  $Mg^{2+}$  were consistent with a motion originating at the catalytic sites and transmitted through the connecting loop (subunit  $\beta$  residues 82–131) to the “crown region”, the  $\beta$ -barrel shaped “ring” located at the binding interface between the  $F_1$  sector and OSCP [104]. In the presence of  $Ca^{2+}$  at the catalytic site the system became more rigid and extremely static at the connecting loop and in the crown region. This suggests that the larger van der Waals radius of  $Ca^{2+}$  induces spatial rearrangements that increase overall  $F_1$  rigidity [102]. We proposed that decreased compliance of the  $Ca^{2+}$ -bound F-ATP synthase transmits mechanical energy to OSCP, the “hinge” through which energy could then be transferred through the peripheral stalk to the inner membrane where the PTP eventually forms [77,109] (Fig. 1). We note that combined conformational changes at the OSCP/ $F_6$  and b subunit at the point of entrance into the membrane have actually been observed [109].

A critical role of OSCP in PTP modulation is emerging. Both CyPD and benzodiazepine 423 (a PTP inducer) affect the PTP by binding to the same site on OSCP [61] and acetylation of OSCP residue K70 promotes its interaction with CyPD sensitizing the PTP to opening

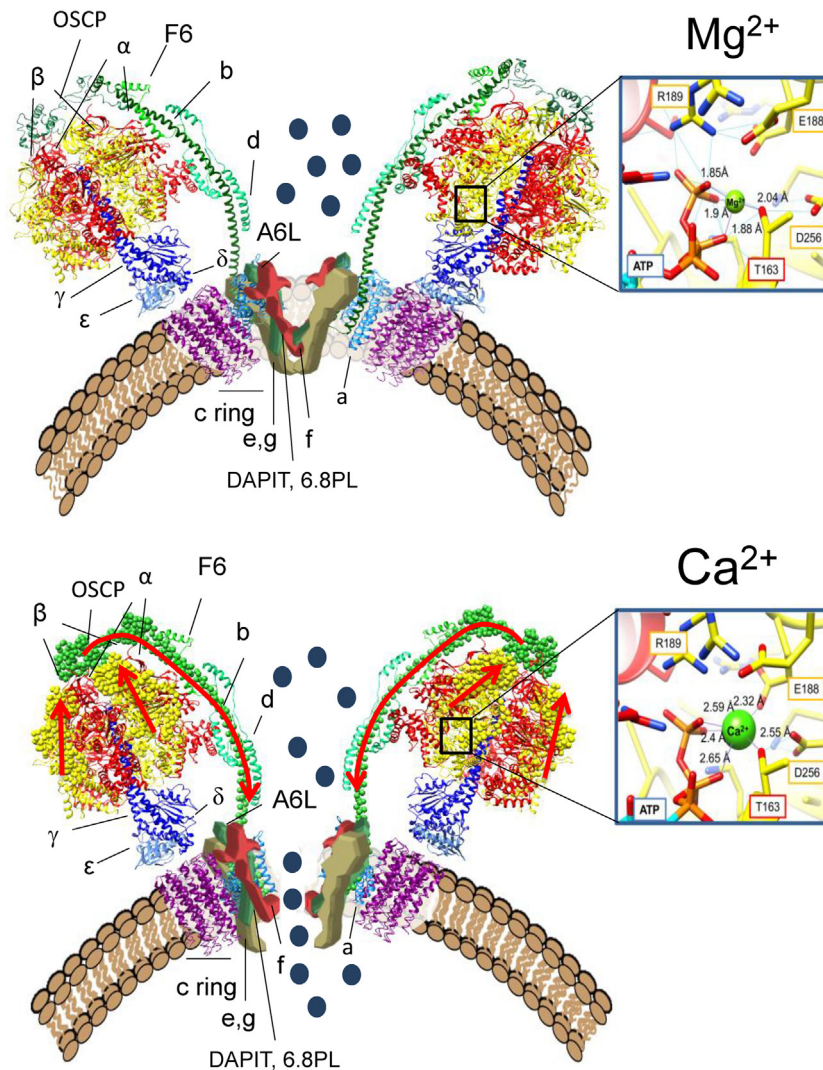


**Fig. 1.** Putative events leading to PTP formation from F-ATP synthase upon  $\text{Ca}^{2+}$  binding. Hypothetical structure of F-ATP synthase dimers with  $\text{Mg}^{2+}$  (upper panel) or  $\text{Ca}^{2+}$  (lower panel) bound at the catalytic sites (insets). The ribbon models are based on the bovine structure of Zhou et al. [109]. Subunits  $\alpha$  and  $\beta$  are colored in red and yellow, respectively. Subunits  $\epsilon$ ,  $\delta$  and  $\gamma$  are rendered in shades of blue and subunits OSCP, b, d, F6 (peripheral stalk) in shades of green. The c-ring is magenta and subunit a light blue. The transmembrane subunits are drawn based on the cryo-EM yeast structure of Hahn et al. [77]. Subunits A6L, f, e and g are colored in grey/green, dark red and yellow, respectively. In the lower panel the  $\alpha$ -carbon of the regions responsible for the putative conformational change occurring upon  $\text{Ca}^{2+}$  binding are highlighted using a sphere representation. Arrows are meant to indicate how the conformational change induced by  $\text{Ca}^{2+}$  binding could be transmitted to the lateral stalk and blue dots represent ion and solutes.

[79]. Thus, changes of OSCP conformation can affect the propensity of PTP opening in the inner membrane, which is more than 100 Å away. This putative mechanism is compatible with recently published structural data showing that the peripheral stalk makes more than one point of contact with  $\text{F}_1$  [77,78].

One last point to be considered is whether the presence of a PTP in HAP1-A12 cells devoid of the c ring undermines our hypothesis that the PTP forms at the peripheral stalk. Indeed (i) absence of the c ring also led to loss of A6L and of a subunit, which is involved in the dimerization surface; and (ii) after extraction with digitonin the resulting vestigial F-ATP synthase did not form fully assembled monomers, dimers or oligomers [100]. On the other hand, the F-ATP synthase of  $\rho^0$  cells (which has a virtually identical composition to that of HAP1-A12 cells except for the presence of the c subunits but obviously lacks subunit a) does display monomeric and dimeric forms of F-ATP synthase after digitonin extraction [100,110], and  $\rho^0$  cells undergo PTP opening *in situ* after detachment of hexokinase from mitochondria [111]. However, none of the subunits we proposed to contribute to PTP formation is downregulated in HAP-A12 cells [100] and as noted by the Authors of this study the vestigial

complex may be artifactually destabilized (i.e. monomerized) by the extraction process and remain dimeric within the membrane [100]. Thus, we think that resolving the issue of whether any or all of the  $\alpha$  helix-containing b, e, f, and g subunits are involved in forming the PTP must await gene disruption and mutagenic strategies.

### 3. Is $\text{Ca}^{2+}$ a permissive factor for PTP opening?

If  $\text{Ca}^{2+}$  must bind to the catalytic site of F-ATP synthase for the PT to occur, then  $\text{Ca}^{2+}$  should be a key permissive factor for PTP opening while other inducers should affect either the accessibility of the  $\text{Me}^{2+}$  binding site or the transmission of the  $\text{Ca}^{2+}$ -dependent conformational change to the inner membrane. The  $\text{Ca}^{2+}$ -dependence of the MMC measured with the patch-clamp in mitoplasts is absolute, in the sense that channel opening has never been observed unless  $\text{Ca}^{2+}$  was added [12]. On the other hand onset of the PT in the absence of added  $\text{Ca}^{2+}$  has been detected with phenylarsine oxide (PhAsO) [112], mastoparan [113,114], *p*-hydroxyphenylglyoxal (OH-PGO) [115], copper-*o*-phenanthroline

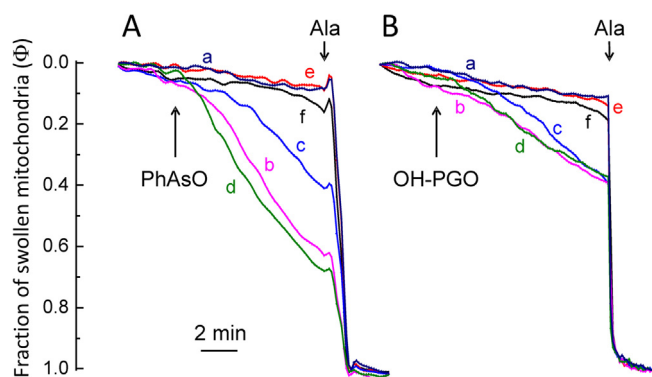


**Fig. 2.** PTP opening requires matrix  $\text{Ca}^{2+}$ . Deenergized mitochondria were incubated in the KCl-based medium specified below. Except for traces (a), PhAsO and OH-PGO were added where indicated. In traces (a) and (c) the medium was supplemented with 1 mM EGTA-Tris; in traces (b) no further additions were made; in traces (d) 50  $\mu\text{M}$   $\text{CaCl}_2$  was added; in traces (e) 1 mM EGTA-Tris and 1  $\mu\text{M}$  CsA were added; in traces (f) 1 mM EGTA-Tris was added and mitochondria had been preloaded with BAPTA. In all experiments Alamethicin (Ala, 5  $\mu\text{M}$ ) was added at the end of the experiments in order to determine the maximal mitochondrial swelling and convert absorbance values to the fraction of swollen mitochondria ( $\Phi$ ) as previously described [121]. Methods. Mouse liver mitochondria were isolated exactly as described [127] in a buffer containing 250 mM sucrose, 10 mM Tris-HCl, 0.1 mM EGTA-Tris, pH 7.4. Mitochondrial BAPTA loading was achieved by incubating mitochondria at 1 mg/ml in their isolation buffer in the presence of 0.2 mM BAPTA-AM (added as 40  $\mu\text{l}$ /ml DMSO from a stock solution) for 20 min at 25 °C. Mitochondria were harvested by centrifugation at 15,300  $\times$  g for 6 min and resuspended at 10 mg/ml in the isolation buffer at 4 °C. Mitochondria not loaded with BAPTA were subjected to the same procedure after the addition of vehicle (40  $\mu\text{l}$ /ml DMSO). Traces are representative of at least 3 replicates per condition. The incubation medium contained 0.1 M KCl, 10 mM Tris-Morpholine propane sulfonic acid pH 7.4, 1 mM  $\text{P}_i$ -Tris, 2  $\mu\text{M}$  rotenone and the additions specified above. The experiments were started by the addition of 0.5 mg/ml mouse liver mitochondria (not shown) and recordings started immediately after. Mitochondrial swelling was followed as the absorbance decrease at 540 nm in an Agilent Cary 100 UV-vis spectrophotometer equipped with magnetic stirring and thermostatic control.

and cyanine dyes [116]. Whether all these conditions reflect the occurrence of a *bona fide* PT, and given that the presence of adventitious and/or matrix  $\text{Ca}^{2+}$  has not been addressed in these studies, we have investigated the problem with the inducers PhAsO and OH-PGO [115,117]. In the following experiments (as is the case for many previous studies) we monitored onset of the PT indirectly from the apparent absorbance changes that mitochondria undergo when the PTP opens, solutes diffuse to the matrix and mitochondria swell. In these protocols (i) we incubated mitochondria in a KCl-based medium because the use of sucrose causes matrix acidification due to  $\text{H}^+/\text{K}^+$  exchange [118], which in turn opposes PTP opening [118,119]; (ii) we did not add respiratory substrates and inhibited endogenous respiration with rotenone since a high membrane potential would oppose PTP opening [120]; and (iii) we added the pore-forming antibiotic alamethicin at the end of each experiment to assess the maximum swelling response, so that swelling can be related to the fraction of mitochondria whose pore(s) have opened [121].

In the absence of any additions the absorbance remained stable, indicating a low basal permeability to  $\text{K}^+$  and  $\text{Cl}^-$  (Fig. 2A and B, traces a). The addition of PhAsO (Fig. 2A) or of OH-PGO (Fig. 2B) was followed by a process of absorbance decrease (traces b) that could be partially slowed down by EGTA (traces c) and marginally if at all altered by the addition of  $\text{Ca}^{2+}$  (traces d), suggesting that uptake of the adventitious  $\text{Ca}^{2+}$  present in the KCl solution was already sufficient to stimulate PTP opening. The swelling response otherwise observed in the presence of EGTA was inhibited by CsA (traces e), which also inhibited swelling induced by both PhAsO and OH-PGO under basal conditions or after the addition of  $\text{Ca}^{2+}$  (omitted for clarity). Remarkably, both PhAsO- and OH-PGO-induced

swelling was blunted by prior treatment with the membrane permeant  $\text{N,N}'$ -[1,2-ethanediylbis(oxy-2,1-phenylene)]bis[N-[2-[(acetyloxy)methoxy]-2-oxoethyl]]-, bis[(acetyloxy)methyl] ester (BAPTA-AM), which generates free BAPTA in the matrix resulting in chelation of  $\text{Ca}^{2+}$ . We conclude that CsA-sensitive swelling observed in previous studies in the absence of added  $\text{Ca}^{2+}$  or in the presence of EGTA [112–114,116] was due to adventitious or residual matrix  $\text{Ca}^{2+}$ , respectively; and that matrix  $\text{Ca}^{2+}$  is necessary (but not always sufficient) to observe PTP opening. We would like to stress that higher concentrations of mastoparan lead to CsA-insensitive permeabilization [113,114], which was also observed in our protocols for longer incubation times, the possible consequence of the opening of latent ion transport pathways for  $\text{K}^+$  and/or  $\text{Cl}^-$ . This is consistent with the fact that mitochondria possess a variety of cation and anion transport systems regulated by  $\text{Mg}^{2+}$  and  $\text{Ca}^{2+}$ . These include  $\text{K}^+$  ( $\text{Na}^+$ ) channels,  $\text{H}^+/\text{K}^+$  and  $\text{H}^+/\text{Na}^+$  antiporters whose molecular nature is being actively pursued [122–124]. In this connection it is noteworthy that activation of a  $\text{K}^+$  channel by PhAsO had been reported as early as in 1986 [125].

#### 4. Conclusions

In summary, we think that the PTP is likely to form from F-ATP synthase through a strictly  $\text{Ca}^{2+}$ -dependent mechanism that still awaits clarification but appears to involve (i) the intramembrane portion of subunits b, e, f, and/or g for channel formation; (ii) the peripheral stalk subunits for transduction of the  $\text{Ca}^{2+}$ -dependent conformational change originating at the  $\text{Ca}^{2+}$ -occupied catalytic site; and (iii) OSCP as a key integrator of regulatory interactions with CyPD and additional proteins and ligands like benzodiazepine 423 and sirtuin 3 [126]. This model is being actively tested by site-directed mutagenesis and by assessment of the structural features conferring species-specific features to the channels formed by F-ATP synthases [61–63]. Although much more work will be needed to solve the riddle of PTP formation, it is encouraging that the F-ATP synthase can accommodate all the key factors ( $\text{Ca}^{2+}/\text{Mg}^{2+}$ , adenine nucleotides, membrane potential, matrix pH,  $-\text{SH}$  oxidants and reductants, CyPD/CsA) that regulate PTP activity.

#### Acknowledgements

This work is in partial fulfillment of the requirements for the PhD of Lishu Guo at the University of Padova. Research in our laboratory is supported by Associazione Italiana Ricerca sul Cancro (AIRC) IG17067, Telethon ItalyGPP14187, and Fondation Leducq (16CVD04).

#### References

- [1] P. Bernardi, A. Rasola, M. Forte, G. Lippe, The mitochondrial permeability transition pore: channel formation by F-ATP synthase, integration in signal transduction, and role in pathophysiology, *Physiol. Rev.* 95 (2015) 1111–1155.
- [2] J. Raaflaub, Die schwellung isolierter leberzell mitochondrien und ihre physikalisch beeinflussbarkeit, *Helv. Physiol. Pharmacol. Acta* 11 (1953) 142–156.
- [3] J. Raaflaub, Über den wirkungsmechanismus von adenosintriphosphat (ATP) als cofaktor isolierter mitochondrien, *Helv. Physiol. Pharmacol. Acta* 11 (1953) 157–165.
- [4] D.R. Hunter, R.A. Haworth, The  $\text{Ca}^{2+}$ -induced membrane transition in mitochondria. I. The protective mechanisms, *Arch. Biochem. Biophys.* 195 (1979) 453–459.
- [5] R.A. Haworth, D.R. Hunter, The  $\text{Ca}^{2+}$ -induced membrane transition in mitochondria. II. Nature of the  $\text{Ca}^{2+}$  trigger site, *Arch. Biochem. Biophys.* 195 (1979) 460–467.
- [6] D.R. Hunter, R.A. Haworth, The  $\text{Ca}^{2+}$ -induced membrane transition in mitochondria. III. Transitional  $\text{Ca}^{2+}$  release, *Arch. Biochem. Biophys.* 195 (1979) 468–477.

- [7] M.C. Sorgato, B.U. Keller, W. Stühmer, Patch-clamping of the inner mitochondrial membrane reveals a voltage-dependent ion channel, *Nature* 330 (1987) 498–500.
- [8] K.W. Kinnally, M.L. Campo, H. Tedeschi, Mitochondrial channel activity studied by patch-clamping mitoplasts, *J. Bioenerg. Biomembr.* 21 (1989) 497–506.
- [9] V. Petronilli, I. Szabó, M. Zoratti, The inner mitochondrial membrane contains ion-conducting channels similar to those found in bacteria, *FEBS Lett.* 259 (1989) 137–143.
- [10] I. Szabó, M. Zoratti, The giant channel of the inner mitochondrial membrane is inhibited by cyclosporin A, *J. Biol. Chem.* 266 (1991) 3376–3379.
- [11] I. Szabó, M. Zoratti, The mitochondrial megachannel is the permeability transition pore, *J. Bioenerg. Biomembr.* 24 (1992) 111–117.
- [12] I. Szabó, M. Zoratti, Mitochondrial channels: ion fluxes and more, *Physiol. Rev.* 94 (2014) 519–608.
- [13] N. Zamzami, G. Kroemer, The mitochondrion in apoptosis: how Pandora's box opens, *Nat. Rev. Mol. Cell Biol.* 2 (2001) 67–71.
- [14] J.E. Kokoszka, K.G. Waymire, S.E. Levy, J.E. Sligh, J. Cai, D.P. Jones, G.R. MacGregor, D.C. Wallace, The ADP/ATP translocator is not essential for the mitochondrial permeability transition pore, *Nature* 427 (2004) 461–465.
- [15] A. Krauskopf, O. Eriksson, W.J. Craigen, M.A. Forte, P. Bernardi, Properties of the permeability transition in *VDAC1<sup>-/-</sup>* mitochondria, *Biochim. Biophys. Acta* 1757 (2006) 590–595.
- [16] C.P. Baines, R.A. Kaiser, T. Sheiko, W.J. Craigen, J.D. Molkenkin, Voltage-dependent anion channels are dispensable for mitochondrial-dependent cell death, *Nat. Cell Biol.* 9 (2007) 550–555.
- [17] M. Gutierrez-Aguilar, D.L. Douglas, A.K. Gibson, T.L. Domeier, J.D. Molkenkin, C.P. Baines, Genetic manipulation of the cardiac mitochondrial phosphate carrier does not affect permeability transition, *J. Mol. Cell. Cardiol.* 72 (2014) 316–325.
- [18] J. Šileikyte, E. Blachly-Dyson, R. Sewell, A. Carpi, R. Menabò, F. Di Lisa, F. Ricchelli, P. Bernardi, M. Forte, Regulation of the mitochondrial permeability transition pore by the outer membrane does not involve the peripheral benzodiazepine receptor (Translocator protein of 18 kDa (TSPO)), *J. Biol. Chem.* 289 (2014) 13769–13781.
- [19] C.P. Baines, R.A. Kaiser, N.H. Purcell, N.S. Blair, H. Osinska, M.A. Hambleton, E.W. Brunskill, M.R. Sayen, R.A. Gottlieb, G.W. Dorn, J. Robbins, J.D. Molkenkin, Loss of cyclophilin D reveals a critical role for mitochondrial permeability transition in cell death, *Nature* 434 (2005) 658–662.
- [20] E. Basso, L. Fante, J. Fowlkes, V. Petronilli, M.A. Forte, P. Bernardi, Properties of the permeability transition pore in mitochondria devoid of cyclophilin D, *J. Biol. Chem.* 280 (2005) 18558–18561.
- [21] T. Nakagawa, S. Shimizu, T. Watanabe, O. Yamaguchi, K. Otsu, H. Yamagata, H. Inohara, T. Kubo, Y. Tsujimoto, Cyclophilin D-dependent mitochondrial permeability transition regulates some necrotic but not apoptotic cell death, *Nature* 434 (2005) 652–658.
- [22] A.C. Schinzel, O. Takeuchi, Z. Huang, J.K. Fisher, Z. Zhou, J. Rubens, C. Hetz, N.N. Danial, M.A. Moskowitz, S.J. Korsmeyer, Cyclophilin D is a component of mitochondrial permeability transition and mediates neuronal cell death after focal cerebral ischemia, *Proc. Natl. Acad. Sci. U. S. A.* 102 (2005) 12005–12010.
- [23] S. Shanmughapriya, S. Rajan, N.E. Hoffman, A.M. Higgins, D. Tomar, N. Nemani, K.J. Hines, D.J. Smith, A. Eguchi, S. Vallem, F. Shaikh, M. Cheung, N.J. Leonard, R.S. Stolakis, M.P. Wolfers, J. Ibbett, J.K. Chuprun, N.R. Jog, S.R. Houser, W.J. Koch, J.W. Elrod, M. Madesh, SPG7 is an essential and conserved component of the mitochondrial permeability transition pore, *Mol. Cell* 60 (2015) 47–62.
- [24] P.M. Quirós, T. Langer, C. Lopez-Otín, New roles for mitochondrial proteases in health, ageing and disease, *Nat. Rev. Mol. Cell Biol.* 16 (2015) 345–359.
- [25] G. Casari, M. De Fusco, S. Ciarmatori, M. Zeviani, M. Mora, P. Fernandez, G. De Michele, A. Filla, S. Coccozza, R. Marconi, A. Durr, B. Fontaine, A. Ballabio, Spastic paraplegia and OXPHOS impairment caused by mutations in paraplegin, a nuclear-encoded mitochondrial metalloprotease, *Cell* 93 (1998) 973–983.
- [26] L. Atorino, L. Silvestri, M. Koppen, L. Cassina, A. Ballabio, R. Marconi, T. Langer, G. Casari, Loss of m-AAA protease in mitochondria causes complex I deficiency and increased sensitivity to oxidative stress in hereditary spastic paraplegia, *J. Cell Biol.* 163 (2003) 777–787.
- [27] D. Di Bella, F. Lazzaro, A. Brusco, M. Plumari, G. Battaglia, A. Pastore, A. Finardi, C. Cagnoli, F. Tempia, M. Frontali, L. Veneziano, T. Sacco, E. Boda, A. Brussino, F. Bonn, B. Castellotti, S. Baratta, C. Mariotti, C. Gellera, V. Fracasso, S. Magri, T. Langer, P. Plevani, S. Di Donato, M. Muzi-Falconi, F. Taroni, Mutations in the mitochondrial protease gene AFG3L2 cause dominant hereditary ataxia SCA28, *Nat. Genet.* 42 (2010) 313–321.
- [28] T.M. Pierson, D. Adams, F. Bonn, P.F. Martinelli, J.K. Cherukuri, N.F. Teer, P. Cruz, Mullikin For The Nisc Comparative Sequencing Program JC, R.W. Blakesley, G. Golas, J. Kwan, A. Sandler, F.K. Fuentes, T. Markello, C. Tiff, C. Blackstone, E.I. Rugarli, T. Langer, W.A. Gahl, C. Toro, Whole-exome sequencing identifies homozygous AFG3L2 mutations in a spastic ataxia-neuropathy syndrome linked to mitochondrial m-AAA proteases, *PLoS Genet.* 7 (2011) e1002325.
- [29] P. Bernardi, M. Forte, Commentary SPG7 is an essential and conserved component of the mitochondrial permeability transition pore, *Front. Physiol.* 6 (2015) 320.
- [30] P. Bernardi, M. Forte, Commentary the m-AAA protease associated with neurodegeneration limits MCU activity in mitochondria, *Front. Physiol.* 7 (2016) 583.
- [31] T. König, S.E. Tröder, K. Bakka, A. Korwitz, R. Richter-Dennerlein, P.A. Lampe, M. Patron, M. Muhlmeister, S. Guerrero-Castillo, U. Brandt, T. Decker, I. Lauria, A. Paggio, R. Rizzuto, E.I. Rugarli, D. De Stefani, T. Langer, The m-AAA protease associated with neurodegeneration limits MCU activity in mitochondria, *Mol. Cell* 64 (2016) 1–15.
- [32] F. Ferreira, A. Quattrini, M. Pirozzi, V. Valsecchi, G. Dina, V. Broccoli, A. Auricchio, F. Piemonte, G. Tozzi, L. Gaeta, G. Casari, A. Ballabio, E.I. Rugarli, Axonal degeneration in paraplegin-deficient mice is associated with abnormal mitochondria and impairment of axonal transport, *J. Clin. Invest.* 113 (2004) 231–242.
- [33] E.R. Almagan, R. Richter, L. Paeger, P. Martinelli, E. Barth, T. Decker, N.G. Larsson, P. Kloppenburg, T. Langer, E.I. Rugarli, AFG3L2 supports mitochondrial protein synthesis and Purkinje cell survival, *J. Clin. Invest.* 122 (2012) 4048–4058.
- [34] R. Imberti, A.L. Nieminen, B. Herman, J.J. Lemasters, Synergism of cyclosporin A and phospholipase inhibitors in protection against lethal injury to rat hepatocytes from oxidant chemicals, *Res. Commun. Chem. Pathol. Pharmacol.* 78 (1992) 27–38.
- [35] J.W. Snyder, J.G. Pastorino, A.M. Attie, J.L. Farber, Protection by cyclosporin A of cultured hepatocytes from the toxic consequences of the loss of mitochondrial energization produced by 1-methyl-4-phenylpyridinium, *Biochem. Pharmacol.* 44 (1992) 833–835.
- [36] J.G. Pastorino, J.W. Snyder, A. Serroni, J.B. Hoek, J.L. Farber, Cyclosporin and carnitine prevent the anoxic death of cultured hepatocytes by inhibiting the mitochondrial permeability transition, *J. Biol. Chem.* 268 (1993) 13791–13798.
- [37] M.R. Duchon, O. McGuinness, L.A. Brown, M. Crompton, On the involvement of a cyclosporin A sensitive mitochondrial pore in myocardial reperfusion injury, *Cardiovasc. Res.* 27 (1993) 1790–1794.
- [38] N. Zamzami, P. Marchetti, M. Castedo, D. Decaudin, A. Macho, T. Hirsch, S.A. Susin, P.X. Petit, B. Mignotte, G. Kroemer, Sequential reduction of mitochondrial transmembrane potential and generation of reactive oxygen species in early programmed cell death, *J. Exp. Med.* 182 (1995) 367–377.
- [39] X. Liu, C.N. Kim, J. Yang, R. Jemerson, X. Wang, Induction of apoptotic program in cell-free extracts: requirement for dATP and cytochrome c, *Cell* 86 (1996) 147–157.
- [40] E.J. Griffiths, A.P. Halestrap, Protection by Cyclosporin A of ischemia/reperfusion-induced damage in isolated rat hearts, *J. Mol. Cell. Cardiol.* 25 (1993) 1461–1469.
- [41] J. Folbergrova, P.A. Li, H. Uchino, M.L. Smith, B.K. Siesjö, Changes in the bioenergetic state of rat hippocampus during 2.5 min of ischemia, and prevention of cell damage by cyclosporin A in hyperglycemic subjects, *Exp. Brain Res.* 114 (1997) 44–50.
- [42] H. Friberg, M. Ferrand-Drake, F. Bengtsson, A.P. Halestrap, T. Wieloch, Cyclosporin A but not FK 506, protects mitochondria and neurons against hypoglycemic damage and implicates the mitochondrial permeability transition in cell death, *J. Neurosci.* 18 (1998) 5151–5159.
- [43] H. Uchino, E. Elmer, K. Uchino, P.A. Li, Q.P. He, M.L. Smith, B.K. Siesjö, Amelioration by cyclosporin A of brain damage in transient forebrain ischemia in the rat, *Brain Res.* 812 (1998) 216–226.
- [44] S. Matsumoto, H. Friberg, M. Ferrand-Drake, T. Wieloch, Blockade of the mitochondrial permeability transition pore diminishes infarct size in the rat after transient middle cerebral artery occlusion, *J. Cereb. Blood Flow Metab.* 19 (1999) 736–741.
- [45] D.O. Okonkwo, A. Buki, R. Siman, J.T. Povlishock, Cyclosporin A limits calcium-induced axonal damage following traumatic brain injury, *Neuroreport* 10 (1999) 353–358.
- [46] M. Forte, B.G. Gold, G. Marracci, P. Chaudhary, E. Basso, D. Johnsen, X. Yu, J. Fowlkes, M. Rahder, K. Stem, P. Bernardi, D. Bourdette, Cyclophilin D inactivation protects axons in experimental autoimmune encephalomyelitis, an animal model of multiple sclerosis, *Proc. Natl. Acad. Sci. U. S. A.* 104 (2007) 7558–7563.
- [47] H. Du, L. Guo, F. Fang, D. Chen, A.A. Sosunov, G.M. McKhann, Y. Yan, C. Wang, H. Zhang, J.D. Molkenkin, F.J. Gunn-Moore, J.P. Vonsattel, O. Arancio, J.X. Chen, S.D. Yan, Cyclophilin D deficiency attenuates mitochondrial and neuronal perturbation and ameliorates learning and memory in Alzheimer's disease, *Nat. Med.* 14 (2008) 1097–1105.
- [48] P.A. Parone, S. Da Cruz, J.S. Han, M. McAlonis-Downes, A.P. Vetto, S.K. Lee, E. Tseng, D.W. Cleveland, Enhancing mitochondrial calcium buffering capacity reduces aggregation of misfolded SOD1 and motor neuron cell death without extending survival in mouse models of inherited amyotrophic lateral sclerosis, *J. Neurosci.* 33 (2013) 4657–4671.
- [49] A. Zulian, M. Schiavone, V. Giorgio, P. Bernardi, Forty years later: mitochondria as therapeutic targets in muscle diseases, *Pharmacol. Res.* 113 (2016) 563–573.
- [50] V. Petronilli, D. Penzo, L. Scorrano, P. Bernardi, F. Di Lisa, The mitochondrial permeability transition, release of cytochrome c and cell death. Correlation with the duration of pore openings in situ, *J. Biol. Chem.* 276 (2001) 12030–12034.
- [51] V. Petronilli, G. Miotto, M. Canton, M. Brini, R. Colonna, P. Bernardi, F. Di Lisa, Transient and long-lasting openings of the mitochondrial permeability transition pore can be monitored directly in intact cells by changes in mitochondrial calcein fluorescence, *Biophys. J.* 76 (1999) 725–734.

- [52] P. Bernardi, S. von Stockum, The permeability transition pore as a  $\text{Ca}^{2+}$  release channel: new answers to an old question, *Cell Calcium* 52 (2012) 22–27.
- [53] J.W. Elrod, R. Wong, S. Mishra, R.J. Vagnozzi, B. Sakthivel, S.A. Goonasekera, J. Karch, S. Gabel, J. Farber, T. Force, J.H. Brown, E. Murphy, J.D. Molkentin, Cyclophilin D controls mitochondrial pore-dependent  $\text{Ca}^{2+}$  exchange, metabolic flexibility, and propensity for heart failure in mice, *J. Clin. Invest.* 120 (2010) 3680–3687.
- [54] A. Barsukova, A. Komarov, G. Hajnoczky, P. Bernardi, D. Bourdette, M. Forte, Activation of the mitochondrial permeability transition pore modulates  $\text{Ca}^{2+}$  responses to physiological stimuli in adult neurons, *Eur. J. Neurosci.* 33 (2011) 831–842.
- [55] X. Lu, J.Q. Kwong, J.D. Molkentin, D.M. Bers, Individual cardiac mitochondria undergo rare transient permeability transition pore openings, *Circ. Res.* 118 (2016) 834–841.
- [56] A. Agarwal, P.H. Wu, E.G. Hughes, M. Fukaya, M.A. Tischfield, A.J. Langseth, D. Wirtz, D.E. Bergles, Transient opening of the mitochondrial permeability transition pore induces microdomain calcium transients in astrocyte processes, *Neuron* 93 (2017) 587–605.
- [57] V. Giorgio, E. Bisetto, M.E. Soriano, F. Dabbeni-Sala, E. Basso, V. Petronilli, M.A. Forte, P. Bernardi, G. Lippe, Cyclophilin D modulates mitochondrial  $\text{F}_0\text{F}_1$ -ATP synthase by interacting with the lateral stalk of the complex, *J. Biol. Chem.* 284 (2009) 33982–33988.
- [58] C.P. Connern, A.P. Halestrap, Recruitment of mitochondrial cyclophilin to the mitochondrial inner membrane under conditions of oxidative stress that enhance the opening of a calcium-sensitive non-specific channel, *Biochem. J.* 302 (1994) 321–324.
- [59] C.P. Connern, A.P. Halestrap, Chaotropic agents and increased matrix volume enhance binding of mitochondrial cyclophilin to the inner mitochondrial membrane and sensitize the mitochondrial permeability transition to  $[\text{Ca}^{2+}]$ , *Biochemistry* 35 (1996) 8172–8180.
- [60] A. Nicolli, E. Basso, V. Petronilli, R.M. Wenger, P. Bernardi, Interactions of cyclophilin with the mitochondrial inner membrane and regulation of the permeability transition pore, a cyclosporin A-sensitive channel, *J. Biol. Chem.* 271 (1996) 2185–2192.
- [61] V. Giorgio, S. von Stockum, M. Antoniel, A. Fabbro, F. Fogolari, M. Forte, G.D. Glick, V. Petronilli, M. Zoratti, I. Szabó, G. Lippe, P. Bernardi, Dimers of mitochondrial ATP synthase form the permeability transition pore, *Proc. Natl. Acad. Sci. U. S. A.* 110 (2013) 5887–5892.
- [62] M. Carraro, V. Giorgio, J. Šileikyte, G. Sartori, M. Forte, G. Lippe, M. Zoratti, I. Szabó, P. Bernardi, Channel formation by yeast F-ATP synthase and the role of dimerization in the mitochondrial permeability transition, *J. Biol. Chem.* 289 (2014) 15980–15985.
- [63] S. von Stockum, V. Giorgio, E. Trevisan, G. Lippe, G.D. Glick, M.A. Forte, C. Da-Rè, V. Checchetto, G. Mazzotta, R. Costa, I. Szabó, P. Bernardi, F-ATPase of *D. melanogaster* forms 53 picosiemens (53-pS) channels responsible for mitochondrial  $\text{Ca}^{2+}$ -induced  $\text{Ca}^{2+}$  release, *J. Biol. Chem.* 290 (2015) 4537–4544.
- [64] K.N. Alavian, G. Beutner, E. Lazrove, S. Sacchetti, H.A. Park, P. Licznarski, H. Li, P. Nabili, K. Hockensmith, M. Graham, G.A. Porter Jr., E.A. Jonas, An uncoupling channel within the c-subunit ring of the  $\text{F}_1\text{F}_0$  ATP synthase is the mitochondrial permeability transition pore, *Proc. Natl. Acad. Sci. U. S. A.* 111 (2014) 10580–10585.
- [65] M. Bonora, A. Bononi, E. De Marchi, C. Giorgi, M. Liebdzinska, S. Marchi, S. Patergnani, A. Rimessi, J.M. Suski, A. Wojtala, M.R. Wieckowski, G. Kroemer, L. Galluzzi, P. Pinton, Role of the c subunit of the  $\text{F}_0$  ATP synthase in mitochondrial permeability transition, *ABV Cell Cycle* 12 (2013) 674–683.
- [66] P.D. Boyer, A perspective of the binding change mechanism for ATP synthesis, *FASEB J.* 3 (1989) 2164–2178.
- [67] A.E. Senior, ATP synthase: motoring to the finish line, *Cell* 130 (2007) 220–221.
- [68] E. Cabezon, P.J. Butler, M.J. Runswick, J.E. Walker, Modulation of the oligomerization state of the bovine  $\text{F}_1\text{F}_0$ -ATPase inhibitor protein  $\text{IF}_1$ , by pH, *J. Biol. Chem.* 275 (2000) 25460–25464.
- [69] F. Di Pancrazio, I. Mavelli, M. Isola, G. Losano, P. Pagliaro, D.A. Harris, G. Lippe, In vitro and in vivo studies of  $\text{F}_0\text{F}_1$  ATP synthase regulation by inhibitor protein  $\text{IF}_1$  in goat heart, *Biochim. Biophys. Acta* 1659 (2004) 52–62.
- [70] J.V. Bason, M.G. Montgomery, A.G. Leslie, J.E. Walker, Pathway of binding of the intrinsically disordered mitochondrial inhibitor protein to  $\text{F}_1\text{F}_0$ -ATPase, *Proc. Natl. Acad. Sci. U. S. A.* 111 (2014) 11305–11310.
- [71] H. Noji, R. Yasuda, M. Yoshida, K. Kinoshita Jr., Direct observation of the rotation of  $\text{F}_1\text{F}_0$ -ATPase, *Nature* 386 (1997) 299–302.
- [72] V.K. Dickson, J.A. Silvester, I.M. Fearnley, A.G. Leslie, J.E. Walker, On the structure of the stator of the mitochondrial ATP synthase, *EMBO J.* 25 (2006) 2911–2918.
- [73] I.R. Collinson, M.J. Runswick, S.K. Buchanan, I.M. Fearnley, J.M. Skehel, M.J. van Raaij, D.E. Griffiths, J.E. Walker, Fo membrane domain of ATP synthase from bovine heart mitochondria: purification, subunit composition, and reconstitution with  $\text{F}_1$ -ATPase, *Biochemistry* 33 (1994) 7971–7978.
- [74] L.A. Baker, I.N. Watt, M.J. Runswick, J.E. Walker, J.L. Rubinstein, Arrangement of subunits in intact mammalian mitochondrial ATP synthase determined by cryo-EM, *Proc. Natl. Acad. Sci. U. S. A.* 109 (2012) 11675–11680.
- [75] J. Habersetzer, W. Ziani, I. Larrieu, C. Stines-Chaumeil, M.F. Giraud, D. Brèthes, A. Dautant, P. Paumard, ATP synthase oligomerization: from the enzyme models to the mitochondrial morphology, *Int. J. Biochem. Cell Biol.* 45 (2013) 99–105.
- [76] J. Lee, S. Ding, T.B. Walpole, A.N. Holding, M.G. Montgomery, I.M. Fearnley, J.E. Walker, Organisation of subunits in the membrane domain of the bovine  $\text{F}_1\text{F}_0$ -ATPase revealed by covalent cross-linking, *J. Biol. Chem.* 290 (2015) 13308–13320.
- [77] A. Hahn, K. Parey, M. Bublitz, D.J. Mills, V. Zickermann, J. Vonck, W. Kühlbrandt, T. Meier, Structure of a complete ATP synthase dimer reveals the molecular basis of inner mitochondrial membrane morphology, *Mol. Cell* 63 (2016) 445–456.
- [78] K.R. Vinothkumar, M.G. Montgomery, S. Liu, J.E. Walker, Structure of the mitochondrial ATP synthase from *Pichia angusta* determined by electron cryo-microscopy, *Proc. Natl. Acad. Sci. U. S. A.* 113 (2016) 12709–12714.
- [79] C.F. Lee, J.D. Chavez, L. Garcia-Menendez, Y.S. Choi, N.D. Roe, Y.A. Chiao, J.S. Edgar, Y.A. Goo, D.R. Goodlett, J.E. Bruce, R. Tian, Normalization of  $\text{NAD}^+$  redox balance as a therapy for heart failure, *Circulation* 134 (2016) 883–894.
- [80] N.V. Dudkina, S. Sunderhaus, H.P. Braun, E.J. Boekema, Characterization of dimeric ATP synthase and cristae membrane ultrastructure from *Saccharomyces* and *Polytomella* mitochondria, *FEBS Lett.* 580 (2006) 3427–3432.
- [81] M. Strauss, G. Hofhaus, R.R. Schröder, W. Kühlbrandt, Dimer ribbons of ATP synthase shape the inner mitochondrial membrane, *EMBO J.* 27 (2008) 1154–1160.
- [82] D. Thomas, P. Bron, T. Weimann, A. Dautant, M.F. Giraud, P. Paumard, B. Salin, A. Cavalier, J. Velours, D. Brèthes, Supramolecular organization of the yeast  $\text{F}_1\text{F}_0$ -ATP synthase, *Biol. Cell* 100 (2008) 591–601.
- [83] K.M. Davies, M. Strauss, B. Daum, J.H. Kief, H.D. Osiewacz, A. Rycovska, V. Zickermann, W. Kühlbrandt, Macromolecular organization of ATP synthase and complex I in whole mitochondria, *Proc. Natl. Acad. Sci. U. S. A.* 108 (2011) 14121–14126.
- [84] K.M. Davies, C. Anselmi, I. Wittig, J.D. Faraldo-Gomez, W. Kühlbrandt, Structure of the yeast  $\text{F}_1\text{F}_0$ -ATP synthase dimer and its role in shaping the mitochondrial cristae, *Proc. Natl. Acad. Sci. U. S. A.* 109 (2012) 13602–13607.
- [85] B. Daum, A. Walter, A. Horst, H.D. Osiewacz, W. Kühlbrandt, Age-dependent dissociation of ATP synthase dimers and loss of inner-membrane cristae in mitochondria, *Proc. Natl. Acad. Sci. U. S. A.* 110 (2013) 15301–15306.
- [86] C. Gerle, On the structural possibility of pore-forming mitochondrial  $\text{F}_0\text{F}_1$  ATP synthase, *Biochim. Biophys. Acta* 1857 (2016) 1191–1196.
- [87] N. Kaludercic, V. Giorgio, The dual function of reactive Oxygen/Nitrogen species in bioenergetics and cell death: the role of ATP synthase, *Oxid. Med. Cell. Longev.* 2016 (2016) 3869610.
- [88] M.C. Sorgato, O. Moran, V. De Pinto, B.U. Keller, W. Stühmer, Further investigation on the high-conductance ion channel of the inner membrane of mitochondria, *J. Bioenerg. Biomembr.* 21 (1989) 485–496.
- [89] I. Arechaga, P.J. Butler, J.E. Walker, Self-assembly of ATP synthase subunit c rings, *FEBS Lett.* 515 (2002) 189–193.
- [90] T. Meier, U. Matthey, F. Henzen, P. Dimroth, D.J. Müller, The central plug in the reconstituted undecameric c cylinder of a bacterial ATP synthase consists of phospholipids, *FEBS Lett.* 505 (2001) 353–356.
- [91] J.E. McGeoch, G. Guidotti, A 0.1–700 Hz current through a voltage-clamped pore: candidate protein for initiator of neural oscillations, *Brain Res.* 766 (1997) 188–194.
- [92] J.E. McGeoch, M.W. McGeoch, R. Mao, G. Guidotti, Opposing actions of cGMP and calcium on the conductance of the  $\text{F}_0$  subunit c pore, *Biochem. Biophys. Res. Commun.* 274 (2000) 835–840.
- [93] J.E. McGeoch, G. Guidotti, Batten disease and the control of the  $\text{F}_0$  subunit c pore by cGMP and calcium, *Eur. J. Paediatr. Neurol.* 5 (Suppl A) (2001) 147–150.
- [94] T.S. Azarashvili, J. Tyynelä, I.V. Odinokova, P.A. Grigorjev, M. Baumann, Y.V. Evtodienko, N.E. Saris, Phosphorylation of a peptide related to subunit c of the  $\text{F}_0\text{F}_1$ -ATPase/ATP synthase and relationship to permeability transition pore opening in mitochondria, *J. Bioenerg. Biomembr.* 34 (2002) 279–284.
- [95] T. Azarashvili, I. Odinokova, A. Bakunts, V. Ternovsky, O. Krestinina, J. Tyynelä, N.-E.L. Saris, Potential role of subunit c of  $\text{F}_0\text{F}_1$ -ATPase and subunit c of storage body in the mitochondrial permeability transition. Effect of the phosphorylation status of subunit c on pore opening, *Cell Calcium* 55 (2014) 69–77.
- [96] A.P. Halestrap, A.P. Richardson, The mitochondrial permeability transition: a current perspective on its identity and role in ischaemia/reperfusion injury, *J. Mol. Cell. Cardiol.* 78 (2015) 129–141.
- [97] I.R. Collinson, M.J. van Raaij, M.J. Runswick, I.M. Fearnley, J.M. Skehel, G.L. Orriss, B. Miroux, J.E. Walker, ATP synthase from bovine heart mitochondria. In vitro assembly of a stalk complex in the presence of  $\text{F}_1$ -ATPase and in its absence, *J. Mol. Biol.* 242 (1994) 408–421.
- [98] Y. Kagawa, E. Racker, Partial resolution of the enzymes catalyzing oxidative phosphorylation. 8. Properties of a factor conferring oligomycin sensitivity on mitochondrial adenosine triphosphatase, *J. Biol. Chem.* 241 (1966) 2461–2466.
- [99] V. Petronilli, A. Nicolli, P. Costantini, R. Colonna, P. Bernardi, Regulation of the permeability transition pore, a voltage-dependent mitochondrial channel inhibited by cyclosporin A, *Biochim. Biophys. Acta* 1187 (1994) 255–259.
- [100] J. He, H.C. Ford, J. Carroll, S. Ding, I.M. Fearnley, J.E. Walker, Persistence of the mitochondrial permeability transition in the absence of subunit c of human ATP synthase, *Proc. Natl. Acad. Sci. U. S. A.* 114 (2017) 3409–3414.
- [101] W. Zhou, F. Marinelli, C. Nief, J.D. Faraldo-Gómez, Atomistic simulations indicate the c-subunit ring of the  $\text{F}_1\text{F}_0$  ATP synthase is not the mitochondrial permeability transition pore, *eLife Sci.* 6 (2017) e23781.

- [102] V. Giorgio, V. Burchell, M. Schiavone, C. Bassot, G. Minervini, V. Petronilli, F. Argenton, M. Forte, S. Tosatto, G. Lippe, P. Bernardi,  $\text{Ca}^{2+}$  binding to F-ATP synthase  $\beta$  subunit triggers the mitochondrial permeability transition, *EMBO Rep.* (2017), <http://dx.doi.org/10.15252/embr.201643354>, in press.
- [103] M.J. Hubbard, N.J. McHugh, Mitochondrial ATP synthase  $F_1$ - $\beta$ -subunit is a calcium-binding protein, *FEBS Lett.* 391 (1996) 323–329.
- [104] D.M. Rees, A.G. Leslie, J.E. Walker, The structure of the membrane extrinsic region of bovine ATP synthase, *Proc. Natl. Acad. Sci. U. S. A.* 106 (2009) 21597–21601.
- [105] P.L. Pedersen, N. Williams, J. Hullihen, Mitochondrial ATP synthase: dramatic  $\text{Mg}^{2+}$ -induced alterations in the structure and function of the  $F_1$ -ATPase moiety, *Biochemistry* 26 (1987) 8631–8637.
- [106] L. Nathanson, Z. Gromet-Elhanan, Mutations in the  $\beta$ -subunit Thr<sup>159</sup> and Glu<sup>184</sup> of the *Rhodospirillum rubrum*  $F_0F_1$  ATP synthase reveal differences in ligands for the coupled  $\text{Mg}^{2+}$ - and decoupled  $\text{Ca}^{2+}$ -dependent  $F_0F_1$  activities, *J. Biol. Chem.* 275 (2000) 901–905.
- [107] Z. Du, W.C. Tucker, M.L. Richter, Z. Gromet-Elhanan, Assembled  $F_1$ -( $\alpha\beta$ ) and Hybrid  $F_1$ - $\alpha_3\beta_3\gamma$ -ATPases from *Rhodospirillum rubrum*  $\alpha$ , wild type or mutant  $\beta$ , and chloroplast  $\gamma$  subunits. Demonstration of  $\text{Mg}^{2+}$  versus  $\text{Ca}^{2+}$ -induced differences in catalytic site structure and function, *J. Biol. Chem.* 276 (2001) 11517–11523.
- [108] S. Papageorgiou, A.B. Melandri, G. Solaini, Relevance of divalent cations to ATP-driven proton pumping in beef heart mitochondrial  $F_0F_1$ -ATPase, *J. Bioenerg. Biomembr.* 30 (1998) 533–541.
- [109] A. Zhou, A. Rohou, D.G. Schep, J.V. Bason, M.G. Montgomery, J.E. Walker, N. Grigorieff, J.L. Rubinstein, Structure and conformational states of the bovine mitochondrial ATP synthase by cryo-EM, *eLife Sci.* 4 (2015) e10180.
- [110] I. Wittig, B. Meyer, H. Heide, M. Steger, L. Bleier, Z. Wumaier, M. Karas, H. Schägger, Assembly and oligomerization of human ATP synthase lacking mitochondrial subunits a and A6L, *Biochim. Biophys. Acta* 1797 (2010) 1004–1011.
- [111] I. Masgras, A. Rasola, P. Bernardi, Induction of the permeability transition pore in cells depleted of mitochondrial DNA, *Biochimica et Biophysica Acta* 1817 (2012) 1860–1866.
- [112] E. Lenartowicz, P. Bernardi, G.F. Azzone, Phenylarsine oxide induces the cyclosporin A-sensitive membrane permeability transition in rat liver mitochondria, *J. Bioenerg. Biomembr.* 23 (1991) 679–688.
- [113] D.R. Pfeiffer, T.I. Gudz, S.A. Novgorodov, W.L. Erdahl, The peptide mastoparan is a potent facilitator of the mitochondrial permeability transition, *J. Biol. Chem.* 270 (1995) 4923–4932.
- [114] T. Yamamoto, M. Ito, K. Kageyama, K. Kuwahara, K. Yamashita, Y. Takiguchi, S. Kitamura, H. Terada, Y. Shinohara, Mastoparan peptide causes mitochondrial permeability transition not by interacting with specific membrane proteins but by interacting with the phospholipid phase, *FEBS J.* 281 (2014) 3933–3944.
- [115] M.D. Linder, S. Morkunaite-Haimi, P.K.J. Kinnunen, P. Bernardi, O. Eriksson, Ligand-selective modulation of the permeability transition pore by arginine modification. Opposing effects of *p*-hydroxyphenylglyoxal and phenylglyoxal, *J. Biol. Chem.* 277 (2002) 937–942.
- [116] Y. Shinohara, S. Bandou, S. Kora, S. Kitamura, S. Inazumi, H. Terada, Cationic uncouplers of oxidative phosphorylation are inducers of mitochondrial permeability transition, *FEBS Lett.* 428 (1998) 89–92.
- [117] M. Johans, E. Milanesi, M. Franck, C. Johans, J. Liobikas, M. Panagiotaki, L. Greci, G. Principato, P.K.J. Kinnunen, P. Bernardi, P. Costantini, O. Eriksson, Modification of permeability transition pore arginine(s) by phenylglyoxal derivatives in isolated mitochondria and mammalian cells: structure-function relationship of arginine ligands, *J. Biol. Chem.* 280 (2005) 12130–12136.
- [118] P. Bernardi, S. Vassanelli, P. Veronese, R. Colonna, I. Szabó, M. Zoratti, Modulation of the mitochondrial permeability transition pore. Effect of protons and divalent cations, *J. Biol. Chem.* 267 (1992) 2934–2939.
- [119] A. Nicolli, V. Petronilli, P. Bernardi, Modulation of the mitochondrial cyclosporin A-sensitive permeability transition pore by matrix pH. Evidence that the pore open-closed probability is regulated by reversible histidine protonation, *Biochemistry* 32 (1993) 4461–4465.
- [120] P. Bernardi, Modulation of the mitochondrial cyclosporin A-sensitive permeability transition pore by the proton electrochemical gradient. Evidence that the pore can be opened by membrane depolarization, *J. Biol. Chem.* 267 (1992) 8834–8839.
- [121] V. Petronilli, C. Cola, S. Massari, R. Colonna, P. Bernardi, Physiological effectors modify voltage sensing by the cyclosporin A-sensitive permeability transition pore of mitochondria, *J. Biol. Chem.* 268 (1993) 21939–21945.
- [122] K. Nowikovsky, T. Pozzan, R. Rizzuto, L. Scorrano, P. Bernardi, The pathophysiology of LETM1, *J. Gen. Physiol.* 139 (2012) 445–454.
- [123] M. Laskowski, B. Augustynek, B. Kulawiak, P. Koprowski, P. Bednarczyk, W. Jarmuszkiewicz, A. Szewczyk, What do we not know about mitochondrial potassium channels? *Biochim. Biophys. Acta – Bioenerg.* 1857 (2016) 1247–1257.
- [124] V. Checchetto, E. Teardo, L. Carraretto, L. Leanza, I. Szabó, Physiology of intracellular potassium channels: a unifying role as mediators of counterion fluxes? *Biochim. Biophys. Acta – Bioenerg.* 1857 (2016) 1258–1266.
- [125] J.J. Diwan, J. Srivastava, C. Moore, T. Haley, Stimulation of  $\text{K}^+$  flux into mitochondria by phenylarsine oxide, *J. Bioenerg. Biomembr.* 18 (1986) 123–134.
- [126] W. Yang, K. Nagasawa, C. Münch, Y. Xu, K. Satterstrom, S. Jeong, S.D. Hayes, M.P. Jedrychowski, F. Sejal Vyas, E. Zaganjor, V. Guarani, A.E. Ringel, S.P. Gygi, J. Wade Harper, M.C. Haigis, Mitochondrial sirtuin network reveals dynamic SIRT3-Dependent deacetylation in response to membrane depolarization, *Cell* 167 (2016) 985–1000.
- [127] P. Costantini, V. Petronilli, R. Colonna, P. Bernardi, On the effects of paraquat on isolated mitochondria. Evidence that paraquat causes opening of the cyclosporin A-sensitive permeability transition pore synergistically with nitric oxide, *Toxicology* 99 (1995) 77–88.



## **6 REFERENCES**

1. Margulis L (1975) Symbiotic theory of the origin of eukaryotic organelles; criteria for proof. *Symp Soc Exp Biol.* 29, 21-38.
2. Martin W, Roettger M, Kloesges T, Thiergart T, Woehle C, Gould S, Dagan T (2012) Modern endosymbiotic theory: Getting lateral gene transfer into the equation. *J Endocytobiosis Cell Res.* 23, 1-5.
3. Poole AM, Penny D (2007) Evaluating hypotheses for the origin of eukaryotes. *BioEssays.* 29, 74-84.
4. Roger AJ, Muñoz-Gómez SA, Kamikawa R (2017) The Origin and Diversification of Mitochondria. *Curr Biol.* 27, R1177-R1192.
5. Timmis JN, Ayliff MA, Huang CY, Martin W (2004) Endosymbiotic gene transfer: Organelle genomes forge eukaryotic chromosomes. *Nat Rev Genet.* 5, 123-135.
6. Allen JF (2015) Why chloroplasts and mitochondria retain their own genomes and genetic systems: Colocation for redox regulation of gene expression. *Proc Natl Acad Sci U S A.* 112, 10231-10238.
7. Rak M, Tzagoloff A (2009) F<sub>1</sub>-dependent translation of mitochondrially encoded Atp6p and Atp8p subunits of yeast ATP synthase. *Proc Natl Acad Sci U S A.* 106, 18509-18514.
8. Ernster L, Schatz G (1981) Mitochondria: A Historical Review. *J Cell Biol.* 91, 227-255.
9. Palade GE (1952) The fine structure of mitochondria. *Anat Rec.* 114, 427-451.
10. Harner M, Körner C, Walther D, Mokranjac D, Kaesmacher J, Welsch U, Griffith J, Mann M, Reggiori F, Neupert W (2011) The mitochondrial contact site complex, a determinant of mitochondrial architecture. *EMBO J.* 30, 4356-4370.
11. Shoshan-Barmatz V, De Pinto V, Zweckstetter M, Raviv Z, Keinan N, Arbel N (2010) VDAC, a multi-functional mitochondrial protein regulating cell life and death. *Mol Aspects Med.* 31, 227-285.
12. Herrmann JM, Riemer J (2010) The Intermembrane Space of Mitochondria. *Antioxid Redox Signal.* 13, 1341-1358.
13. McStay GP (2017) Complex formation and turnover of mitochondrial transporters and ion channels. *J Bioenerg Biomembr.* 49, 101-111.
14. Horvath SE, Rampelt H, Oeljeklaus S, Warscheid B, Van Der Laan M, Pfanner N (2015) Role of membrane contact sites in protein import into mitochondria. *Protein Sci.* 24, 277-297.
15. Matouschek A (1997) Active unfolding of precursor proteins during mitochondrial protein import. *EMBO J.* 16, 6727-6736.
16. Liu X, Kim CN, Yang J, Jemmerson R, Wang X (1996) Induction of apoptotic program in cell-free extracts: Requirement for dATP and cytochrome *c*. *Cell.* 86, 147-157.

17. Tait SWG, Green DR (2010) Mitochondria and cell death: outer membrane permeabilization and beyond. *Nat Rev Mol Cell Biol.* 11, 621-632.
18. Danial NN, Korsmeyer SJ (2004) Cell Death: Critical Control Points. *Cell.* 116, 205-219.
19. Wang X (2001) The expanding role of mitochondria in apoptosis. *Gene Dev.* 15, 2922-2933.
20. Fontanesi F (2015) Mitochondria: Structure and Role in Respiration. *eLS.* 1–13.
21. Lewis MR, Lewis WH. (1914) Mitochondria in tissue culture. *Science.* 39, 330-333.
22. van der Blik AM, Shen Q, Kawajiri S (2013) Mechanisms of mitochondrial fission and fusion. *Cold Spring Harb Perspect Biol.* 5, 1-16.
23. Twig G, Shirihai OS. (2011) The Interplay Between Mitochondrial Dynamics and Mitophagy. *Antioxid Redox Signal.* 14, 1939-1951.
24. Mouli PK, Twig G, Shirihai OS (2009) Frequency and selectivity of mitochondrial fusion are key to its quality maintenance function. *Biophys J.* 96, 3509-3518.
25. Cipolat S, de Brito OM, Dal Zilio B, Scorrano L (2004) OPA1 requires mitofusin 1 to promote mitochondrial fusion. *Proc Natl Acad Sci U S A.* 101, 15927-15932.
26. Osellame LD, Blacker TS, Duchen MR (2012) Cellular and molecular mechanisms of mitochondrial function. *Best Pract Res Clin Endocrinol Metab.* 26, 711-723.
27. Mitchell P (1961) Coupling of phosphorylation to electron and hydrogen transfer by a chemiosmotic type of mechanism. *Nature.* 191, 144-148.
28. Mitchell P (1979) Keilin's respiratory chain concept and its chemiosmotic consequences. *Science* 206, 1148-1159.
29. Papa S, Martino PL, Capitanio G, Gaballo A, Rasmussen D De, Signorile A, Petruzzella V (2012) The oxidative phosphorylation system in mammalian mitochondria. *Adv Exp Med Biol.* 942, 3-37.
30. Berrisford JM, Sazanov LA (2009) Structural basis for the mechanism of respiratory complex I. *J Biol Chem.* 284, 29773-29783.
31. Efremov RG, Sazanov LA (2011) Respiratory complex I: “steam engine” of the cell? *Curr Opin Struct Biol.* 21, 532-540.
32. Correia K, Yu SM, Mahadevan R (2017) Reconstructing the evolution of metabolism in budding yeasts. *bioRxiv.* 237974. doi: <https://doi.org/10.1101/237974>
33. De Deken RH (1966) The Crabtree Effect: A Regulatory System in Yeast. *J Gen Microbiol.* 44, 149-156.
34. Hunte C, Zickermann V, Brandt U (2010) Functional modules and structural basis of conformational coupling in mitochondrial complex I. *Science.* 329, 448-451.

35. Kluckova K, Bezawork-Geleta A, Rohlena J, Dong L, Neuzil J (2013) Mitochondrial complex II, a novel target for anti-cancer agents. *Biochim Biophys Acta-Bioenerg.* 1827, 552-564.
36. Xia D, Yu CA, Kim H, Xia JZ, Kachurin AM, Zhang L, Yu L & Deisenhofer J (1997) Crystal structure of the cytochrome bc<sub>1</sub> complex from bovine heart mitochondria. *Science* 277, 60-66.
37. Crofts AR (2004) The Cytochrome bc<sub>1</sub> Complex: Function in the Context of Structure. *Annu Rev Physiol.* 66, 689-733.
38. Murphy MP (2009) How mitochondria produce reactive oxygen species. *Biochem J.* 417, 1-13.
39. Guarás A, Perales-Clemente E, Calvo E, Acín-Pérez R, Loureiro-Lopez M, Pujol C, Martínez-Carrascoso I, Nuñez E, García-Marqués F, Rodríguez-Hernández MA, Cortés A, Diaz F, Pérez-Martos A, Moraes CT, Fernández-Silva P, Trifunovic A, Navas P, Vazquez J, Enríquez JA (2016) The CoQH<sub>2</sub>/CoQ Ratio Serves as a Sensor of Respiratory Chain Efficiency. *Cell Rep.* 15, 197-209.
40. Chouchani ET, Pell VR, Gaude E, Aksentijević D, Sundier SY, Robb EL, Logan A, Nadtochiy SM, Ord ENJ, Smith AC, Eyassu F, Shirley R, Hu CH, Dare AJ, James AM, Rogatti S, Hartley RC, Eaton S, Costa ASH, Brookes PS, Davidson SM, Duchon MR, Saeb-Parsy K, Shattock MJ, Robinson AJ, Work LM, Frezza C, Krieg T, Murphy MP (2014) Ischaemic accumulation of succinate controls reperfusion injury through mitochondrial ROS. *Nature.* 515, 431-435.
41. Lanciano P, Khalfaoui-Hassani B, Selamoglu N, Ghelli A, Rugolo M, Daldal F. (2013) Molecular mechanisms of superoxide production by complex III: a bacterial versus human mitochondrial comparative case study. *Biochim Biophys Acta.* 1827, 1332-1339.
42. Abramson J, Svensson-Ek M, Byrne B, Iwata S (2001) Structure of cytochrome c oxidase: A comparison of the bacterial and mitochondrial enzymes. *Biochim Biophys Acta-Protein Struct Mol Enzymol.* 1544, 1-9.
43. Kaila VRI, Sharma V, Wikström M (2011) The identity of the transient proton loading site of the proton-pumping mechanism of cytochrome c oxidase. *Biochim Biophys Acta-Bioenerg.* 1807, 80-84.
44. Cooper GM (2000) *The Cell: A Molecular Approach*. 2nd edition. The Mechanism of Oxidative Phosphorylation. Available from: <https://www.ncbi.nlm.nih.gov/books/NBK9885/>
45. Dudkina N V., Sunderhaus S, Boekema EJ, Braun HP (2008) The higher level of organization of the oxidative phosphorylation system: Mitochondrial supercomplexes. *J Bioenerg Biomembr.* 40, 419-424.
46. Winge DR (2012) Sealing the Mitochondrial Respirasome. *Mol Cell Biol.* 32, 2647-2652.
47. Guo R, Gu J, Zong S, Wu M, Yang M (2018) Structure and mechanism of mitochondrial electron transport chain. *Biomed J.* 41, 9-20.

48. Chandel NS (2015) Evolution of Mitochondria as Signaling Organelles. *Cell Metab.* 22, 204-206.
49. Schito L & Semenza GL (2016) Hypoxia-Inducible Factors: Master Regulators of Cancer Progression. *Trends Cancer* 2, 758-770.
50. Xia X, Lemieux ME, Li W, Carroll JS, Brown M, Liu XS, Kung AL (2009) Integrative analysis of HIF binding and transactivation reveals its role in maintaining histone methylation homeostasis. *Proc Natl Acad Sci U S A.* 106, 4260-4265.
51. Semenza GL (2003) Targeting HIF-1 for cancer therapy. *Nat Rev Cancer.* 3, 721-732.
52. Gong T, Cui L, Wang H, Wang H, Han N (2018) Knockdown of KLF5 suppresses hypoxia-induced resistance to cisplatin in NSCLC cells by regulating HIF-1 $\alpha$ -dependent glycolysis through inactivation of the PI3K/Akt/mTOR pathway. *J Transl Med.* 16, 164.
53. Woo YM, Shin Y, Lee EJ, Lee S, Jeong SH, Kong HK, Park EY, Kim HK, Han J, Chang M, Park JH (2015) Inhibition of aerobic glycolysis represses Akt/mTOR/HIF-1 $\alpha$  axis and restores tamoxifen sensitivity in antiestrogen-resistant breast cancer cells. *PLoS One.* 10, e0132285.
54. Pillai VB, Sundaresan NR, Kim G, Gupta M, Rajamohan SB, Pillai JB, Samant S, Ravindra PV, Isbatan A, Gupta MP (2010) Exogenous NAD blocks cardiac hypertrophic response via activation of the SIRT3-LKB1-AMP-activated kinase pathway. *J Biol Chem.* 285, 3133-3144.
55. Ahn BH, Kim HS, Song S, Lee IH, Liu J, Vassilopoulos A, Deng CX, Finkel T (2008) A role for the mitochondrial deacetylase Sirt3 in regulating energy homeostasis. *Proc Natl Acad Sci U S A.* 105, 14447-14452.
56. Zhang M, Deng Y, Zhang J, Liu J, Li Y, Su H (2018) SIRT3 Protects Rotenone-induced Injury in SH-SY5Y Cells by Promoting Autophagy through the LKB1-AMPK-mTOR Pathway. *Aging Dis.* 9, 273-286.
57. Zhang Q li, Cui B ri, Li H yan, Li P, Hong L, Liu LP, Ding DZ, Cui X (2013) MAPK and PI3K pathways regulate hypoxia-induced atrial natriuretic peptide secretion by controlling HIF-1 alpha expression in beating rabbit atria. *Biochem Biophys Res Commun.* 438, 507-512.
58. Khan AUH, Allende-Vega N, Gitenay D, Garaude J, Vo DN, Belkhala S, Gerbal-Chaloin S, Gondeau C, Daujat-Chavanieu M, Delettre C, Orecchioni S, Talarico G, Bertolini F, Anel A, Cuezva JM, Enriquez JA, Cartron G, Lecellier CH, Hernandez J & Villalba M (2018) Mitochondrial Complex I activity signals antioxidant response through ERK5. *Sci Rep.* 8, 7420.
59. Hajnóczky G, Robb-Gaspers LD, Seitz MB & Thomas AP (1995) Decoding of cytosolic calcium oscillations in the mitochondria. *Cell.* 82, 415-424.
60. Logan CV, Szabadkai G, Sharpe JA, Parry DA, Torelli S, Childs AM, Kriek M, Phadke R, Johnson CA, Roberts NY, Bonthron DT, Pysden KA, Whyte T, Munteanu I, Foley AR, Wheway G, Szymanska K, Natarajan S, Abdelhamed ZA, Morgan JE, Roper H, Santen GWE,

- Niks EH, van der Pol WL, Lindhout D, Raffaello A, De Stefani D, den Dunnen JT, Sun Y, Ginjaar I, Sewry CA, Hurles M, Rizzuto R, Consortium K, Duchen MR, Muntoni F & Sheridan E (2014) Loss-of-function mutations in MICU1 cause a brain and muscle disorder linked to primary alterations in mitochondrial calcium signaling. *Nat Genet.* 46, 188-193.
61. Antony AN, Paillard M, Moffat C, Juskeviciute E, Correnti J, Bolon B, Rubin E, Csordas G, Seifert EL, Hoek JB & Hajnóczky G (2016) MICU1 regulation of mitochondrial Ca<sup>2+</sup> uptake dictates survival and tissue regeneration. *Nat Commun.* 7, 10955.
  62. Patergnani S, Suski JM, Agnoletto C, Bononi A, Bonora M, De Marchi E, Giorgi C, Marchi S, Missioli S, Poletti F, Rimessi A, Duszynski J, Wieckowski MR, Pinton P (2011) Calcium signaling around Mitochondria Associated Membranes (MAMs). *Cell Commun Signal.* 9, 19.
  63. De Stefani D, Rizzuto R & Pozzan T (2016) Enjoy the Trip: Calcium in Mitochondria Back and Forth. *Annu Rev Biochem.* 85, 161-192.
  64. Hajnóczky G, Booth D, Csordas G, Debattisti V, Golénar T, Naghdi S, Niknejad N, Paillard M, Seifert EL & Weaver D (2014) Reliance of ER-mitochondrial calcium signaling on mitochondrial EF-hand Ca<sup>2+</sup> binding proteins: Miros, MICUs, LETM1 and solute carriers. *Curr Opin Cell Biol.* 29, 133-141.
  65. Csordás G, Thomas AP, Hajnóczky G (1999) Quasi synaptic calcium signal transmission between endoplasmic reticulum and mitochondria. *Embo J.* 18, 96-108.
  66. Kerkhofs M, Bittremieux M, Morciano G, Giorgi C, Pinton P, Parys JB, Bultynck G (2018) Emerging molecular mechanisms in chemotherapy: Ca<sup>2+</sup> signaling at the mitochondria-associated endoplasmic reticulum membranes. *Cell Death Dis.* 9, 334.
  67. Decuypere JP, Monaco G, Missiaen L, De Smedt H, Parys JB, Bultynck G (2011) IP<sub>3</sub> Receptors, Mitochondria, and Ca<sup>2+</sup> Signaling: Implications for Aging. *J Aging Res.* 2011, 920178.
  68. De Stefani D, Raffaello A, Teardo E, Szabó I & Rizzuto R (2011) A forty-kilodalton protein of the inner membrane is the mitochondrial calcium uniporter. *Nature* 476, 336-340.
  69. Baughman JM, Perocchi F, Girgis HS, Plovanich M, Belcher-Timme CA, Sancak Y, Bao XR, Strittmatter L, Goldberger O, Bogorad RL, Kotliansky V & Mootha VK (2011) Integrative genomics identifies MCU as an essential component of the mitochondrial calcium uniporter. *Nature.* 476, 341-345.
  70. Kirichok, Krapivinsky, Clapham, Kirichok Y, Krapivinsky G, Clapham DE (2004) The Mitochondrial Calcium Uniporter is a Highly Selective Ion Channel. *Nature.* 427, 360-364.
  71. Palty R, Silverman WF, Hershfinkel M, Caporale T, Sensi SL, Parnis J, Nolte C, Fishman D, Shoshan-Barmatz V, Herrmann S, Khananshvilid D & Sekler I (2010) NCLX is an essential component of mitochondrial Na<sup>+</sup>/Ca<sup>2+</sup> exchange. *Proc Natl Acad Sci U S A.* 107, 436-441.

72. Dash RK, Beard DA (2008) Analysis of cardiac mitochondrial Na<sup>+</sup>-Ca<sup>2+</sup> exchanger kinetics with a biophysical model of mitochondrial Ca<sup>2+</sup> handling suggests a 3:1 stoichiometry. *J Physiol.* 586, 3267-3285.
73. Nicholls DG, Chalmers S. (2004) The integration of mitochondrial calcium transport and storage. *J Bioenerg Biomembr.* 36, 277-281.
74. Nicholls DG (2005) Mitochondria and calcium signaling. *Cell Calcium.* 38, 311-317.
75. Colombini M (1979) A candidate for the permeability pathway of the outer mitochondrial membrane. *Nature.* 279, 643-645.
76. Raghavan A, Sheiko T, Graham BH & Craigen WJ (2012) Voltage-dependant anion channels: novel insights into isoform function through genetic models. *Biochim Biophys Acta.* 1818, 1477-1485.
77. Becker T, Wagner R (2018) Mitochondrial Outer Membrane Channels: Emerging Diversity in Transport Processes. *BioEssays.* 40, 1-8.
78. Campo ML, Peixoto PM, Martínez-Caballero S (2017) Revisiting trends on mitochondrial mega-channels for the import of proteins and nucleic acids. *J Bioenerg Biomembr.* 49, 75-99.
79. Mertins B, Psakis G, Essen LO (2014) Voltage-dependent anion channels: the wizard of the mitochondrial outer membrane. *Biol Chem.* 395, 1435-1442.
80. Shoshan-Barmatz V, Ben-Hail D, Admoni L, Krelin Y, Tripathi SS (2015) The mitochondrial voltage-dependent anion channel 1 in tumor cells. *Biochim Biophys Acta-Biomembr.* 1848, 2547-2475.
81. Szabó I, Zoratti M (2014) Mitochondrial Channels: Ion Fluxes and More. *Physiol Rev.* 94, 519-608.
82. Midzak A, Zirkin B & Papadopoulos V (2015) Translocator protein: pharmacology and steroidogenesis. *Biochem Soc Trans.* 43, 572-578.
83. Gatliff J & Campanella M (2016) TSPO: kaleidoscopic 18-kDa amid biochemical pharmacology, control and targeting of mitochondria. *Biochem J.* 473, 107-121.
84. Perocchi F, Gohil VM, Girgis HS, Bao XR, McCombs JE, Palmer AE & Mootha VK (2010) MICU1 encodes a mitochondrial EF hand protein required for Ca<sup>2+</sup> uptake. *Nature* 467, 291-296.
85. Csordàs G, Golenar T, Seifert EL, Kamer KJ, Sancak Y, Perocchi F, Moffat C, Weaver D, de la Fuente Perez S, Bogorad R, Koteliansky V, Adijanto J, Mootha VK & Hajnóczky G (2013) MICU1 controls both the threshold and cooperative activation of the mitochondrial Ca<sup>2+</sup> uniporter. *Cell Metab.* 17, 976-987.
86. Sancak Y, Markhard AL, Kitami T, Kovacs-Bogdan E, Kamer KJ, Udeshi ND, Carr SA, Chaudhuri D, Clapham DE, Li AA, Calvo SE, Goldberger O & Mootha VK (2013) EMRE is

- an essential component of the mitochondrial calcium uniporter complex. *Science*. 342, 1379-1382.
87. Vais H, Mallilankaraman K, Mak DO, Hoff H, Payne R, Tanis JE & Foskett JK (2016) EMRE Is a Matrix Ca<sup>2+</sup> Sensor that Governs Gatekeeping of the Mitochondrial Ca<sup>2+</sup> Uniporter. *Cell Rep*. 14, 403-410.
  88. Joiner ML, Koval OM, Li J, He BJ, Allamargot C, Gao Z, Luczak ED, Hall DD, Fink BD, Chen B, Yang J, Moore SA, Scholz TD, Strack S, Mohler PJ, Sivitz WI, Song LS & Anderson ME (2012) CaMKII determines mitochondrial stress responses in heart. *Nature*. 491, 269-273.
  89. Zhang T, Zhang Y, Cui M, Jin L, Wang Y, Lv F, Liu Y, Zheng W, Shang H, Zhang J, Zhang M, Wu H, Guo J, Zhang X, Hu X, Cao CM & Xiao RP (2016) CaMKII is a RIP3 substrate mediating ischemia- and oxidative stress-induced myocardial necroptosis. *Nat Med*. 22, 175-182.
  90. Raffaello A, De Stefani D, Sabbadin D, Teardo E, Merli G, Picard A, Checchetto V, Moro S, Szabó I & Rizzuto R (2013) The mitochondrial calcium uniporter is a multimer that can include a dominant-negative pore-forming subunit. *EMBO J*. 32, 2362-2376.
  91. Moore CL (1971) Specific inhibition of mitochondrial Ca<sup>++</sup> transport by ruthenium red. *Biochem Biophys Res Commun*. 42, 298-305.
  92. de Jesús García-Rivas G, Guerrero-Hernandez A, Guerrero-Serna G, Rodriguez-Zavala JS & Zazueta C (2005) Inhibition of the mitochondrial calcium uniporter by the oxo-bridged dinuclear ruthenium amine complex (Ru360) prevents from irreversible injury in postischemic rat heart. *FEBS J*. 272, 3477-3488.
  93. Marchi S, Pinton P (2014) The mitochondrial calcium uniporter complex: Molecular components, structure and physiopathological implications. *J Physiol*. 592, 829-839.
  94. Leanza L, Zoratti M, Gulbins E, Szabó I (2014) Mitochondrial ion channels as oncological targets. *Oncogene*. 33, 5569-5581.
  95. O-Uchi J, Pan S, Sheu SS (2012) Molecular identities of mitochondrial Ca<sup>2+</sup> influx mechanism: Updated passwords for accessing mitochondrial Ca<sup>2+</sup>-linked health and disease. *J Gen Physiol*. 139, 435-443.
  96. Bernardi P & Petronilli V (1996) The permeability transition pore as a mitochondrial calcium release channel: a critical appraisal. *J Bioenerg Biomembr*. 28, 131-138.
  97. Nicholls DG & Rial E (1999) A history of the first uncoupling protein, UCP1. *J Bioenerg Biomembr*. 31, 399-406.
  98. Ricquier D & Bouillaud F (2000) The uncoupling protein homologues: UCP1, UCP2, UCP3, StUCP and AtUCP. *Biochem J*. 345, 161-179.



99. Mao W, Yu XX, Zhong A, Li W, Brush J, Sherwood SW, Adams SH & Pan G (1999) UCP4, a novel brain-specific mitochondrial protein that reduces membrane potential in mammalian cells. *FEBS Lett.* 443, 326-330.
100. Yu XX, Mao W, Zhong A, Schow P, Brush J, Sherwood SW, Adams SH & Pan G (2000) Characterization of novel UCP5/BMCP1 isoforms and differential regulation of UCP4 and UCP5 expression through dietary or temperature manipulation. *FASEB J.* 14, 1611-1618.
101. Kunji ER (2004) The role and structure of mitochondrial carriers. *FEBS Lett.* 564, 239-244.
102. Papa S, Francavilla A, Paradies G, Meduri B (1971) The transport of pyruvate in rat liver mitochondria. *FEBS Lett.* 12, 285-288.
103. Herzig S, Raemy E, Montessuit S, Veuthey JL, Zamboni N, Westermann B, Kunji ER, Martinou JC (2012) Identification and functional expression of the mitochondrial pyruvate carrier. *Science.* 337, 93-96.
104. Bricker DK, Taylor EB, Schell JC, Orsak T, Boutron A, Chen YC, Cox JE, Cardon CM, Van Vranken JG, Dephoure N, Redin C, Boudina S, Gygi SP, Brivet M, Thummel CS, Rutter J (2012) A mitochondrial pyruvate carrier required for pyruvate uptake in yeast, *Drosophila*, and humans. *Science.* 337, 96-100.
105. Rauckhorst AJ, Taylor EB (2016) Mitochondrial pyruvate carrier function and cancer metabolism. *Curr Opin Genet Dev.* 38, 102-109.
106. Monné M, Palmieri F (2014) Antiporters of the mitochondrial carrier family. *Curr Top Membr.* 73, 289-320.
107. Taylor EB (2017) Functional Properties of the Mitochondrial Carrier System. *Trends Cell Biol.* 27, 633-644.
108. Bernardi P (1999) Mitochondrial transport of cations: channels, exchangers, and permeability transition. *Physiol Rev.* 79, 1127-1155.
109. Hunter R, Haworth RA, Southard JH (1976) Relationship between configuration, function, and permeability in calcium-treated mitochondria. *J Biol Chem.* 251, 5069-5077.
110. Hunter DR, Haworth RA (1979) The  $\text{Ca}^{2+}$ -induced membrane transition in mitochondria. I. The protective mechanisms. *Arch Biochem Biophys.* 195, 453-459.
111. Haworth RA, Hunter DR (1979) The  $\text{Ca}^{2+}$ -induced membrane transition in mitochondria. II. Nature of the  $\text{Ca}^{2+}$  trigger site. *Arch Biochem Biophys.* 195, 460-467.
112. Hunter DR, Haworth RA (1979) The  $\text{Ca}^{2+}$ -induced membrane transition in mitochondria. III. Transitional  $\text{Ca}^{2+}$  release. *Arch Biochem Biophys.* 195, 468-477.
113. Haworth RA, Hunter DR (1980) Allosteric inhibition of the  $\text{Ca}^{2+}$ -activated hydrophilic channel of the mitochondrial inner membrane by nucleotides. *J Membr Biol.* 54, 231-236.

114. Haworth R, Hunter D (2000) Control of the mitochondrial permeability transition pore by high-affinity ADP binding at the ADP/ATP translocase in permeabilized mitochondria. *J Bioenerg Biomembr.* 32, 91-96.
115. Fournier N, Ducet G, Crevat A (1987) Action of cyclosporine on mitochondrial calcium fluxes. *J Bioenerg Biomembr.* 19, 297–303.
116. Crompton M, Ellinger H, Costi A (1988) Inhibition by cyclosporin A of a Ca<sup>2+</sup>-dependent pore in heart mitochondria activated by inorganic phosphate and oxidative stress. *Biochem J.* 255, 357-360.
117. Broekemeier KM, Dempsey ME, Pfeiffer DR (1989) Cyclosporin A is a potent inhibitor of the inner membrane permeability transition in liver mitochondria. *J Biol Chem.* 264, 7826-7830.
118. Halestrap AP & Davidson AM (1990) Inhibition of Ca<sup>2+</sup>-induced large-amplitude swelling of liver and heart mitochondria by cyclosporin is probably caused by the inhibitor binding to mitochondrial-matrix peptidyl-prolyl *cis-trans* isomerase and preventing it interacting with the adenine nucleotide translocase. *Biochem J.* 268, 153-160.
119. Sorgato MC, Keller BU, Stühmer W (1987) Patch-clamping of the inner mitochondrial membrane reveals a voltage-dependent ion channel. *Nature.* 330, 498–500.
120. Petronilli V, Szabó I, Zoratti M (1989) The inner mitochondrial membrane contains ion-conducting channels similar to those found in bacteria. *FEBS Lett.* 259, 137-143.
121. Kinnally KW, Campo ML, Tedeschi H (1989) Mitochondrial channel activity studied by patch-clamping mitoplasts. *J Bioenerg Biomembr.* 21, 497-506.
122. Zoratti M, Szabó I. (1995) The mitochondrial permeability transition. *Biochim Biophys Acta.* 1241, 139-176.
123. Szabó I, Zoratti M (1992) The mitochondrial megachannel is the permeability transition pore. *J Bioenerg Biomembr.* 24, 111-117.
124. Szabó I, Bernardi P, Zorattis M (1992) Modulation of the Mitochondrial Megachannel by Divalent Cations and Protons. *J Biol Chem.* 267, 940-2946.
125. Bernardi P, Rasola A, Forte M, Lippe G (2015) The Mitochondrial Permeability Transition Pore: Channel Formation by F-ATP Synthase, Integration in Signal Transduction, and Role in Pathophysiology. *Physiol Rev.* 95, 1111-1155.
126. Giorgio V, Guo L, Bassot C, Petronilli V, Bernardi P (2018) Calcium and regulation of the mitochondrial permeability transition. *Cell Calcium.* 70, 56-63.
127. Bernardi P, Veronese P & Petronilli V (1993) Modulation of the mitochondrial cyclosporin A-sensitive permeability transition pore. I. Evidence for two separate Me<sup>2+</sup> binding sites with opposing effects on the pore open probability. *J Biol Chem.* 268, 1005-1010.

128. Al-Nasser I, Crompton M (1986) The reversible  $\text{Ca}^{2+}$ -induced permeabilization of rat liver mitochondria. *Biochem J.* 239, 19-29.
129. Crompton M, Costi A (1988) Kinetic evidence for a heart mitochondrial pore activated by  $\text{Ca}^{2+}$ , inorganic phosphate and oxidative stress. A potential mechanism for mitochondrial dysfunction during cellular  $\text{Ca}^{2+}$  overload. *Eur J Biochem.* 178, 489-501.
130. Crompton M, Costi A (1990) A heart mitochondrial  $\text{Ca}^{2+}$ -dependent pore of possible relevance to re-perfusion-induced injury. Evidence that ADP facilitates pore interconversion between the closed and open states. *Biochem J.* 266, 33-39.
131. Petronilli V, Nicolli A, Costantini P, Colonna R & Bernardi P (1994) Regulation of the permeability transition pore, a voltage-dependent mitochondrial channel inhibited by cyclosporin A. *Biochim Biophys Acta.* 1187, 255-259.
132. Bernardi P (1992) Modulation of the mitochondrial cyclosporin A-sensitive permeability transition pore by the proton electrochemical gradient. Evidence that the pore can be opened by membrane depolarization. *J Biol Chem.* 267, 8834-8839.
133. Jiang Y, Ruta V, Chen J, Lee A, Mackinnon R (2003) The principle of gating charge movement in a voltage-dependent  $\text{K}^+$  channel. *Nature.* 423, 42-48.
134. Swartz KJ. (2008) Sensing voltage across lipid membranes. *Nature.* 456, 891-897.
135. Krepiy D, Mihailescu M, Freitas JA, Schow EV, Worcester DL, Gawrisch K, Tobias DJ, White SH, Swartz KJ (2009) Structure and hydration of membranes embedded with voltage-sensing domains. *Nature.* 462, 473-479.
136. Nicolli A, Petronilli V, Bernardi P (1993) Modulation of the Mitochondrial Cyclosporin A-Sensitive Permeability Transition Pore by Matrix pH. Evidence That the Pore Open-Closed Probability Is Regulated by Reversible Histidine Protonation. *Biochemistry.* 32, 4461-4465.
137. Kristian T, Bernardi P, Siesjö BK (2001) Acidosis promotes the permeability transition in energized mitochondria: implications for reperfusion injury. *J Neurotrauma.* 18, 1059-1074.
138. Novgorodov SA, Kultayeva EV, Yaguzhinsky LS, Lemeshko VV (1987) Ion permeability induction by the SH cross-linking reagents in rat liver mitochondria is inhibited by the free radical scavenger, butylhydroxytoluene. *J Bioenerg Biomembr.* 19, 191-202.
139. Petronilli V, Costantini P, Scorrano L, Colonna R, Passamonti S, Bernardi P (1994) The voltage sensor of the mitochondrial permeability transition pore is tuned by the oxidation-reduction state of vicinal thiols: Increase of the gating potential by oxidants and its reversal by reducing agents. *J Biol Chem.* 269, 16638-16642.
140. Traber J, Suter M, Walter P, Richter C (1992) In vivo modulation of total and mitochondrial glutathione in rat liver. Depletion by phorone and rescue by N-acetylcysteine. *Biochem Pharmacol.* 43, 961-964.

141. Costantini P, Chernyak BV, Petronilli V & Bernardi P (1996) Modulation of the mitochondrial permeability transition pore by pyridine nucleotides and dithiol oxidation at two separate sites. *J Biol Chem.* 271, 6746-6751.
142. Cumming RC, Andon NL, Haynes PA, Park M, Fischer WH, Schubert D (2004) Protein Disulfide Bond Formation in the Cytoplasm during Oxidative Stress. *J Biol Chem.* 279, 21749-21758.
143. Pfeiffer DR, Schmid PC, Beatrice MC, Schmid HH (1979) Intramitochondrial phospholipase activity and the effects of Ca<sup>2+</sup> plus N-ethylmaleimide on mitochondrial function. *J Biol Chem.* 254, 11485-11494.
144. Beatrice MC, Palmer JW, Pfeiffer DR (1980) The relationship between mitochondrial membrane permeability, membrane potential, and the retention of Ca<sup>2+</sup> by mitochondria. *J Biol Chem.* 255, 8663-8671.
145. Broekemeier KM & Pfeiffer DR (1995) Inhibition of the mitochondrial permeability transition by cyclosporin A during long time frame experiments: relationship between pore opening and the activity of mitochondrial phospholipases. *Biochemistry.* 34, 16440-16449.
146. Wojtczak L & Lehninger AL (1961) Formation and disappearance of an endogenous uncoupling factor during swelling and contraction of mitochondria. *Biochim Biophys Acta.* 51, 442-456.
147. Wang P & Heitman J (2005) The cyclophilins. *Genome Biol.* 6, 226.1-226.6.
148. Nicolli A, Basso E, Petronilli V, Wenger RM & Bernardi P (1996) Interactions of cyclophilin with the mitochondrial inner membrane and regulation of the permeability transition pore, a cyclosporin A-sensitive channel. *J Biol Chem.* 271, 2185-2192.
149. Connern CP & Halestrap AP (1996) Chaotropic agents and increased matrix volume enhance binding of mitochondrial cyclophilin to the inner mitochondrial membrane and sensitize the mitochondrial permeability transition to Ca<sup>2+</sup>. *Biochemistry.* 35, 8172-8180.
150. Giorgio V, Soriano ME, Basso E, Bisetto E, Lippe G, Forte MA, Bernardi P (2010) Cyclophilin D in mitochondrial pathophysiology. *Biochim Biophys Acta.* 1797, 1113-1118.
151. Baines CP, Kaiser RA, Purcell NH, Blair NS, Osinska H, Hambleton MA, Brunskill EW, Sayen MR, Gottlieb RA, Dorn GW, Robbins J, Molkenin JD. (2005) Loss of cyclophilin D reveals a critical role for mitochondrial permeability transition in cell death. *Nature.* 434, 658-662.
152. Nakagawa T, Shimizu S, Watanabe T, Yamaguchi O, Otsu K, Yamagata H, Inohara H, Kubo T, Tsujimoto Y (2005) Cyclophilin D-dependent mitochondrial permeability transition regulates some necrotic but not apoptotic cell death. *Nature.* 434, 652-658.

153. Basso E, Fante L, Fowlkes J, Petronilli V, Forte MA, Bernardi P (2005) Properties of the permeability transition pore in mitochondria devoid of cyclophilin D. *J Biol Chem.* 280, 18558-18561.
154. Schinzel AC, Takeuchi O, Huang Z, Fisher JK, Zhou Z, Rubens J, Hetz C, Danial NN, Moskowitz MA & Korsmeyer SJ (2005) Cyclophilin D is a component of mitochondrial permeability transition and mediates neuronal cell death after focal cerebral ischemia. *Proc Natl Acad Sci U S A.* 102, 12005-12010.
155. Schonbrunner ER, Mayer S, Tropschug M, Fischer G, Takahashi N, Schmid FX (1991) Catalysis of protein folding by cyclophilins from different species. *J Biol Chem.* 266, 3630-3635.
156. Matouschek A, Rospert S, Schmid K, Glick BS, Schatz G (1995) Cyclophilin catalyzes protein folding in yeast mitochondria. *Proc Natl Acad Sci U S A.* 92, 6319-6123.
157. Jung DW, Bradshaw PC, Pfeiffer DR (1997) Properties of a cyclosporin-insensitive permeability transition pore in yeast mitochondria. *J Biol Chem.* 272, 21104-21112.
158. Carraro M, Giorgio V, Sileikyte J, Sartori G, Forte M, Lippe G, Zoratti M, Szabò I, Bernardi P (2014) Channel Formation by Yeast F-ATP Synthase and the Role of Dimerization in the Mitochondrial Permeability Transition. *J Biol Chem.* 289, 15980-15985.
159. Kamei Y, Koushi M, Aoyama Y, Asakai R (2018) The yeast mitochondrial permeability transition is regulated by reactive oxygen species, endogenous Ca<sup>2+</sup> and Cpr3, mediating cell death. *Biochim Biophys Acta-Bioenerg.* pii: S0005-2728(18)30197-X.
160. Bernardi P & Pietrobon D (1982) On the nature of Pi-induced, Mg<sup>2+</sup>-prevented Ca<sup>2+</sup> release in rat liver mitochondria. *FEBS Lett.* 139, 9-12.
161. Zoccarato F, Nicholls D (1982) The role of phosphate in the regulation of the independent calcium-efflux pathway of liver mitochondria. *Eur J Biochem.* 127, 333-338.
162. Giorgio V, Bisetto E, Soriano ME, Dabbeni-Sala F, Basso E, Petronilli V, Forte MA, Bernardi P, Lippe G (2009) Cyclophilin D modulates mitochondrial FoF<sub>1</sub>-ATP synthase by interacting with the lateral stalk of the complex. *J Biol Chem.* 284, 33982-33988.
163. Giorgio V, von Stockum S, Antoniel M, Fabbro A, Fogolari F, Forte M, Glick GD, Petronilli V, Zoratti M, Szabó I, Lippe G, Bernardi P (2013) Dimers of mitochondrial ATP synthase form the permeability transition pore. *Proc Natl Acad Sci U S A.* 110, 5887-5892.
164. Basso E, Petronilli V, Forte MA, Bernardi P (2008) Phosphate is essential for inhibition of the mitochondrial permeability transition pore by cyclosporin A and by cyclophilin D ablation. *J Biol Chem.* 283, 26307-26311.
165. Von Stockum S, Basso E, Petronilli V, Sabatelli P, Forte MA, Bernardi P (2011) Properties of Ca<sup>2+</sup> transport in mitochondria of *Drosophila melanogaster*. *J Biol Chem.* 286, 41163-41170.

166. Bernardi P, Von Stockum S (2012) The permeability transition pore as a  $\text{Ca}^{2+}$  release channel : New answers to an old question. *Cell Calcium*. 52, 22-27.
167. Carraro M, Bernardi P (2016) Calcium and reactive oxygen species in regulation of the mitochondrial permeability transition and of programmed cell death in yeast. *Cell Calcium*. 60, 102-107.
168. Von Stockum S, Giorgio V, Trevisan E, Lippe G, Glick GD, Forte MA, Da-Rè C, Checchetto V, Mazzotta G, Costa R, Szabò I, Bernardi P (2015) F-ATPase of *Drosophila melanogaster* forms 53-picosiemen (53-pS) channels responsible for mitochondrial  $\text{Ca}^{2+}$ -induced  $\text{Ca}^{2+}$  release. *J Biol Chem*. 290, 4537-4544.
169. Means JC, Muro I, Clem RJ (2006) Lack of involvement of mitochondrial factors in caspase activation in a *Drosophila* cell-free system. *Cell Death Differ*. 13, 1222-1234.
170. Zorov DB, Juhaszova M, Sollott SJ (2014) Mitochondrial Reactive Oxygen Species (ROS) and ROS-Induced ROS Release. *Physiol Rev*. 94, 909-950.
171. Wang W, Fang H, Groom L, Cheng A, Zhang W, Liu J, Wang X, Li K, Han P, Zheng M, Yin J, Wang W, Mattson MP, Kao JP, Lakatta EG, Sheu SS, Ouyang K, Chen J, Dirksen RT, Cheng H (2008) Superoxide Flashes in Single Mitochondria. *Cell*. 134, 279-290.
172. Wei-LaPierre L, Gong G, Gerstner BJ, Ducreux S, Yule DI, Pouvreau S, Wang X, Sheu SS, Cheng H, Dirksen RT, Wang W. (2013) Respective contribution of mitochondrial superoxide and pH to mitochondria-targeted circularly permuted yellow fluorescent protein (mt-cpYFP) flash activity. *J Biol Chem*. 288, 10567-10577.
173. Shang W, Gao H, Lu F, Ma Q, Fang H, Sun T, Xu J, Ding Y, Lin Y, Wang Y, Wang X, Cheng H, Zheng M (2016) Cyclophilin D regulates mitochondrial flashes and metabolism in cardiac myocytes. *J Mol Cell Cardiol*. 91, 63-71.
174. Schwarzländer M, Logan DC, Fricker MD, Sweetlove LJ (2011) The circularly permuted yellow fluorescent protein cpYFP that has been used as a superoxide probe is highly responsive to pH but not superoxide in mitochondria: implications for the existence of superoxide “flashes.” *Biochem J*. 437, 381-387.
175. Schwarzländer M, Murphy MP, Duchon MR, Logan DC, Fricker MD, Halestrap AP, Müller FL, Rizzuto R, Dick TP, Meyer AJ, Sweetlove LJ (2012) Mitochondrial “flashes”: A radical concept reHined. *Trends Cell Biol*. 22, 503-508.
176. Bernardi P, Di Lisa F (2015) The mitochondrial permeability transition pore: Molecular nature and role as a target in cardioprotection. *J Mol Cell Cardiol*. 78, 100-106.
177. Schiavone M, Zulian A, Menazza S, Petronilli V, Argenton F, Merlini L, Sabatelli P, Bernardi P. (2017) Alisporivir rescues defective mitochondrial respiration in Duchenne muscular dystrophy. *Pharmacol Res*. 125, 122-131.

178. Aquila H, Misra D, Eulitz M & Klingenberg M (1982) Complete amino acid sequence of the ADP/ATP carrier from beef heart mitochondria. *Hoppe Seylers Z Physiol Chem.* 363, 345-349.
179. Klingenberg M (1989) Molecular aspects of the adenine nucleotide carrier from mitochondria. *Arch Biochem Biophys.* 270, 1-14.
180. Klingenberg M (2008) The ADP and ATP transport in mitochondria and its carrier. *Biochim Biophys Acta.* 1778, 1978-2021.
181. Halestrap AP, Brenner C (2003) The Adenine Nucleotide Translocase : A Central Component of the Mitochondrial Permeability Transition Pore and Key Player in Cell Death. *Curr Med Chem.* 10, 1507-1525.
182. Crompton M, Virji S & Ward JM (1998) Cyclophilin-D binds strongly to complexes of the voltage-dependent anion channel and the adenine nucleotide translocase to form the permeability transition pore. *Eur J Biochem.* 258, 729-735.
183. Brustovetsky N, Klingenberg M (1996) Mitochondrial ADP/ATP carrier can be reversibly converted into a large channel by  $Ca^{2+}$ . *Biochemistry.* 2960, 8483-8488.
184. Brustovetsky N, Tropschug M, Heimpel S, Heidka D, Klingenberg M (2002) A large  $Ca^{2+}$ -dependent channel formed by recombinant ADP/ATP carrier from *Neurospora crassa* resembles the mitochondrial permeability transition pore. *Biochemistry.* 41, 11804-11811.
185. Vieira HL, Haouzi D, El Hamel C, Jacotot E, Belzacq AS, Brenner C, Kroemer G (2000) Permeabilization of the mitochondrial inner membrane during apoptosis: impact of the adenine nucleotide translocator. *Cell Death Differ.* 7, 1146-1154.
186. Kokoszka JE, Waymire KG, Levy SE, Sligh JE, Cai J, Jones DP, MacGregor GR, Wallace DC (2004) The ADP/ATP translocator is not essential for the mitochondrial permeability transition pore. *Nature.* 427, 461-465.
187. Szabó I, De Pinto V, Zoratti M (1993) The mitochondrial permeability transition pore may comprise VDAC molecules. II. The electrophysiological properties of VDAC are compatible with those of the mitochondrial megachannel. *FEBS Lett.* 330, 206-210.
188. Krauskopf A, Eriksson O, Craigen WJ, Forte MA, Bernardi P (2006) Properties of the permeability transition in *VDAC1<sup>-/-</sup>* mitochondria. *Biochim Biophys Acta.* 1757, 590-595.
189. Baines CP, Kaiser RA, Sheiko T, Craigen WJ, Molkenin JD (2007) Voltage-dependent anion channels are dispensable for mitochondrial-dependent cell death. *Nat Cell Biol.* 9, 550-555.
190. Manon S, Roucou X, Guérin M, Rigoulet M, Guérin B (1998) Characterization of the yeast mitochondria unselective channel: a counterpart to the mammalian permeability transition pore? *J Bioenerg Biomembr.* 30, 419-429.

191. Roucou X, Manon S, Guérin M (1997) Conditions allowing different states of ATP- and GDP-induced permeability in mitochondria from different strains of *Saccharomyces cerevisiae*. *Biochim Biophys Acta*. 1324, 120-132.
192. Kolbe HV, Costello D, Wong A, Lu RC, Wohlrab H (1984) Mitochondrial phosphate transport. Large scale isolation and characterization of the phosphate transport protein from beef heart mitochondria. *J Biol Chem*. 259, 9115-9120.
193. Alcalá S, Klee M, Fernández J, Fleischer A, Pimentel-Muiños FX (2008) A high-throughput screening for mammalian cell death effectors identifies the mitochondrial phosphate carrier as a regulator of cytochrome *c* release. *Oncogene*. 27, 44-54.
194. Leung AWC, Varanyuwatana P, Halestrap AP (2008) The Mitochondrial Phosphate Carrier Interacts with Cyclophilin D and May Play a Key Role in the Permeability Transition. *J Biol Chem*. 283, 26312-26323.
195. Varanyuwatana P, Halestrap AP (2012) The roles of phosphate and the phosphate carrier in the mitochondrial permeability transition pore. *Mitochondrion*. 12, 120-125.
196. Gutiérrez-aguilar M, Douglas DL, Gibson AK, Domeier TL, Molkentin JD, Baines CP (2014) Genetic manipulation of the cardiac mitochondrial phosphate carrier does not affect permeability transition. *J Mol Cell Cardiol*. 72, 316-325.
197. Kwong JQ, Davis J, Baines CP, Sargent MA, Karch J, Wang X, Huang T, Molkentin JD (2014) Genetic deletion of the mitochondrial phosphate carrier desensitizes the mitochondrial permeability transition pore and causes cardiomyopathy. *Cell Death Differ*. 21, 1209-1217.
198. McEnery MW, Snowman AM, Trifiletti RR, Snyder SH. (1992) Isolation of the mitochondrial benzodiazepine receptor: association with the voltage-dependent anion channel and the adenine nucleotide carrier. *Proc Natl Acad Sci U S A*. 89, 3170-3174.
199. Pastorino JG, Simbula G, Gilfor E, Hoek JB, Farber JL. (1994) Protoporphyrin IX, an endogenous ligand of the peripheral benzodiazepine receptor, potentiates induction of the mitochondrial permeability transition and the killing of cultured hepatocytes by rotenone. *J Biol Chem*. 269, 31041-31046.
200. Azarashvili T, Grachev D, Krestinina O, Evtodienko Y, Yurkov I, Papadopoulos V, Reiser G. (2007) The peripheral-type benzodiazepine receptor is involved in control of Ca<sup>2+</sup>-induced permeability transition pore opening in rat brain mitochondria. *Cell Calcium*. 42, 27-39.
201. Šileikytė J, Blachly-Dyson E, Sewell R, Carpi A, Menabò R, Di Lisa F, Ricchelli F, Bernardi P, Forte M. (2014) Regulation of the mitochondrial permeability transition pore by the outer membrane does not involve the peripheral benzodiazepine receptor (Translocator Protein of 18 kDa (TSPO)). *J Biol Chem*. 289, 13769-13781.



202. Antonsson B, Montessuit S, Lauper S, Eskes R, Martinou JC (2000) Bax oligomerization is required for channel-forming activity in liposomes and to trigger cytochrome c release from mitochondria. *Biochem J.* 345 Pt 2, 271-278.
203. Karch J, Kwong JQ, Burr AR, Sargent MA, Elrod JW, Peixoto PM, Martinez-Caballero S, Osinska H, Cheng EH, Robbins J, Kinnally KW, Molkenin JD (2013) Bax and Bak function as the outer membrane component of the mitochondrial permeability pore in regulating necrotic cell death in mice. *Elife.* 2, e00772.
204. Whelan RS, Konstantinidis K, Wei AC, Chen Y, Reyna DE, Jha S, Yang Y, Calvert JW, Lindsten T, Thompson CB, Crow MT, Gavathiotis E, Dorn GW 2nd, O'Rourke B, Kitsis RN. (2012) Bax regulates primary necrosis through mitochondrial dynamics. *Proc Natl Acad Sci U S A.* 109, 6566-6571.
205. Narita M, Shimizu S, Ito T, Chittenden T, Lutz RJ, Matsuda H, Tsujimoto Y. (1998) Bax interacts with the permeability transition pore to induce permeability transition and cytochrome c release in isolated mitochondria. *Proc Natl Acad Sci U S A.* 95, 14681-14686.
206. Fontaine E, Eriksson O, Ichas F, Bernardi P (1998) Regulation of the permeability transition pore in skeletal muscle mitochondria. Modulation By electron flow through the respiratory chain complex i. *J Biol Chem.* 273, 12662-12668.
207. Fontaine E, Bernardi P (1999) Progress on the mitochondrial permeability transition pore: Regulation by complex I and ubiquinone analogs. *J Bioenerg Biomembr.* 31, 335-345.
208. Chauvin C, Oliveira D, Ronot X, Mousseau M, Leverage X, Fontaine E (2001) Rotenone Inhibits the Mitochondrial Permeability Transition- induced Cell Death in U937 and KB Cells. *J Biol Chem.* 276, 41394-41398.
209. Li B, Chauvin C, De Paulis D, De Oliveira F, Gharib A, Vial G, Lablanche S, Leverage X, Bernardi P, Ovize M, Fontaine E. (2012) Inhibition of complex I regulates the mitochondrial permeability transition through a phosphate-sensitive inhibitory site masked by cyclophilin D. *Biochim Biophys Acta.* 1817, 1628-1634.
210. Starkov AA. (2008) The role of mitochondria in reactive oxygen species metabolism and signaling. *Ann N Y Acad Sci.* 1147, 37-52.
211. He L, Lemasters JJ (2002) The Regulated and unregulated mitochondrial permeability transition pores: a new paradigm of pore structure and function? *FEBS Lett.* 512, 1-7.
212. Kowaltowski AJ, Castilho RF, Vercesi AE (2001) Mitochondrial permeability transition and oxidative stress. *FEBS Lett.* 495, 12-15.
213. Walker JE (2013) ATP synthase: the understood, the uncertain and the unknown. *Biochem Soc Trans.* 41, 1-16.

214. Walker JE, Fearnley IM, Gay NJ, Gibson BW, Northrop FD, Powell SJ, Runswick MJ, Saraste M, Tybulewicz VL (1985) Primary structure and subunit stoichiometry of F<sub>1</sub>-ATPase from bovine mitochondria. *J Mol Biol.* 184, 677-701.
215. Abrahams JP, Leslie AGW, Lutter R, Walker JE (1994) Structure at 2.8 Å resolution of F<sub>1</sub>-ATPase from bovine heart mitochondria. *Nature.* 370, 621-628.
216. Cabezón E, Montgomery MG, Leslie AGW, Walker JE (2003) The structure of bovine F<sub>1</sub>-ATPase in complex with its regulatory protein IF<sub>1</sub>. *Nat Struct Biol.* 10, 744-750.
217. Stock D, Leslie AG, Walker JE (1999) Molecular architecture of the rotary motor in ATP synthase. *Science.* 286, 1700-1705.
218. Watt IN, Montgomery MG, Runswick MJ, Leslie AGW, Walker JE (2010) Bioenergetic cost of making an adenosine triphosphate molecule in animal mitochondria. *Proc Natl Acad Sci U S A.* 107, 16823-16827.
219. Mitome N, Ono S, Sato H, Suzuki T, Sone N, Yoshida M (2010) Essential arginine residue of the F<sub>0</sub>-a subunit in F<sub>0</sub>F<sub>1</sub>-ATP synthase has a role to prevent the proton shortcut without c-ring rotation in the F<sub>0</sub> proton channel. *Biochem J.* 430, 171-177.
220. Symersky J, Pagadala V, Osowski D, Krah A, Meier T, Faraldo-Gómez JD, Mueller DM (2012) Structure of the c<sub>10</sub> ring of the yeast mitochondrial ATP synthase in the open conformation. *Nat Struct Mol Biol.* 19, 485-491.
221. Dickson VK, Silvester JA, Fearnley IM, Leslie AG, Walker JE (2006) On the structure of the stator of the mitochondrial ATP synthase. *EMBO J.* 25, 2911-2918.
222. Rees DM, Leslie AG, Walker JE (2009) The structure of the membrane extrinsic region of bovine ATP synthase. *Proc Natl Acad Sci U S A.* 106, 21597-21601.
223. Baker LA, Watt IN, Runswick MJ, Walker JE, Rubinstein JL (2012) Arrangement of subunits in intact mammalian mitochondrial ATP synthase determined by cryo-EM. *Proc Natl Acad Sci U S A.* 109, 11675-11680.
224. Lee J, Ding SJ, Walpole TB, Holding AN, Montgomery MG, Fearnley IM, et al. (2015) Organization of subunits in the membrane domain of the bovine F-ATPase revealed by covalent cross-linking. *J Biol Chem.* 290, 13308–13320.
225. Vaillier J, Arselin G, Graves PV, Camougrand N, Velours J. Isolation of supernumerary yeast (1999) ATP synthase subunits e and i: Characterization of subunit i and disruption of its structural gene ATP18. *J Biol Chem.* 274, 543–548.
226. He J, Ford HC, Carroll J, Douglas C, Gonzales E, Ding S, Fearnley IM, Walker JE (2018) Assembly of the membrane domain of ATP synthase in human mitochondria. *Proc Natl Acad Sci U S A.* 115, 2988-2993.

227. Mueller DM (2000) Partial assembly of the yeast mitochondrial ATP synthase. *J Bioenerg Biomembr.* 32, 391-400.
228. Lau WCY, Baker LA, Rubinstein JL (2008) Cryo-EM Structure of the Yeast ATP Synthase. *J Mol Biol.* 382, 1256-1264.
229. Hahn A, Parey K, Bublitz M, Mills DJ, Zickermann V, Vonck J, Kühlbrandt W, Meier T (2016) Structure of a Complete ATP Synthase Dimer Reveals the Molecular Basis of Inner Mitochondrial Membrane Morphology. *Mol Cell.* 63, 445-456.
230. Guo H, Bueler SA, Rubinstein JL (2017) Atomic model for the dimeric F<sub>O</sub> region of mitochondrial ATP synthase. *Science.* 358, 936-940.
231. Gledhill JR, Walker JE (2005) Inhibition sites in F<sub>1</sub>-ATPase from bovine heart mitochondria. *Biochem J.* 386, 591-598.
232. Pullman ME, Monroy GC (1963) A Naturally Occurring Inhibitor of Mitochondrial Adenosine Triphosphatase. *J Biol Chem.* 238, 3762-3769.
233. Walker JE (1994) The regulation of catalysis in ATP synthase. *Curr Opin Struct Biol.* 4, 912-918.
234. Cabezón E, Butler PJG, Runswick MJ, Walker JE (2000) Modulation of the oligomerization state of the bovine F<sub>1</sub>-ATPase inhibitor protein, IF<sub>1</sub>, by pH. *J Biol Chem.* 275, 25460-25464.
235. Cabezón E, Runswick MJ, Leslie AG, Walker JE (2001) The structure of bovine IF(1), the regulatory subunit of mitochondrial F-ATPase. *EMBO J.* 20, 6990- 6996.
236. Gledhill JR, Montgomery MG, Leslie AGW, Walker JE (2007) How the regulatory protein, IF<sub>1</sub>, inhibits F<sub>1</sub>-ATPase from bovine mitochondria. *Proc Natl Acad Sci U S A.* 104, 15671-15676.
237. Robinson GC, Bason J V, Montgomery MG, Fearnley IM, Mueller DM, Leslie AG, Walker JE (2013) The structure of F<sub>1</sub>-ATPase from *Saccharomyces cerevisiae* inhibited by its regulatory protein IF<sub>1</sub>. *Open Biol.* 3, 120164.
238. Feniouk BA, Junge W (2005) Regulation of the F<sub>O</sub>F<sub>1</sub>-ATP synthase: The conformation of subunit ε might be determined by directionality of subunit γ rotation. *FEBS Lett.* 579, 5114-5118.
239. Havlíčková V, Kaplanová V, Nůsková H, Drahotka Z, Houstek J (2010) Knockdown of F<sub>1</sub> epsilon subunit decreases mitochondrial content of ATP synthase and leads to accumulation of subunit c. *Biochim Biophys Acta.* 1797, 1124-1129.
240. Montgomery MG, Leslie AGW, Walker JE (2003) The structure of bovine F<sub>1</sub>-ATPase in complex with its regulatory protein IF<sub>1</sub>. *Nat Struct Biol.* 10, 744-750.

241. He J, Ford HC, Carroll J, Ding S, Fearnley IM, Walker JE (2017) Persistence of the mitochondrial permeability transition in the absence of subunit c of human ATP synthase. *Proc Natl Acad Sci U S A.* 114, 3409-3414.
242. He J, Carroll J, Ding S, Fearnley IM, Walker JE (2017) Permeability transition in human mitochondria persists in the absence of peripheral stalk subunits of ATP synthase. *Proc Natl Acad Sci U S A.* 114, 9086-9091.
243. Fujikawa M, Sugawara K, Tanabe T, Yoshida M (2015) Assembly of human mitochondrial ATP synthase through two separate intermediates, F<sub>1</sub>-c-ring and b-e-g complex. *FEBS Lett.* 589, 2707-2712.
244. Wittig I, Meyer B, Heide H, Steger M, Bleier L, Wumaier Z, Karas M, Schägger H (2010) Assembly and oligomerization of human ATP synthase lacking mitochondrial subunits a and A6L. *Biochim Biophys Acta.* 1797, 1004-1011.
245. Vrbacký M, Kovalčíková J, Chawengsaksophak K, Beck IM, Mráček T, Nůsková H, Sedmera D, Papoušek F, Kolář F, Sobol M, Hozák P, Sedlacek R, Houštěk J (2016) Knockout of Tmem70 alters biogenesis of ATP synthase and leads to embryonal lethality in mice. *Hum Mol Genet.* 25, 4674-4685.
246. Osman C, Wilmes C, Tatsuta T, Langer T (2007) Prohibitins interact genetically with Atp23, a novel processing peptidase and chaperone for the F<sub>1</sub>F<sub>0</sub>-ATP synthase. *Mol Biol Cell.* 18, 627-35.
247. Naumenko N, Morgenstern M, Rucktäschel R, Warscheid B, Rehling P (2017) INA complex liaises the F<sub>1</sub>F<sub>0</sub>-ATP synthase membrane motor modules. *Nat Commun.* 8, 1237.
248. Rak M, Gokova S, Tzagoloff A (2011) Modular assembly of yeast mitochondrial ATP synthase. *EMBO J.* 30, 920-930.
249. Ackerman SH, Tzagoloff A (1990) Identification of two nuclear genes (ATP11, ATP12) required for assembly of the yeast F<sub>1</sub>-ATPase. *Proc Natl Acad Sci U S A.* 87, 4986-4990.
250. Rühle T, Leister D (2015) Assembly of F<sub>1</sub>F<sub>0</sub>-ATP synthases. *Biochim Biophys Acta.* 1847, 849-860.
251. Song J, Pfanner N, Becker T (2018) Assembling the mitochondrial ATP synthase. *Proc Natl Acad Sci U S A.* 115, 2850-2852.
252. Anselmi C, Davies KM, Faraldo-Gómez JD (2018) Mitochondrial ATP synthase dimers spontaneously associate due to a long-range membrane-induced force. *J Gen Physiol.* 150, 763-770.
253. Fronzes R, Weimann T, Vaillier J, Velours J, Brèthes D (2006) The peripheral stalk participates in the yeast ATP synthase dimerization independently of e and g subunits. *Biochemistry.* 45, 6715-6723.

254. Arselin G, Vaillier J, Salin B, Schaeffer J, Giraud MF, Dautant A, Brèthes D, Velours J (2004) The modulation in subunits e and g amounts of yeast ATP synthase modifies mitochondrial cristae morphology. *J Biol Chem.* 279, 40392-40399.
255. Soubannier V, Vaillier J, Paumard P, Couлары B, Schaeffer J, Velours J (2002) In the absence of the first membrane-spanning segment of subunit 4(b), the yeast ATP synthase is functional but does not dimerize or oligomerize. *J Biol Chem.* 277, 10739-10745.
256. Soubannier V, Rusconi F, Vaillier J, Arselin G, Chaignepain S, Graves PV, Schmitter JM, Zhang JL, Mueller D, Velours J (1999) The second stalk of the yeast ATP synthase complex: Identification of subunits showing cross-links with known positions of subunit 4 (subunit b). *Biochemistry.* 38, 15017-15024.
257. Spannagel C, Vaillier J, Arselin G, Graves PV, Grandier-Vazeille X, Velours J (1998) Evidence of a subunit 4 (subunit b) dimer in favor of the proximity of ATP synthase complexes in yeast inner mitochondrial membrane. *Biochim Biophys Acta-Biomembr.* 1414, 260-264.
258. Brunner S, Everard-Gigot V, Stuart RA (2002) Subunit e of the yeast F<sub>1</sub>F<sub>0</sub>-ATP synthase forms homodimers. *J Biol Chem.* 277, 48484-48489.
259. Arselin G, Giraud MF, Dautant A, Vaillier J, Brèthes D, Couлары-Salin B, Schaeffer J, Velours J (2003) The GxxxG motif of the transmembrane domain of subunit e is involved in the dimerization/oligomerization of the yeast ATP synthase complex in the mitochondrial membrane. *Eur J Biochem.* 270, 1875-1884.
260. Bustos DM, Velours J (2005) The modification of the conserved GXXXG motif of the membrane-spanning segment of subunit g destabilizes the supramolecular species of yeast ATP synthase. *J Biol Chem.* 280, 29004-29010.
261. Saddar S, Stuart RA (2005) The yeast F<sub>1</sub>F<sub>0</sub>-ATP synthase: Analysis of the molecular organization of subunit g and the importance of a conserved GXXXG motif. *J Biol Chem.* 280, 24435-24442.
262. Arnold I, Pfeiffer K, Neupert W, Stuart RA, Schägger H (1998) Yeast mitochondrial F<sub>1</sub>F<sub>0</sub>-ATP synthase exists as a dimer: identification of three dimer-specific subunits. *EMBO J.* 17, 7170-7178.
263. Paumard P, Vaillier J, Couлары B, Schaeffer J, Soubannier V, Mueller DM, Brèthes D, di Rago JP, Velours J (2002) The ATP synthase is involved in generating mitochondrial cristae morphology. *EMBO J.* 21, 221-230.
264. Strauss M, Hofhaus G, Schröder RR, Kühlbrandt W (2008) Dimer ribbons of ATP synthase shape the inner mitochondrial membrane. *EMBO J.* 27, 1154-1160.

265. Davies KM, Anselmi C, Wittig I, Faraldo-Gómez JD, Kühlbrandt W (2012) Structure of the yeast F<sub>1</sub>F<sub>0</sub>-ATP synthase dimer and its role in shaping the mitochondrial cristae. *Proc Natl Acad Sci U S A.* 109, 13602-13607.
266. Jiko C, Davies KM, Shinzawa-Itoh K, Tani K, Maeda S, Mills DJ, Tsukihara T, Fujiyoshi Y, Kühlbrandt W, Gerle C (2015) Bovine F<sub>1</sub>F<sub>0</sub> ATP synthase monomers bend the lipid bilayer in 2D membrane crystals. *Elife.* 4, e06119.
267. Habersetzer J, Ziani W, Larrieu I, Stines-Chaumeil C, Giraud MF, Brèthes D, Dautant A, Paumard P (2013) ATP synthase oligomerization: From the enzyme models to the mitochondrial morphology. *Int J Biochem Cell Biol.* 45, 99-105.
268. Wagner K, Perschil I, Fichter CD, van der Laan M (2010) Stepwise Assembly of Dimeric F<sub>1</sub>F<sub>0</sub>-ATP Synthase in Mitochondria Involves the Small F<sub>0</sub>-Subunits k and i. *Mol Biol Cell.* 21, 1494-1504.
269. Wittig I, Velours J, Stuart R, Schägger H (2008) Characterization of domain interfaces in monomeric and dimeric ATP synthase. *Mol Cell Proteomics.* 7, 995-1004.
270. Davies KM, Strauss M, Daum B, Kief JH, Osiewacz HD, Rycovska A, Zickermann V, Kühlbrandt W (2011) Macromolecular organization of ATP synthase and complex I in whole mitochondria. *Proc Natl Acad Sci U S A.* 108, 14121-14126.
271. Papakonstantinou T, Galanis M, Nagley P, Devenish RJ (1993) Each of three positively-charged amino acids in the C-terminal region of yeast mitochondrial ATP synthase subunit 8 is required for assembly. *Biochim Biophys Acta.* 1144, 22-32.
272. Raffin R, Stevens PW, Boogaard C, Schiffer M, Stevens FJ (1998) Reengineering immunoglobulin domain interactions by introduction of charged residues. *Protein Eng.* 11, 303-309.
273. Pedersen SW, Moran GE, Sereikaitė V, Haugaard-Kedström LM, Strømgaard K (2016) Importance of a Conserved Lys/Arg Residue for Ligand/PDZ Domain Interactions as Examined by Protein Semisynthesis. *Chembiochem.* 17, 1936-1944.
274. Neves MAC, Yeager M, Abagyan R (2012) Unusual arginine formations in protein function and assembly: Rings, strings, and stacks. *J Phys Chem B.* 116, 7006-7013.
275. Giorgio V, Burchell V, Schiavone M, Bassot C, Minervini G, Petronilli V, Argenton F, Forte M, Tosatto S, Lippe G, Bernardi P (2017) Ca<sup>2+</sup> binding to F-ATP synthase β subunit triggers the mitochondrial permeability transition. *EMBO Rep.* 18, 1065-1076.
276. Bernardi P, Lippe G (2018) Channel formation by F-ATP synthase and the permeability transition pore: an update. *Curr Opin Physiol.* 3, 1–5.
277. Antoniel M, Jones K, Antonucci S, Spolaore B, Fogolari F, Petronilli V, Giorgio V, Carraro M, Di Lisa F, Forte M, Szabó I, Lippe G, Bernardi P (2018) The unique histidine in OSCP subunit

- of F-ATP synthase mediates inhibition of the permeability transition pore by acidic pH. *EMBO Rep.* 19, 257-268.
278. Hubbard MJ, McHugh NJ (1996) Mitochondrial ATP synthase F<sub>1</sub>-beta-subunit is a calcium-binding protein. *FEBS Lett.* 391, 323-329.
279. Chernyak BV, Bernardi P (1996) The mitochondrial permeability transition pore is modulated by oxidative agents through both pyridine nucleotides and glutathione at two separate sites. *Eur J Biochem.* 238, 623-630.
280. Eriksson O, Fontaine E, Petronilli V, Bernardi P (1997) Inhibition of the mitochondrial cyclosporin A-sensitive permeability transition pore by the arginine reagent phenylglyoxal. *FEBS Lett.* 409, 361-364.
281. Eriksson O, Fontaine E, Bernardi P (1998) Chemical modification of arginines by 2,3-butanedione and phenylglyoxal causes closure of the mitochondrial permeability transition pore. *J Biol Chem.* 273, 12669-12674.
282. Linder MD, Morkunaite-Haimi S, Kinnunen PKJ, Bernardi P, Eriksson O (2002) Ligand-selective modulation of the permeability transition pore by arginine modification: Opposing effects of p-hydroxyphenylglyoxal and phenylglyoxal. *J Biol Chem.* 277, 937-942.
283. Speer O, Morkunaite-Haimi S, Liobikas J, Franck M, Hensbo L, Linder MD, Kinnunen PK, Wallimann T, Eriksson O (2003) Rapid suppression of mitochondrial permeability transition by methylglyoxal: Role of reversible arginine modification. *J Biol Chem.* 278, 34757-34763.
284. Johans M, Milanese E, Franck M, Johans C, Liobikas J, Panagiotaki M, Greci L, Principato G, Kinnunen PK, Bernardi P, Costantini P, Eriksson O (2005) Modification of permeability transition pore arginine(s) by phenylglyoxal derivatives in isolated mitochondria and mammalian cells: Structure-function relationship of arginine ligands. *J Biol Chem.* 280, 12130-12136.
285. Papageorgiou S, Melandri AB, Solaini G (1998) Relevance of divalent cations to ATP-driven proton pumping in beef heart mitochondrial F<sub>0</sub>F<sub>1</sub>-ATPase. *J Bioenerg Biomembr.* 30, 533-541.
286. Nathanson L, Gromet-Elhanan Z (2000) Mutations in the beta-subunit Thr<sup>159</sup> and Glu<sup>184</sup> of the *Rhodospirillum rubrum* F<sub>0</sub>F<sub>1</sub> ATP synthase reveal differences in ligands for the coupled Mg<sup>2+</sup>- and decoupled Ca<sup>2+</sup>-dependent F<sub>0</sub>F<sub>1</sub> activities. *J Biol Chem.* 275, 901-905.
287. Du Z, Tucker WC, Richter ML, Gromet-Elhanan Z (2001) Assembled F<sub>1</sub>-(αβ) and Hybrid F<sub>1</sub>-α3β3γ-ATPases from *Rhodospirillum rubrum* α, Wild Type or Mutant β, and Chloroplast γ Subunits. Demonstration of Mg<sup>2+</sup> versus Ca<sup>2+</sup>-induced differences in catalytic site structure and function. *J Biol Chem.* 276, 11517-11523.
288. Bonora M, Bononi A, De Marchi E, Giorgi C, Lebiedzinska M, Marchi S, Patergnani S, Rimessi A, Suski JM, Wojtala A, Wieckowski MR, Kroemer G, Galluzzi L, Pinton P (2013)

- Role of the c subunit of the F<sub>0</sub> ATP synthase in mitochondrial permeability transition. *Cell Cycle*. 12, 674-683.
289. Alavian KN, Beutner G, Lazrove E, Sacchetti S, Park H-A, Licznanski P, Li H, Nabili P, Hockensmith K, Graham M, Porter GA Jr, Jonas EA (2014) An uncoupling channel within the c-subunit ring of the F<sub>1</sub>F<sub>0</sub> ATP synthase is the mitochondrial permeability transition pore. *Proc Natl Acad Sci U S A*. 111, 10580-10585.
290. Zhou W, Marinelli F, Nief C, Faraldo-Gómez JD (2017) Atomistic simulations indicate the c-subunit ring of the F<sub>1</sub>F<sub>0</sub>ATP synthase is not the mitochondrial permeability transition pore. *Elife*. 6, e23781.
291. Bragadin M, Pozzan T, Azzone GF (1979) Kinetics of Ca<sup>2+</sup> carrier in rat liver mitochondria. *Biochemistry*. 18, 5972-5978.
292. Sakaguchi T (2005) The modification of Arginine. *Proteins*. 4, 95–122.
293. Takahashi K (1968) The Reaction of Phenylglyoxal with Arginine Residues in Proteins. *J Biol Chem*. 243, 6171-6179.
294. Takahashi K (1977) The reactions of phenylglyoxal and related reagents with amino acids. *J Biochem*. 81, 395-402.
295. Oya T, Hattori N, Mizuno Y, Miyata S, Maeda S, Osawa T, Uchida K (1999) Methylglyoxal modification of protein. Chemical and immunochemical characterization of methylglyoxal-arginine adducts. *J Biol Chem*. 274, 18492-18502.
296. Godfrey L, Yamada-Fowler N, Smith J, Thornalley PJ, Rabbani N (2014) Arginine-directed glycation and decreased HDL plasma concentration and functionality. *Nutr Diabetes*. 4, e134.
297. Ahmed N, Thornalley PJ, Dawczynski J, Franke S, Strobel J, Stein G, Haik GM (2003) Methylglyoxal-derived hydroimidazolone advanced glycation end-products of human lens proteins. *Invest Ophthalmol Vis Sci*. 44, 5287-5292.
298. Ellis EM (2007) Reactive carbonyls and oxidative stress: Potential for therapeutic intervention. *Pharmacol Ther*. 115, 13-24.
299. Hoon S, Gebbia M, Costanzo M, Davis RW, Giaever G, Nislow C (2011) A Global Perspective of the Genetic Basis for Carbonyl Stress Resistance. *G3 (Bethesda). Genes/Genomes/Genetics*. 1, 219-231.
300. Maessen DEM, Stehouwer CDA, Schalkwijk CG (2015) The role of methylglyoxal and the glyoxalase system in diabetes and other age-related diseases. *Clin Sci*. 128, 839-861.
301. Lindblom R, Higgins G, Coughlan M, De Haan JB (2015) Targeting mitochondria-and reactive oxygen species-driven pathogenesis in diabetic nephropathy. *Rev Diabet Stud*. 12, 134–56.



302. Choksi KB, Boylston WH, Rabek JP, Widger WR, Papaconstantinou J (2004) Oxidatively damaged proteins of heart mitochondrial electron transport complexes. *Biochim Biophys Acta-Mol Basis Dis.* 1688, 95-101.
303. Westwood ME, Thornalley PJ (1995) Molecular characteristics of methylglyoxal-modified bovine and human serum albumins. Comparison with glucose-derived advanced glycation endproduct- modified serum albumins. *J Protein Chem.* 14, 359-372.
304. Gomes RA, Silva MS, Vicente Miranda H, Ferreira AEN, Cordeiro CAA, Freire AP (2005) Protein glycation in *Saccharomyces cerevisiae*: Argpyrimidine formation and methylglyoxal catabolism. *FEBS J.* 272, 521-531.
305. Martins AMTBS, Cordeiro CAA, Ponces Freire AM (2001) In situ analysis of methylglyoxal metabolism in *Saccharomyces cerevisiae*. *FEBS Lett.* 499, 41-44.
306. Bezanilla F. (2000) The voltage sensor in voltage-dependent ion channels. *Physiol Rev.* 80, 555-592.
307. Schwaiger CS, Börjesson SI, Hess B, Wallner B, Elinder F, Lindahl E (2012) The Free Energy Barrier for Arginine Gating Charge Translation Is Altered by Mutations in the Voltage Sensor Domain. *PLoS One.* 7, e45880.
308. Armstrong CT, Mason PE, Anderson JLR, Dempsey CE (2016) Arginine side chain interactions and the role of arginine as a gating charge carrier in voltage sensitive ion channels. *Sci Rep.* 6, 21759.
309. Chen DC, Yang BC, Kuo TT (1992) One-step transformation of yeast in stationary phase. *Curr Genet.* 21, 83-84.
310. Bradshaw PC, Pfeiffer DR (2013) Characterization of the respiration-induced yeast mitochondrial permeability transition pore. *Yeast.* 30, 471-483.
311. Gunter TE, Pfeiffer DR (1990) Mechanisms by which mitochondria transport calcium. *Am J Physiol.* 258, C755-C786.
312. Lenartowicz E, Bernardi P, Azzone GF (1991) Phenylarsine oxide induces the cyclosporin A-sensitive membrane permeability transition in rat liver mitochondria. *J Bioenerg Biomembr.* 23, 679-688.
313. Pfeiffer DR, Gudz TI, Novgorodov SA, Erdahl WL (1995) The peptide mastoparan is a potent facilitator of the mitochondrial permeability transition. *J Biol Chem.* 270, 4923-4932.
314. Yamamoto T, Ito M, Kageyama K, Kuwahara K, Yamashita K, Takiguchi Y, Kitamura S, Terada H, Shinohara Y (2014) Mastoparan peptide causes mitochondrial permeability transition not by interacting with specific membrane proteins but by interacting with the phospholipid phase. *FEBS J.* 281, 3933-3944.

315. Shinohara Y, Bandou S, Kora S, Kitamura S, Inazumi S, Terada H (1998) Cationic uncouplers of oxidative phosphorylation are inducers of mitochondrial permeability transition. *FEBS Lett.* 428, 89-92.
316. Bernardi P, Vassanelli S, Veronese P, Colonna R, Szabó I, Zoratti M (1992) Modulation of the mitochondrial permeability transition pore: Effect of protons and divalent cations. *J Biol Chem.* 267, 2934-2939.
317. Petronilli V, Cola C, Massari S, Colonna R, Bernardi P (1993) Physiological effectors modify voltage sensing by the cyclosporin A-sensitive permeability transition pore of mitochondria. *J Biol Chem.* 268, 21939-21945.
318. Roy S, Šileikytė J, Schiavone M, Neuenswander B, Argenton F, Aubé J, Hedrick MP, Chung TD, Forte MA, Bernardi P, Schoenen FJ (2015) Discovery, Synthesis, and Optimization of Diarylisoxazole-3-carboxamides as Potent Inhibitors of the Mitochondrial Permeability Transition Pore. *ChemMedChem.* 10, 1655-1671.
319. Guo L, Carraro M, Sartori G, Minervini G, Eriksson O, Petronilli V, Bernardi P (2018) Arginine 107 of yeast ATP synthase subunit g mediates sensitivity of the mitochondrial permeability transition to phenylglyoxal. *J Biol Chem.* 293, 14632-14645.
320. Carraro M, Checchetto V, Sartori G, Kucharczyk R, di Rago JP, Minervini G, Franchin C, Arrigoni G, Giorgio V, Petronilli V, Tosatto SCE, Lippe G, Szabó I, Bernardi P (2018) High-Conductance Channel Formation in Yeast Mitochondria is Mediated by F-ATP Synthase e and g Subunits. *Cell Physiol Biochem.* 50, 1840-1855.